VIRGINIA DIVISION OF MINERAL RESOURCES
PUBLICATION 88

CONTRIBUTIONS TO VIRGINIA GEOLOGY - VI

N. H. Evans, Editor

COMMONWEALTH OF VIRGINIA

DEPARTMENT OF MINES, MINERALS AND ENERGY
DIVISION OF MINERAL RESOURCES
Robert C. Milici, Commissioner of Mineral Resources and State Geologist

CHARLOTTESVILLE, VIRGINIA

1989

FRONT COVER: Pillow structures in the Catoctin Formation. Small pillows showing well defined rims are exposed in this outcrop located beside the Appalachian Trail about 300 meters north of State Road 636 (north of the Lynchburg Reservoir). These lavas are thought to have been extruded into a lake or shallow body of marine water.

VIRGINIA DIVISION OF MINERAL RESOURCES
PUBLICATION 88

CONTRIBUTIONS TO VIRGINIA GEOLOGY - VI

N. H. Evans, Editor

COMMONWEALTH OF VIRGINIA

DEPARTMENT OF MINES, MINERALS AND ENERGY
DIVISION OF MINERAL RESOURCES
Robert C. Milici, Commissioner of Mineral Resources and State Geologist

CHARLOTTESVILLE, VIRGINIA

1989

DEPARTMENT OF MINES, MINERALS AND ENERGY
RICHMOND, VIRGINIA
O. GENE DISHNER, Director

COMMONWEALTH OF VIRGINIA
DEPARTMENT OF PURCHASES AND SUPPLY
RICHMOND

Copyright 1989
Commonwealth of Virginia

Portions of this publication may be quoted if credit is given to the Virginia Division of Mineral Resources.

Memorial of David R. Wones [1]
July 13, 1932—October 25, 1984

David B. Stewart
National Center 959, U.S. Geological Survey
Reston, Virginia 22092

David R. Wones was born in San Francisco to Colonel Edward M. and Mrs. Hannah Pearson Wones, their second son and third child. Colonel Wones was a hospital administrator in the U.S. Army and had assignments in Colorado, Hawaii, Illinois, Kansas, Oklahoma, and Texas during Dave's youth. The Wones family loved literature, drama, and music. Dave's father was especially fond of opera and poetry, and Dave and his father spent their last moments together reciting poetry. Dave was particularly interested in the theater throughout his life; he also was shamelessly addicted to composing limericks on short notice, wherein humor and zeal pseudomorphed meter.

Dave graduated in 1950 from Thomas Jefferson High School in San Antonio, Texas. In 1954, he received an S.B. from Massachusetts Institute of Technology, where he studied with H. W. Fairbairn and acquired a life-long interest in the plutonic rocks of northeastern Massachusetts. Dave's graduate work at MIT, at the suggestion of his advisor, G. J. F. MacDonald, combined thermodynamics with experimental geochemistry and petrology. As recipient of the Vannevar Bush Fellowship, he was able to do this work at the Geophysical Laboratory of the Carnegie Institution of Washington. It was there on his first visit that I met him in 1956, and we became close friends for the rest of his life. As a predoctoral fellow at the Geophysical Laboratory in the extraordinarily good times of 1957-1959, Dave worked closely with Han P. Eugster on the phase relations of biotites, on the join phlogopite-annite, and on ferriannite. These studies led to his Ph.D. in 1960 from MIT. He and his colleagues continued to work on micas through the years. One of his last papers, coauthored with his close friend and colleague, David A. Hewitt, summarized 25 years of experimental data on mica stability and noted how deceptive, complex, and difficult this mineral group is. The Mica volume, No. 13 of this Society's Reviews in Mineralogy, was dedicated to his memory by colleagues to acknowledge his contributions and the stimulus of his interactions with them on mica problems. Wonesite, a Na-rich trioctaheral mica like phlogopite, was named in his honor in 1981 by his friends Frank S. Spear, Robert M. Hazen, and Douglas Rumble, III.

Dave joined the geological thermometry project at the U.S. Geological Survey in 1959 and performed experimental work on micas and feldspars, while interacting with a large group of experimentalists, crystallographers, and field geologists. To better formulate the experiments that would contribute most to an understanding of geological problems, he spent summers with Robert L. Smith and Roy A. Bailey in long-established Survey field mapping projects in the Jemez Mountains, New Mexico, and with Paul C. Bateman in the Sierra Nevada. His interests in the stability of micas in the presence of silicate melt and in the relative stability of biotite and hornblende in granitic magma stem from these field seasons. With field observations as his guide, he focussed his experimental work to calibrate the physical properties of phases so that they could be measured and be interpreted to yield estimates of the intensive parameters prevailing during their formation. He also stimulated many colleagues, most notably H. R. Shaw, to develop new methods of controlling hydrogen fugacity for experiments on rock-forming minerals.

In 1967 Frank Press enticed Dave back to MIT as associate professor of geology to teach mineralogy, phase equilibria, and physical geology. Dave enjoyed teaching very much, and his enthusiasm and giving of himself attracted students, several of whom completed advanced degrees in geochemistry and petrology of New England granites. When the Apollo 12 and 14 lunar landings took place in 1969-71, Dave was part of the preliminary examination team that described and catalogued the lunar samples immediately after their delivery to Houston.

In 1971 Dave returned to the U.S. Geological Survey as Chief of the Branch of Experimental Geochemistry and Mineralogy. While managing and leading this diverse research group, he also began field mapping of the Lucerne pluton in Maine to meet Paul Bateman's challenge that he should obtain data for New England granitic plutons to complement the data available for Sierra Nevada plutons. He also began to compile data on the granitic plutons of the northern Appalachians, seeking patterns from their chemistry that might yield clues to magma source regions and be used to constrain models for continental accretion. On completion of his branch chief responsibilities, Dave returned to experimental petrology and intensified his mapping and petrographic and geochemical work on plutonic rocks from Maine and Massachusetts. By then he was becoming chronically overcommitted and recognized that he had more ideas and exciting things to do than there ever would be time for. He realized that he needed the interactions with many colleagues to bring some of his hopes to fruition. When the opportunity to teach was offered again in 1977 as Professor of Geology at Virginia Polytechnic Institute and State University, he accepted, knowing that the questions of thoughtful students would prevent his ever becoming "old and stodgy."

The Virginia Tech environment was ideal, and six master's degrees and one doctorate were completed under his direction. Studies by seven other students are in progress. Important new evidence for the juxtaposition of discrete crustal blocks in the northern Appalachians has been developed with his guidance and inspiration.

Dave thought very deeply about what the distribution of granitic rocks in the northern Appalachians can tell us about geologic processes. His own contributions had just begun to be published. His presidential address to this

1. Reprinted from American Mineralogist, v. 70, p. 1321-1323, 1985.

Society in 1979 on the Lucerne batholith was but the beginning. Another installment, the paper with Andrew and Loiselle in 1983, considered oxygen and strontium isotopes for a transect across the orogen from northwestern to eastern Maine. In two abstracts published posthumously, Wones considered the tectonic environment of magma generation in New England; papers on the distribution of plutons and their chemistry and field relations that were in preparation will be completed by colleagues.

Dave contributed much to the International Geological Correlation Project on the Caledonides, especially by his leadership in the study of plutonic rocks, by lecturing at IGCP conferences, by organizing a conference at Blacksburg and editing its proceedings volume, and by hosting and participating in many field trips.

Although some of us remember him more as a scientist than as an administrator, Wones served with dedication for four years as Chairman of the Department of Geological Sciences at Virginia Tech, ending his term in September 1984. A month later he was tragically killed in an automobile accident while fulfilling with typical dedication the additional responsibility to meet an old friend who came to visit the Department.

A scientist with many skills, Dave Wones to a greater extent than anyone I have known brought theory, experiment, and field observations together to interpret the origin of granitic rocks and their constituent minerals. Although technically not a great lecturer (he usually omitted labels on coordinates on graphs, for example), he was so easily able to share his excitement and the joy of discovery that all who listened understood, and old colleagues and young students alike were stimulated to greater effort, new ideas, and more commitment. Charles Gilbert has aptly cited Dave's capacity for developing and holding more relationships than most of us do, and his great patience with others and little with himself. David A. Hewitt tells of Dave's ability to increase the feeling of self-worth of all his associates. Dave could convey to everyone a deep and transforming sense of the joy in sharing scientific and social life. He once told Douglas W. Rankin that one of the worst things he could think of would be to eat lunch alone. One of my greatest frustrations with his passing is the inability to share newfound knowledge from seismology about the crust in Maine that we both had sought for years to understand. I know that many others have the same sorts of frustrations in other topics, because Dave's interests and influence were very broad.

Dave Wones was interested in all aspects of natural history, especially birds. Dependent upon eye glasses and afflicted by the limited width of field of view through binoculars, he characteristically made a challenge of adversity and kept a seasonal list of species he had observed at a close enough distance to identify without binoculars. This list was long; and every field trip had the added excitement of possibly adding a new bird to his life list.

Dave's numerous allergies denied him many of the joys of life such as honey, string beans, beer, and clams. He gamely balanced his diet, when appropriate, with fruits such as pinot noir, cabernet sauvignon, chardonnay, riesling, and oaky zinfandel. There simply were no challenges - intellectual or physical - that he turned away from.

Dave was much involved with this Society. He joined it in 1959, was elected a Fellow in 1965, and was President of the Society in 1978-79. He was also a Fellow of the American Geophysical Union and of the Geological Society of America.

Dave married Constance Gilman in 1958, and she and their four children Edward, Andres, Sarah, and Suzanne survive him. He was devoted to his family and to his church. He had many social concerns and took a leading role in community responsibilities.

Dave Wones was a scholar, a naturalist, a generous and sharing person, and an exceptionally intelligent and broad scientist who happily contributed much to the lives of everyone he knew. His joyful spirit, zest for life, and boundless energy were vital parts of many lives, and he is sorely missed. At a memorial service for him at Virginia Tech on November 16, 1984, his student, Diana N. Solie, expressed all this in his favorite verse form:

"Twas biotites that first gave him fame
Petrologists all know his name;
But to us Dave was more;
Teacher, friend, and mentor—
To learn from his life is our aim."

Selected Bibliography

Eugster, H. P. and Wones, D. R. (1962) Phase relations of the ferruginous biotite, annite. Journal of Petrology, 3, 82-125.

Wones, D. R. (1963) Phase equilibria of ferriannite, $KFe_3^{+2}Fe^{+3}Si_3O_{10}(OH)_2$. American Journal of Science, 261, 581-596.

Wones, D. R. and Appleman, D. E. (1963) Properties of synthetic triclinic $KFeSi_3O_8$, and some observations on the iron microcline-iron-sanidine transition. Journal of Petrology, 4, 313-317.

Wones, D. R. (1963) Physical properties of synthetic biotites on the join phlogopite-annite. American Mineralogist, 43, 1300-1321.

Wones, D. R. and Eugster, H. P. (1965) Stability of biotite: experiment, theory, and application. American Mineralogist, 50, 1228-1272.

Wones, D. R., Tatlock, D. B., and von Limbach, Dora (1967) Coexisting orthoclase and microcline in altered volcanic rocks; West Humboldt Range, Pershing County, Nevada.

Schweizerische Mineralogische and Petrographische Mitteilungen, 47, 169-176.
Wones, D. R. (1967) A low pressure investigation of the stability of phlogopite. Geochimica et Cosmochimica Acta, 31, 2248-2253.

Wones, D. R. and Gilbert, M. C. (1969) The fayalite-magnetite-quartz assemblage between 600° and 800° C. American Journal of Science, 267-A (Schairer Vol.), 480-488.

Buma, G., Frey, F. A., and Wones, D. R. (1971) New England granites: trace element evidence regarding their origin and differentiation. Contributions to Mineralogy and Petrology, 31, 300-320.

Bateman, P. E. and Wones, D. R. (1972) Huntington Lake quadrangle, central Sierra Nevada, California—analytic data. U.S. Geological Survey Professional Paper 724-A.

Hazen, R. M. and Wones, D. R. (1972) The effect of cation substitutions on the physical properties of trioctahedral micas. American Mineralogist, 57, 103-129.

Czamanske, G. K. and Wones, D. R. (1973) Oxidation during magmatic differentiation, Finmarka, Oslo area, Norway. Part 2, The mafic silicates. Journal of Petrology, 14, 349-380.

Wones, D. R. (1973) Igneous petrology of some plutons in the northern part of the Penobscot Bay area. Geology of East Central and North Central Maine, New England Intercollegiate Geological Conference Guidebook, 1974, 99-125.

Stewart, D. B. and Wones, D. R. (1974) Bedrock geology of Northern Penobscot Bay area. Geology of East Central and North Central Maine, New England Intercollegiate Geological Conference Guidebook, 1974, 223-239.

Barker, Fred, Wones, D. R., Sharp, W. N., and Desborough, G. A. (1975) The Pikes Peak batholith, Colorado Front Range, and a model for the origin of the gabbro-anorthosite-syenite potassic granite suite. Precambrian Research, 2, 97-160.

Hewitt, D. A. and Wones, D. R. (1975) Physical properties of some Fe-Mg-Al trioctahedral biotites. American Mineralogist, 60, 854-862.

Wones, D. R. (1975) The mare basins—characterization and evolution. Geotimes, 20, 22-23.

Wones, D. R. (1976) Granitic intrusives of the Penobscot Bay region, Maine and their structural setting. in Pajari, G. E., Jr. (ed.), Field Guide to the Geology and Plutonic Rocks of South-western New Brunswick and the Penobscot Bay Area of Maine, I.G.C.P. Canadian Plutonics Study Group, Project Caledonide Orogen, 1, 39-69.

Wones, D. R. and Dodge, F. C. W. (1977) The stability of phlogopite in the presence of quartz and diopside. *in* Fraser, D. G. (ed.), Thermodynamics and Geology Reidel. Dordrecht, 229-247.

Czamanske, G. K., Wones, D. R., and Eichelberger, J. C. (1977) Mineralogy and petrology of the intrusive complex in the Pliny Range, New Hampshire. American Journal of Science, 277, 1073-1123.

Hazen, R. M. and Wones, D. R. (1978) Predicted and observed compositional limits of trioctahedral micas. American Mineralogist, 63, 885-892.

Wones, D. R. (1979) The fractional resorption of complex minerals and the formation of strongly femic alkaline rocks. in Yoder, H. S. (ed.), The Evolution of the Igneous Rocks: Fiftieth Anniversary Perspectives, Princeton University Press, Chapter 14, 413-422.

Wones, D. R. (1980) A comparison between granitic plutons of New England, U.S.A., and the Sierra Nevada batholith, California: in California. *in* Wones, D. R. (ed.), Caledonides in the U.S.A., Department of Geological Sciences, VPI & SU, Memoir No. 2, 123-129.

Wones, D. R. (1980) Contributions of crystallography, mineralogy, and petrology to the geology of the Lucerne pluton, Hancock County, Maine. American Mineralogist, 65, 411-437.

Ayuso, R. A. and Wones, D. R. (1980) Geology of the Bottle Lake Complex, Maine: *in* Roy, D. C., and Naylor, R. S. (eds.), The Geology of Northeastern Maine and Neighboring New Brunswick, 72nd New England Intercollegiate Geological Conference Guidebook, 32-64.

Wones, D. R. (1981) Mafic silicates as indicators of intensive variables in granitic magmas. Mining Geology, 31, 191-212.

Wones, D. R. and Gilbert, M. C. (1982) Amphiboles in the igneous environment, *in* Veblen, D. R., and Ribbe, P. H. (eds.), Reviews of Mineralogy, Amphiboles: Petrology and experimental phase relations. Mineralogical Society of America, 9B, 355-390.

Andrew, A. S., Loiselle, M. C., and Wones, D. R. (1983) Granitic plutonism as an indicator of microplates in the Paleozoic of central and eastern Maine. Earth and Planetary Science Letters, 66, 151-165.

Noyes, H. J., Wones, D. R., and Frey, F. A. (1983) A tale of two plutons: petrographic and mineralogic constraints on the

petrogenesis of the Red Lake and Eagle peak plutons, Central Sierra Nevada, California. Journal of Geology, 91, 353-379.
Noyes, H. J., Frey, F. A., and Wones, D. R. (1983) A tale of two plutons: geochemical evidence bearing on the origin and differentiation of the Red Lake and Eagle Peak pluton, Central Sierra Nevada, California Journal of Geology, 91, 487-509.

Loiselle, M. and Wones, D. R. (1983) Plutonism and post-Acadian faulting in east-central Maine: Maine Geology, Bulletin No. 3, 72-84.

Hewitt, D. A. and Wones, D. R. (1984) Phase equilibria of the micas. *in* Bailey, S. W. (Ed.), Micas, Mineralogical Society of America Reviews in Mineralogy, 13, 201-256.

CONTRIBUTIONS TO VIRGINIA GEOLOGY - VI

CONTENTS

Page

Vein copper mineralization of the Virgilina district, Virginia and North Carolina, by Neil E. Johnson, James R. Craig, and J. Donald Rimstidt 1

Exploration for magnetic sulfide deposits in the Virginia Blue Ridge, by Carol Walsh-Stovall, Edwin S. Robinson, J. Donald Rimstidt, and Robert L. Stovall 17

Mineralogy and geochemistry of the lead-zinc ores of the Austinville-Ivanhoe district, Wythe County, Virginia, by Nora K. Foley, and James R. Craig 23

Interpretation of gravity and magnetic anomalies of the Richmond Triassic basin, by Ali A. Nowroozi, and Arnold Wong 41

Gravity anomalies and geology in the Blue Ridge province near Floyd, Virginia, by Robert L. Stovall, Edwin S. Robinson, and Mervin J. Bartholomew 61

Pillow lavas in the Catoctin Formation of central Virginia, by Edgar W. Spencer, Christopher Bowring, and J. D. Bell .. 83

VEIN COPPER MINERALIZATION OF THE VIRGILINA DISTRICT, VIRGINIA AND NORTH CAROLINA

Neil E. Johnson[1], James R. Craig[1], and J. Donald Rimstidt[1]

CONTENTS

	Page
Abstract	2
Introduction	2
Regional geology	3
Ore mineralogy	3
Bornite	3
Chalcocite and djurleite	6
Anilite	6
Digenite	6
Chalcopyrite	7
Hematite	7
Magnetite	8
Pyrite	9
Ilmenite	9
Hessite	9
Gold	9
Rutile	9
Malachite	10
Covellite	10
Cuprite	10
Spionkopite and yarrowite	10
Azurite	10
Intergrowths, textures, and paragenesis	11
Bornite, chalcocite/djurleite, and digenite	11
Anilite and djurleite	11
Bornite and chalcopyrite	11
Bornite and chalcocite (kamacite-like)	12
Textural interpretations and paragenesis	12
Origin and metamorphism of the copper-bearing veins	13
Acknowledgments	15
References cited	15

ILLUSTRATIONS

Figure	Page
1. Location of the Virgilina district	2
2. Composite geologic map of the Virgilina district	4
3. Typical cross-cutting quartz veins	5
4. Mineralization along vein/wall-rock boundary	5
5. Supergene veinlets in bornite displaying reaction rim of digenite	5
6. Phase relations on the Cu-S binary system	7
7. Chalcocite, djurleite, and bornite in myrmekitic intergrowths	9
8. Primary hypogene hematite displaying bireflectance	9
9. Gold associated with bornite, digenite, and hessite	10

1. Department of Geological Sciences, Virginia Polytechnic Institute and State University, Blacksburg, VA 24061

10. Spionkopite and yarrowite pseudomorphs after anilite 10
11. Anilite/djurleite lamellar intergrowths 11
12. "Orange bornite", microscopic intergrowth of bornite and chalcopyrite 12
13. Kamacite-like intergrowth of bornite and chalcocite 12
14. A section of the Cu-Fe-S ternary diagram 13
15. Paragenetic diagram showing the sequence of formation of ore minerals 14

TABLES

1. Ore mineralogy of the Virgilina district 6
2. Representative microprobe analyses of ore minerals from the Virgilina district 8

ABSTRACT

The Virgilina district of the Carolina slate belt of Virginia and North Carolina yielded over 300,000 tons of copper and significant amounts of silver and gold between 1852 and 1916. A detailed examination of the ore and gangue mineralization from the district reveals that the ores display two stages of hypogene deposition and a significant phase of supergene alteration.

Hypogene minerals, in decreasing order of abundance, are bornite, chalcocite/djurleite, anilite, digenite, hematite, chalcopyrite, pyrite, magnetite, ilmenite, rutile, hessite, and gold (fineness approximately 850). Supergene minerals, in decreasing order of abundance, are malachite, covellite, cuprite, digenite, hematite, chalcopyrite, chalcocite/djurleite, azurite, spionkopite, and yarrowite. This represents the first reported occurrence of djurleite, anilite, hessite, spionkopite, and yarrowite in Virginia.

Lamellar intergrowths of anilite and djurleite on their close-packed planes, myrmekitic intergrowths of bornite and chalcocite/djurleite, coexisting chalcocite and djurleite, and gradational transitions from anilite to digenite were determined to have formed by secondary hypogene reactions. These reactions removed iron and sulfur from the bornite and increased the copper to sulfur ratio, which shifted the Cu-S binary phases towards copper-enriched compositions producing delicate textures and intergrowths.

The source of ore fluids and the timing of the mineralization are not known precisely, but fragments of wall rock that are contained within the veins and have schistosity at an angle to the regional schistosity constrain the veins to be post-metamorphic. Metals were probably derived in part from the metamorphism of mafic volcanic rocks in the area.

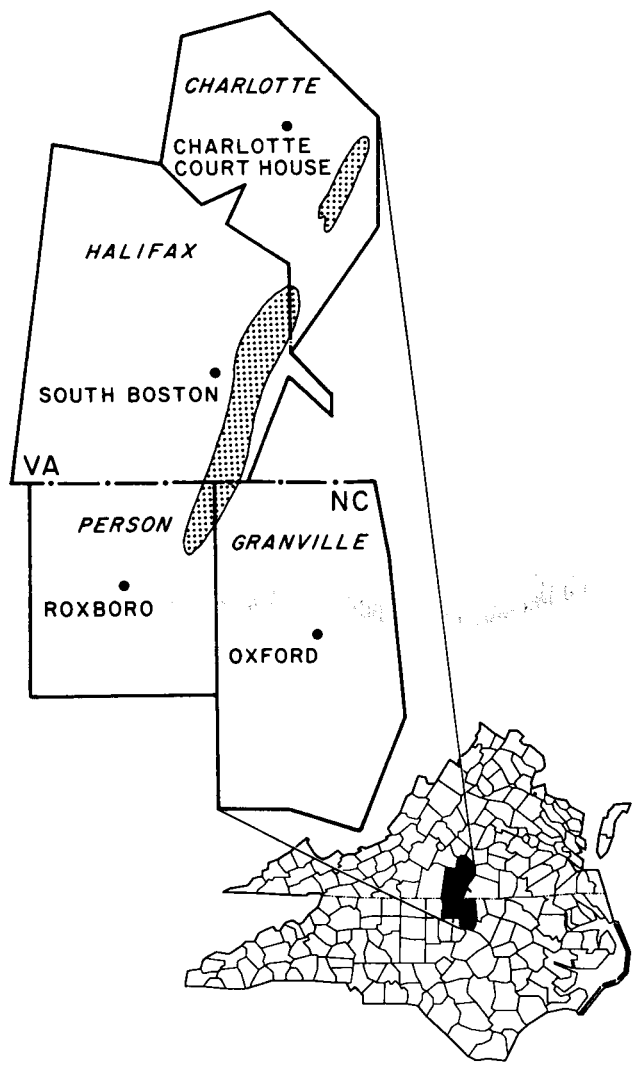

Figure 1. Location of the Virgilina district in Halifax and Charlotte counties, Virginia, and Person and Granville counties, North Carolina.

INTRODUCTION

The Virgilina district, which extends from Keysville, Virginia, to Roxboro, North Carolina (Figure 1), a distance of about 55 miles, was a major producer of copper in the late 19th and early 20th centuries. There is evidence that some prospecting and mining was accomplished between 1700 and

1750 and mining began in earnest in about 1852. The bulk of production was from a few large mines and took place between 1890 and 1916. Mining ceased in 1916. More than 30 named mines and prospects can be located today (Sweet, 1976), and there are others that are unnamed or are named but whose locations are no longer known. Copper mineralization occurs either as sulfides in distinct quartz veins or as native copper disseminated through epidotized host rocks within the Virgilina Formation. The Virgilina is a series of mixed metavolcanic rocks and epiclastic sediments of Precambrian to Cambrian age (Glover and Sinha, 1973; Kreisa, 1980; Harris, 1982).

Although the geology of the area has been subjected to increasing scrutiny in recent years (Tobisch and Glover, 1969, 1971; Glover and others, 1971; Glover and Sinha, 1973; Glover, 1974; Black, 1978; Briggs and others, 1978; Kreisa, 1980; Wright and Seiders, 1980; Harris, 1982), there have been no modern studies of the copper mineralization. Watson (1902) and Weed (1911) catalog the known occurrences; Newberry and others (1948) summarize the economic potential; and Laney (1917) provides the only detailed description of the deposits. Studies of the host rock trace-element chemistry (Stein and Kish, 1978), and the gold mineralization in the district (Linden, 1981) have been completed. The present study describes the mineralogic and textural relations of the ore minerals at the located mines in light of modern mineralogy and ore petrology (see Johnson, 1983 for detailed locality maps and descriptions).

REGIONAL GEOLOGY

The Virgilina district (Figure 2) is part of the Carolina slate belt of the southern Appalachians and is in the Piedmont physiographic province. The district is underlain by Precambrian to Cambrian volcanic, volcaniclastic, and epiclastic rocks that are folded into a broad synclinorium and metamorphosed to greenschist facies. Scattered throughout the district are plutons and dikes that range compositionally from granite to gabbro. Quartz veins also crosscut the rocks and are host to copper, silver, and gold ore that was mined in the late 19th and early 20th centuries.

The metasedimentary sequence consists of, from oldest to youngest, the Hyco, Aaron, and Virgilina Formations (Laney, 1917). The Hyco consists primarily of andesitic to basaltic pyroclastic rocks; the Aaron, of arenites, siltstones, and conglomerates derived in part from the Hyco; and the Virgilina of interlayered rhyolitic to dacitic volcanic and volcaniclastic rocks, mudstones, and graywackes (Harris, 1982). All of these rocks have been metamorphosed to the greenschist facies. Kreisa (1980) proposed that the Virgilina Formation be considered the middle member of a redefined Aaron Formation.

Intrusive rocks in the district include the Redoak and Roxboro metagranites, gabbroic bodies including the Abbeyville gabbro, and other unnamed bodies of granodiorite, quartz diorite, and quartz monzonite. Most of these are poorly exposed (Glover and Sinha, 1973; Kreisa, 1980) but are believed to be pre-metamorphic. Some of the plutons may be subvolcanic shallow intrusives related to the Hyco Formation (Glover and Sinha, 1973). Scattered throughout the district are post-metamorphic dikes of diabase and granite that are compositionally similar to many of the plutons but are generally considered to be younger (Glover and Sinha, 1973; Harris, 1982).

The ubiquitous quartz veins in the district are commonly subparallel to the regional schistosity (N75° to 80°E), are sharply bounded, and range in width from a few inches to 15 feet (Figure 3). Although the veins occur in all formations, only those found in the Virgilina Formation contain significant copper mineralization.

The major structural feature in the district is the Virgilina synclinorium (Brown, 1953). The rocks have undergone at least two episodes of deformation and possess a penetrative slaty cleavage (Harris, 1982). There are steeply dipping faults in the district, some of which predate and some of which postdate the regional metamorphism.

ORE MINERALOGY

The ore minerals of the Virgilina district can be subdivided into hypogene and supergene ores (Table 1). Descriptions of each of the minerals observed are given below, and examples of the textures are shown in Figures 5 and 7 through 13. The ore-bearing veins consist of coarse- grained, white to clear quartz with local concentrations of manganocalcite and orthoclase. Most of the ore mineralization occurs as local concentrations in the veins, but minor amounts are disseminated in the veins and in the adjacent metavolcanic rocks. Fragments of the metavolcanic rocks, both altered to epidosite and unaltered, are often included in the veins, usually along the margins. Ore mineralization is commonly associated with these fragments. Locally the ore is disseminated within the individual fragments.

In general, ore mineralization occurs near or at the interface zone of the vein and the metavolcanic country rock (Figure 4). This interface is almost always altered to epidote or epidote plus chlorite. Veins that do not display this alteration halo tend not to be mineralized. This suggests that the reactions of metalliferous hydrothermal fluids with the country rock were partially responsible for ore deposition. Grain sizes of ore minerals range from less than 0.002 mm to as much as 3 cm. Representative electron microprobe analyses of minerals are listed in Table 2.

BORNITE

Bornite (Cu_5FeS_4) is the most abundant ore mineral

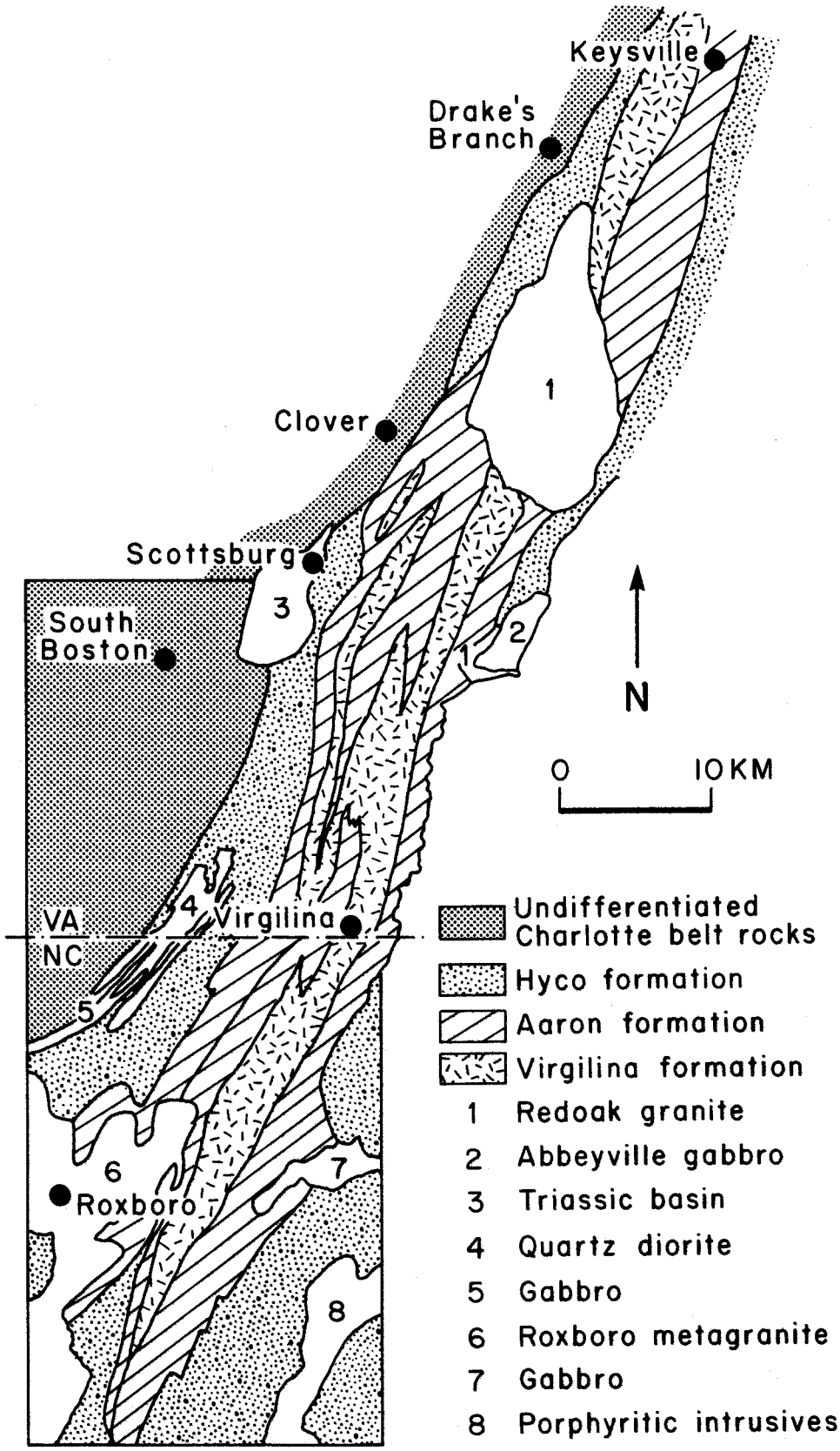

Figure 2. Composite geologic map of the Virgilina district, from Laney (1917), LeGrand (1960), Glover and Sinha (1973) and Kreisa (1980).

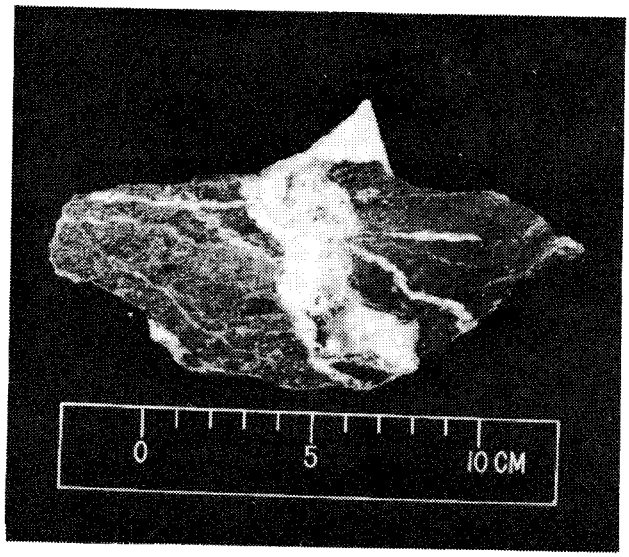

A

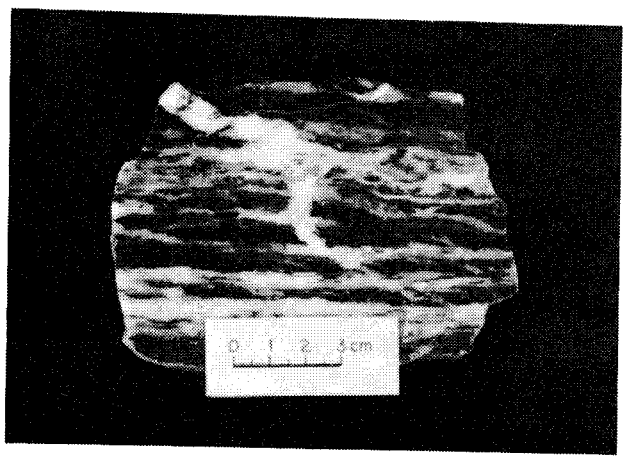

B

Figure 3. Typical cross-cutting quartz veins from the Virgilina district: (A) Durgy mine, Person County, North Carolina, (B) Holloway mine, Granville County, North Carolina.

in the veins of the Virgilina district, constituting approximately 45 percent of the hypogene ore minerals. It occurs as disseminated blebs less than 0.015 mm to masses more than 3 cm in size in both the veins and the country rock. Compositions range from virtually stoichiometric to 3 weight percent copper-depleted (Table 2). There is no apparent relationship between composition and location in the district.

Bornite is generally highly fractured and contains abundant veins of digenite (Figure 5). Tooth-shaped crystals of chalcocite or djurleite and flame-like structures of supergene chalcopyrite are present locally. Bornite may also contain randomly distributed blebs of chalcocite, djurleite, and chalcopyrite, and euhedral to subhedral crystals of hematite. Bornite rarely displays a weak bireflectance, and examination under crossed nicols indicates that masses of bornite are primarily of homogeneous. Bornite may also be found in myrmekitic intergrowths with both chalcocite/djurleite and digenite, as well as kamacite-like intergrowths with chalcocite. It is replaced by chalcocite and djurleite and replaces anilite.

Peculiar orange-tinted bornite that displays high relief and tends to tarnish more slowly than normal bornite was found throughout the district in association with covellite, spionkopite, yarrowite, cuprite, and malachite. High-magnification petrographic examination and microprobe analysis indicate that this "orange bornite" is, in fact, bornite with microscopic to submicroscopic (50 to 250 micron) lamellae of chalcopyrite oriented parallel to (111) and (100) in the bornite.

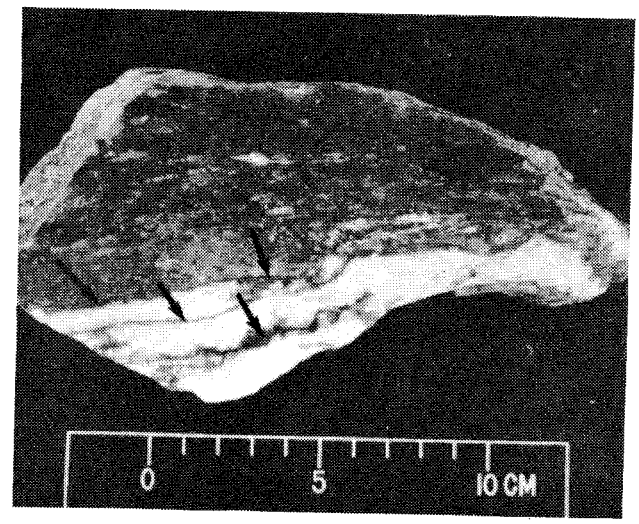

Figure 4. Mineralization (chalcocite/djurleite with minor bornite) along vein/wall-rock boundary, Littlejohn mine, Halifax County, Virginia.

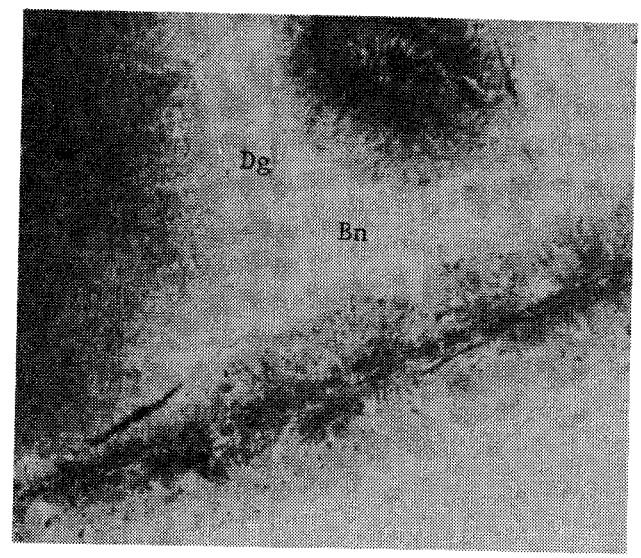

Figure 5. Supergene veinlets in bornite (Bn) displaying reaction rim of digenite (Dg); sample 80, High Hill mine, 100X, field oof view 1.05 mm.

Table 1. Ore mineralogy of the Virgilina district.

Ore minerals observed in this study.

HYPOGENE		SUPERGENE	
Name	Formula	Name	Formula
Bornite	Cu_5FeS_4	Malachite	$Cu_2(CO_3)(OH_)2$
Chalcocite	Cu_2S	Covelite	CuS
Djurleite*	$Cu_{31}S_{16}$	Cuprite	Cu_2O
Anilite*	Cu_7S_4	Digenite	Cu_9S_5
Digenite	Cu_9S_5	Hematite	Fe_2O_3
Chalcopyrite	$CuFeS_2$	Spionkopite	$Cu_{39}O_{28}$
Hematite	Fe_2O_3	Yarrowite	Cu_9S_8
Magnetite	Fe_3O_4	Chalcopyrite	$CuFeS_2$
Hessite*	Ag_2Te	Azurite	$Cu_3(CO_3)_2(OH)_2$
Gold	(Au,Ag)		
Ilmenite	$FeTiO_3$		
Pyrite	FeS_2		

Ore minerals previously reported.

Name	Formula	Reference
Argentite	Ag_2S	Laney (1917)
Chrysocolla	$(Cu,Al)_2H_2Si_2O_5(H0)_4nH_2O)$	Laney (1917)
Copper	Cu	Laney (1917)
Klaprothite**	$CuBiS_2$	Laney (1917)
Silver	Ag	Laney (1917)
Tenorite	CuO	Laney (1917)
Hemimorphite	$Zn_4Si_2O_7(OH)_2H_2O$	Carpenter (1976)
Pyrrhotite	$Fe_{1-x}S$	Carpenter (1976)

* First reported occurrence in Virginia or North Carolina.
** According to Nuffield (1947b), all klaprothite available to him for examination proved to be either wittichenite or emplectite (Uytenbogaart and Burke, 1971).

CHALCOCITE AND DJURLEITE

Chalcocite and djurleite ($Cu_2S/Cu_{31}S_{16}$) represent approximately 30 percent of the hypogene and 5 percent of the supergene ores. Distinguishing between the two minerals is virtually impossible by petrographic or microprobe analysis; the only reliable method of identification is X-ray diffraction. Accordingly, positive determination can only be made for large, inclusion-free areas. The X-ray powder analyses undertaken (Johnson, 1983) indicate that chalcocite is only present where the ores do not contain anilite. This is consistent with the phase relations determined by Barton (1973) and Potter (1977) (Figure 6). However, the absence of visible anilite does not necessarily imply the presence of chalcocite. Unless the presence or absence of one or the other can be conclusively proven by X-ray methods, it is deemed prudent to describe the two minerals together.

Chalcocite/djurleite occur as disseminated blebs less than 0.015 mm to masses more than 3 cm in size. Both minerals tend to be more restricted to the vein rocks than the bornite. Microprobe analyses of samples from several mines show no obvious compositional trends across the district. Of special interest are trace amounts of silver, ranging from the limits of detection (0.01 weight percent) to a maximum of 0.46 weight percent silver. Comparison of the amounts of silver produced as by-products of the mining operations with the amount of silver detected indicates that much of the reported production could have been accounted for by trace amounts of silver in chalcocite and djurleite. This implies that the free silver and argentite described by Laney (1917) may have been of minor and supergene origin.

Neither the chalcocite nor the djurleite display any deformational features, and both are generally free of the fracturing and veining that are common in the bornite. Some supergene chalcocite/djurleite does occur, commonly as tooth-shaped crystals lining the walls of cuprite veinlets in the bornite and anilite. In places the minerals were observed with malachite in reprecipitated masses filling fractures in the ore and gangue.

Hypogene chalcocite and djurleite occur in myrmekitic intergrowths with bornite (Figure 7). Intergrowths are more common when chalcocite is present. Both chalcocite and djurleite replace bornite, and the djurleite replaces anilite as well as forming lamellar intergrowths with it.

ANILITE

Anilite (Cu_7S_4) is common in the district, but less so than bornite, chalcocite, or djurleite. It constitutes approximately 15 percent of the hypogene mineralization and is found in most of the mines. The presence of anilite was determined by X-ray diffraction and microprobe analyses. Anilite, a good indicator for presence of chalcocite or djurleite, occurs within ore veins as isolated grains 0.05 to 0.1 mm in size and as 1- to 20-mm masses of interlocked grains.

As is the case with bornite, anilite is highly fractured. Although some of the fractures have random orientation, most are parallel to (001) cleavage. Anilite appears optically homogeneous, but Morimoto and others (1969) note that any anisotropic effects are probably masked by a surface layer of an isotropic digenite-like phase created by polishing. It is usually free of inclusions, except for occasional subhedral to euhedral crystals of hematite. Microprobe analyses (Johnson, 1983) indicate that anilite may contain trace amounts of iron and up to 0.42 weight percent silver. Anilite occurs in lamellar intergrowths with, and is replaced by, djurleite, bornite, and digenite.

DIGENITE

Digenite (Cu_9S_5), which makes up approximately 10 percent of the hypogene and 5 percent of the supergene ore minerals, occurs primarily as reaction rims between other ore minerals. In the hypogene ores digenite is commonly found between bornite and anilite in myrmekitic textures. Super-

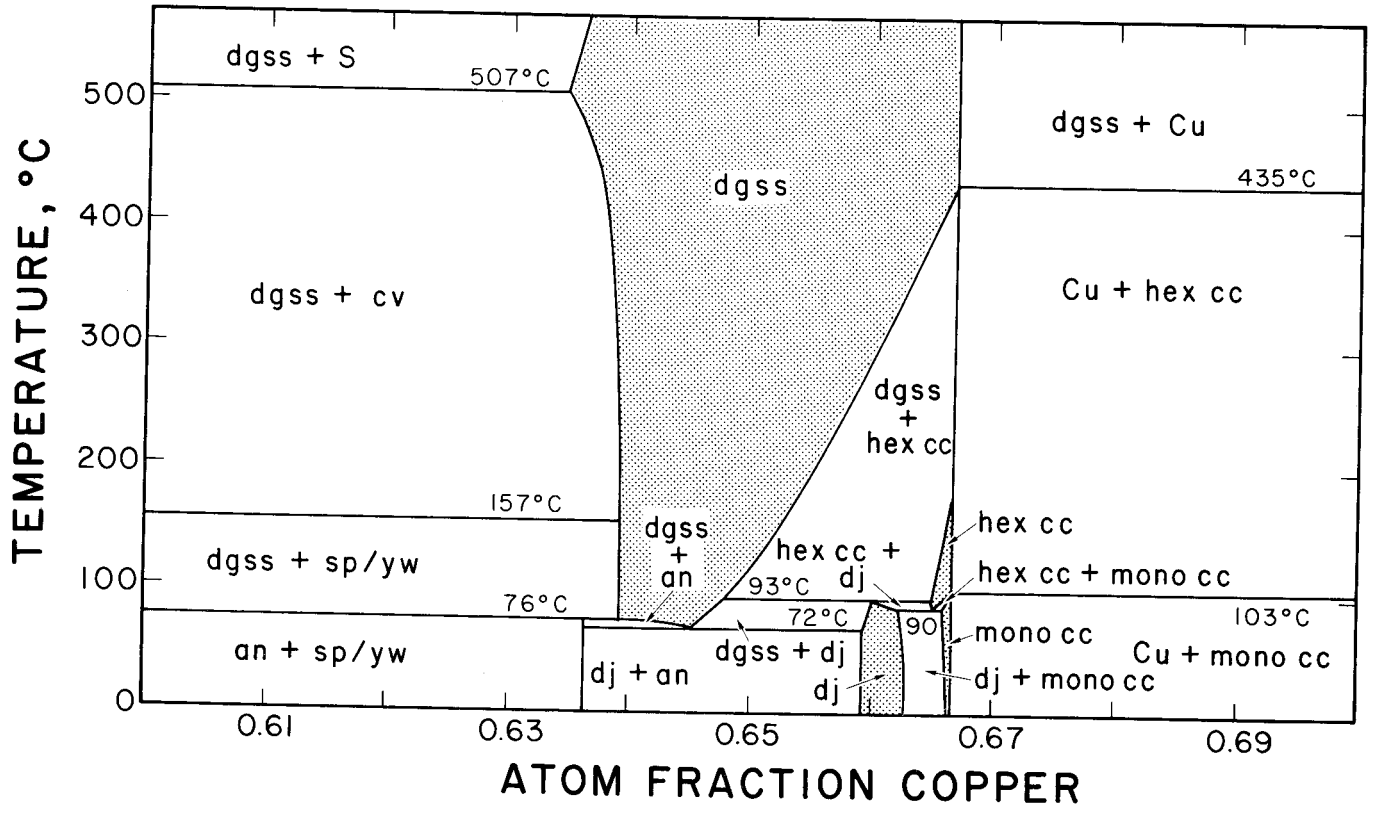

Figure 6. Phase relations on the Cu-S binary system from 0.60 to 0.70 atom percent copper, after Barton (1973) and Potter (1977); dgss = high digenite solid solution; cv = covellite; sp/yw = spionkopite/yarrowite; an = anilite; hex cc = hexagonal chalcocite; mono cc = monoclinic chalcocite; dj = djurleite.

gene digenite forms a border between quartz and cuprite veinlets and hypogene bornite or chalcopyrite. In both cases, the digenite is massive.

Although the formula is usually given as Cu_9S_5, Morimoto and Koto (1970) determined that digenite is unstable below 70° C unless there is approximately 1 percent iron in the structure. Microprobe analyses of zones of anilite reacting to digenite indicate that the transition is gradational from iron-poor (less than 0.05 weight percent) to iron-rich (more than 2.0 weight percent). In this study, an arbitrary limit of 0.50 weight percent Fe is used for distinguishing digenite from anilite.

CHALCOPYRITE

Chalcopyrite ($CuFeS_2$) is the least common ore mineral, constituting less than 1 percent of the total mineralization. It constitutes up to 20 percent of the hypogene ore at the Seaboard mine and the Glascock shaft of the Pontiac mine but elsewhere is limited to minor supergene mineralization. It occurs as 0.003- to 0.1-mm blebs and 0.001- to 0.01-mm lamellae in bornite, 0.5- to 3-mm masses, and rarely as 0.003- to 0.015-mm supergene flame-like structures along fractures in bornite.

Hypogene chalcopyrite is fractured in the same manner as bornite; fractures are commonly filled with digenite and less commonly follow grain boundaries. Examination under crossed nicols indicates that, unlike bornite, chalcopyrite masses consist of interlocked grains in various orientations. Some of the masses contain grains with 120° triple junctions; this feature is peculiar to chalcopyrite and suggests annealing following ore deposition. The supergene chalcopyrite, as noted above, is exceedingly rare, occurring in bornite fractures with cuprite and digenite. The compositions of both hypogene and supergene chalcopyrite are stoichiometric within the limits of analysis.

HEMATITE

Hematite (Fe_2O_3) is ubiquitous in the hypogene and

Table 2. Representative microprobe analyses of ore minerals from the Virgilina district.

Sulfide Mineral	Cu	Ag	Fe	S	Total	Sample
Bornite	63.08	0.02	11.82	25.91	100.83	167, Glasscock shaft, Pontiac mine.
Bornite	61.52	0.08	11.49	25.79	98.88	208, Daniel's mine.
Bornite	61.17	0.04	12.21	26.69	100.11	122, High Hill mine.
Chalcocite/ Djurleite	78.44	0.18	0.06	21.03	99.72	149, Seaboard mine.
Chalcocite/ Djurleite	79.24	0.07	0.06	20.84	100.21	65, Tuck shaft, Pontiac mine.
Chalcocite/ Djurleite	78.59	0.01	0.05	20.84	99.49	190, Littlejohn mine.
Anilite	77.59	0.02	0.00	22.35	99.96	77, High Hill mine.
Anilite	76.40	0.11	0.02	22.02	98.55	69, Anaconda mine.
Digenite	77.12	0.04	1.62	22.00	100.78	161, Chappell mine.
Digenite	75.44	0.01	1.46	22.70	99.61	206, Crenshaw mine.
Covellite	65.90	0.18	0.00	32.41	98.49	159, Chappell mine.
Covellite	66.66	0.11	0.00	32.81	00.58	80, High Hill mine.
Chalcopyrite	34.60	0.02	30.50	34.28	99.40	193, Barnes mine.
Spionkopite/ Yarrowite	68.65	0.02	0.12	30.80	99.59	80, High Hill mine.
Spionkopite/ Yarrowite	66.42	0.27	0.10	31.28	98.07	70, Pandora mine.

Oxide Mineral	Fe_2O_3	FeO	TiO_2	MnO	MgO	Al_2O_3	SiO_2	Total	Sample
Hematite	86.31	6.48	7.13	0.00	0.00	0.02	0.00	99.94	197, Barnes mine.
Hematite	99.04	0.22	0.19	0.00	0.07	0.00	0.00	99.45	68, Anaconda mine.
Hematite	100.35	0.02	0.03	0.00	0.00	0.00	0.00	100.40	157, Chappell mine.
Ilmenite	0.00	43.81	52.69	3.54	0.00	0.02	0.03	100.09	202, Crenshaw mine.
Magnetite	70.82	28.75	0.02	0.08	0.00	0.05	0.00	99.72	204, Crenshaw mine.

supergene ores but occurs in only minor (1 to 2 percent) amounts. It is present as tabular single crystals 0.05 to 10 mm in length and as polycrystalline masses or radiating sprays. Crystals and masses are commonly folded or otherwise deformed.

Hypogene hematite is associated with anilite, chalcocite, djurleite, bornite, and rarely, chalcopyrite. In addition, martitic hematite is associated with magnetite. Supergene hematite is associated with covellite, malachite, and cuprite. Hypogene hematite can be divided into two groups: primary hematite that displays a distinct bireflectance (Figure 8), and secondary hematite that exhibits no bireflectance. Microprobe analyses of the primary bireflectant hematite indicate that it contains up to 17 weight percent $FeTiO_3$, whereas both secondary and supergene hematite are closer to stoichiometric Fe_2O_3.

Although titanohematite is often distinctly heterogeneous, systematic zonation within grains is not evident. Some titanohematite from the Barnes mine has exsolved small (1.5 to 3 micron) blebs of ilmenite along the edges of grains. Ilmenite and hematite are completely miscible at high temperatures (above 800°C), however, at lower temperatures there is a miscibility gap (Lindsley, 1973).

MAGNETITE

Magnetite (Fe_3O_4) is uncommon in the Virgilina ore veins. It occurs as subhedral to euhedral crystals, 0.02 to 0.4 mm in size, generally disseminated through the country rock adjacent to the vein. The grains are usually fractured but otherwise show no evidence of deformation. Martitization

replacement by hematite along edges and certain crystallographic planes is very common and ranges from slight to nearly complete. Microprobe analyses of the magnetites failed to reveal any minor constituents above a concentration of 0.5 weight percent.

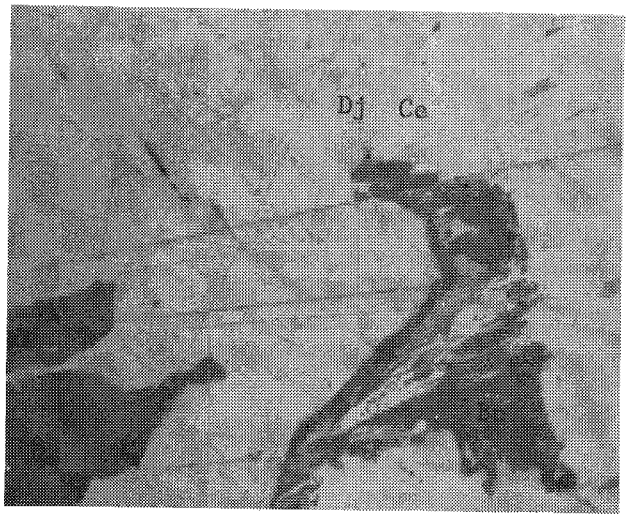

Figure 7. Chalcocite (Cc), djurleite (Dj), and Bornite (Bn) in myrmekitic intergrowth; sample 208, Daniels mine, 200X, field of view 1.05 mm.

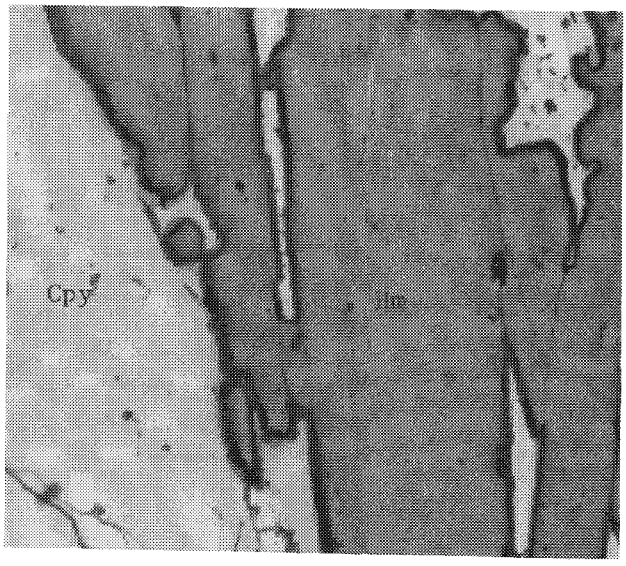

Figure 8. Primary hypogene hematite (Hm) displaying bireflectance, associated with chalcopyrite (Cpy); sample 159, Chappell mine, 100X, field of view 1.05 mm.

PYRITE

Pyrite (FeS_2) has been found only in samples from the Morong (Mother Lode) mine. The grains are subhedral to euhedral, 0.2 to 2 mm in size and are disseminated through both the vein and the country rock. Pyrite displays no apparent pressure fringes or other evidence of deformation, and most grains contain small inclusions of quartz.

ILMENITE

Ilmenite ($FeTiO_3$) occurs as disseminated blades and blebs 0.03 to 0.4 mm in size disseminated through the country rock at the Crenshaw and Daniels mines and as 1.5- to 3-micron blebs exsolved from titanohematite at the Barnes mine. Both the blades and blebs show embayments and curved boundaries indicative of resorption. Disseminated through the ilmenite grains are small (3 to 10 micron) blebs of titanohematite and rutile.

HESSITE

Hessite (Ag_2Te) has been found only in polished sections of samples from the Daniel's mine. It occurs as 0.002 to 0.066 mm blebs disseminated through the bornite, anilite, and digenite and displays the spotty anisotropism characteristic of inversion at 155°C from the cubic polymorph (Uytenbogaart and Burke, 1971). Microprobe analyses indicate that hessite contains up to 7 weight percent copper and 1 weight percent iron.

GOLD

Gold (Au) grains were observed in polished sections of samples from only the Daniels mine. The gold ranges in size from 0.002 to 0.05 mm, is disseminated along the ore-gangue boundary, and is associated with covellite, cuprite, malachite, and digenite. Gold also occurs with hessite in disseminated blebs (Figure 9). Microprobe analyses of the gold indicate that it has a fineness of approximately 850. This is comparable with the average fineness of 840 determined by Linden (1981) for material from the abandoned gold mines of the district.

Based on the similarities of the gold-bearing and the copper-bearing veins, both Laney (1917) and Linden (1981) concluded that the gold and copper mineralization were related. The similarity of the gold from the Daniels mine to that from the gold mines also supports a relationship.

RUTILE

Rutile (TiO_2) occurs as finely disseminated blebs in ilmenite associated with titanohematite at the Crenshaw and Daniels mines.

replacement by hematite along edges and certain crystallographic planes is very common and ranges from slight to nearly complete. Microprobe analyses of the magnetites failed to reveal any minor constituents above a concentration of 0.5 weight percent.

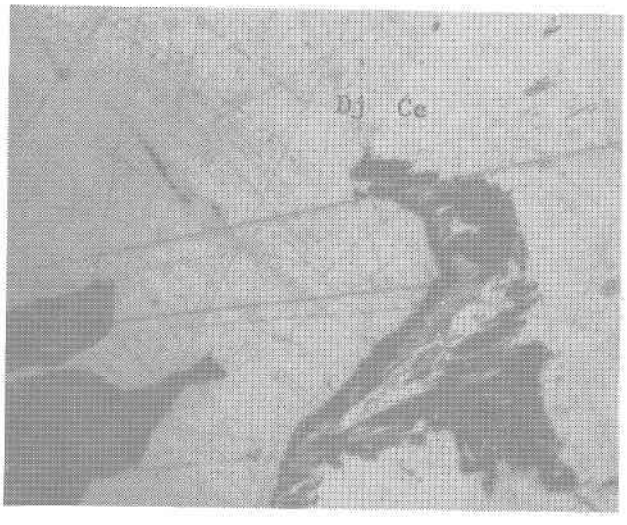

Figure 7. Chalcocite (Cc), djurleite (Dj), and Bornite (Bn) in myrmekitic intergrowth; sample 208, Daniels mine, 200X, field of view 1.05 mm.

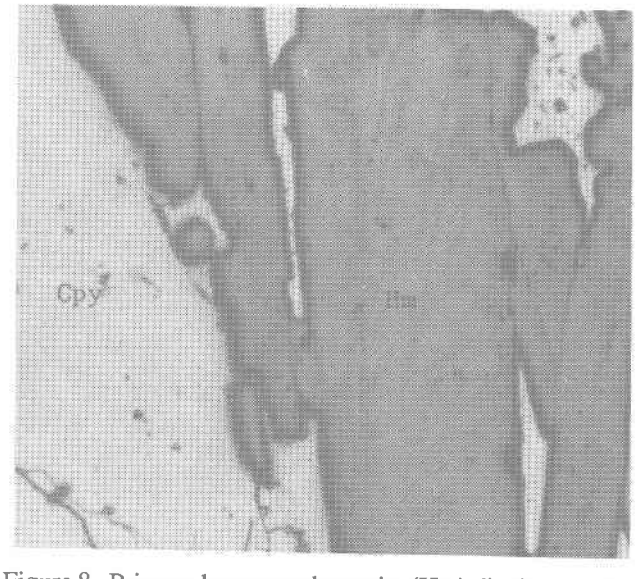

Figure 8. Primary hypogene hematite (Hm) displaying bireflectance, associated with chalcopyrite (Cpy); sample 159, Chappell mine, 100X, field of view 1.05 mm.

PYRITE

Pyrite (FeS_2) has been found only in samples from the Morong (Mother Lode) mine. The grains are subhedral to euhedral, 0.2 to 2 mm in size and are disseminated through both the vein and the country rock. Pyrite displays no apparent pressure fringes or other evidence of deformation, and most grains contain small inclusions of quartz.

ILMENITE

Ilmenite ($FeTiO_3$) occurs as disseminated blades and blebs 0.03 to 0.4 mm in size disseminated through the country rock at the Crenshaw and Daniels mines and as 1.5- to 3-micron blebs exsolved from titanohematite at the Barnes mine. Both the blades and blebs show embayments and curved boundaries indicative of resorption. Disseminated through the ilmenite grains are small (3 to 10 micron) blebs of titanohematite and rutile.

HESSITE

Hessite (Ag_2Te) has been found only in polished sections of samples from the Daniel's mine. It occurs as 0.002 to 0.066 mm blebs disseminated through the bornite, anilite, and digenite and displays the spotty anisotropism characteristic of inversion at 155'C from the cubic polymorph (Uytenbogaart and Burke, 1971). Microprobe analyses indicate that hessite contains up to 7 weight percent copper and 1 weight percent iron.

GOLD

Gold (Au) grains were observed in polished sections of samples from only the Daniels mine. The gold ranges in size from 0.002 to 0.05 mm, is disseminated along the ore-gangue boundary, and is associated with covellite, cuprite, malachite, and digenite. Gold also occurs with hessite in disseminated blebs (Figure 9). Microprobe analyses of the gold indicate that it has a fineness of approximately 850. This is comparable with the average fineness of 840 determined by Linden (1981) for material from the abandoned gold mines of the district.

Based on the similarities of the gold-bearing and the copper-bearing veins, both Laney (1917) and Linden (1981) concluded that the gold and copper mineralization were related. The similarity of the gold from the Daniels mine to that from the gold mines also supports a relationship.

RUTILE

Rutile (TiO_2) occurs as finely disseminated blebs in ilmenite associated with titanohematite at the Crenshaw and Daniels mines.

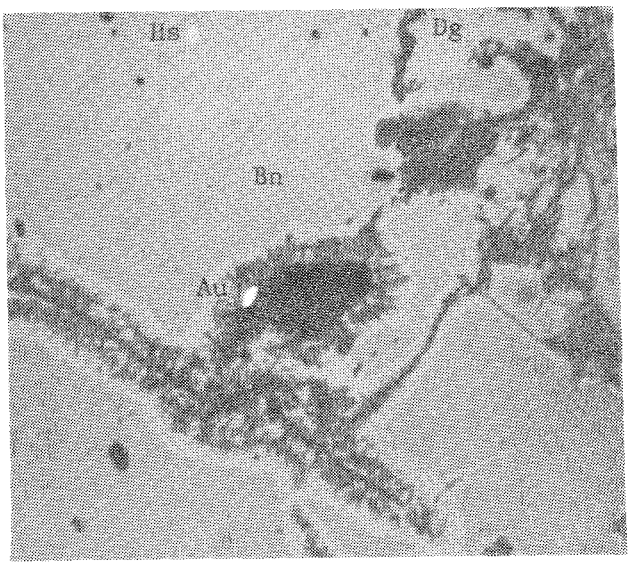

Figure 9. Gold (Au) associated with bornite (Bn), digenite (Dg), and hessite (Hs); sample 208 Daniels mine, 200X, field of view 0.52 mm.

MALACHITE

Malachite ($Cu_2(CO_3)OH)_2$) is the most common supergene mineral of the district, constituting 55 percent of the total supergene mineralization. It occurs on dump rocks as small druses in cavities, botryoidal crusts and stains and in the ore, as massive or disseminated grains, or as veinlets. Crystal size may range from less than 0.02 to 3 mm. Malachite is always associated with the other common supergene minerals cuprite and covellite. In polished section, malachite generally occurs as radiating sprays of crystals filling the interstices between partially altered relict grains of hypogene ore minerals.

COVELLITE

Covellite (CuS) makes up approximately 25 percent of the supergene ores in the Virgilina district. It occurs as alteration rims on bornite, chalcocite, djurleite, chalcopyrite, and anilite, and as masses replacing the same hypogene minerals, usually in a matrix of malachite. Microprobe analyses indicate that it usually is stoichiometric CuS; however, it may contain up to 0.5 weight percent silver. It is rarely associated with spionkopite and yarrowite.

CUPRITE

Cuprite (Cu_2O) is ubiquitous in the Virgilina district, despite the fact that it makes up only 15 percent of the supergene ores. It is usually associated with malachite and covellite, occurring in fine-grained masses. Cuprite also occurs in anastomosing and/or dendritic veinlets in bornite and chalcopyrite, with quartz, hematite, digenite, chalcocite, and djurleite.

SPIONKOPITE AND YARROWITE

Spionkopite and yarrowite ($Cu_{39}S_{28}$ /Cu_9S_8) make up less than 2 percent of the supergene mineralization but are distributed throughout the district. Both occur as small (0.008 to 0.16 mm) grains associated with covellite, malachite, and cuprite (Figure 10). Spionkopite and yarrowite resemble covellite when viewed in air; however, when viewed in oil-immersion, covellite displays a purplish-red bireflectance, whereas spionkopite and yarrowite remain blue. Hence they are referred to as "blue-remaining covellites." Microprobe analyses indicate that these blue-remaining covellites may consist of either yarrowite or a mixture of both spionkopite and yarrowite. In addition, up to 0.7 weight percent silver was detected.

Spionkopite and yarrowite apparently are derived from the supergene leaching and oxidation of copper from anilite (Goble, 1981; Whiteside and Goble, 1986). In the Virgilina district they always occur as pseudomorphs after anilite. Locally, edges of the pseudomorphs are further leached to covellite.

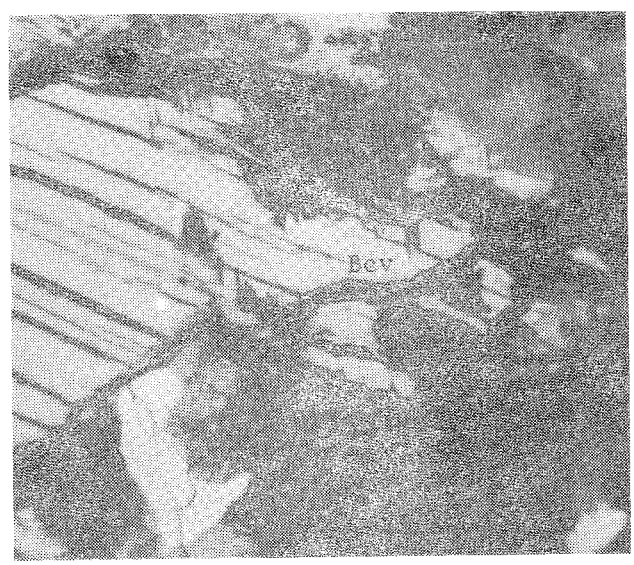

Figure 10. Spionkopite and yarrowite (Bcv) pseudomorphous after anilite, with one area altering to covellite (Cv); sample 159, Chappell mine, 100X, field of view 1.05 mm.

AZURITE

Azurite ($Cu_3(CO_3)_2(OH)_2$) is very uncommon in the Virgilina district, occurring only at the Pontiac mine. It is of

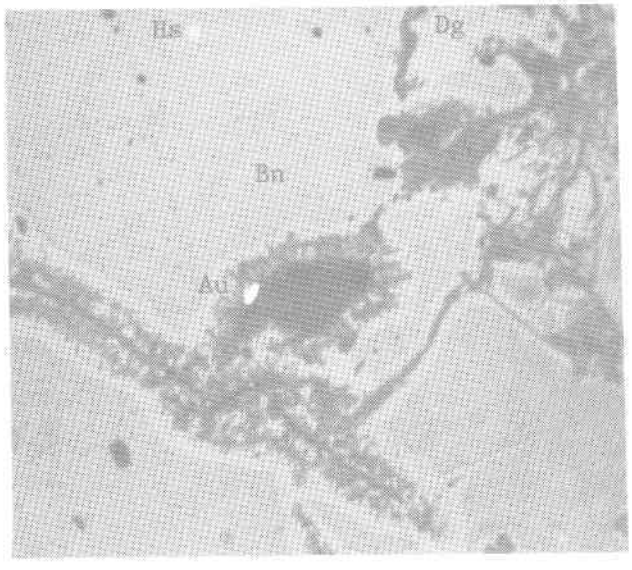

Figure 9. Gold (Au) associated with bornite (Bn), digenite (Dg), and hessite (Hs); sample 208 Daniels mine, 200X, field of view 0.52 mm.

MALACHITE

Malachite ($Cu_2(CO_3)OH)_2$) is the most common supergene mineral of the district, constituting 55 percent of the total supergene mineralization. It occurs on dump rocks as small druses in cavities, botryoidal crusts and stains and in the ore, as massive or disseminated grains, or as veinlets. Crystal size may range from less than 0.02 to 3 mm. Malachite is always associated with the other common supergene minerals cuprite and covellite. In polished section, malachite generally occurs as radiating sprays of crystals filling the interstices between partially altered relict grains of hypogene ore minerals.

COVELLITE

Covellite (CuS) makes up approximately 25 percent of the supergene ores in the Virgilina district. It occurs as alteration rims on bornite, chalcocite, djurleite, chalcopyrite, and anilite, and as masses replacing the same hypogene minerals, usually in a matrix of malachite. Microprobe analyses indicate that it usually is stoichiometric CuS; however, it may contain up to 0.5 weight percent silver. It is rarely associated with spionkopite and yarrowite.

CUPRITE

Cuprite (Cu_2O) is ubiquitous in the Virgilina district, despite the fact that it makes up only 15 percent of the supergene ores. It is usually associated with malachite and covellite, occurring in fine-grained masses. Cuprite also occurs in anastomosing and/or dendritic veinlets in bornite and chalcopyrite, with quartz, hematite, digenite, chalcocite, and djurleite.

SPIONKOPITE AND YARROWITE

Spionkopite and yarrowite ($Cu_{39}S_{28}$ /Cu_9S_8) make up less than 2 percent of the supergene mineralization but are distributed throughout the district. Both occur as small (0.008 to 0.16 mm) grains associated with covellite, malachite, and cuprite (Figure 10). Spionkopite and yarrowite resemble covellite when viewed in air; however, when viewed in oil-immersion, covellite displays a purplish-red bireflectance, whereas spionkopite and yarrowite remain blue. Hence they are referred to as "blue-remaining covellites." Microprobe analyses indicate that these blue-remaining covellites may consist of either yarrowite or a mixture of both spionkopite and yarrowite. In addition, up to 0.7 weight percent silver was detected.

Spionkopite and yarrowite apparently are derived from the supergene leaching and oxidation of copper from anilite (Goble, 1981; Whiteside and Goble, 1986). In the Virgilina district they always occur as pseudomorphs after anilite. Locally, edges of the pseudomorphs are further leached to covellite.

Figure 10. Spionkopite and yarrowite (Bcv) pseudomorphous after anilite, with one area altering to covellite (Cv); sample 159, Chappell mine, 100X, field of view 1.05 mm.

AZURITE

Azurite ($Cu_3(CO_3)_2(OH)_2$) is very uncommon in the Virgilina district, occurring only at the Pontiac mine. It is of

nealed. This assemblage is only rarely associated with titanohematite, and never with secondary hematite. The fine intergrowths of chalcopyrite and bornite, considering their appearance and associations, are likely of supergene origin

These data are interpreted to indicate that the primary ores underwent some sort of reaction subsequent to their formation. This reaction, at a temperature high enough to anneal the primary chalcopyrite, created hematite or digenite at the expense of bornite, and increased the copper-to-sulfur ratio of the remaining minerals. This increase resulted in a shift in the bulk compositions of the copper-sulfides from anilite and djurleite to chalcocite, often leaving a copper-depleted bornite. The final and most common assemblage in the Virgilina ores is therefore bornite plus chalcocite. A paragenetic diagram derived from these interpretations is given in Figure 15.

ORIGIN AND METAMORPHISM OF THE COPPER-BEARING VEINS

The copper-bearing veins of the Virgilina district are similar in many respects to the gold-bearing and barren veins of the district, as well as to other mineralized and non-mineralized veins of the Piedmont province. These veins have been attributed both to fluids derived from intrusive bodies and to metamorphic expulsions of water. Laney (1917) interpreted the veins as originating from an intrusive source and cited as evidence his observations that a significant number of the veins crosscut the regional schistosity, following preexisting fractures or faults, and that the silica and potassium feldspar content of the veins implies a more silicic source than the mafic rocks of the district. Laney also stated that insufficient copper occurs in the greenstones to

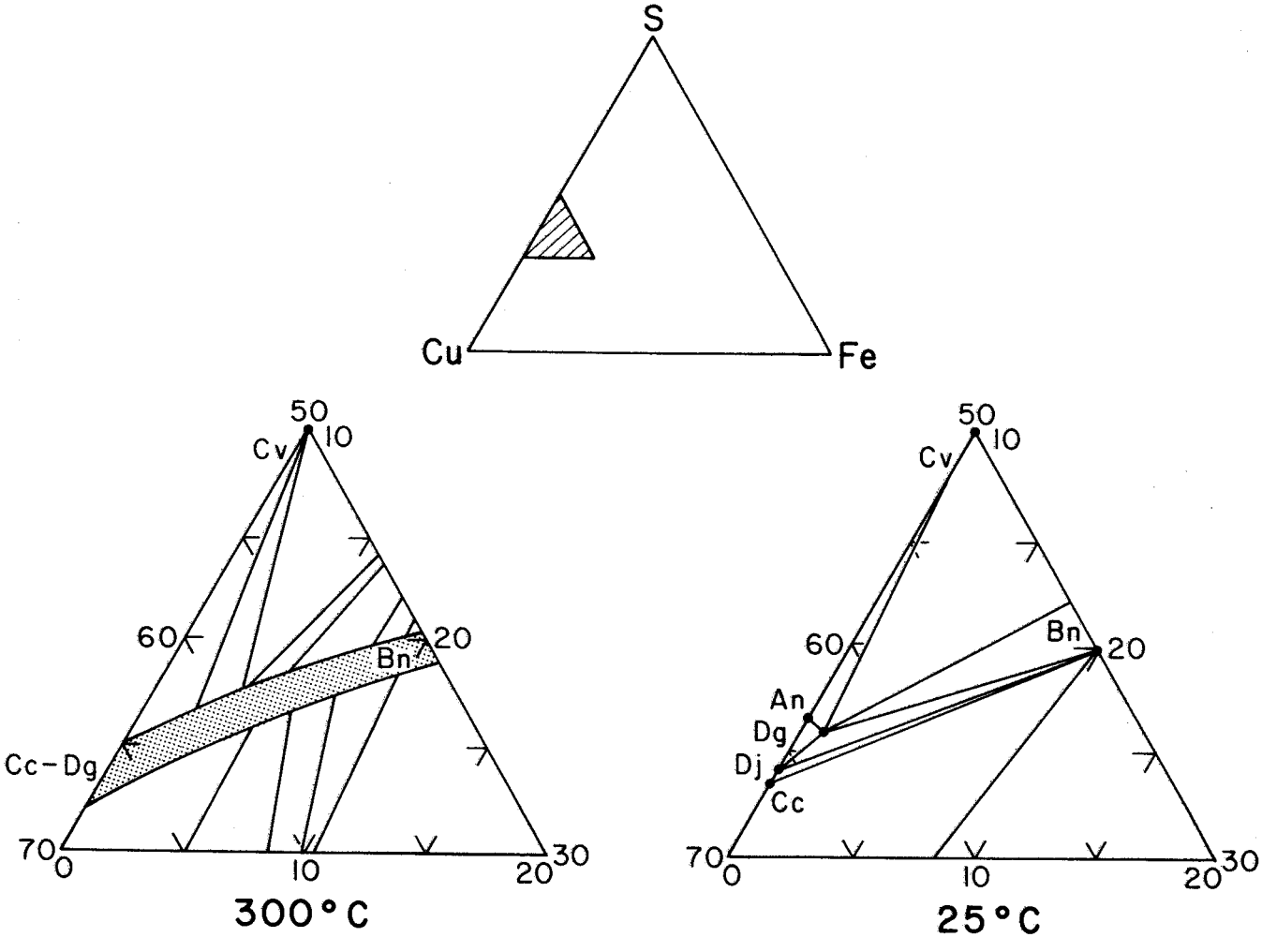

Figure 14. A secton of the Cu-Fe-S ternary diagram at 300°C and at 25°C, after Craig and Vaughn (1981); Cc-Dg = chalcocite-digenite solid solution; Bn = bornite; An = anilite; Dj = djurleite; Cv = covellite.

account for the copper in the veins. Stein and Kish (1978) argue instead for an in situ metamorphic origin, pointing out that the veins are commonly subparallel to parallel to the regional schistosity, contain few strained ore and gangue minerals, and are associated with epidosite bodies that are depleted in copper relative to nonmineralized areas.

The observations of the present study appear to contradict parts of both of these hypotheses: 1) there appears to be no direct association between any known plutons and the belt of mineralized veins; 2) strain is apparent in both ore and gangue minerals in the veins; 3) alteration zones consisting of epidotized country rock are less extensive than previously indicated; and 4) fragments of wall rock contained within the veins are often rotated so that their schistosity is no longer parallel to the regional schistosity. It has been noted (F. LeSure, personal communication) that the copper mineralization occurs in relatively mafic rocks with higher than normal nickel and chromium contents, and the gold mineralization occurs in more felsic rocks with lower nickel andchromium contents. Although the copper-mineralized veins are confined to the Virgilina Formation, it is not possible to establish a genetic relationship. Fluids traversing fractures in the Virgilina Formation apparently reacted sufficiently with the rocks to deposit large quantities of ore, whereas fluids entering the Hyco and Aaron did not.

The low solubility of quartz (Rimstidt and Barnes, 1980) and the very large volume of quartz present in the veins indicate that very large quantities of water must have flowed through the vein systems, much more than can be reasonably considered as originating solely from either an intrusive or a metamorphic source or even the two sources combined. Such quantities do not necessarily rule out contributions by intrusive or metamorphic fluids but strongly suggest the recirculation of meteoric waters as part of a convective cell.

In summary, although the fluids that produced the veins clearly came from outside the country rock in which the veins now reside, the original source of the mineralizing fluids cannot be definitively determined at this time. The presence of disoriented schistose wall rock fragments within the veins indicates that they formed after the peak of metamorphism, but the presence of deformation features such as strained ore and gangue minerals indicates that they formed before the end of deformation.

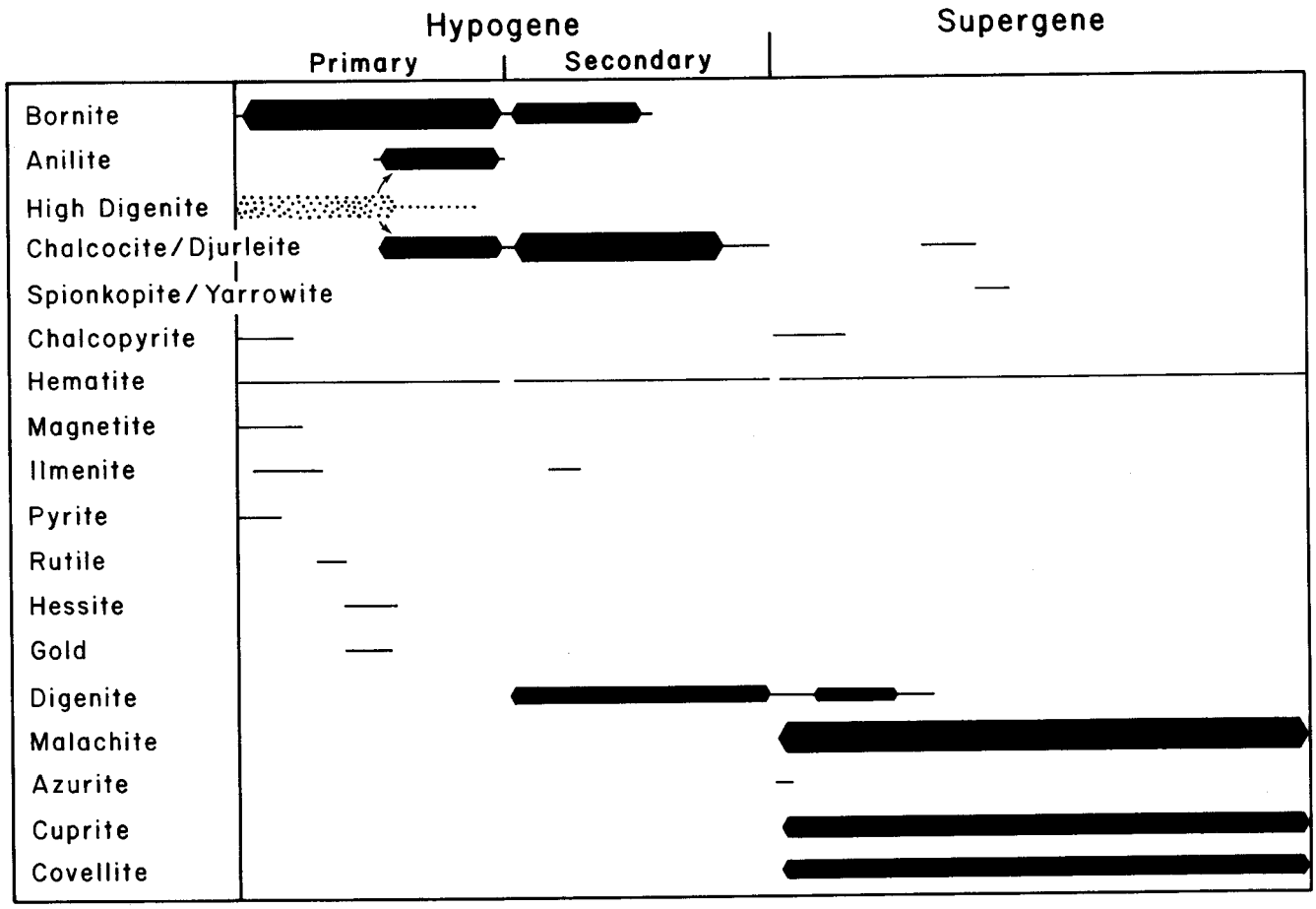

Figure 15. Paragenetic diagram showing the sequence of ore minerals in terms of hypogene (primary and secondary) and supergene development. High digenite, shown in the stippled pattern is no longer present, but its pre-existence is inferred from textural evidence and the known Cu-S phase equilibra.

ACKNOWLEDGMENTS

The authors would like to thank Frank LeSure, Palmer Sweet, and Todd Solberg for their invaluable aid in this project. Helpful comments were provided by G. V. Gibbs and P. H. Ribbe. This study was funded in part by an allotment grant from the Virginia Mining and Minerals Resource Research Institute.

REFERENCES CITED

Barton, P. B., Jr., 1973, Solid solutions in the system Cu-Fe-S. part I: the Cu-S and Cu-Fe-S joins: Economic Geology, v. 68, n. 4, p. 455-465.

Black, W. W., 1978, Chemical characteristics and Rb/Sr ages of metavolcanics from the Carolina slate belt of North Carolina (abs.): Geological Society America Abstracts with Programs, v. 10, n. 4, p. 162-163.

Briggs, D. R., Gilbert, M. C., and Glover, Lynn, III, 1978, Petrology and regional significance of the Roxboro metagranite, North Carolina: Geological Society America Bulletin, v. 8, n. 4, p. 511-521.

Brown, W. R., 1953, Structural framework and mineral resources of the Virginia piedmont, in McGrain, Preston, ed., Proceedings of the Southeast Mineral Symposium, 1950: Kentucky Geological Survey Reprint series 9, Spec. Pub 1, p. 88-111.

Evans, H. T., Jr., 1979, The crystal structures of low chalcocite and djurleite: Zeitschrift Fur Kristallographie, Band 150, p. 299-300.

Glover, Lynn, III, 1974, Speculations on the relation between eastern and western Piedmont volcanism (abs.): Geological Society America Abstracts with Programs, v. 6, n. 7, p. 757.

Glover, Lynn, III, and Sinha, A. K., 1973, The Virgilina deformation, a late Precambrian to early Cambrian (?) orogenic event in the central piedmont of Virginia and North Carolina: American Journal Science, v. 273-A, Cooper Volume, p. 234-251.

Glover, Lynn, III, Sinha, A. K., Higgins, M. W., and Kirk, W. S., 1971, U-Pb dating of Carolina slate belt and Charlotte belt rocks, Virgilina district, Virginia and North Carolina (abs.): Geological Society America Abstracts with Programs, v. 3, n. 5, p. 313.

Goble, R. J., 1981, The leaching of copper from anilite and the production of a metastable copper sulfide structure: Canadian Mineralogist, v. 19, n. 4, p. 583-591.

Harris, C. H., 1982, An unconformity in the Carolina slate belt of central North Carolina: New evidence for the areal extent of the ca. 600 Ma. Virgilina deformation [M. S. thesis]: Blacksburg, Virginia, Virginia Polytechnic Institute and State University, 90 p.

Johnson, N. E., 1983, A study of the vein copper mineralization of the Virgilina district, Virginia and North Carolina [M. S. thesis]: Blacksburg, Virginia, Virginia Polytechnic Institute and State University, 195 p.

Koto, Kichiro, and Morimoto, Nubuo, 1970, The crystal structure of anilite: Acta Crystallographica, v. B26, n. 7, p. 915-924.

Kreisa, R. D., 1980, Geology of the Omega, South Boston, Cluster Springs, and Virgilina quadrangles: Virginia Division of Mineral Resources Publication 5, 22 p.

Laney, F. B., 1911, The relation of bornite and chalcocite in the copper ores of the Virgilina district of North Carolina and Virginia: Economic Geology, v. 6, n. 2, p. 399-411.

Laney, F. B., 1917, Geology and ore deposits of the Virgilina district of Virginia and North Carolina: Virginia Geological Survey Bulletin 14, 176 p.

Legrand, H. E., 1960, Geology and groundwater resources of Pittsylvania and Halifax counties: Virginia Division of Mineral Resources Bull. 75, 86 p.

Linden, M. A., 1981, Mineralogical and chemical characteristics of gold occurrences in the Virgilina district, Halifax County, Virginia [M. S. thesis]: Blacksburg, Virginia, Virginia Polytechnic Institute and State University, 125 p.

Lindsley, D. H., 1973, Delimitization of the hematite-ilmenite miscibility gap: Geological Society America Bulletin, v. 84, p. 657-661.

Morimoto, Nubuo, and Koto, Kichiro, 1970, Phase relations of the Cu-S system at low temperatures: stability of anilite: American Mineralogist, v. 55, n. 1, p. 106-117.

Morimoto, Nubuo, Koto, Kichiro, and Shimazaki, Y., 1969, Anilite, Cu S , a new mineral: American Mineralogist, v. 54, n. 9, p. 1256-1268.

Newberry, A. W., Roos, Alford, Robertson, A. F., Dahners, L. A., and Cohen, C. J., 1948, Investigation of the Virgilina copper district, Virginia and North Carolina: U.S. Bureau of Mines, Report of Investigations 4384, 14 p.

Potter, R. W., 1977, An electrochemical investigation of the system copper-sulfur: Economic Geology, v. 72, n. 8, p. 1524-1542.

Ramdohr, Paul, 1980, The ore minerals and their intergrowths, 2nd edition: Berlin, Pergamon Press, 1207 p.

Rimstidt, J. D., and Barnes, H. L., 1980, The kinetics of silica-water reactions: Geochimica Et Cosmochimicia Acta, v. 44, n. 11, p. 1683-1699.

Stein, H. J., and Kish, S. A., 1978, The Virgilina mining district of North Carolina and Virginia - preliminary evidence for a copper deposit of metamorphic origin (abs.): Geological Society America Abstracts with Programs, v. 10, n. 4, p. 198.

Sweet, P. C., 1976, Abandoned copper mines and prospects in the Virgilina district, Virginia: Virginia Division of Mineral Resources, Virginia Minerals, v. 22, n. 3, p. 25-34.

Tobisch, O. T., and Glover, Lynn, III, 1969, Metamorphic change across part of the Carolina slate belt - Charlotte belt boundary, North Carolina and Virginia, in Geological survey research 1969: U.S. Geological Survey Professional Paper 650-C, p. C1-C7.

Tobish, O. T., and Glover, Lynn, III, 1971, Nappe formationin part of the southern Appalachian piedmont: Geological Society America Bulletin, v. 82, n. 8, p. 2209- 2230.

Uytenbogaart, W., and Burke, E. A. J., 1971, Tables for microscopic identification of ore minerals: Amsterdam, Elsevier Science Publishers, 430 p.

Watson, T. L., 1902, Copper bearing rocks of Virgilina copper district, Virginia and North Carolina: Geological Society America Bulletin, v. 13, p. 353-376.

Weed, W. H., 1911, Copper deposits of the Appalachian states: U.S. Geological Survey Bulletin 455, 166 p.

Whiteside, L. S., and Goble, R. J., 1986, Structural and compositional changes in copper sulfides during leaching and dissolution: Canadian Mineralogist v. 24, n. 2, p. 247-258.

Wright, J. E., and Seiders, V. M., 1980, Age of zircons from volcanic rocks of the central North Carolina piedmont and tectonic implications for the Carolina volcanic slate belt: Geological Society America Bulletin, v. 91, p. 287-294.

EXPLORATION FOR MAGMATIC SULFIDE DEPOSITS IN THE VIRGINIA BLUE RIDGE

Carol Walsh-Stovall[1], E. S. Robinson[2], J. D. Rimstidt[2], and R.L. Stovall[1]

CONTENTS

	Page
Abstract	17
Introduction	17
Magnetic survey	18
Geochemical survey	19
Conclusions	20
Acknowledgments	21
References cited	21

ILLUSTRATIONS

Figure
1. Location of the Lick Fork and Vest prospects 18
2. Magnetic map of the Lick Fork prospect 19
3. Magnetic map of the Vest prospect 19
4. Nickel concentrations in soils surrounding the Lick Fork prospect 20
5. Nickel concentrations in soils surrounding the Vest prospect 20

ABSTRACT

The mafic and ultramafic rocks in the Blue Ridge province of Virginia are possible hosts of nickel and cobalt mineralization that might become economic if the present supplies to the United States were cut off. Rugged terrain, dense vegetation, poor rock exposures, and unavailability of detailed maps demand that indirect exploration methods be used to locate areas of mineralization. Coincident geophysical (aeromagnetic) and geochemical (high nickel concentrations in soil) anomalies appear to be good indicators of sulfide-bearing mafic or ultramafic rocks. This concept was tested by performing magnetic and geochemical surveys at the Vest and Lick Fork prospects in Floyd County.

INTRODUCTION

The United States is currently dependent upon foreign suppliers for certain strategic materials such as chromium, platinum group metals, tungsten, cobalt, and nickel. If a political or economic event were to disrupt the supply of these materials, stockpiled reserves may be sufficient to allow for business-as-usual for several months to a few years, and emergency conservation and recycling of these materials might allow a buffer of several years in which to develop domestic supplies. Because the development of a mine often requires more than ten years and is rarely accomplished in less than five years, the successful transition from foreign to domestic supplies of a critical mineral requires the mobilization of an exploration program that can assess the mineral potential of vast tracts of land very rapidly. This paper suggests a strategy for such an exploration program based upon screening aeromagnetic anomalies to find those associated with high nickel content in the overlying soils. This strategy could be used to locate magmatic sulfide deposits, which often contain nickel and cobalt minerals and are often associated with deposits of platinum-group elements and with chromium deposits.

There are numerous ultramafic-mafic intrusions in the Blue Ridge province of Virginia (Scotford and Williams, 1983) that might contain strategic minerals. The Blue Ridge terrain is rugged, the vegetation is dense, and the rocks are, in general, poorly exposed. In addition, the geology is complex and detailed maps of sufficient quality to guide mineral exploration are not available for many areas. This means that an exploration program must depend upon indirect geophysical and geochemical clues to locate prospects.

Two nickel-bearing prospects, the Lick Fork and the Vest, in the vicinity of Check, Virginia are used here to illustrate the proposed exploration concept. At each of these prospects (Figure 1), iron-nickel-cobalt sulfides and iron-

1. Conoco, Inc., Ponca City, Oklahoma 74601
2. Department of Geological Sciences, Virginia Polytechnic Institute and State University, Blacksburg, VA 24061

titanium oxides occur in ultramafic or altered ultramafic bodies. These bodies are contained in the deformed granitic gneisses on the north side of the Fries fault zone in Floyd County, Virginia. The rocks that contain this mineralization were probably a part of a larger sulfide-bearing mafic body that was dissected by the fault so that they now appear as small slices within the highly sheared rocks adjacent to the Fries fault. Fluids moving through the sheared rocks penetrated and altered these mafic bodies. The sulfides at the Lick Fork prospect have been partly oxidized, converting primary pentlandite to secondary violarite. Craig and Higgins (1975) examined the violaritic specimens from the Lick Fork prospect and found that they contain up to 43 weight percent iron and up to 9.7 weight percent cobalt. The sulfide assemblage at Lick Fork now consists of: pyrrhotite (hexagonal and monoclinic), pentlandite, violarite, chalcopyrite, pyrite, ilmenite, and magnetite. The mafic body is described by Watson (1907a, b) as gabbro to pyroxene syenite enclosed in a medium-grained leucocratic gneiss. The mafic body at the Vest prospect has undergone complete retrograde metamorphism to a green-gray, chlorite-tremolite schist enclosed in a quartz-biotite gneiss. Weathering has destroyed the sulfide minerals in samples accessible at the surface; however, Luttrell (1966) reports that the rocks in this altered mafic body contain nickel, gold, arsenic, and traces of cobalt which suggests that the original sulfide assemblage was probably quite similar to that at the Lick Fork prospect.

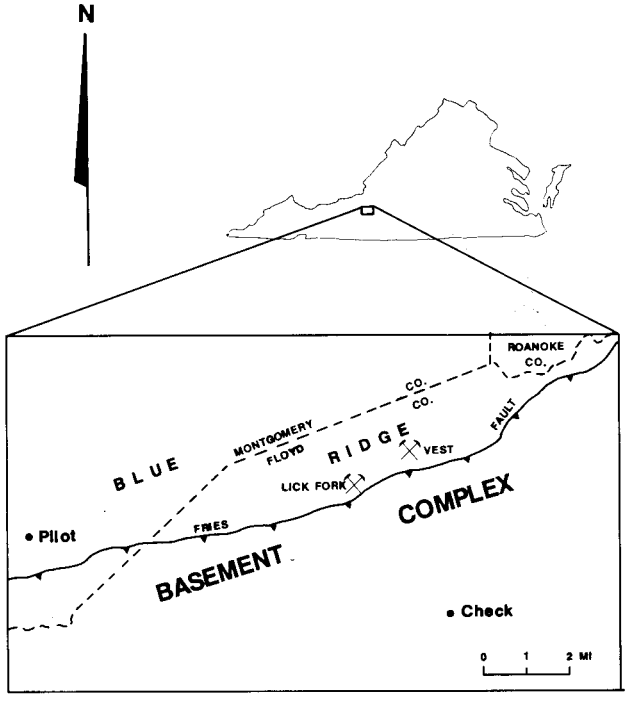

Figure 1. Location of the Lick Fork and Vest prospects, Floyd County, Virginia.

The Lick Fork prospect is located along Lick Fork 330 m southeast of the confluence of Lick Fork and Flat Run creeks (Check 7.5-minute quadrangle). The prospect was worked before the Civil War and subsequently changed owners several times with some promotional work during each period of ownership. The workings consist of an exposed face about 20 feet long and test pits and dump piles in the immediate area.

The Vest prospect is located approximately 1.45 km west of State Road 653 on State Road 657, 548 m northwest of the Willis Store (Check 7.5-minute quadrangle). The prospect was first worked in 1924 when a 5-m vertical shaft and a 23-m adit were opened (Grosh, 1949). The property was later leased to C. H. Thompson and in 1936 four churn-drill drill holes were put down. In January 1944, the U. S. Bureau of Mines sponsored the drilling of two holes, totaling 97.5 m. Two test pits approximately 30 m east of the original shaft location and a flowing test well are all that remain of these workings. There is no record of production from this prospect.

MAGNETIC SURVEY

The minerals pentlandite, magnetite, and monoclinic pyrrhotite show significant magnetism. The common association of these minerals with mafic rocks that contain magmatic sulfides suggests they should produce a recognizable magnetic anomaly. Detailed, local, ground magnetic surveys were carried out at the Lick Fork and Vest sites to determine the intensity and nature of their associated magnetic fields. The Lick Fork survey (Figure 2) revealed three anomalies lying along a trend of N24°E, with approximate total intensity amplitudes of 450 gammas, 250 gammas, and 150 gammas. Comparison with stimulated fields calculated for anomaly source models shows that these anomalies could be produced by pyrrhotite concentrations of 2.9 percent, 1.5 percent, and 0.7 percent, in tabular zones approximate 12 m long by 12 m wide by 6 m thick. This analysis suggests a total pyrrhotite mass of about 230 metric tons.

The magnetic map of the Vest prospect showed two magnetic anomalies (Figure 3). The largest has an approximate diameter of 70 m and a total intensity amplitude of 150 gammas. It could be produced by a pyrrhotite concentration of 31 percent in a zone 40 m long by 23 m wide by 15 m thick. The smaller anomaly with a diameter of about 12 m and a total intensity amplitude of 200 gammas could be produced by a 31 percent concentration of pyrrhotite in a zone 9 m long by 3 m wide by 3 m thick. This analysis suggests a total pyrrhotite mass of 2150 metric tons for both anomalies. The total nickel plus cobalt sulfide mineralization in these bodies is unlikely to exceed the total pyrrhotite content. It is important to note that a measurable magnetic anomaly accompanies the rocks of the highly altered Vest prospect. This shows that even though this body has undergone extensive retrograde meta-

morphism, it can still be identified by a magnetic survey.

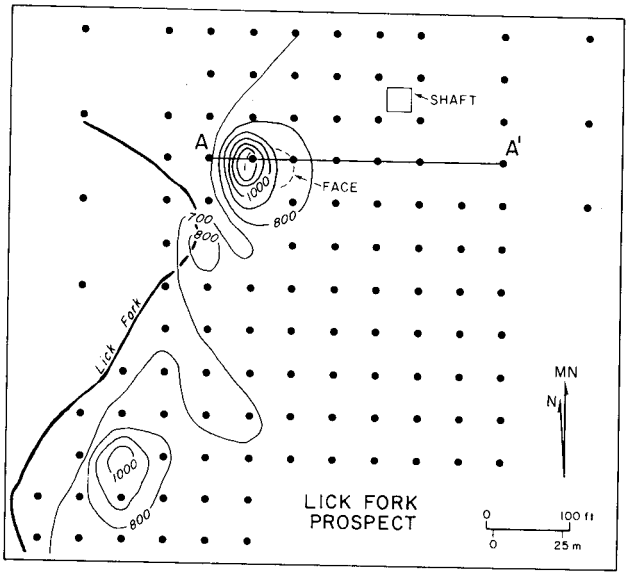

Figure 2. Magnetic map of the Lick Fork prospect, contour interval 100 gammas; data from proton-precession magnetometer, measurements at locations indicated by dots; a constant value of 54,000 gammas was subtracted from the total field intensity measurements to obtain the contoured values. Soil samples for the geochemical analyses collected at the grid points along A-A'.

Perusal of the 1:62,500-scale aeromagnetic maps, prepared by the Virginia Division of Mineral Resources, shows many magnetic anomalies scattered throughout the Blue Ridge province. Most of these are related to magnetite-rich rocks that contain no significant sulfide mineralization whereas a few may represent economic magmatic sulfide mineralization. Clearly it is not practical to investigate each of these anomalies. Simulated magnetic fields calculated for tabular source models show that mineralized bodies similar in composition to the Lick Fork and Vest prospects must be larger than 9.1 metric tons in order to produce a recognizable anomaly on 1:62,500-scale aeromagnetic maps. The minimum tonnage of ore that would be economic can be used to model the amplitude and size of the anomaly; smaller anomalies do not warrant further investigation. Larger anomalies in areas where detailed mapping shows no sulfide-bearing mafic or altered mafic rocks can also be eliminated. The remaining anomalies require on-site investigation beginning with the largest and/or most accessible.

GEOCHEMICAL SURVEY

Sulfide minerals oxidize rapidly in the weathering environment so that finding significant sulfide mineralization in Blue Ridge rocks by a ground survey is very unlikely.

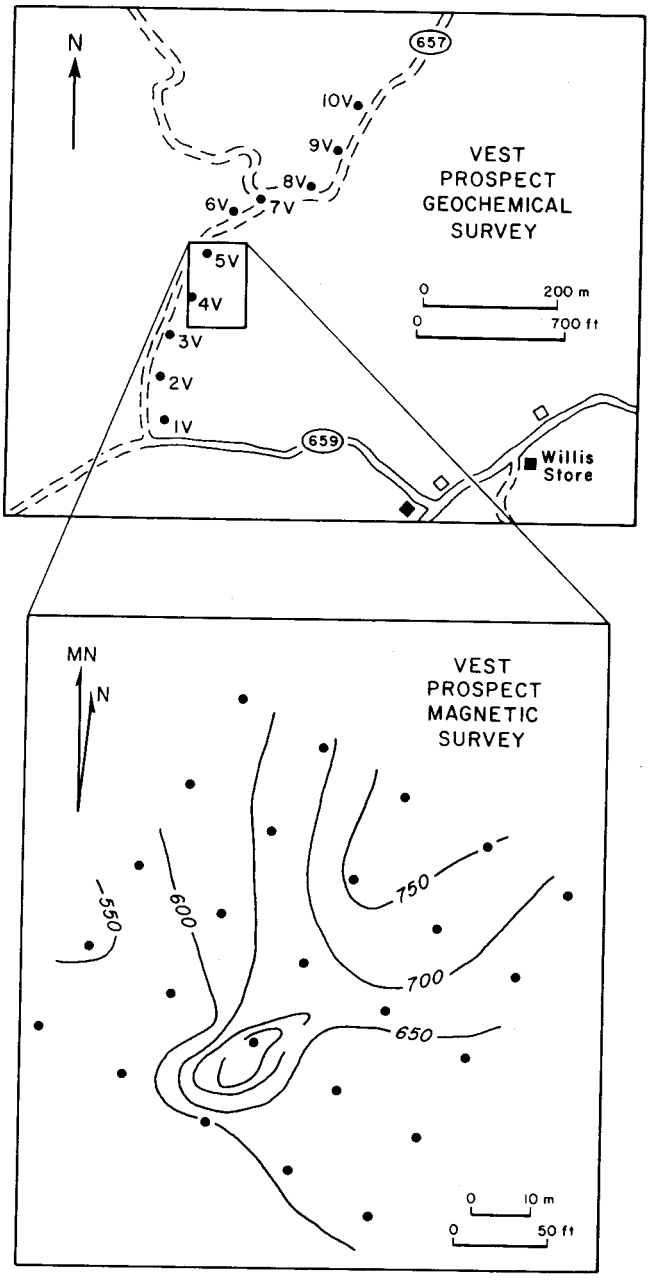

Figure 3. Magnetic map of the Vest prospect, contour interval 50 gammas; data from proton-precession magnetometer, measurements at locations indicated by dots; a constant value of 54,000 gammas was subtracted from the total field intensity measurements to obtain the contoured values. Sample sites for the geochemical survey indicated by Vs.

The most effective method to identify mineralized areas is to look for residual elements from the weathered sulfide minerals in the soil. Nickel is an ideal candidate for such a soil geochemical survey because it is extremely immobile in the weathering environment. It is easily incorporated by iron oxy-hydroxides that are formed by the oxidation of the iron

minerals in the mafic body (Rose and others, 1979). The nickel-bearing oxy-hydroxides that accumulate in the soil horizon can be broken down in a molten potassium pyrosulfate flux to produce a water soluble complex that can be detected colorimetrically (Ward and others, 1963).

Geochemical surveys were performed at the Lick Fork and Vest prospects. Samples from the B-horizon soil were collected at both sites; at the Lick Fork prospect the samples (1LF through 7LF) were collected at the magnetic survey grid points along section A-A' (Figure 2) and at the Vest prospect the samples (1V to 10V) were collected at 200-foot intervals along State Road 657 (Figure 3). In addition, at each sample location at the Vest prospect samples of sediment and water were collected from a small stream that parallels State Road 657. The soil and sediment samples from this survey were digested in molten potassium pyrosulfate; the cooled mixtures were dissolved in a 2 M HCl solution; and the nickel was reacted with -furildoxime (Ward and others, 1963). The nickel complex was extracted into benzene layers whose optical densities at 350 mm were determined using a Bausch and Lomb Spectronic 21 spectrophotometer.

The soil-sample analyses from both prospects show distinct nickel anomalies with values ranging up to 1000 ppm at the Lick Fork prospect (Figure 4) and values up to 425 ppm at the Vest prospect (Figure 5). Samples located away from the magnetic anomalies (1V, 2V, 8V, 9V, and 10V) show relatively low nickel values; these are probably near background levels (around 25 ppm). Stream sediment samples collected at the Vest prospect show nickel concentrations of 25 ppm or less and the associated water samples all contained less than 0.25 ppm nickel. This indicates that the nickel released by weathering at these sites is very immobile and flowing water is unlikely to disperse it to create a false anomaly at a distance from the mineralized rock. This pattern, consistent with observations in other areas (Nriagu, 1980), suggests that this simple method of determining the nickel content of grab samples of B-horizon soils from areas that show magnetic anomalies can be used to identify quickly areas that deserve a more thorough geologic investigation.

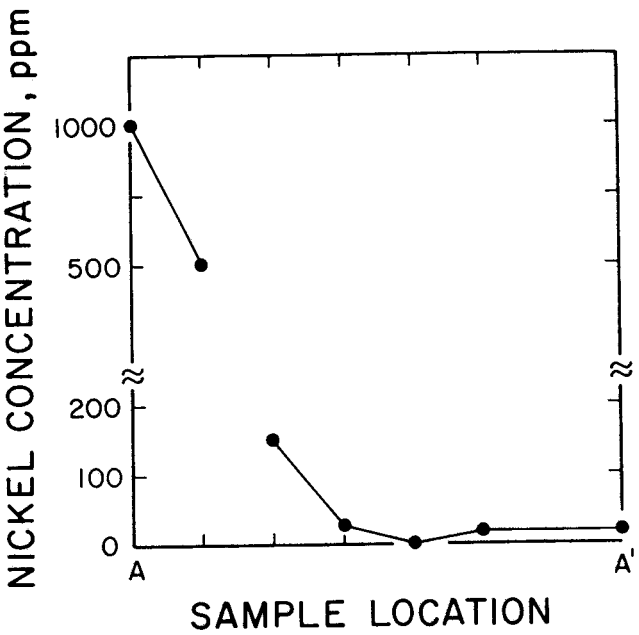

Figure 4. Nickel concentrations in soils surrounding the Lick Fork prospect; see Figure 2 for the sample locations.

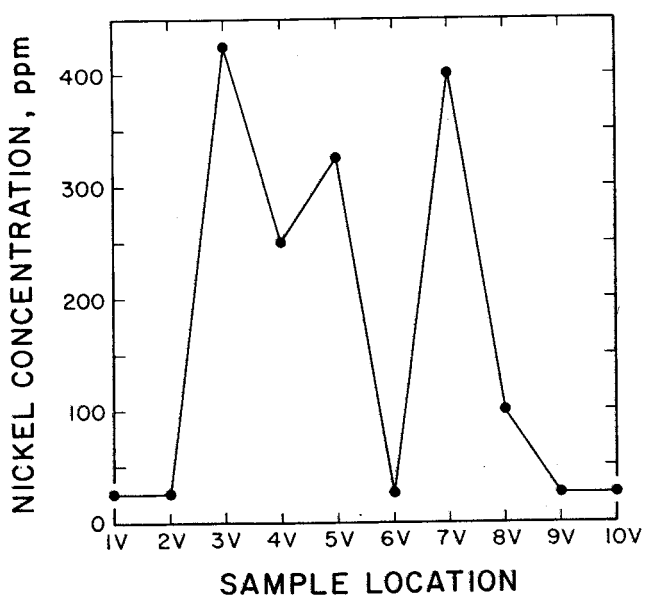

Figure 5. Nickel concentrations in soils surrounding the Vest prospect; see Figure 3 for the sample locations.

CONCLUSIONS

In the event that a political or economic situation cuts off supplies of critical materials such as nickel or cobalt, the exploration approach described offers an effective and rapid method to explore for magmatic sulfide deposits of economic size. This approach involves four steps. 1) Search 1:62,500-scale aeromagnetic maps for prospective anomalies that might be caused by a pyrrhotite-rich magmatic sulfide body large enough to be economic. 2) Screen the selected anomalies to eliminate those that are caused by known nonmineralized lithologies. This will require a careful study of existing geologic maps to identify units that are rich in magnetite but not in sulfide. 3) Visit, in the order of most accessible to least accessible and/or largest to smallest, each of these anomalies and obtain a sample of the B-horizon soil for the determination of nickel values following the described procedure. Samples from nonmineralized areas must also be taken to determine background levels. 4) Carefully scrutinize areas showing both a large magnetic anomaly and high nickel concentrations in the soil. Shallow drilling at these sites may be required to locate enough unweathered rock to determine if significant mineralization exists.

ACKNOWLEDGMENTS

We appreciate John Wonderly's help with the magnetic surveying. M. J. Bartholomew contributed to the geologic interpretation. Sharon Chaing drafted the figures. This report benefited from reviews by R. S. Good and N. H. Evans. Financial support was provided by the Virginia Mining and Mineral Resources Institute and the Virginia Division of Mineral Resources. Computing was done by the Virginia Tech Computing Center.

REFERENCES CITED

Craig, J. R., and Higgins, J. B., 1975, Cobalt- and iron-rich violarites from Virginia: American Mineralogist, v. 60, p. 35-38.

Grosh, W. A., 1949, Investigation of Vest nickel prospect, Floyd County, Virginia: U. S. Bureau of Mines Report of Investigations, 4491, 4 p.

Luttrell, G. W., 1966, Base- and precious-metal and related ore deposits of Virginia: Virginia Division of Mineral Resources Mineral Resources Report 7, 167 p.

Nriagu, J. O., ed., 1980, Nickel in three environments: New York, Wiley Interscience, 833 p.

Rose, A. W., Hawkes, H. E., and Webb, J. S., 1979, Geochemistry in mineral exploration, 2nd edition: New York, Academic Press, 657 p.

Scotford, D. M., and Williams, J. R., 1983, Petrology and geochemistry of metamorphosed ultramafic bodies in a portion of the Blue Ridge of North Carolina and Virginia: American Mineralogist, v. 68, p. 78-94.

Ward, F. N., Lakin, H. W., Canney, F. C., and others, 1963, Analytical methods used in geochemical exploration by the U. S. Geological: U. S. Geological Survey Bulletin 1152, 100 p.

Watson, T. L., 1907a, Mineral resources of Virginia: Lynchburg, Virginia,J. P. Bell and Co., 681 p.

Watson, T. L., 1907b, The occurrence of nickel in Virginia: American Institute of Mining Engineering Bulletin 17, p. 829-843.

MINERALOGY AND GEOCHEMISTRY OF THE LEAD-ZINC ORES OF THE AUSTINVILLE-IVANHOE DISTRICT, WYTHE COUNTY, VIRGINIA

Nora K. Foley[1], and James R. Craig[2]

CONTENTS

	Page
Abstract	24
Introduction	24
Mining history	24
Geological setting and previous studies	24
Ore textures	27
Mineralogy and paragenesis	27
Sphalerite stratigraphy	30
Environment of ore deposition	31
Discussion: Comparison of the Austinville-Ivanhoe district with other carbonated-hosted lead-zinc deposits	35
References cited	38

ILLUSTRATIONS

1. Aerial view of the Austinville-Ivanhoe mine, Wythe County, southwestern Virginia 24
2. Sketch map of the ore bodies and major faults of the Austinville-Ivanhoe district, Virginia 25
3. Geologic map of the Austinville-Ivanhoe district 25
4. Stratigraphic cross section, Austinville area 26
5. Sphalerite showing initial multiple hemispheroidal centers 27
6. General paragenetic sequence for the sulfides of the Austinville-Ivanhoe district 28
7. Variations in paragenesis associated with the three major fault blocks 29
8. Sphalerite zones identified in the mineralization sequence 30
9. Plot of iron and cadmium content in banded sphalerite 31
10. Microprobe traverse across banded sphalerite 32
11. Stratigraphic correlation of sphalerite banding within the Fisher Field area 33
12. Stratigraphic correlation of sphalerite banding between the Fisher Field area, the Brown ore body, and the 100 ore body 34
13. Two-phase inclusions in sphalerite crystal 35
14. Histogram of fluid inclusion temperatures 35
15. Stability fields of ore deposition 37
16. Stability fields of mineralization for the three periods of ore deposition 38
17. Isotopic composition of lead from Mississippi Valley-type deposits 38

TABLE

1. Comparison of the Austinville-Ivanhoe district with other carbonate-hosted lead-zinc deposits 36

1. Present address: U.S. Geological Survey, 959 National Center, Reston, Va 22092
2. Department of Geological Sciences, Virginia Polytechnic Institute and State University, Blacksburg, VA 24061

ABSTRACT

The Austinville-Ivanhoe mine is the most continuously mined base-metal deposit in North America. The ore bodies of the district are contained within a 400-meter stratigraphic interval of the Patterson and Austinville members of the Cambrian-age Shady Formation. Individual ore bodies are crudely lens-shaped and are situated on the flanks of the Austinville anticline. Sphalerite, pyrite, galena, marcasite, and minor chalcopyrite were deposited during three periods of mineralization separated by intervals of sulfide dissolution and dolomite deposition. The minerals occur as disseminated dolomite replacements and as crustiform coatings along fractures in and around breccia fragments. The banded sphalerite has a consistent pattern which may be correlated for over 2.7 km across the district. Iron contents of the delicately banded sphalerite range from 0.3 to 3.3 weight percent and appear to be inversely correlated with cadmium contents (0.0 to 0.3 weight percent). The color of the bands is probably not related to variations in iron content but may reflect the presence of inclusion-rich zones. Geothermometry measurements of fluid inclusions in sphalerite from the middle and late periods of mineralization indicate that the ores formed in the temperature range of 100° C to 160° C. Galena from the three generations have progressively high $^{208}Pb/^{204}Pb$, $^{207}Pb/^{204}Pb$, and $^{206}Pb/^{204}Pb$ values. In addition, the smaller ore bodies have a wider range in lead values and seem to be more radiogenic than larger bodies.

INTRODUCTION

The Austinville-Ivanhoe district (Figure 1) is located 2 km north of the Wythe-Carroll county line in southwestern Virginia and extends northeastward for over 11 km, roughly paralleling the New River (Figure 2). The elongated lenses make up one of the few major base-metal sulfide districts situated in sedimentary rocks of Cambrian age in the eastern United States and constitute the only recently active base-metal mine in the Appalachians between Tennessee and Pennsylvania. The highly mineralized sphalerite-, galena-, and pyrite-bearing bodies are crudely pencil-shaped with lenticular cross sections and range from tens to hundreds of meters in length.

MINING HISTORY

Mining operations began at Austinville in 1756 with the application of surface and shallow underground techniques. Over 21,000 tons of lead ore were extracted during a period of mining which lasted until the 1860s. Iron was mined near Austinville from surficial goethite and limonite during the years ranging from 1800 to the early 1900s and this contributed to Virginia's moderately high position in the

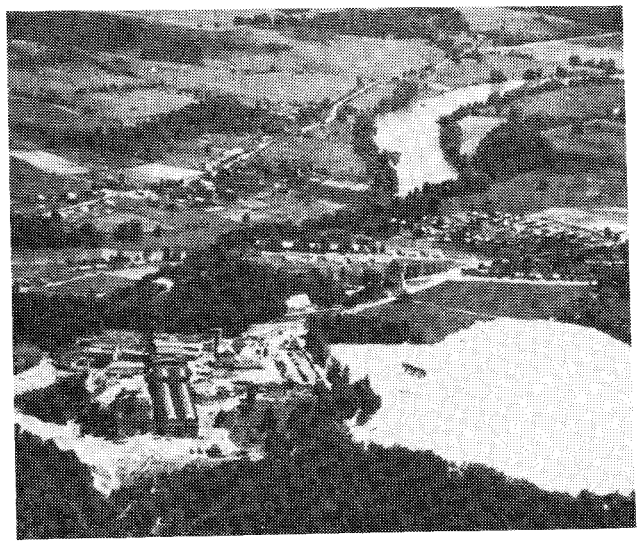

Figure 1. Aerial view of the Austinville-Ivanhoe mine, Wythe County, Virginia, from Weinberg (1971).

19th century pig-iron production (Weinberg, 1971). The mining of zinc from oxidized ores (mainly hemimorphite) was initiated during the post-Civil War years and lasted until 1902 when The New Jersey Zinc Company purchased the mine for its zinc oxide potential. During the next quarter century, the company developed reserves of sulfide ore and, after the perfection of the flotation process in the early 1920s, a separation plant was built and put into production. During 230 years, over 1,000,000 tons of zinc metal and 200,000 tons of lead metal were extracted from more than 30,000,000 tons of ore mined at Austinville. In the recent past, approximately 500,000 tons of ore averaging 3 percent zinc and 0.4 percent lead were mined each year using modified open stope methods (Weinberg, 1980). The residual dolomite gangue was crushed and sold as agricultural dolomitic limestone. The mine ceased operation in December 1981 and was allowed to flood.

GEOLOGICAL SETTING AND PREVIOUS STUDIES

The Austinville-Ivanhoe deposit is situated near the southeast margin of the folded and faulted Valley and Ridge province (Figure 3). The basal stratigraphic sequence consists of Precambrian basement rocks nonconformably overlain by the Chilhowie Group of Early Cambrian age. The uppermost formation in the Chilhowie Group, the Erwin Formation, is gradationally overlain by the Early to Middle Cambrian Shady Dolomite. The Early to Middle Cambrian Rome Formation overlies the Shady and is overlain by the Early to Middle Cambrian Elbrook Formation (Butts, 1940; Cooper and others, 1961).

The Shady Formation, the ore host, is approximately 640 meters thick in the Austinville area, where it has

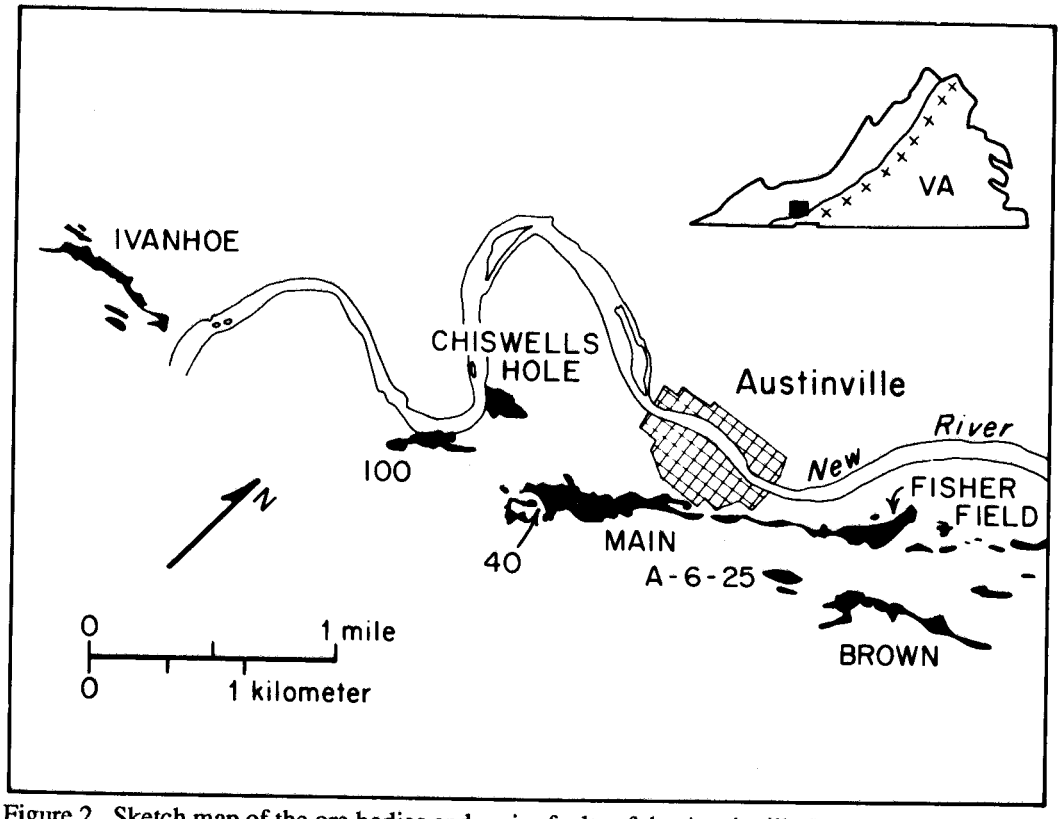

Figure 2. Sketch map of the ore bodies and major faults of the Austinville-Ivanhoe district, Virginia, modified from Brown and Weinberg (1967); inset map shows the location of the district at the southeast edge of the Valley and Ridge province, marked by solid line.

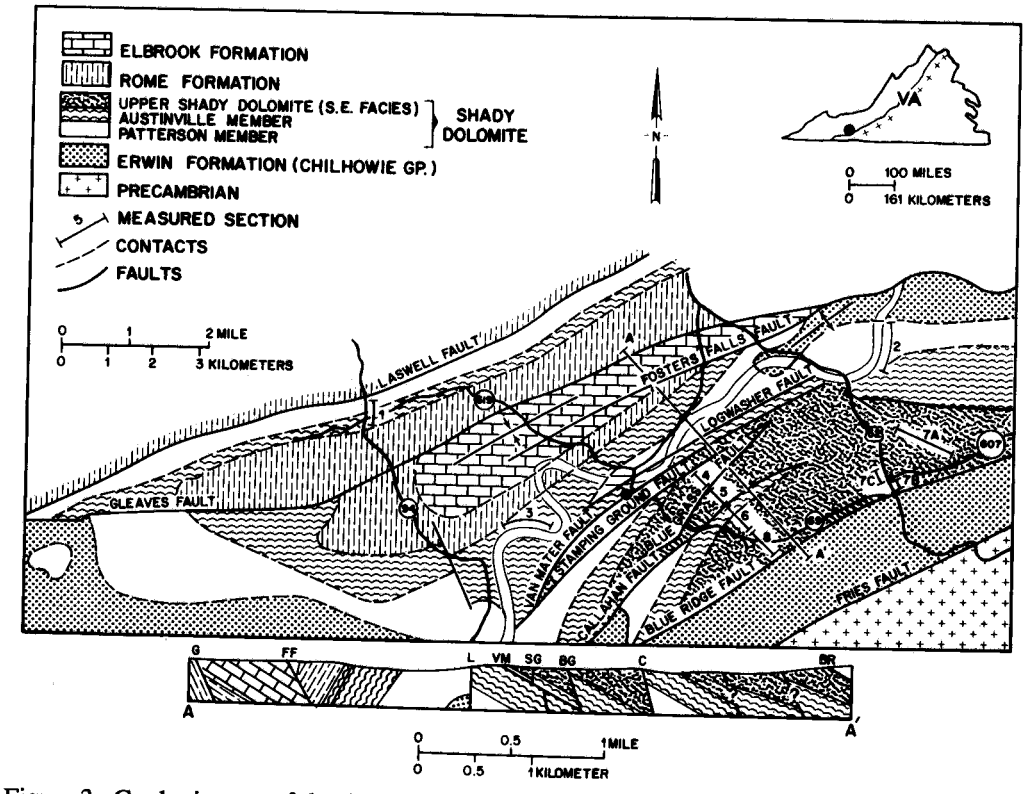

Figure 3. Geologic map of the Austinville-Ivanhoe area after Pheil and Read (1980); numbers refer to sections measured by Pheil and Read.

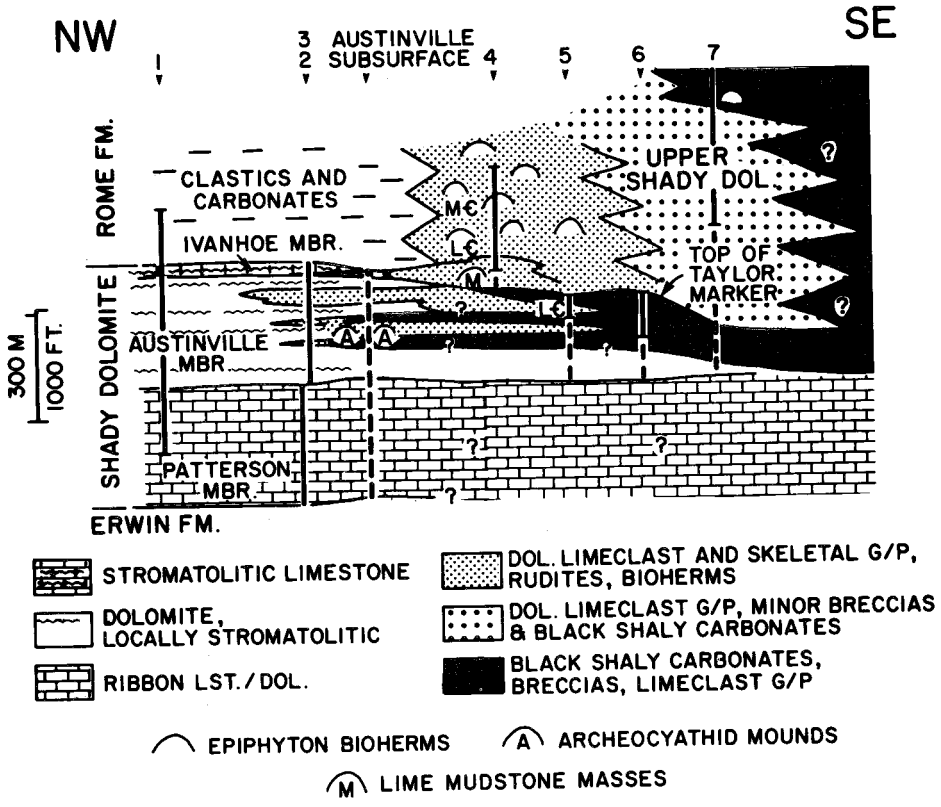

Figure 4. Stratigraphic cross section, Austinville area (Pheil and Read, 1980).

three conformable members (Figure 4). The Patterson member is a 300 meter thick sequence of ribbon-laminated limestones and dolomites. The Austinville member consists of a 300 meter thick section of stromatolitic and massive dolomite that has minor quartzose grainstones and, in the subsurface, archeocyathid mounds and black shaly carbonate tongues (Figure 4). The Ivanhoe member consists of a thick-bedded stromatolitic limestone with minor dolomite and shale and is up to 43 meters in thickness (Pfeil and Read, 1980). Southeast of Austinville, the Patterson does not crop out and the Austinville equivalent consists of black shaly carbonates, breccias and skeletal and limeclast sands. The mineralized zones lie within a 400-meter stratigraphic interval that straddles the contact between the Patterson and Austinville members of the Shady Formation. Pfeil and Read (1980) have suggested that the Austinville region represents a Cambrian platform to platform margin, foreslope and slope facies transition.

The ore bodies are situated on the northwest and southeast flanks of the Austinville anticline (Weinberg, 1971). The mining district is cut by two high-angle faults, the Logwasher and the Stamping Ground. These faults separate but do not intersect the ore bodies (Figure 2). The Van Mater fault is subparallel to bedding and cuts the Stamping Ground (Figure 3). Displacement on these faults is apparently on the order of 200 to 400 meters. Numerous cross faults with minor displacement are present throughout the area. These commonly display reverse sense of movement and locally cut the ore bodies.

The age of the mineralization in the Austinville-Ivanhoe District is not known. The Cambrian carbonate rocks that host the ore contain many breccias that are similar to those seen in the Ordovician carbonate rocks in the East Tennessee zinc district. Breccias of the East Tennessee district are attributed to collapse following extensive karst development in late Early Ordovician time. East Tennessee zinc ores have generally been considered to be late Early Ordovician to early Middle Ordovician in age because of absence of mineralization in the overlying Middle Ordovician limestones. More recently, Kyle (1976), Gorody (1980) and Grover (1981) suggested that the age of much Zn-Pb mineralization in the Appalachians may be as late as Mississippian, on the basis of the occurrence of minor zinc mineralization which cuts Mississippian beds in central Tennessee, and studies of carbonate cements.

The earliest mineralogic work on the Austinville-Ivanhoe deposit was published in 1907 by Thomas L. Watson in his treatise on the mineral deposits of Virginia (Watson, 1907). This was followed by a study of the ore zoning (Brown, 1935). Subsequently, Brown and Weinberg (1967) and Weinberg (1971, 1980) described the general geologic setting, the textures and mineralogy of the ores, and presented mine statistics.

ORE TEXTURES

The ore minerals occur within a 400-meter stratigraphic interval defined by marker beds in the Austinville and Patterson members of the Shady Formation. Samples were collected only from the high-grade ore lenses. These ore bodies are separated from each other by faults and areas of sub-economic mineralization. In the vicinity of the ore bodies, the dolomite is ribbon-laminated and stromatolitic. The ores occur as ribbon and disseminated replacements and as open-space fillings.

Ribbon and disseminated sphalerite replacements occur within shaly carbonate layers in both ribbon-laminated and stromatolitic dolomites. Selective replacement is the primary mode of ore mineralization. Ribbon and disseminated replacements of dolomite by sphalerite, galena and pyrite are usually accompanied by total recrystallization of the surrounding dolomite. In many parts of the deposit two generations of replacement ore are present, in others only one generation exists. Typically, the first generation of sulfides is present as a thin horizon within the replaced dolomite. Evidence in thin section suggests that early sulfide mineralization was replaced extensively by dolomite associated with the later sulfides. Rarely, small (<5 mm) vugs were left unfilled in the centers of partially replaced ribbon-laminated layers. Coarse-grained dolomite and euhedral quartz crystals line the sides of these vugs.

The open-space-filling ore consists of symmetrically and asymmetrically banded coatings and rosettes on brecciated dolomite fragments (Figure 5). The fine-grained dolomite blocks range in size from a few millimeters to tens of meters, but most are less than 10 to 20 centimeters in their long dimension. Polycrystalline aggregates of pyrite, admixed with minor marcasite and galena, encrust the dolomite fragments. The pyrite and overlying sphalerite grew outward radially from centers on the underlying material; succeeding crystals coalesced to form continuous layers (Figure 5). Three generations of crustiform pyrite, sphalerite, and galena exist in the open-space-filling ore. During the hiatuses that separate the generations, the earlier galena and sphalerite were replaced by dolomite. Low-grade metamorphism and deformation have resulted in minor recrystallization and microfaulting of all generations of ore minerals. Textural evidence suggests that replacement mineralization occurred prior to, or concurrently with, crustiform ore mineralization.

MINERALOGY AND PARAGENESIS

The mineralized zones of the Austinville-Ivanhoe deposit contain sphalerite, galena, pyrite, and traces of marcasite and chalcopyrite intergrown with at least three generations of dolomite gangue; minor amounts of quartz, fluorite, barite, gypsum, anhydrite, and calcite also are present. Alteration minerals occur in near-surface parts of the ore lenses

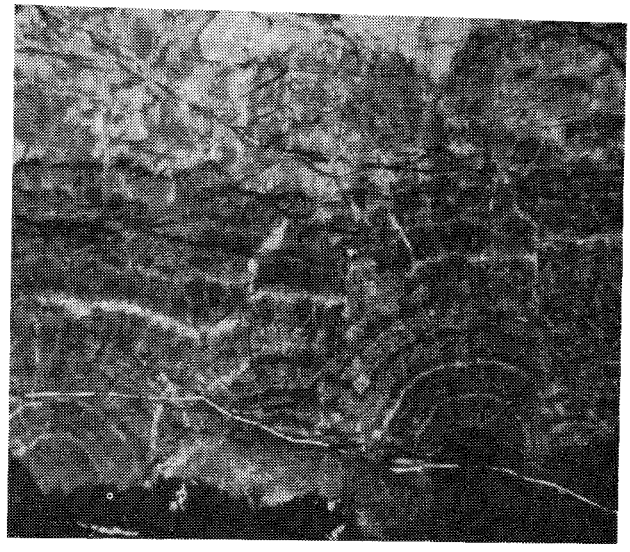

Figure 5. Sphalerite showing initial multiple hemispheroidal centers on underlying pyrite (lower part of photograph); later crystals coalesced to form continuous layers (upper part of photograph); field of view 1.1 cm.

and, locally, at depth near faults; these include smithsonite, cerussite, anglesite, iron-oxides, hydrozincite, plumbo-aragonite and hemimorphite (Watson, 1907; Weinburg, 1971).

Sphalerite is the most abundant of the primary ore minerals, followed by pyrite, galena, marcasite, and chalcopyrite. Pyrite and marcasite comprise less than five percent of the total sulfide content, although they are very abundant locally, as in the Pyrite ore body. The paragenetic sequence of the primary hydrothermal minerals is illustrated in Figure 6. The order of mineral deposition appears to be uniform throughout the district except for minor variations in the late stages of sulfide mineralization and in the local appearance of chalcopyrite as intergrowths in early sphalerite. Chalcopyrite has been identified as epitaxial intergrowths in early sphalerite in the Ivanhoe, Brown, and A-6-25 ore lenses. Figure 7 demonstrates the variations in paragenesis which occur in three major fault-bounded areas: the Brown ore body, the 40 ore body-Fisher Field area, and the Ivanhoe lens.

The depositional sequence consists of two major periods of mineralization, separated by a hiatus during which sulfides were dissolved and dolomite was deposited locally. During the first interval of sulfide deposition, pyrite containing minor marcasite and interstitial galena was deposited on brecciated dolomite fragments. Crystallization of sphalerite followed with minor chalcopyrite and galena. The second interval of mineralization mimics the first, except that simultaneous deposition of galena and sphalerite is more common and chalcopyrite is absent. Late-stage mineralization consisted of sphalerite, fluorite, quartz, barite, gypsum, and anhydrite.

Pyrite, the first sulfide mineral to form, is ubiquitous. It occurs as polycrystalline, crustiform overgrowths 100 microns to 3 mm in thickness on dolomite fragments, as

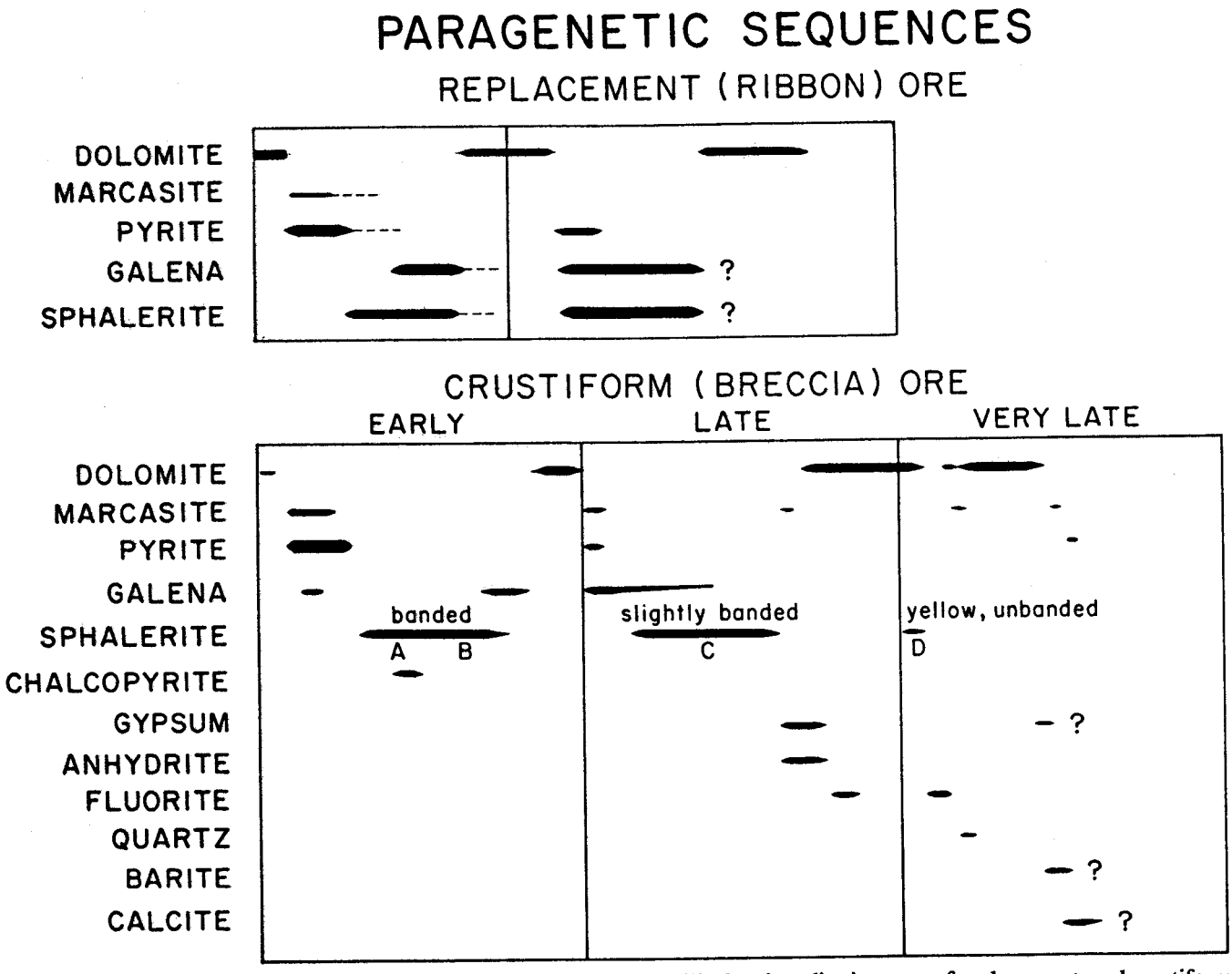

Figure 6. General paragenetic sequence for the sulfides of the Austinville-Ivanhoe district; ores of replacement and crustiform textures have a similar history of mineralization.

layers in banded sphalerite, and as cubes scattered in sphalerite, dolomite and most of the late-stage minerals. The pyrite overgrowths contain thin layers of dolomite and sphalerite, interstitial galena and, rarely, laths of marcasite.

The second sulfide mineral to crystallize in significant quantity was sphalerite. Four zones of sphalerite can be distinguished in the paragenetic sequence based on optical characteristics. Zone A, the earliest, consists of red-brown to yellow, delicately banded sphalerite that grew outward radially from multiple hemispheroidal centers on the underlying pyrite (Figure 8). Overlying layers of alternating light and dark sphalerite coalesce to form continuous bands parallel to the surface of fragments or fractures. Commonly, the cyclic banding begins with a broad, diffuse, reddish-brown layer, which grades into fine, lighter bands. Sphalerite may contain discontinuous, thin pyrite layers within zones A to C, local disseminations of chalcopyrite in zone A, and galena in zones A to C. Chalcopyrite occurs locally in sphalerite as oriented rods which are interpreted to be epitaxial intergrowths. The intergrowths always appear in the same paragenetic position and have been observed in samples from Ivanhoe, the Brown ore body, and the Fisher Field area. The A and B zone sphalerite samples have iron and cadmium contents ranging from 0.09 to 3.16 and 0.00 to 0.21 weight percent respectively.

Sphalerite in Zone C is commonly separated from that of Zones A and B by pyrite and dolomite. Zone C sphalerite ranges from light brown to pale yellow, and the banding is less distinct than in zones A and B. Zone C sphalerite is chemically distinct from the first, having lower and more uniform iron and cadmium contents. The iron contents range from 0.0 to 1.3 weight percent and the cadmium from 0.0 to 0.12 weight percent.

The last generation of sphalerite (Zone D) is dominantly lemon yellow and has minor-element contents that range from 0.08 to 0.35 weight percent for cadmium and 0.14 to 0.21 weight percent for iron. Locally, along mircofaults and fractures, the sphalerite has been stained red with traces

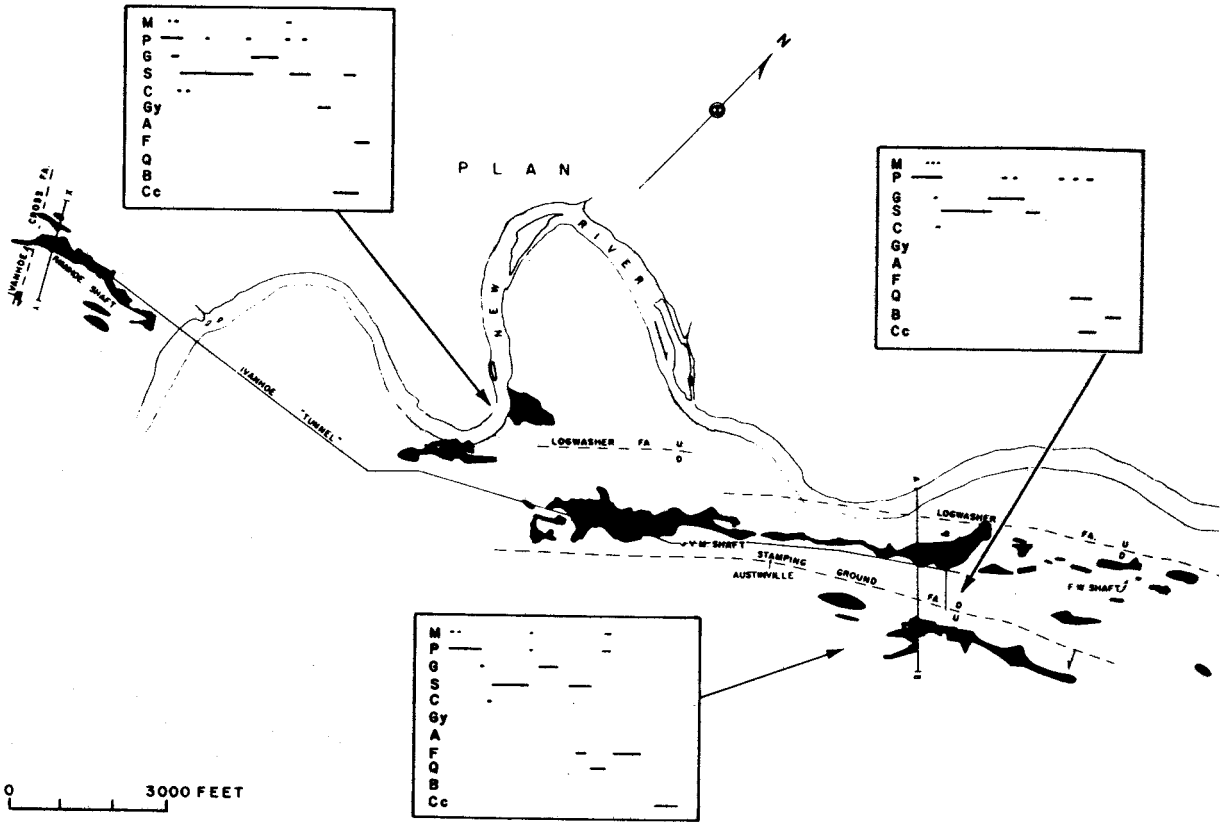

Figure 7. Variations in paragenesis associated with the three major fault blocks; M - marcasite, P - pyrite, G - galena, S - sphalerite, C - chalcopyrite, Gy - gypsum, A - anhydrite, F - flourite, Q - quartz, B - barite, CC - calcite.

of hematite resulting from oxidation of pyrite.

The zinc sulfides in Zones A, B, C, and some in Zone D are anisotropic; minute domains have undulatory extinction reminiscent of deformed quartz. A single crystal precession photograph taken of the sphalerite indicates the presence of deformation twins. The radially diffuse reflections do not broaden along lattice rows with equivalent hexagonal indices (H - K = 3n). These results are in agreement with those of Fleet (1977) who in a similar study of an unlocated ore sample from Austinville concluded that the origin of the twin lamellae was closely-spaced deformation faults. This interpretation agrees well with the tectonic history of the ores (Weinberg, 1971). Slight recrystallization, microfaulting, and minor amounts of element redistribution resulting from a period of post-ore deformation are evident in minerals throughout the deposit.

An electron microprobe study of delicately banded sphalerite indicates that, in general, an inverse relationship exists between the iron and cadmium contents of the sphalerite bands. Iron contents of the sphalerite bands range from 0.0 to 3.0 weight percent and the cadmium contents range from 0.0 to 0.3 weight percent (Figure 9). The color zonation of the sphalerite bands is not strictly due to the variation in iron content, although sphalerites of zones A and B are generally darker and have higher and more variable iron contents. Figure 10 demonstrates the lack of correlation between iron content and band color on a local scale. The traverse is taken across a 2.5 millimeter-wide sphalerite layer and indicates that although a particular dark band may have a high iron content, other bands of the same opacity contain little iron. Roedder and Dwornik (1968) found a similar lack of correlation of color and iron content in the sphalerites of Pine Point, Northwest Territories, Canada, whereas McLimans (1977) noted that such a correlation does exist in the zinc sulfide of the Upper Mississippi Valley district. Some of the color inherent in the bands may be due to the presence of minute fluid and solid inclusions (Foley and others, 1981).

Sphalerite has two occurrences in the replacement-type ore. Millimeter- to centimeter-wide crystals of resinous-brown to yellow sphalerite have selectively replaced the coarse carbonate layers in the ribbon-laminated dolomite. Sphalerite also occurs as millimeter-wide rosettes in black shaly carbonate.

The last sulfide mineral to form in major proportions was galena. It crystallized as millimeter-wide grains disseminated in sphalerite and as millimeter- to centimeter-wide crystals which appear to have replaced layers in ribbon-laminated carbonates. Galena crystals have included fragments of pyrite, sphalerite, and dolomite. Exsolution features are absent. The cleavage traces within galena are curved, suggestive of post-depositional deformation. Ball and Thompson (1916) reported galena analyses with silver contents ranging

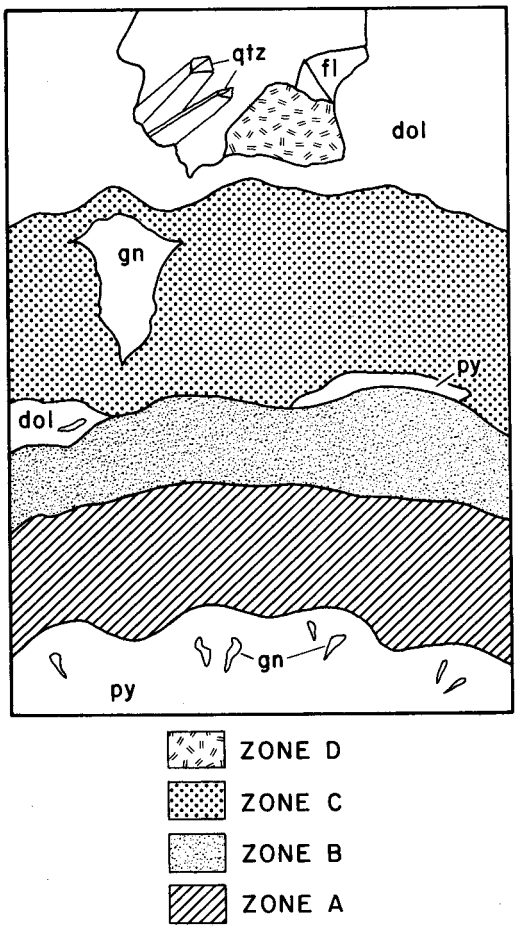

Figure 8. Sphalerite zones identified in the mineralization sequence; zones A and B correspond to early mineralization, zone C to the middle period, and zone D to the final vug-filling stage; qtz - quartz, fl - fluorite, dol - dolomite, gn - galena, py - pyrite,

from nil to 0.7 ounces of silver per ton of ore with an average of slightly less than 0.13 ounces (4 ppm). Mineral production figures for the years 1955-1958 (Weinberg, 1980) indicate that the silver contents of the galena for those years averaged about 0.5 ounces of silver per ton of lead concentrate (17 ppm) or about .003 ounces per ton for the entire ore (0.11 ppm).

During the later stages of mineralization, fluorite, quartz, barite, gypsum, and anhydrite were deposited locally in vugs and veins. Fluorite crystals are commonly colorless to pale purple and range up to 5 millimeters in width. Sprays of euhedral quartz crystals, 2 to 3 millimeters in length, are present in open spaces throughout the deposit. Gypsum and anhydrite usually contain scattered cubes of pyrite and feather-like aggregates of marcasite. Barite contains pyrite cubes aligned along growth planes.

SPHALERITE STRATIGRAPHY

The banding in sphalerite may reflect episodic changes in the nature of the chemical and physical environment of ore deposition. Correlating sphalerite banding throughout an ore body and across an entire district can yield important information of the physical extent and chemical regularity of the ore-depositing environment. At Austinville incomplete stratigraphic sequences, nondeposition, and late fracturing of the host rock are present at many localities, in general, enough characteristics of a particular zone are retained to enable tentative stratigraphic correlation of sphalerite.

Oriented samples of sphalerite were collected from the Brown, A-6-25, 40, and 100 ore lenses and the Fisher Field area and were examined for correlative features. Doubly polished thin sections of the symmetrically and asymmetrically banded sphalerites were prepared for study as described in Foley (1980) and Craig and Vaughan (1981). The delicate, colorless to resinous-brown banding is nearly invisible in standard polished thin sections but the banding is readily visible after the thin sections are doubly polished. As mentioned earlier, four general sphalerite zones (A, B, C, and D) can be identified on the basis of color, texture, and association. The zones have the following characteristics:

Zone A: The bands in this zone range in color from pale yellow to resinous brown. The earliest bands contain rare chalcopyrite rods and tend to be darker and more diffuse in color than the later bands. The terminal band of Zone A is a thin (0.1 mm), colorless layer of sphalerite.

Zone B: The bands in this zone are thinner and more sharply defined than those in Zone A. They also range in color from pale yellow to resinous brown. The boundary between zones B and C usually shows evidence of dissolution.

Zone C: Zone C is significantly lighter in color than the earlier zones. The bands at the base of Zone C typically are yellow-brown, broad, and diffuse. Later bands in the zone are thinner, fewer in number, and sharply defined.

Zone D: The sphalerite in Zone D grew as light yellow to red, euhedral crystals and is associated with the latest-stage mineralization. This zone was not used in the stratigraphic correlation because it is not a continuous layer.

The sphalerite stratigraphy for the Fisher Field area is represented in Figure 11 by sections taken from three locations within the lens. Samples 419, 334-B, and 334-A demonstrate the stratigraphic continuity over a distance of 188 meters. The thickness in millimeters of Zones A, B, and C ranges from 1.0 to 3.0, 0.5 to 2.0, and 1.0 to 4.0, respectively. Stratigraphic correlation of sphalerite bands across the district is more tenuous than within a single ore body because of widely spaced sampling. Samples taken from the Fisher Field area, the Brown ore body, and the 100 ore body possess the general characteristics attributable to the individual zones. As Figure 12 demonstrates, the sphalerite bands

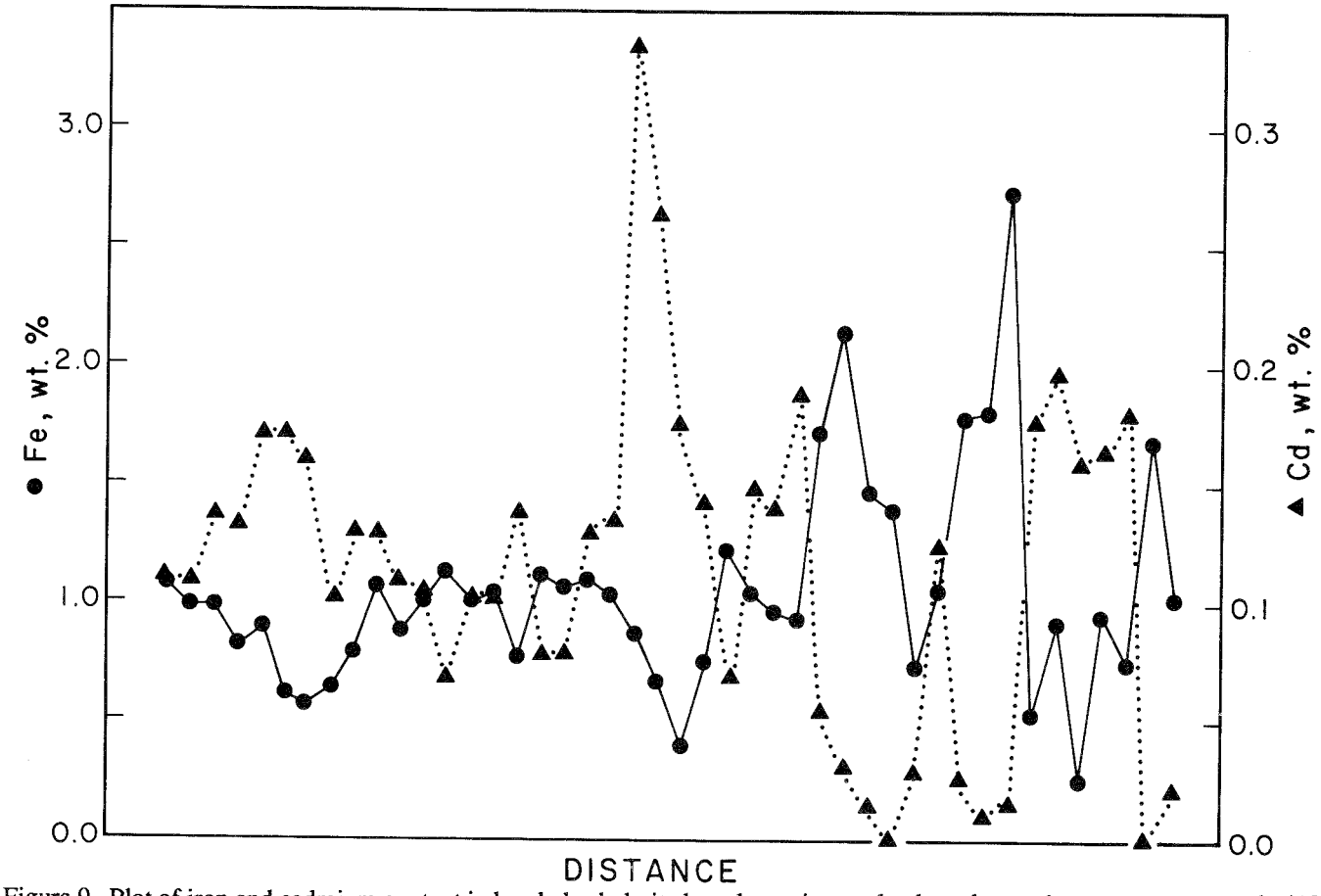

Figure 9. Plot of iron and cadmium content in banded sphalerite based on microprobe data along a 1 cm traverse, sample 419.

can be tentatively correlated over a distance of 2.7 kilometers. In some areas a distinction between Zones A and B is less obvious than in others, but the boundary between Zones B and C is usually easily recognized.

The stratigraphy suggests that deposition was probably not uniform over the entire district. Within a single ore body (for example, Fisher Field), the rate or total amount of deposition may have varied by a factor of two. Samples 334 and 419, which are 188 meters apart, have total thicknesses of approximately 3 mm and 7 mm, respectively. This suggests that either different vugs started filling at different times or that the depositional rate was higher in some locations than in others. Banding such as this is present in many carbonate-hosted zinc ores of the Appalachians (Foley and Craig, 1980) and is similar to banding in sphalerite of the Mississippi Valley-type districts of the central United States (McLimans and others, 1980).

ENVIRONMENT OF ORE DEPOSITION

The coexisting sulfide and gangue minerals reflect changes in the physical and chemical characteristics of the environment of ore deposition during the three episodes of mineralization. The delicate growth banding and the coarse-grained nature of the crystals that are present throughout the deposit indicate that the minerals were deposited under quiescent conditions and that the deposition rate was slow (McLimans, 1977).

Fluid inclusion geothermometry studies of 30 to 70 micron-wide fluid inclusions in sphalerite that crystallized during the later stages of mineralization were conducted on samples from the Ivanhoe, A-6-25, 100, 40, and Brown ore lenses. The criteria used to distinguish between primary and secondary inclusions are those described by Roedder (1979). Measurements were conducted on a gas-flow heating stage modelled after Werre and others (1979). The stage was calibrated against the boiling point of water and reproducibility was estimated by repeating runs on each specimen three times. The stage also was calibrated against a fluid inclusion stage at the U.S. Geological Survey in Reston, Virginia. Inclusion runs repeated on both stages yielded temperatures within the probable range of error. The accumulated error on the measured temperatures is estimated at less than ± 3.0°C.

Most of the 30- to 70-micron wide fluid inclusions examined consisted of a gas and a liquid phase (Figure 13) at room temperature. Two inclusions contained daughter minerals in addition to liquid plus vapor; these have been tentatively identified as gypsum based on crystal shape and optical properties. The results of the thermal measurements indicate that the sphalerite in the later part of mineralization (Zones C and D) crystallized in the temperature range 100°C to 160°

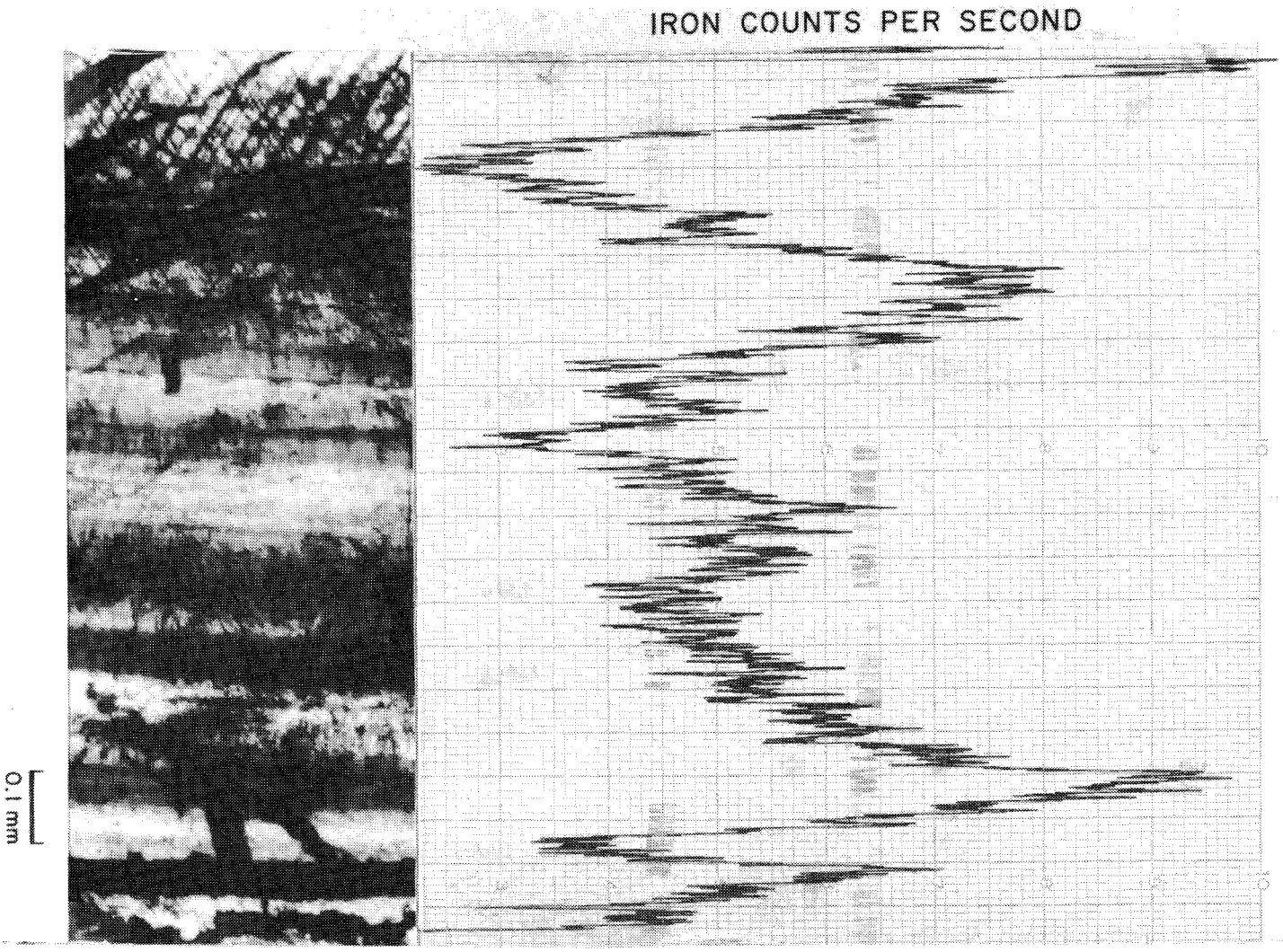

Figure 10. Microprobe traverse across banded sphalerite showing lack of correlation between iron content and sphalerite color.

C (Figure 14). The dark nature of the banding in early sphalerite (Zones A and B) and the small size of the inclusions within the bands inhibited estimates of the temperature of mineralization during these periods. This temperature range (100° C-160° C) is consistent with the temperatures derived from other Mississippi Valley-type deposits by fluid inclusion geothermometry (Roedder, 1979; McLimans, 1977).

Estimates were made of the activities of O_2, CO_2, and S_2 for the mineralizing fluids based on the fluid inclusion thermometry results and the coexisting mineral assemblages. It was assumed for the calculations that Zones A and B sphalerite was deposited at higher temperatures (175° C) than sphalerite from Zones C and D. For a given temperature an area on an activity of O_2 versus activity of CO_2 plot is defined by the absence of graphite and presence of carbonates, the presence of pyrite instead of magnetite and the absence of wollastonite and presence of calcite and quartz. Although calcite is not present in the early stages of ore deposition, it does occur in equilibrium with late-stage dolomite, quartz, and sphalerite. The ore presumably crystallized within this range of aO_2 and aCO_2. The activity of sulfur in the stable assemblages is calculated on the basis of the FeS content of sphalerite coexisting with pyrite (Vaughan and Craig, 1978). The iron content of banded sphalerite varies within each zone but, in general, results of analyses of samples from the deposit indicate that early sphalerites have a slightly higher iron content than middle and late zinc sulfides (Table 1). Zones A and B sphalerites have iron con-

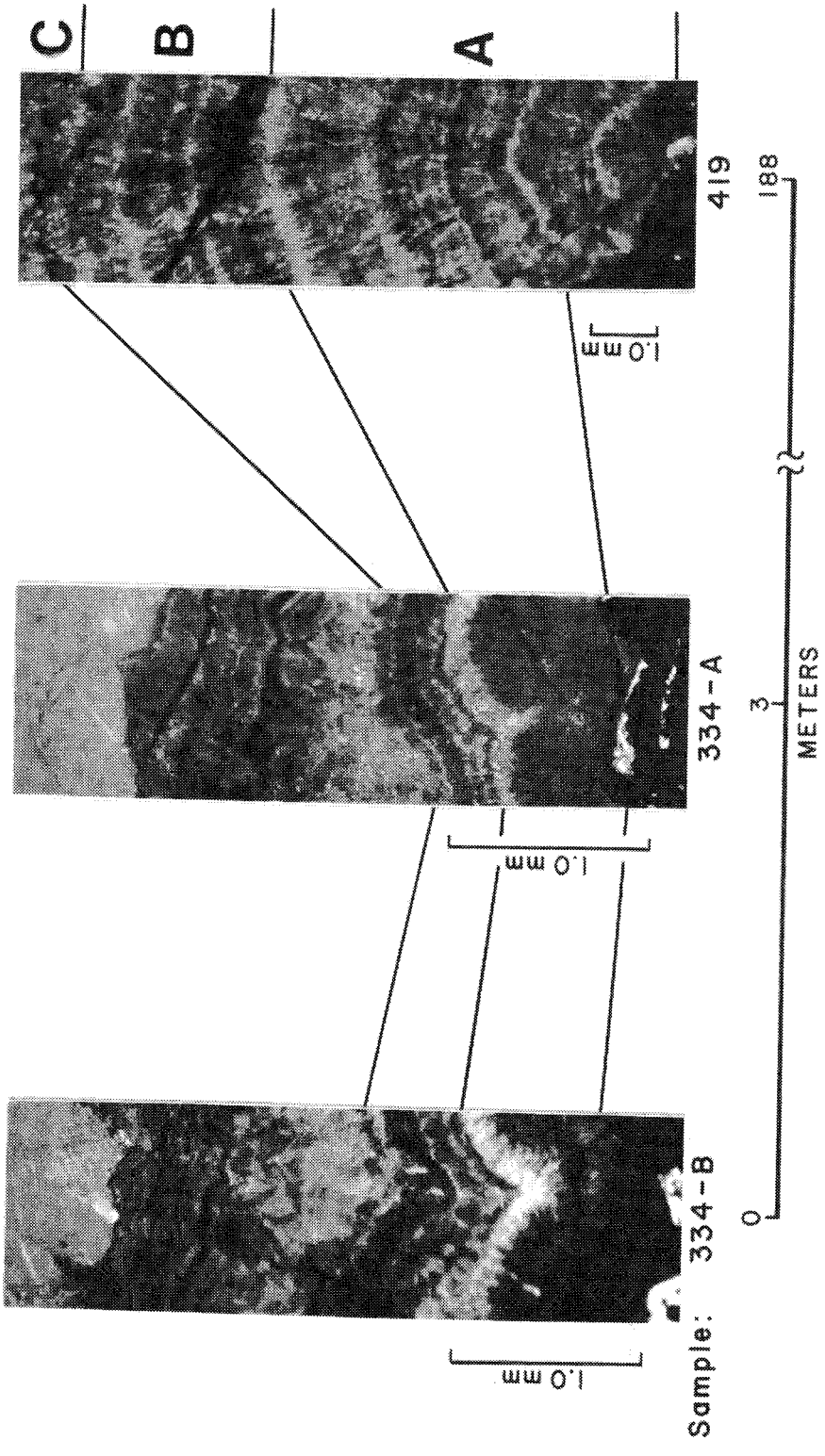

Figure 11. Stratigraphic correlation of sphalerite banding within the Fisher Field area; A, B, and C refer to sphalerite zones described in text.

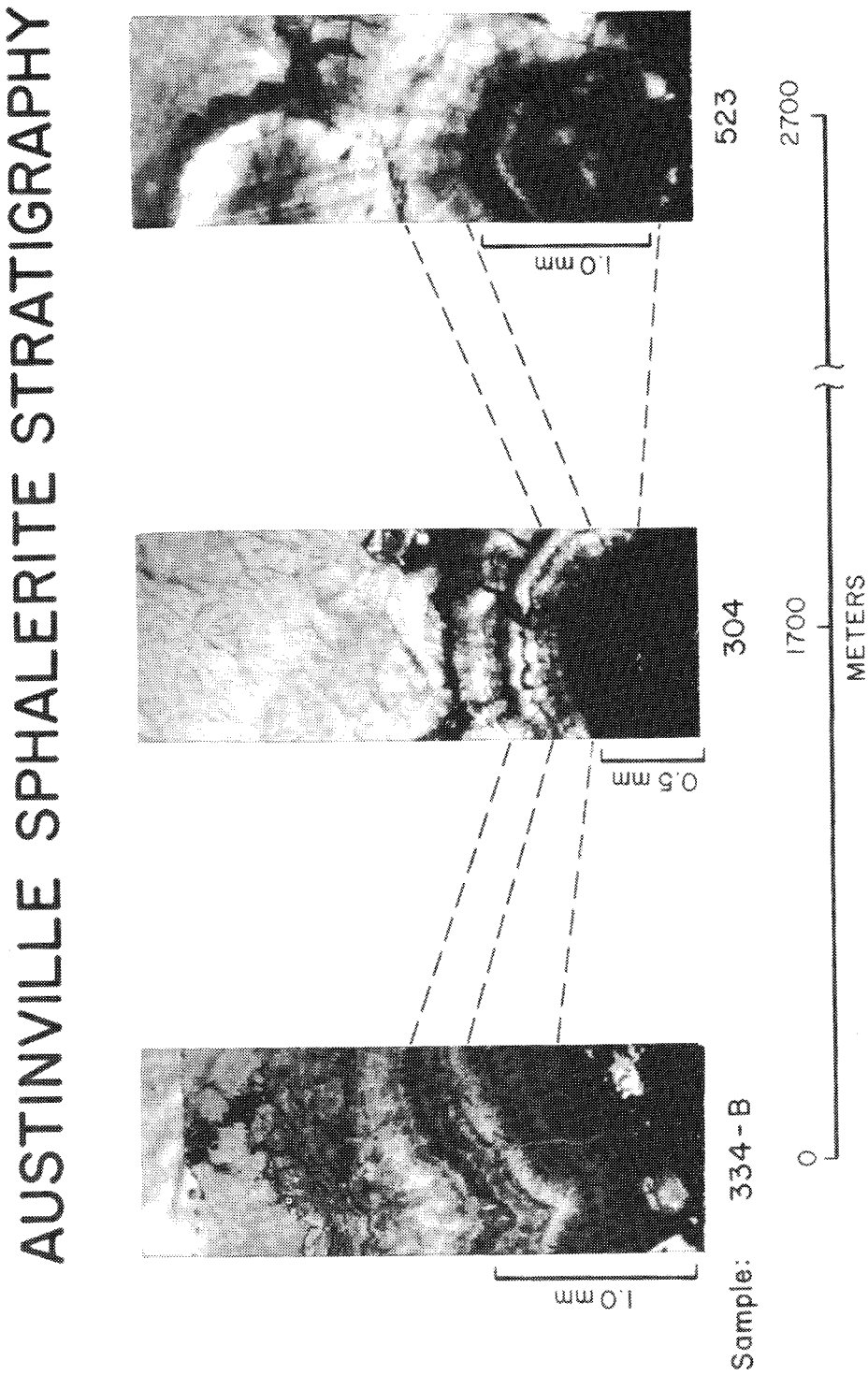

Figure 12. Stratigraphic correlation of sphalerite banding between the Fisher Field area (334B), the Brown ore body (304), and the 100 ore body (523); A, B, and C refer to sphalerite zones described in text.

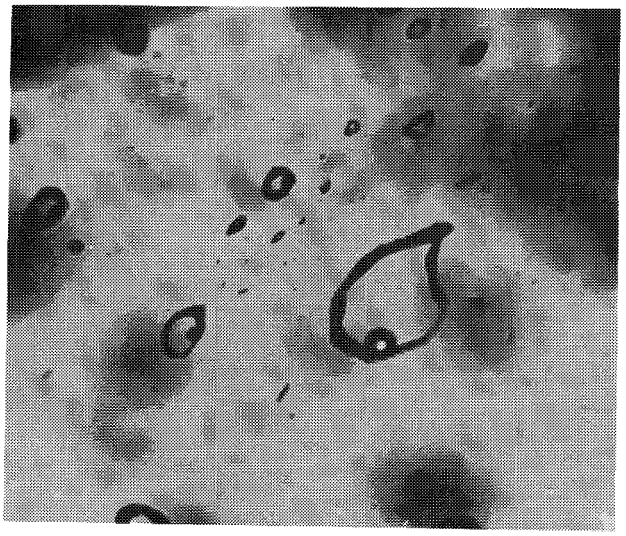

Figure 13. Two-phase inclusions in sphalerite crystal; inclusions were trapped as the crystals grew in vugs; field of view 0.33 mm.

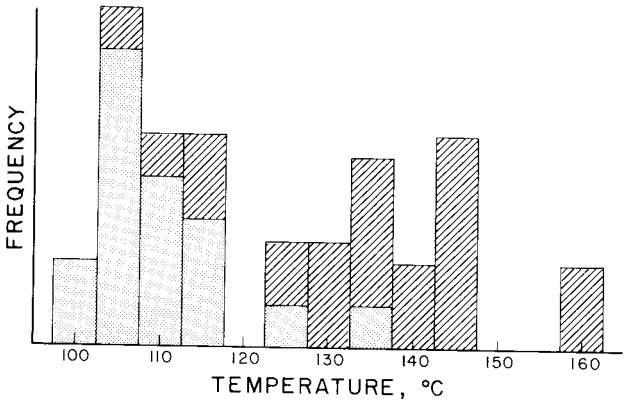

Figure 14. Histogram of fluid inclusion temperatures; the ruled area represents inclusions from sphalerite associated with dolomite; the dotted area pertains to inclusions from sphalerite associated with barite and/or calcite.

tents ranging from 0.0 to 3.2 weight percent, and Zone C sphalerites have iron contents ranging from 0.0 to 0.4 weight percent. If a point in the center of each log aO_2 versus log aCO_2 field (Figure 15) is taken as the average value for that interval of mineralization, a log aO_2 versus log aS_2 plot can be constructed (Figure 16). Activity of both sulfur and oxygen decreased throughout the sequence of ore deposition.

DISCUSSION: COMPARISON OF THE AUSTINVILLE-IVANHOE DISTRICT WITH OTHER CARBONATE-HOSTED LEAD-ZINC DEPOSITS

Carbonate-hosted lead-zinc deposits constitute the principal source of lead and zinc in both the United States and Europe. Examples include the Appalachian district, the Tri-state district, the southeast Missouri district, the upper Mississippi Valley district, and the Pine Point district in North America and the Pennine district in Western Europe. The deposits occur in dolomite and limestone ranging in age from Early Cambrian to Triassic and many are related to reef or platform structures. In most cases, mineralization appears to have been structurally controlled. Some deposits are situated near unconformities; others are on the flanks and axes of anticlines and domes; most are associated with fault systems. The volume of ore in this type of deposit ranges from a few tons to hundreds of millions of tons; the average grade ranges from 2 to 7 weight percent zinc and from 0 to 3 weight percent lead.

The primary sulfide mineralogy of the deposits is simple; most contain only sphalerite, galena, pyrite, and minor chalcopyrite. Sphalerite is commonly banded and contains a number of trace constituents including cadmium. The deposits characteristically form at low temperature (100° C to 200°C) from high salinity brines (approximately 10 to 25 equivalent weight percent NaCl).

The isotopic composition of lead in galena from carbonate-hosted lead-zinc deposits is distinctive. The galena has lead isotopic ratios that commonly plot above and to the right of the zero million year isochron of single and two-stage lead evolution models (Doe and Zartman, 1979). Age calculations based on these ratios yield negative or future ages of formation. An exception is the Pine Point district, Northwest Territories, Canada, which has a lead isotopic composition that conforms to a two-stage model. The lead ratios of the deposits in the drainage basin of the Mississippi River are commonly greater than 19.0 in $^{206}Pb/^{204}Pb$, and greater than 39.0 in $^{208}Pb/^{204}Pb$ (Doe and Zartman, 1979). The Austinville-Ivanhoe district has ratios that range from 18.95 to 19.16 in $^{206}Pb/^{204}Pb$, from 15.66 to 15.75 in $^{207}Pb/^{204}Pb$, and from 38.66 to 39.0 in $^{208}Pb/^{209}Pb$ (Foley, 1980; Foley and others, 1981). These ratios are isotopically similar to only the least radiogenic of other Mississippi Valley-type deposits (Figure 17).

Lead isotopic studies from the Austinville-Ivanhoe district (Foley and others, 1981) also demonstrate that galena of different generations has distinct lead isotopic compositions. Within a single ore body paragenetically early galena has lower lead isotopic ratios than later galenas. In addition smaller ore lenses characteristically show a more radiogenic signature than larger ore lenses. This suggests that during the paragenesis of the ores an increasing amount of more radiogenic lead became involved in the formation of galena. The smaller ore lenses may have been more easily contaminated by more radiogenic crustal leads. The lead isotopic composition of galena in the district may have been derived by mixing of lead from the enclosing sedimentary sequence with less radiogenic leads derived from underlying basement rocks (Foley and others, 1981).

Table 1. Comparison of the Austinville-Ivanhoe district with other carbonate-hosted lead-zinc deposits in the United States, Canada, and Great Britain. Reference numbers (3) listed at end of References Cited.

Location	Host Rock	Age of Host Rock	Genesis of Host Rock	Structural Setting	Tonnage and Grade	Reported Sulfide Mineralogy*	Formation Temperature	Salinity (Equiv. wt % NaCl)
Austinville, Va.	Shady Fm.	Lower Cambrian	Reef to platform sequence	Flanks of Austinville anticline	>30 million tons: 4% Zn, 0.6% Pb	sph, gn, py, marc, ccp	100 - 160°C	18.5 - 22.5
	(3)	(3)	(2)	(3)	(4)	(1)	(1)	
Timberville, Va.	Beekmantown Fm.	Lower Ordovician		Breccia pipe on west limb of syncline	Small	sph, gn, py, ccp	140 - 150°C	17.1 - 24.5
	(6)	(6)		(17)		(6)	(14)	(14)
Friedensville Pa.	Beekmantown Fm.	Lower Ordovician	Paleokarst unconformity	Anticline and faults	>3 million tons: 6% Zn	sph, py		16.1 - 26.7
	(5)	(5)	(5)	(5)	(12)	(5)		(14)
East Tennessee	Kingsport and Mascot Fms.	Lower Ordovician	Unconformity in platform sequence	Footwall block of thrust	50 million tons: 4% Zn	sph, py, ccp	100 - 150°C	14.0 - 29.5
	(5)	(5)	(5)	(5)	(12)	(5)	(14)	(14)
Central Tennessee	Mascot Fm.	Lower to Middle Ordovician	Paleokarst unconformity	Under thrust sheet, Nashville	>20 million tons: 4.5 - 5% Zn	sph, gn	110°C	22.6
	(5)	(5)	(15)	(5)	(16)	(5)	(14)	(14)
Illinois-Kentucky	St. Louis and St. Genevieve Fms.	Mississippian	Platform	Hicks dome		gn, sph, py, marc, ccp	110°C	18.5 - 22.5
	(12)	(12)	(5)	(12)		(12)	(14)	(14)
Upper Mississippi Valley	Galena, Decorah, and Platteville Fms.	Middle Ordovician	Platform sequence	SW flank of Wisconsin arch	50 million tons: 4% Zn	sph, gn, py, marc, ccp, enargite	80 - 120°C	22.6
	(9)	(9)	(9)	(9)	(12)	(9)	(9)	(14)
Southeast Missouri	Bonneterre Fm.	Cambrian	Reef environment	Flanks of St. Francois Mts.		sph, gn, py, marc, ccp, siegenite, bravoite	94 - 120°C	9.9 - 24.5
	(8)	(8)	(12)	(8)		(8)	(14)	(14)
Tri-state Area	Boone Fm.	Mississippian	Platform carbonates	NW flank of Ozark dome	500 million tons: 2.3% Zn, 9.6% Pb	sph, gn, py, marc, ccp	80 - 120°C	24.1 - 24.5
	(11)	(11)	(11)	(11)	(12)	(11)	(11)	(11)
Pine Point, Canada	Presquile Fm.	Middle Devonian	Reef environment	Folds and faults	65 million tons: 7% Zn, 3% Pb	sph, py, gn	51 - 97°C	25.5
					(12)		(14)	(14)
Pennines Great Britain	Great Limestone	Lower Carboniferous		Folds and faults		sph, gn, py, marc, ccp, bravoite, tetrahedrite, arsenopyrite, pyrrhotite	130 - 160°C	22.4
	(13)	(13)		(13)		(13)	(14)	(14)

*sph - sphalerite, gn - galena, py - pyrite, marc - marcasite, ccp - chalcopyrite.

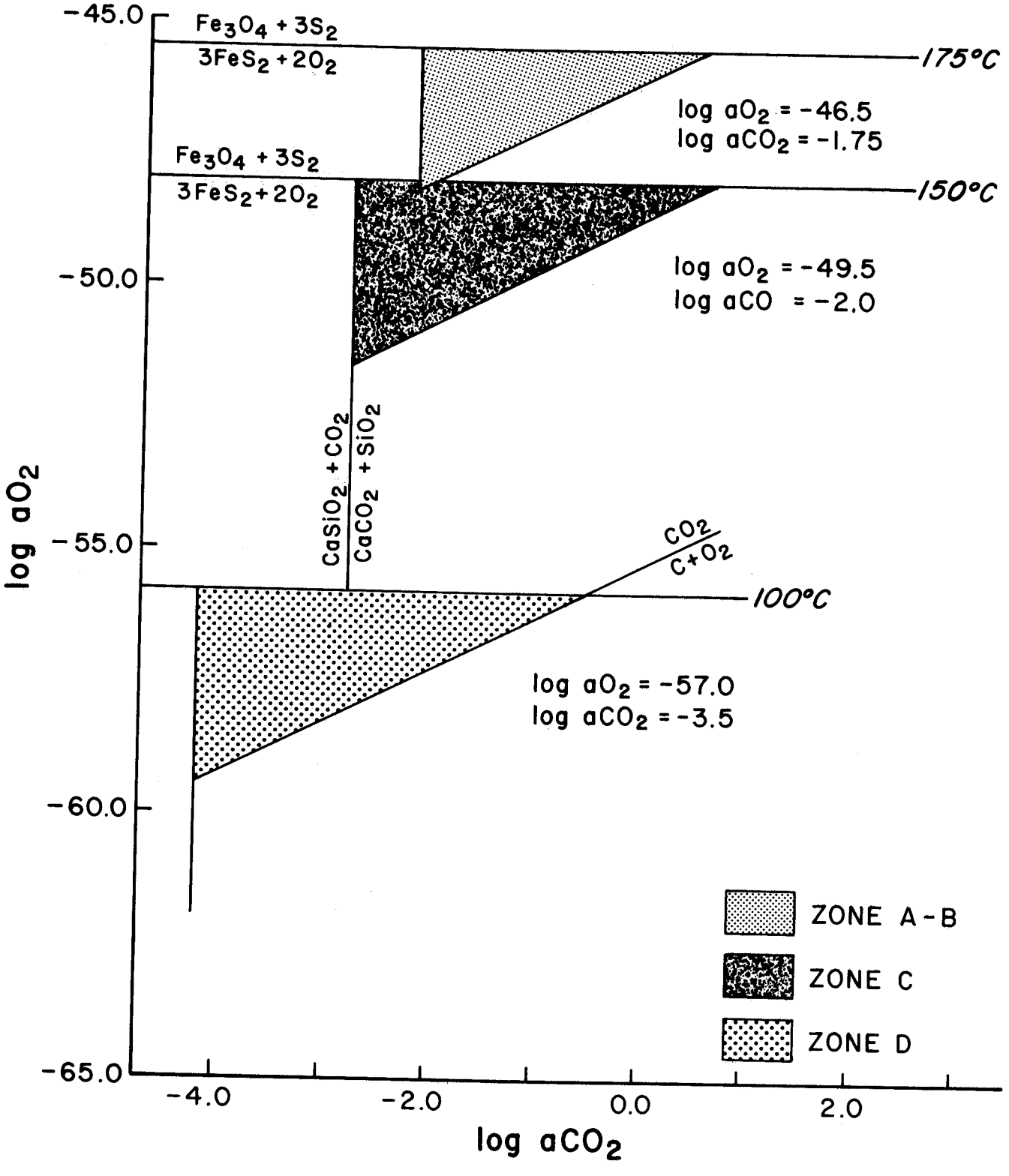

Figure 15. Stability fields of ore deposition in terms of aO_2 and aCO_2; sphalerite zones A, B, C, and D as described in text.

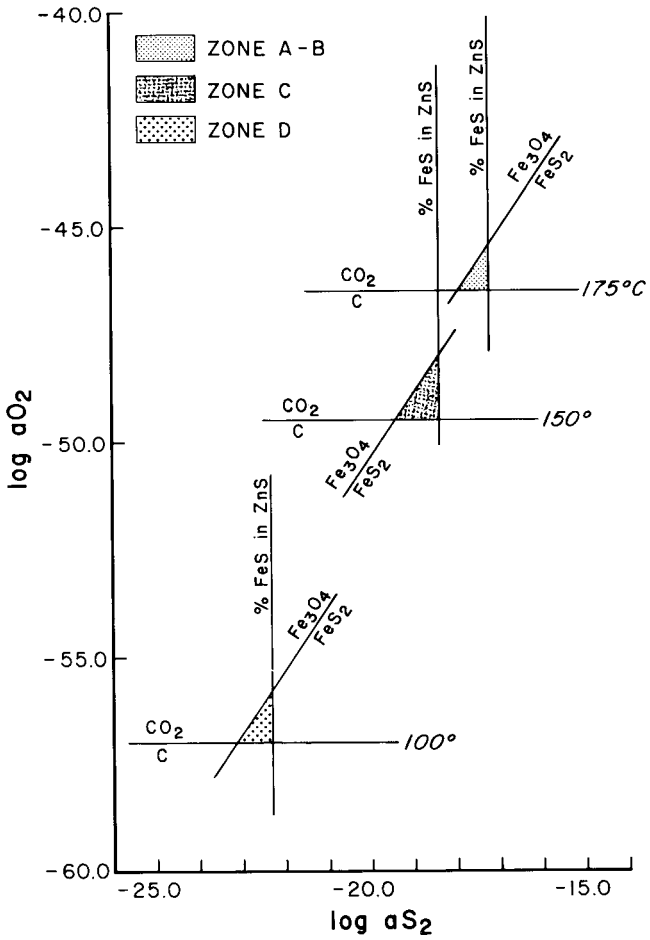

Figure 16. Stability fields of mineralization for the three periods of ore deposition in terms of aO_2 and aS_2; sphalerite Zones A, B, C, and D as described in text.

The form and structural setting of the ore lenses of the Austinville-Ivanhoe district are similar to many other Appalachian zinc deposits. The open space filling and minor replacement textures are common to all deposits of this type and the mineralogy of the district is characteristically simple (Foley and Craig, 1980). Stratigraphic correlation of the sphalerite is possible over an extensive area, though not as great as was possible in the upper Mississippi Valley (McLimans and others, 1980). The mineral chemistry, the Fe/Cd zonation, and the banding of the sphalerite are similar to that in other Appalachian deposits (Foley and others, 1981) and to other deposits of the central United States and Pine Point, Northwest Territories, Canada (Roedder and Dwornik, 1968; McLimans and others, 1980; Sangster, 1976).

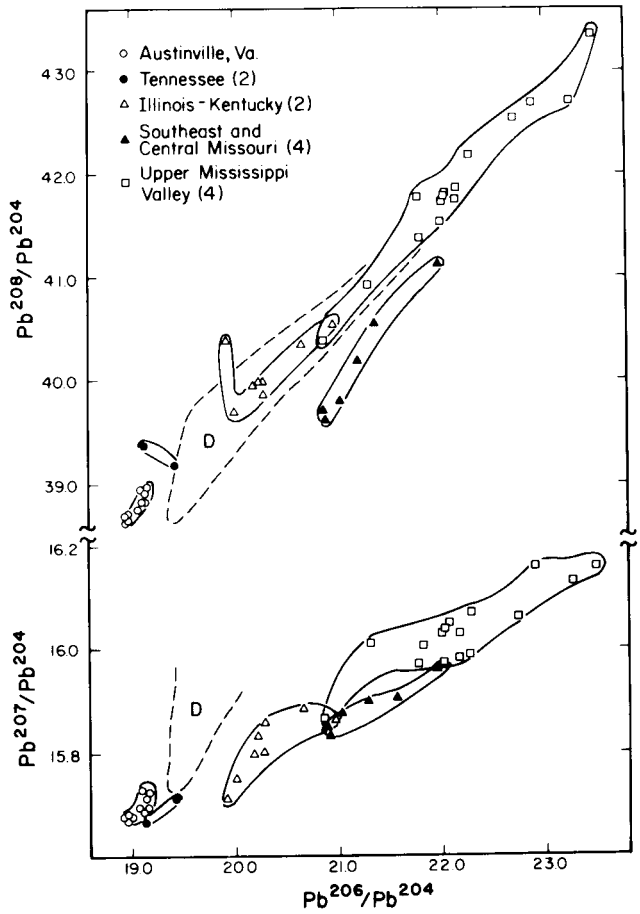

Figure 17. Isotopic composition of lead from Mississippi Valley-type deposits.

REFERENCES CITED

Ball, S. H., and Thompson, L. S., 1916, The Southeast Virginia lead-zinc deposits: Engineering and Mining Journal, v. 102, p. 735-737.

Brown, W. Horatio, 1935, Quantitative study of ore zoning, Austinville mine, Wythe County, Virginia: Economic Geology, v. 30, p. 425-433.

Brown, W. H., and Weinberg, E. L., 1967, Geology of the Austinville-Ivanhoe district, Virginia, *in* Ridge, J. D., ed., Ore deposits of the United States, 1933-1967: American Institute of Mining, Metallurgical, and Petroleum Engineers, v. 1, p. 169-186.

Butts, Charles, 1940, Geology of the Appalachian Valley in Virginia: Virginia Geological Survey Bulletin 52, pt. 1, 568 p.

Cooper, B. N., Arkle, T., Jr., and Latimer, I. S., Jr., 1961, Grand Appalachian Excursion: Guidebook no. 1, Virginia Polytechnic Institute, 114 p.

Craig, J. R., and Vaughan, D. J., 1981, Ore microscopy and ore petrography: New York, Wiley Interscience, 406 p.

Currier, L. W., 1935, Zinc and lead region of southwestern Virginia: Virginia Geological Survey Bulletin 43, 122 p.

Doe, B. R., and Delevaux, M. H., 1972, Source of lead in southeast Missouri galena ores: Economic Geology, v. 67, p. 409-425.

Doe, B. R., and Zartman, R. E., 1979, Plumbotectonics, the Phanerozoic, *in* Barnes, H. L., ed., Geochemistry of hydrother mal ore deposits, Second edition: New York, Wiley-Interscience, p. 24-70.

Fleet, M., 1977, Structural transformations in natural ZnS: American Mineralogist, v. 62, p. 540-546.

Foley, N. K., 1980, Mineralogy and geochemistry of the Austinville-Ivanhoe district [M. S. thesis]: Blacksburg, Virginia Polytechnic Institute and State University, 83 p.

Foley, N. K., and Craig, J. R., 1980, Ore and gangue mineralogy of the Austinville-Ivanhoe district, Wythe County, Virginia [abs.]: Geological Society of America Abstracts with Programs, v. 12, p. 177.

Foley, N. K., Sinha, A. K., and Craig, J. R., 1981, Isotopic composition of lead in the Austinville-Ivanhoe Pb-Zn district, Virginia: Economic Geology, v. 76, p. 2012-2017.

Gorody, A. W., 1980, The Lower Ordovician Mascot Formation, Upper Knox Group, in North Central Tennessee [Ph.D. dissert.]: Houston, Texas, Rice University, 181 p.

Grover, G. A., 1981, Cement types and cementation patterns of middle Ordovician ramp-to-basin carbonates, Virginia [Ph.D. dissert.]: Blacksburg, Virginia Polytechnic Institute and State University, 164 p.

Hagni, R. D., 1976, Tri-state ore deposits: the character of their host rocks and their genesis, *in* Wolf, K. H., ed., Handbook of stratiform and stratabound ore deposits: Amsterdam; Elsevier Scientific Publishing Co., v. 6, p. 457-494.

Herbert, Paul, and Young, Robert S., 1956, Sulfide mineralogy in the Shenandoah Valley of Virginia: Virginia Division of Geology Bulletin 70, 121 p.

Heyl, A. V., Delevaux, M. H., Zartman, R. E., and Brock, M. R., 1966, Isotopic study of galenas from the upper Mississippi Valley, the Illinois-Kentucky and some Appalachian Valley mineral districts: Economic Geology, v. 61, p. 933-961.

Hoagland, A. D., 1976, Appalachian zinc-lead deposits, in Wolf, K. H., ed., Handbook of stratiform and stratabound ore deposits: Amsterdam, Elsevier Scientific Publishing Co., v. 6, p. 495-534.

Kearns, L. E., and Campbell, F. H., 1978, The Elmwood and Gordonsville zinc mines near Carthage, Tennessee: The Mineralogical Record, v. 9, p. 213-218.

Kyle, J. R., 1976, Brecciation, alteration and mineralization in the central Tennessee zinc deposit: Economic Geology, v. 71, p. 892-903.

Maher, S. W., and Fagan, J. M., 1970, Trace element contents of some ore deposits in the southeastern states: Tennessee Division of Geology Information Circular, n. 16, 42 p.

McLimans, R. K., 1977, Geological fluid inclusion and stable isotope studies of the upper Mississippi Valley zinc-lead district, southwest Wisconsin [Ph.D. dissert.]: State College, The Pennsylvania State University, 175 p.

McLimans, R. K., Barnes, H. L., and Ohmoto, H., 1980, Sphalerite stratigraphy of the upper Mississippi Valley zinc-lead district, southwest Wisconsin: Economic Geology, v. 75, p. 351-362.

Pfeil, R. W., and Read, J. F., 1980, Cambrian carbonate platform margin facies, Shady Dolomite, southwestern Virginia, U.S.A.: Journal of Sedimentary Petrology, v. 50, p. 91-116.

Roedder, Edwin, 1979, Fluid inclusions as samples of ore fluids, *in* Barnes, H. L., ed., Geochemistry of hydrothermal ore deposits, Second edition: New York, Wiley-Interscience, p. 684-737.

Roedder, Edwin, 1976, Fluid-inclusion evidence on the genesis of ores in sedimentary and volcanic rocks, *in* Wolf, K. H.,ed., Handbook of stratiform and stratabound ore deposits: Amsterdam, Elsevier Scientific Publishing Co., v. 2, p. 67-110.

Roedder, Edwin, and Dwornik, Edward J., 1968, Sphalerite color banding: lack of correlation with iron content, Pine Point, NWT, Canada: American Mineralogist, v. 53, p. 1523-1529.

Sangster, D. R., 1976, Carbonate-hosted lead-zinc deposits, *in* Wolf, K. H., ed., Handbook of stratiform and stratabound ore deposits: Amsterdam, Elsevier Scientific Publishing Co., v. 6, p. 447-456.

Vaughan, D. J., and Craig, J. R., 1978, Mineral chemistry of metal sulfides: Cambridge University Press, 476 p.

Vaughan, D. J., and Ixer, R. A., 1980, Studies of the sulfide mineralogy of North Pennine ores and its contribution to genetic models: Transactions of the Institute of Mining and Metallurgy, v. 89, p. B99-B109.

Watson, T. L., 1907, Mineral resources of Virginia: Lynch-burg, Virginia, J. P. Bell Co., 618 p.

Weinberg, E. L., 1971, Sulfide mineralization in southwest Virginia, Austinville-Ivanhoe mine, *in* Guidebook to Appalachian tectonics and sulfide mineralization: Geological Society America, p. 7-23.

Weinberg, E. L., 1980, Austinville mining - 1756 to present:Virginia Division of Mineral Resources Virginia Minerals, v. 26, n. 1, p. 11.

Werre, R. W., Jr., Bodnar, R. J., Bethke, P. M., and Barton, P. B., Jr., 1979, A novel gas-flow fluid inclusion heating/freezing stage [abs.]: Geological Society of America Abstracts with Programs, v. 11, p. 539.

References for Table 1.

1. Foley (1980)
2. Pfeil and Read (1980)
3. Brown and Weinberg (1967)
4. Weinberg (1980)
5. Hoagland (1976)
6. Herbert and Young (1956)
7. Heyl and others, (1966)
8. Doe and Delevaux (1972)
9. McLimans (1977)
10. Maher and Fagan (1970)
11. Hagni (1976)
12. Sangster (1976)
13. Vaughan and Ixer (1980)
14. Roedder (1976)
15. Kearns and Cambell (1978)
16. Kyle (1976)
17. Weinberg (pers. comm.)

INTERPRETATION OF GRAVITY AND MAGNETIC ANOMALIES OF THE RICHMOND TRIASSIC BASIN

Ali A. Nowroozi[1] and Arnold Wong[1]

CONTENTS

	Page
Abstract	42
Introduction	42
Regional geologic setting	43
Geology of the Richmond basin	43
Review of geophysical data	45
Field procedures	45
Interpretation of gravity data	46
Regional interpretation	46
Hylas fault zone	47
Theoretical anomalies and gravity modeling	48
Gravity modeling of the basin	50
Interpretation of the magnetic data	52
Discussion	53
Acknowledgments	59
References cited	59

ILLUSTRATIONS

Figure	Page
1. Location of State roads and U.S. highways along which gravity and magnetic profiles were measured	43
2. Geologic map of the Richmond Triassic basin and vicinity	43
3. Geologic map of the Richmond Triassic basin	44
4. Simple Bougoer gravity map	46
5. Profile H1	47
6. Profile H2	47
7. Variation of the gravity anomaly over a fault due to variation of the fault plane	47
8. Six possible fault planes for the Hylas fault	47
9. An interpretation of the Hylas fault	48
10. An interpretive geometry for the Hylas fault along profile H1	48
11. An interpretive geometry for the Hylas fault along profile H2	48
12. Variation of the theoretical anomaly due to variation of depth	49
13. Variation of the theoretical anomaly due to variation of basin width	49
14. Variation of the theoretical anomaly due to variation in depth of a half graben	49
15. Variation of the position of maximum theoretical anomaly	49
16. Two interpretive models for the basin along profile R1	50
17. Two interpretive models for the basin along profile R2	50
18. Interpretive model for the basin along profile R3	50
19. Interpretive model for the basin along profile R4	51
20. Interpretive model for the basin along profile R5	51
21. Interpretive model for the basin along profile R6	51
22. Interpretive model for the basin along profile R7	51
23. Interpretive model for the basin along profile R8	52
24. Interpretive model for the basin along profile R9	52
25. Three structural interpretations of the gravity profile along State Road 602	53
26. General interpretation of the total magnetic field of the Richmond basin and vicinity	54

1. Department of Geological Sciences, Old Dominion University, Norfolk, Virginia 23508

27. Location of the longest diabase dike in the southern part of the Richmond basin and the position of the ten profiles across the dike 55
28 through 37. Observed and calculated values of the vertical component of the magnetic field 56

TABLE

1. Densities and susceptibilities of certain rock units and specific lithologies 58

ABSTRACT

New detailed gravity and magnetic profiles along several State roads and highways which cross the Early Mesozoic age Richmond basin augment existing data for the analysis of the structure of the basin.

The gravity profiles display steep gradients across the western border of the basin where the Triassic lithologies are in fault contact with older metamorphic rocks. The surface geology indicates that this gradient probably marks the southern continuation of the Hylas fault zone. The displacement of this fault may be as much as a few kilometers. A gravity gradient is also apparent along the southern segment of the eastern border of the basin. The eastern edge of the basin is generally bounded by the Petersburg granite of Mississippian age. All available data indicate that the basin is a half graben in which depth decreases toward the east. Theoretical modeling shows that the gravity gradient due to the Hylas fault may be interpreted in the vicinity of Hylas as a thrust fault which dips toward the east from about 26° to 18° to a depth of about 4 km and then becomes nearly horizontal. The eastern block is the Petersburg granite which is thrust over the Goochland complex on the western block. This fault is the source of the dominant gravitational feature of the Richmond basin as far south as the middle of the basin.

A lumped-sum mass model is used to simplify the structure of the basin. The Hylas fault zone and its relation to the basin is modeled. The results indicate that the basin's western border dips steeply toward the east and reaches a depth of over 2 km whereas its eastern border has a gentle dip toward the west. Several diabase dikes which intrude the Triassic rocks are apparent from the magnetic map. Magnetic modeling of the longest dike, over 12 km long, yields a range of widths of from 15 to 30 meters and a range of depths of from 5 to 35 meters. The dikes also crop out at the surface in many areas.

INTRODUCTION

A number of petroleum-producing continental rift basins have been found around the world. Many similar basins in the eastern United States are being actively explored for petroleum and some of these could prove to be productive. Although in the eastern United States several continental basins of early Mesozoic age have been recognized, the interest of oil companies has only recently emerged (Gentz, 1982; Cochran, 1984). Exploration and drilling have been hampered largely because subsurface data are insufficient to evaluate even those basins that are partly or completely exposed in the Piedmont province. Generation of much needed data through random exploratory drilling and seismic exploration is expensive and, therefore, has not been widely attempted. In this study we have completed a detailed gravity and magnetic survey of the Richmond basin in order to generate the requisite data for subsequent detailed seismic exploration. Our detailed work augments the existing data of Johnson and others (1985) and facilitates the analysis of the structure of the basin and the thickness of sedimentary rocks (Figure 1).

REGIONAL GEOLOGICAL SETTING

The Richmond Triassic basin is a north-northeast trending faulted structure that contains Late Triassic clastic rocks (Figure 2). This basin is one of many elongated faulted basins of early Mesozoic age, which are exposed along the eastern coast of North America from Nova Scotia to Georgia. All of these exposed Mesozoic age basins are aligned with the Appalachian structural trend. Other basins exist under Coastal Plain sediments and offshore. Many workers (Van Houten, 1969; Grow, 1981; Bally, 1981; Watts, 1981; Johnson and others, 1985) agree that these basins are dominantly clastic sedimentary rocks in contrast to the generally metamorphic rocks of the basement complex.

The Richmond basin is located about 12 miles west of the city of Richmond and has a length and width of about 33 and 10 miles respectively. Its exposed surface area is about 260 square miles (Weems, 1980). Drill-hole results indicate that approximately 7300 feet of Triassic-age rocks are present in the central part of the basin (Johnson and others, 1985).

The Richmond basin is bounded mainly by igneous and metamorphic rocks (Lutz, 1986). The central and northern segment of the eastern border of the basin is bounded by the Petersburg granite and a veneer of Tertiary sedimentary units. The southern segment of the eastern border and a section of the southern and western border are bounded by undifferentiated mica gneiss. The central and northwestern

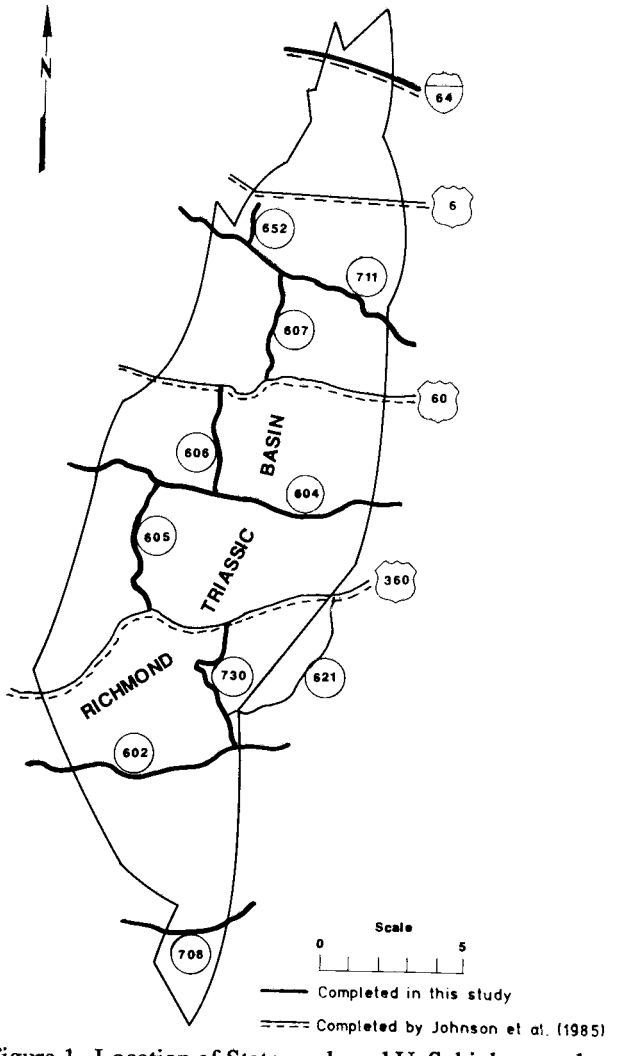

Figure 1. Location of State roads and U. S. highways along which gravity and magnetic profiles were measured. Profiles along Interstate Highway 64, U. S. highways 250, 60, and 360, and State Road 6 were measured by Johnson and others (1985). The other profiles were measured for this study. The horizontal spacing for measurements of the gravity and magnetic fields for these profiles is about 100 meters.

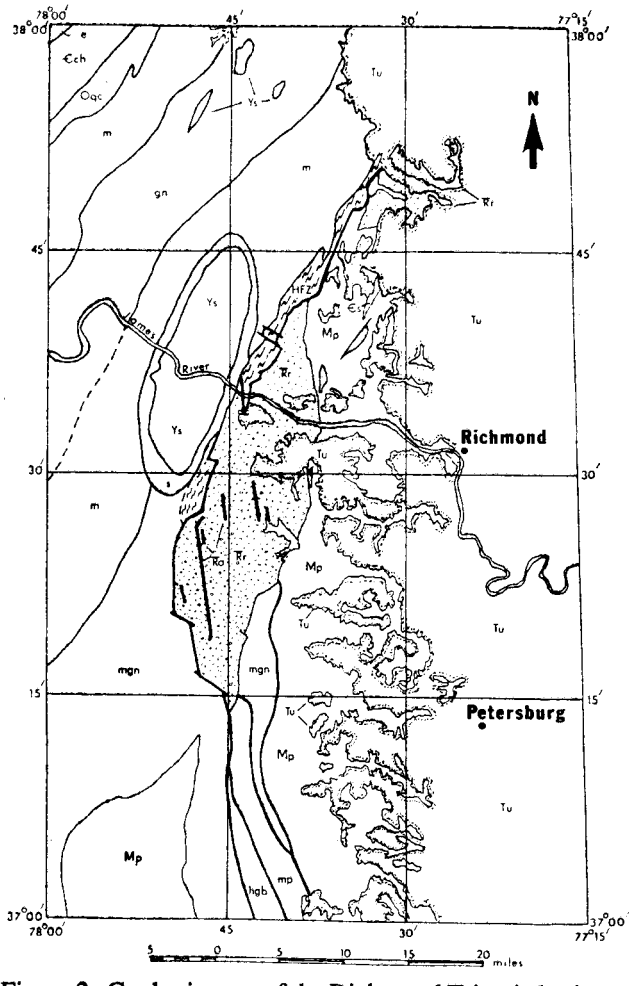

Figure 2. Geologic map of the Richmond Triassic basin and vicinity (modified from Lutz, 1986 and Farrar, 1984); Tu - Tertiart sediment, Jd - diabase dikes, Trr - red-beds, HFZ - Hylas fault zone, Mp - Petersburg granite, Oqc - Quantico Creek Slate, Oe - Ellisville Granodiorite, Cs - Chopawamic Formation, m - Madins gneiss, s - Sabot amphobolite, Ys - State Farm Gneiss, gn - granite gneiss, mgn - mica gneiss, mp - mica phyllite, hgb - hornblende gabbro.

border is bounded by Goochland complex rocks which consist of the State Farm gneiss, Sabot amphibolite, and Maidens gneiss (Bobyarchick and Glover, 1979; Farrar, 1984). The State Farm gneiss has been deformed into a northeastward-trending doubly plunging antiform and is overlain by the Sabot amphibolite interbedded with mafic and felsic gneiss (Glover and others, 1978). The Sabot is overlain by the Maidens gneiss which consists of a lower massive biotite gneiss with interbedded amphibolite and an upper micaceous gneiss (Glover and others, 1978; Harris and others, 1982). The Petersburg granite is of batholithic proportion and extends as far south as the Virginia-North Carolina border. Zircon ages determined by Wright and others (1975) indicate an age of 330±8 million years (Mississippian) for the Petersburg granite.

The Hylas fault zone is located on the western side of the basin. The fault has a complex history of movement (Bobyarchick and Glover, 1979) and is exposed from the town of Hylas northward (Figure 2) where it defines the western boundary of the Taylorsville Triassic basin. The Hylas fault zone continues northward and may connect with the Brandywine fault system near the Maryland-Virginia border (Mixon and Newell, 1977). The Hylas zone is composed of mylonitized granite gneiss, biotite gneiss, and amphibolite with a linear northeast trend (Bobyarchick and Glover, 1979; and Goodwin, 1970). The zone is important to the interpretation of the gravity and magnetic anomalies associated with the Richmond basin. Previous gravity work (Johnson and others, 1985) and aeromagnetic surveys (U. S. Geological Survey, 1972; Virginia Division of Mineral Resources, 1971) indicate strong gradients across the fault zone

which continue southward and are observed over most of the western border of the basin. These gradients are the dominant geophysical features of the basin.

GEOLOGY OF THE RICHMOND BASIN

The Richmond basin is over 50 kilometers long and has a maximum width of nearly 15 kilometers (Figure 3). The maximum depth of the basin is about 2200 meters. The

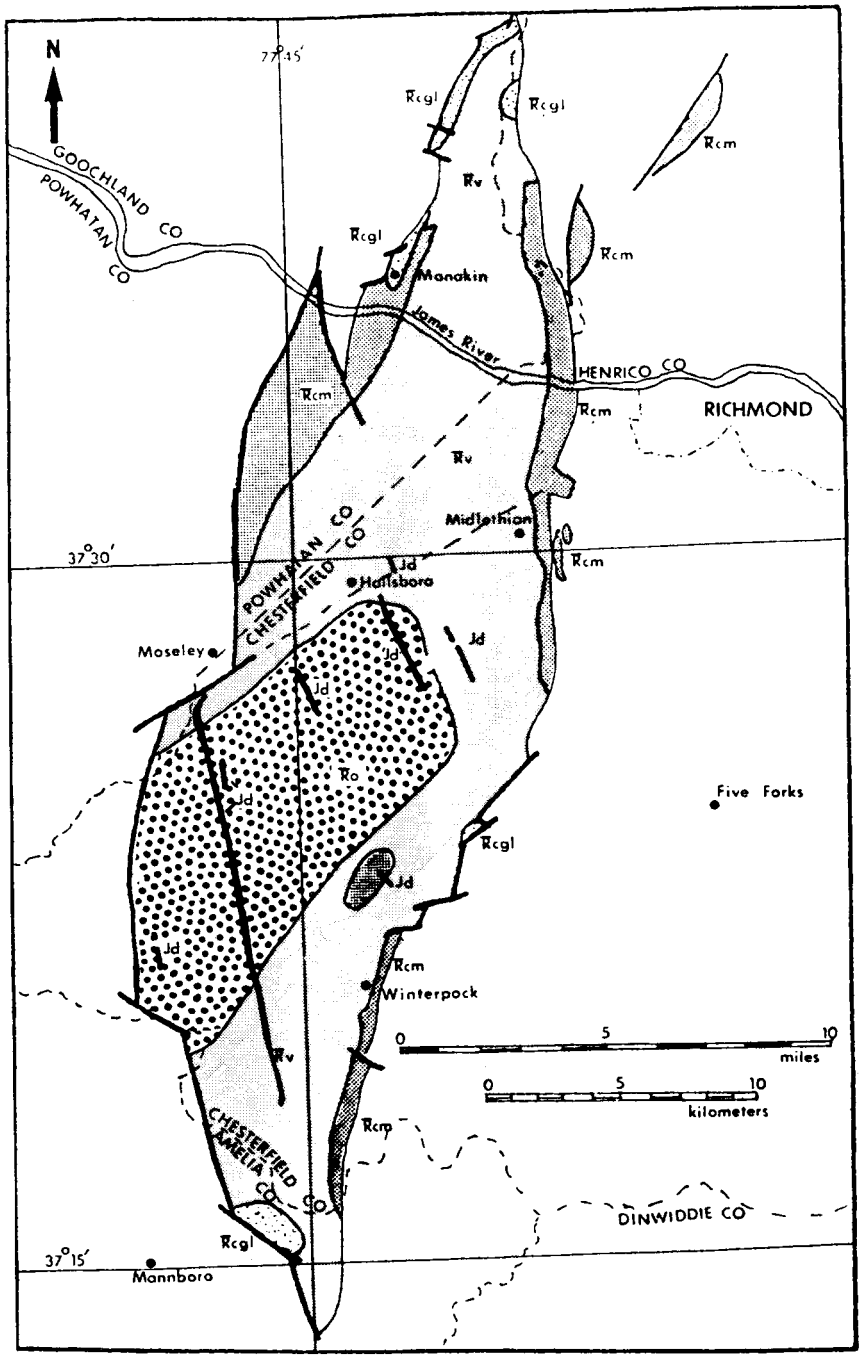

Figure 3. Geologic map of the Richmond Triassic basin, after Johnson and others (1985) with some modifications; Jd - diabase dike, Ꞧo - Otterdale Sandstone, Ꞧcm - coal measures (shale, sandstone, and coal), Ꞧcgl - boulder and conglomerate beds (gneiss, granite, and mylonite clasts), unlabeled - pre- and post-Triassic/Jurassic units.

sedimentary rocks consist of conglomerate or fanglomerate, arkosic sandstone, and siltstone deposited in a fluvial environment. Lenses of lacustrine limestone and shale, as well as coal beds, are also locally present (Bobyarchick and Glover, 1979; Weems, 1980; Johnson and others, 1985).

The stratigraphy of the basin was first described by Lyell (1847). He recognized a lower coal bearing zone and an upper series of sandstones, these were described as the Tuckahoe group, and the Chesterfield group respectively. The Tuckahoe group is comprised of three members:

1. Boulder conglomerate bed with gneiss, granite, and mylonite clasts (0 to 50 feet in thickness),
2. Lower barren sandstone and shale beds (0 to 300 feet in thickness), and
3. Interstratified beds of bituminous coal, coke, shale, siltstone, and sandstone (up to 500 feet in thickness).

The Chesterfield group is comprised of two members:

1. Vinita bed composed of fissile shale, grading upward to sandstone (this is the thickest sequence in the basin, in excess of 2000 feet) and
2. Otterdale sandstone (about 500 feet thick).

Northwest trending diabase dikes cut the Tuckahoe and Chesterfield Groups. The dikes are exposed mainly in creeks. There is no evidence to suggest that the dikes are offset by cross faults. Lutz (1986) studied these dikes using ground magnetic surveys and found several elongated, thin magnetic bodies within the basin. These bodies are found in aeromagnetic surveys (Virginia Division of Mineral Resources, 1971; Lutz, 1986).

Radiometric dating of similar dikes along the eastern continental margin of North America (DeBoer and Snyder, 1979; Ragland and others, 1983) suggests a Late Triassic to Early Jurassic age. A veneer of Tertiary gravel and loosely consolidated alluvium has been mapped by Goodwin (1970) in the vicinity of the James River. This material is considered Tertiary in age because, in part, it lies unconformably over Cretaceous sediments beyond the limits of the basin (Weems, 1974; Bobyarchick and Glover, 1979; Virginia Division of Mineral Resources, 1963).

REVIEW OF GEOPHYSICAL DATA

Le Van and Pharr (1963) collected ground magnetic data with relatively large station spacing. A major northeast trending magnetic high, about 6.5 km to 20 km in width, extending northeast from the vicinity of Sussex County into Maryland, was determined from their study. They also reported a magnetic high extending northwest from near Whaleyville, Suffolk County, to the James River. These highs were further confirmed on the Aeromagnetic Map of Virginia (Zietz and others, 1977). The total intensity aeromagnetic map of Southeastern Virginia (U. S. Geological Survey, 1972) shows the Richmond basin border fault and diabase dikes. The interior of the basin is shown as nearly featureless magnetically except for the diabase dikes. The ground magnetic profiles and the detailed work of Lutz (1986) show several elongated, narrow, and near-vertical magnetic bodies.

A Bouguer gravity contour map of southeastern Virginia (Johnson, 1975), using 1900 gravity stations over an area of 17,612 square kilometers, which includes the Richmond basin, was the first regional gravity survey completed in that area.

Published detailed gravity and magnetic data in the area of study are not available. Johnson and others (1985) conducted a detailed gravity profile along Interstate Highway 64 (I-64), using a station interval of 130 meters. This profile crosses the most northern part of the Richmond basin. Harris and others (1982) interpreted a Vibroseis profile along I-64 from just east of Staunton to a few miles west of Hampton. The I-64 gravity profile was used as an aid in the seismic interpretation. Harris and others (1982) associated the Ellisville granodiorite and State Farm gneiss with gravity lows, and the Sabot amphibolite and the Maidens gneiss with gravity highs. They also associated one amphibolite unit with high magnetic anomalies.

Johnson and others (1985) published the Simple Bouguer Anomaly Map of the Richmond Basin and Vicinity. A total of 1627 gravity observations were used for this contour map. These observations utilized benchmarks, spot elevations, surveyed elevations, and road construction centerline elevations. In Figure 4 we have constructed a new Simple Bouguer anomaly map of the Richmond basin by adding 1300 new observations. Common profiles across both anomaly maps were used for comparisons. For Figures 16 through 24 the profiles from the map published by Johnson and others (1985) are referred to with the letter J, while the profiles obtained from Figure 4 are referred to with the letter N.

FIELD PROCEDURES

State roads and U. S. highways which cross the Richmond basin were selected for gravity and magnetic surveys (Figure 1). Four profiles traverse the basin in a nearly east-west trend: the remaining cross the length of the basin in a nearly north-south trend. The vertical position of each station was determined by surveying. Benchmarks were used as base stations. A forward surveying technique was employed for calculation of station elevation. The latitude and longitude of each station was measured from 7.5-minute topographic maps. The positional accuracy of each station is about ± 25 meters in the horizontal plane and about ± 10 centimeters in the vertical plane. Five profiles shown in Figure 1 were completed by Johnson and others (1985).

A surveying transit and leveling rod were used for

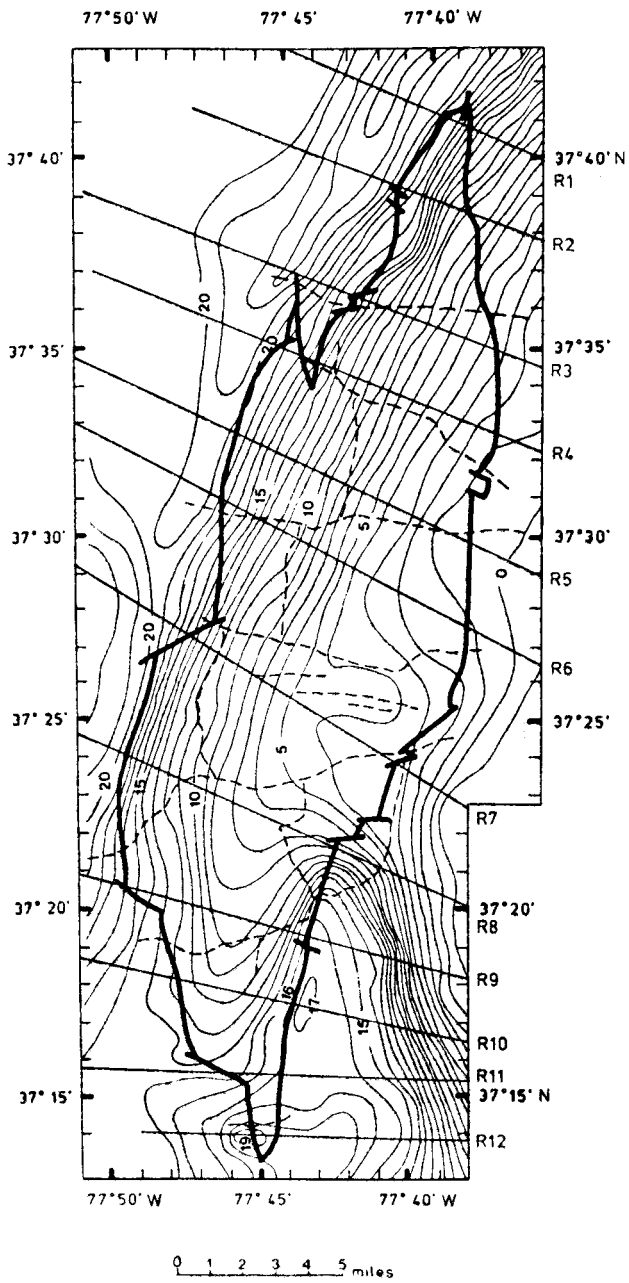

Figure 4. Simple Bouguer gravity map based on the data of Johnson and others (1985) with over 1300 new observations. The positions of profiles R1 to R12 are shown; the contoured values are in milligals.

elevation determinations. The exact horizontal distances were determined from the appropriate trigonometric relations. When possible, surveying started and ended at a bench mark. The observed errors in calculated elevation from benchmark to benchmark were about ±1.5 feet for a traverse distance of 2 to 5 miles. This error was uniformly distributed among all the stations in the traverse. The distance between stations is about 100 meters.

A Lacoste-Romberg Model G gravity meter was used for the gravity survey. This meter has a range of over 7000 milligals and a reading accuracy of ±0.1 milligal, with a drift rate of less than 1 milligal per month.

A Scintrex model MFD-4 digital fluxgate magnetometer was used for measurement of the relative value of the vertical component of the magnetic field. The magnetometer has a resolution of 1 gamma and a range of -99.999 to +99.999 gammas.

Each gravity survey started and ended at the Virginia Gravity Net Base Station located at Chesterfield Court House (latitude = 37°22'34" N; longitude = 77°30'25" W; elevation = 209.652 feet). The absolute gravity value of the Chesterfield Base Station is 979929.27 ±.02 milligals (Johnson and Ziegler, 1972). All gravity and magnetic observations were made by utilization of a modified ladder-sequence loop technique. The time interval between two consecutive occupations of auxiliary base stations was kept to less than two hours. The gravity anomalies are reduced with respect to the International Gravity Formula of 1930.

INTERPRETATION OF GRAVITY DATA

REGIONAL INTERPRETATION

The simple Bouguer gravity anomaly map, Figure 4, indicates a gravity gradient, with a range of about 25 milligals, extending in a north-northeast direction. This gravity gradient corresponds closely with the Hylas fault zone. Profiles HI and H2 (Figures 5 and 6) are gravity cross sections constructed from data obtained by Johnson and others (1985). Positions of profiles HI and H2 are slightly outside Figure 4, and therefore not shown. These profiles indicate the magnitude of the gravity anomaly caused by the Hylas fault zone. The Petersburg granite is exposed in this and nearby areas. West of the Hylas fault zone, the Maidens gneiss is exposed at the surface and the State Farm gneiss and the Sabot amphibolite are at depth (Figure 2). The Hylas fault zone is interpreted as causing the Bouguer anomaly shown in the cross sections. The Richmond basin does not influence these two profiles.

Additional cross sections across the Richmond basin are labeled as R1 through R12 on Figure 4. The basin increases in width to the vicinity of profile R6. Profile R1 extends across only about 2 km of the basin and profile R6 extends across about 12 km. These cross sections have the same characteristics as profiles H1 and H2. The gravity gradients seen on these profiles are interpreted as anomalies due to the basin and indicate further extension of the Hylas fault southward. The gravity signature of the Hylas fault zone continues to profile R6 and dominates the expected Bouguer gravity anomaly low due to the basin. As a preliminary interpretation, the subsurface mass distribution was made to match profiles H1 and H2. Modifications were then made by appropriate supposition of a basin with various depths. Well

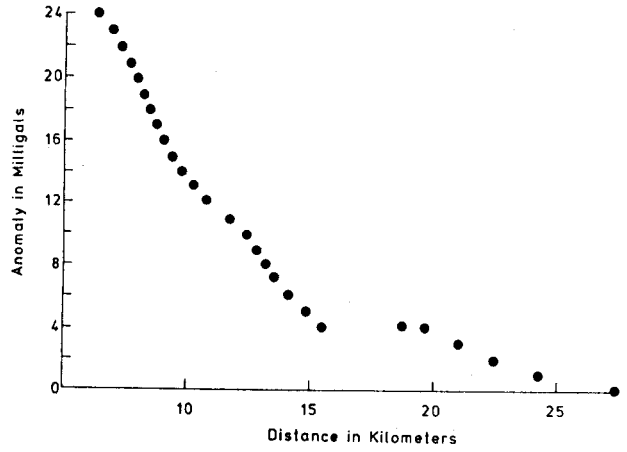

Figure 5. Profile H1, taken from Johnson and others (1985). The Y axis is the simple Bouguer anomaly in milligals; the X axis is the horizontal distance in kilometers. Profiles are located slightly off the northeast corner of Figure 4. The orientation of these two profiles is nearly parallel to the orientation of profile R1 (Figure 4).

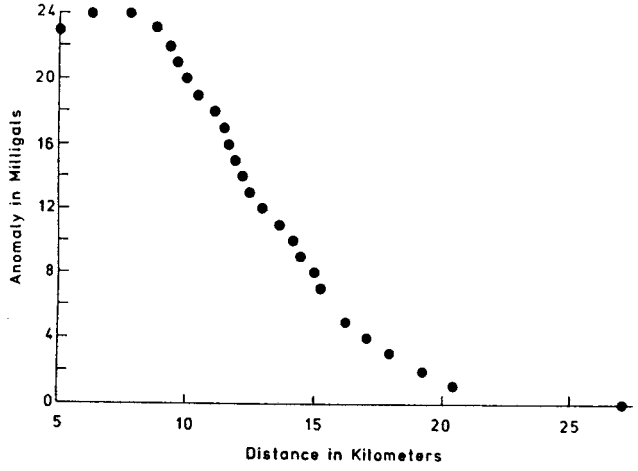

Figure 6. Profile H2, see Figure 5 for explanation.

data indicate that Triassic lithologies are present to a depth of about 2200 meters within the basin (Johnson and others, 1985).

HYLAS FAULT ZONE

Interpretation of gravity data is difficult because the solutions are non-unique and a variety of models may satisfy the same data set. In Figure 7, three models, and in Figure 8, six models are presented that produce an anomaly similar to that of profiles H1, H2, and R1 through R6. In all cases, west of the fault, the gravity high is about 24 milligals, and to the east of the fault it is around zero. Although the general character of the theoretical curves given in Figures 7 and 8 is similar, a maximum of 24 milligals at the left which de-

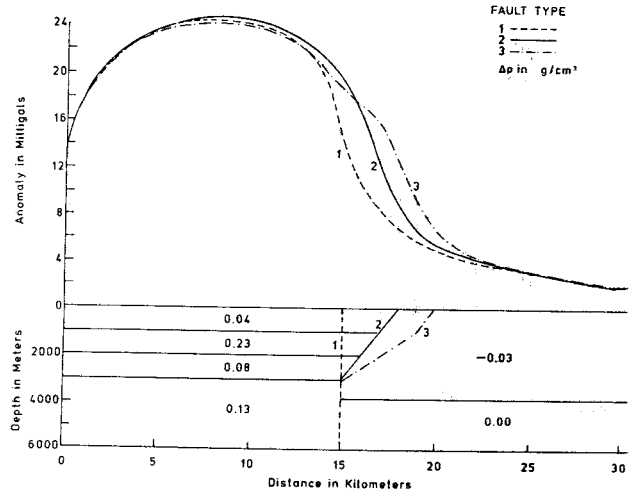

Figure 7. Variation of the gravity anomaly over a fault due to variation of the fault plane. In this figure the Hylas fault is marked by the contact between a series of horizontal layers on the west with the Petersburg granite on the east. Three curves indicate the three anomalies resulting from the three forms of contact given in the lower section. These models were not in agreement with the other geophysical data, Harris and others (1982), and were discarded. The numbers on the layers refer to density contrast in g/cm³. The reference density is 2.67 g/cm³.

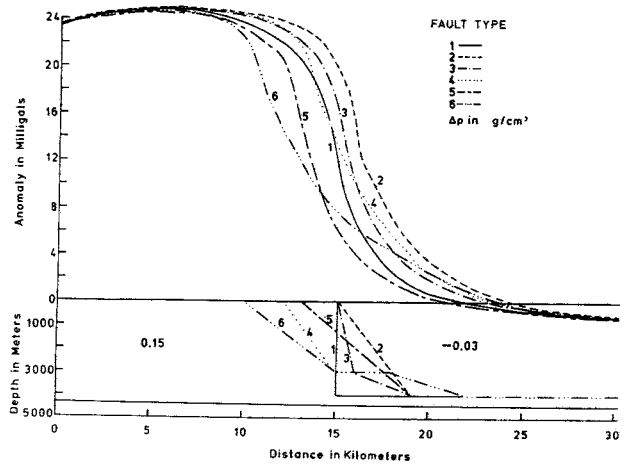

Figure 8. Six possible fault planes for the Hylas fault. In this figure a "lumped-sum" mass model consisting of only two materials is used for simplicity. The models, however, are in better agreement with the other geophysical and geological data than the previous models. Density contrast is in g/cm³.

creases to near zero on the right, the two subcrustal mass distributions are quite different. In Figure 7, the subsurface mass distribution is a "pancake" model, that is, there are horizontal layers with different thicknesses and densities. Figure 8 is a simple "lumped-sum" mass model. These

models contain only two layers which have different thicknesses and densities. For both models, rather minute variations in the gravity anomalies around the fault surface can be obtained by variation in the configuration of the layers on both sides of the fault plane. For this study, the gravitational effect of the fault and the basin were examined. The "lumped-sum" mass model was chosen as the preferred model. The seismic interpretation of Harris and others (1982) indicates that the Hylas fault zone dips toward the east. The type 4 model given in Figure 9, defined by a granitic layer with thickness of about 4500 to 5000 meters, agrees with the seismic interpretation. The fault plane varies in dip with depth. In the preferred model the fault has a dip of about 26° toward the east to a depth of about 3 km, then dips east at about 18° to a depth of 4 km; at 4 km the fault plane is horizontal. This is interpreted as a thrust fault where the Petersburg granite is thrust over the Goochland complex to the west.

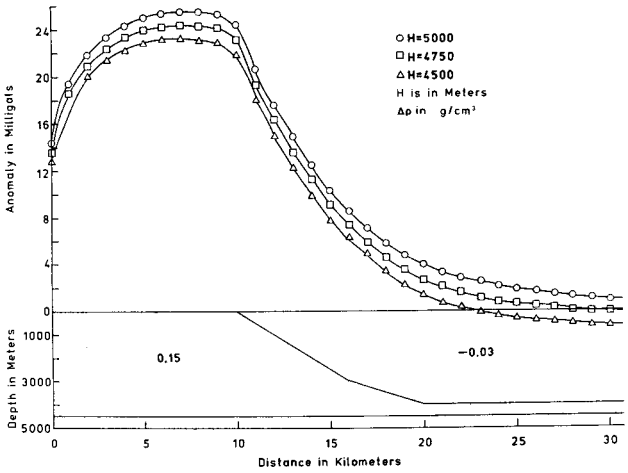

Figure 9. An interpretation of the Hylas fault; three depths for the master decollement are assumed.

Figure 10 shows the structure and the gravity anomaly of profile H1. This model agrees satisfactorily with the profile. There is some difference between profile H1 and profile H2 at distances greater than 20 km. This is probably caused by a slight variation in the thickness of the granite due to the westward thrusting. Theoretical gravity, subsurface mass distribution, and profile H2 are shown in Figure 11. The match indicated is very good except in the area near the 14 and 15 km marks. Slight variation in the dip of the thrust plane in this area might improve the model.

THEORETICAL ANOMALIES AND GRAVITY MODELING

The shape of the gravity anomaly caused by a basin about the size and shape of the Richmond basin was considered in some detail. A density contrast of -0.2 g/cm³ was arbitrarily selected. Many researchers believe that the density contrast for this area is between -0.10 and -0.2 g/cm³ (Davison, 1985). Density acts as a scale factor for the gravity anomaly. Thus, if a density of -0.1 g/cm³ were assumed, the values of the gravity anomaly shown would have been half the values presented. If Δp = -0.15 g/cm³, the values presented must be multiplied by 0.15/0.2.

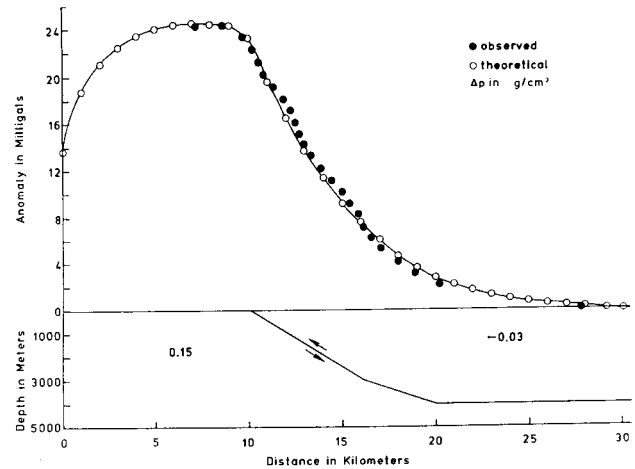

Figure 10. An interpretive geometry for the Hylas fault along profile H1. The model indicates a granitic layer, (-0.03 g/cm³) , thrust over the Goochland complex, (0.15 g/cm³) .

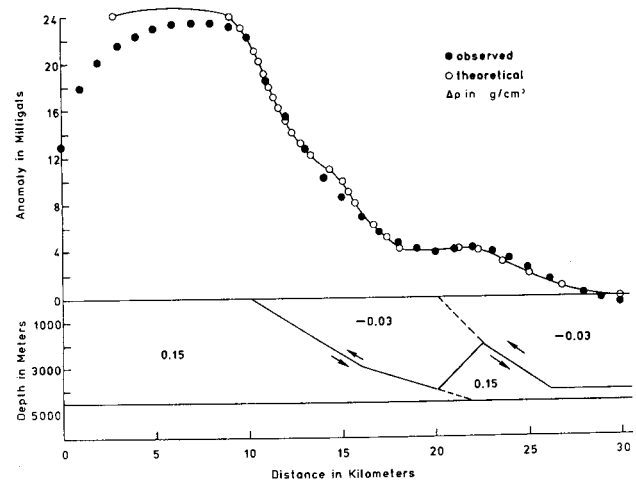

Figure 11. An interpretive geometry for the Hylas fault along profile H2. A second thrust has been added due to the variation in the Bouguer anomaly between 17 and 26 km.

Figure 12 shows the shape of anomalies, as a function of depth, for a rectangular basin of 10 km width as the depth increases from 500 to 3000 meters. As depth increases, the maximum value of the anomaly increases. This increase, however, is not linear and the rate of increase decreases with depth. As depth increases, the shape of the anomaly changes from a rectangular shape at a depth of 500 meters to a domal shape at a depth of 3000 meters. The position of the basin

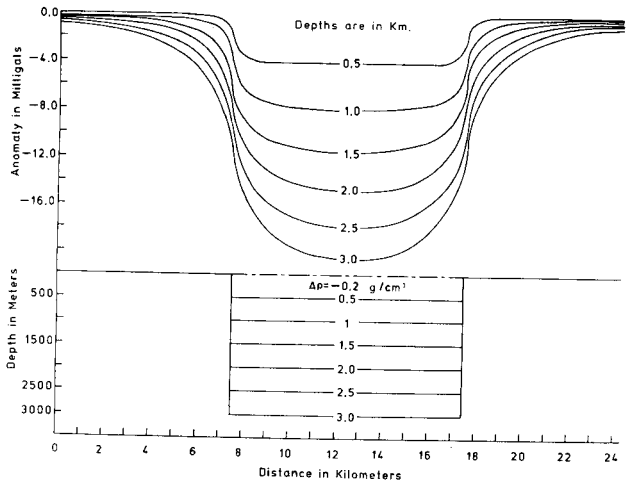

Figure 12. Variation of the theoretical anomaly due to variation of depth of a rectangular basin. The width of the basin is assumed constant, 10 km; the depth ranges from 0.5 to 3.0 km in steps of 0.5 km.

borders are closely related to the inflection points of the graph of a computed anomaly.

Figure 13 shows the change of the width of the anomaly as the basin width is increased. For the sake of simplicity, the depth was kept constant at 500 meters. It is clear from this figure that although the increased width changes the maximum value of the anomaly, these variations are only a few tenths of a milligal. However, as the width increases, the distance between the inflection points increases. For a rectangular basin, the basin's width can be obtained from the distances between the inflection points of the anomaly's graph.

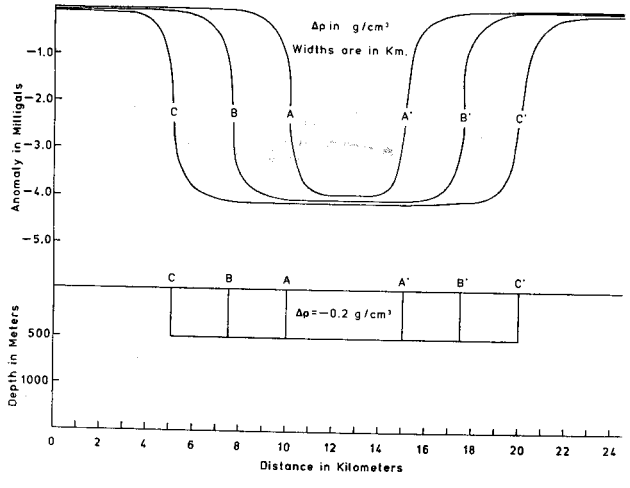

Figure 13. Variation of the theoretical anomaly due to variation of basin width.

The Richmond basin is interpreted as a half graben. This model is indicated in Figures 14 and 15. Figure 14 shows the theoretical anomaly for a half graben model as a function of depth. The left side of the graben is vertical, and the depth is varied from 500 to 2000 meters. The gravity anomaly varies in accordance with the depth and is asymmetrical. The maximum value moves toward the right as depth increases. The inflection point on the graph of an anomaly gives the position of the fault. Figure 15 shows the shape of the anomaly when the depth is kept constant at 2000 meters. The deepest point of the basin was moved toward the right at an increment of one kilometer. The maximum value of the anomaly occurs about one kilometer to the right of the point of maximum depth.

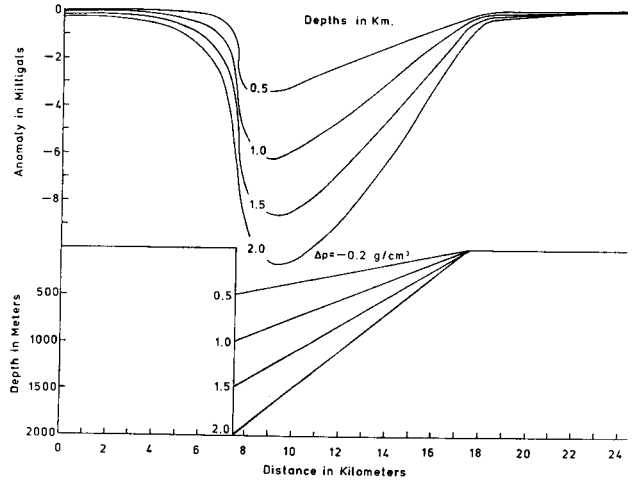

Figure 14. Variation of the theoretical anomaly due to variation in depth of a half graben. Depths range from 0.5 to 2.0 km.

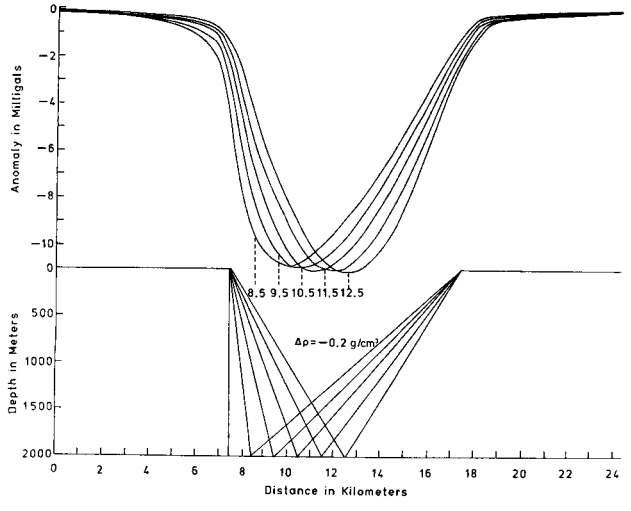

Figure 15. Variation of the position of maximum theoretical anomaly due to variation of the position of maximum depth in a half graben. In all the theoretical calculations $\Delta p = -0.2$ g/cm³ was assumed. Δp acts as a scaling factor; thus the anomaly for $\Delta p = \Delta p_1$ can be read by multiplication of the theoretical anomaly by $\Delta p_1/0.2$. Positions are in kilometers from the origin.

GRAVITY MODELING OF THE BASIN

In order to determine a cross section for the basin, a curve-matching modeling technique was adopted. In this method, a theoretical anomaly is computed for a possible subsurface structure, and the resulting anomaly is then compared to the observed anomaly. The shape of the model; the mass distribution; the position of the fault, or faults, and the layers were modified while the computations were repeated until a reasonable match was obtained. This method does not find a unique structure, that is, many models may give the same anomaly. To reduce this number of models to a few, knowledge of the regional geology is essential. In constructing the subsurface structure, the tectonic style of the region as shown by Harris and others (1982) was used. For the calculation of the theoretical anomalies, the rapid computational technique proposed by Talwani and others (1959) for the calculation of a gravity anomaly due to two-dimensional bodies was adopted.

Figure 16 gives an interpretation of profile R1. The Hylas fault zone is under the basin near its western edge. Two possible shapes of the basin and their corresponding theoretical anomalies are seen in the upper part of the figure. This profile traverses about 2 km of the basin. The observed anomaly is mainly determined by the Hylas fault zone and is affected only slightly by the structure of the basin.

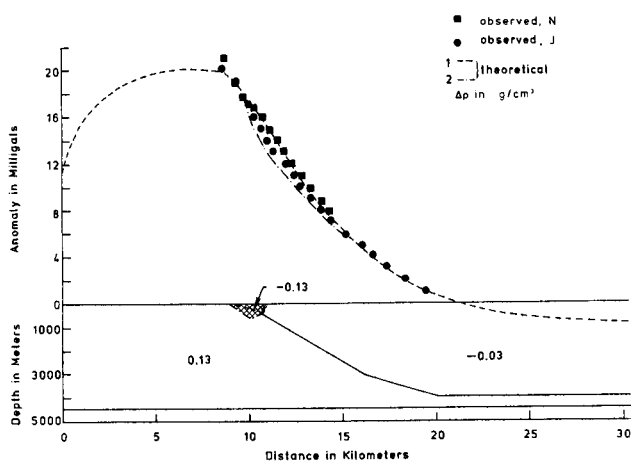

Figure 16. Two interpretive models for the basin along profile R1. Maximum depth is between 300 to 750 meters. The Hylas fault is at the bottom near the eastern edge of the basin. In this figure and the following figures the boundariesof the two basins are marked by cross hatches. In this profile and all other profiles, the density contrast is in g/cm³. In Figures 16 through 24, J refers to a profile across the Simple Bouguer Anomaly Map by Johnson and others (1985) and N refers to a profile across the Bouguer Anomaly Map given in Figure 4.

Figure 17 gives an interpretation of profile R2. The Hylas fault zone forms the western border of the basin. A thin layer of a dense material, $\Delta\rho = 0.23$ g/cm³ probably the Sabot amphibolite (s), is thrusted and underlain by the fault plane. A second thrust, at a distance of 17 to 20 km, has been proposed. This profile traverses about 3.8 km of the basin. Two models of the basin are presented; both have a maximum depth of about 1000 meters.

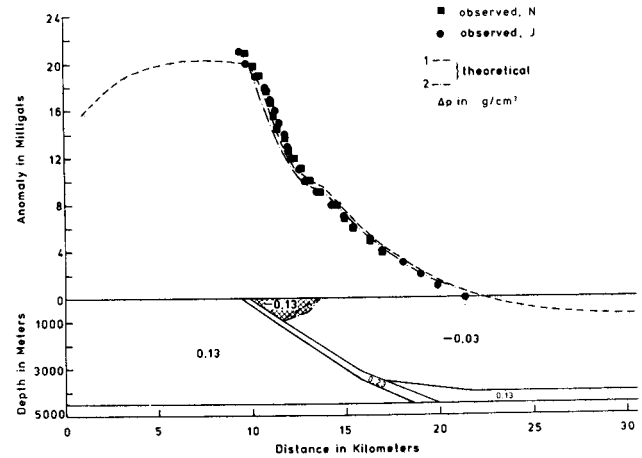

Figure 17. Two interpretive models for the basin along profile R2. Maximum depth is about 1000 meters.

Figure 18 presents an interpretation of profile R3. The denser layer, $\Delta\rho = 0.23$ g/cm³, is thicker, probably due to a bedding fault, and the proposed thrust at a distance of 17 to 20 km appears more pronounced. This cross section traverses about 7.5 km of the basin. The basin in this model has a flat bottom at a depth of about 1000 meters. Figures 19 and 20 present interpretations of profiles R4 and R5. The profiles traverse about 11.5 and 13.5 km of the basin, respectively. The dense layer is thicker, probably because of additional bedding faults. The basin fill thickness in both profiles is about 1500 meters.

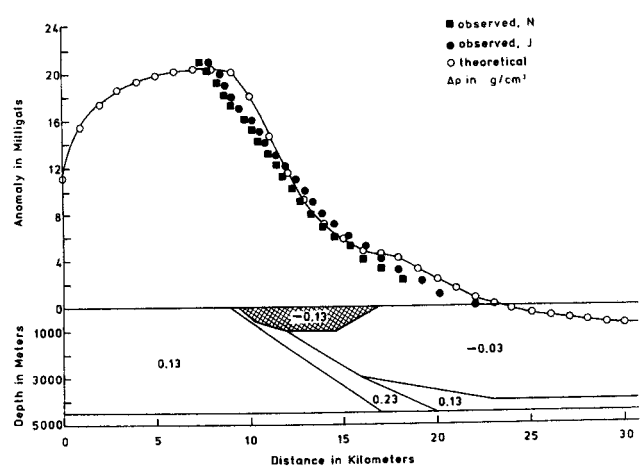

Figure 18. Interpretive model for the basin along profile R3. Maximum depth is about 1000 meters.

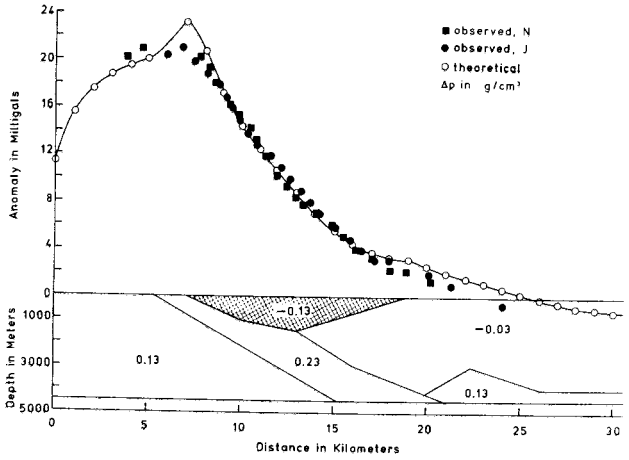

Figure 19. Interpretive model for the basin along profile R4. Maximum depth is about 1500 meters.

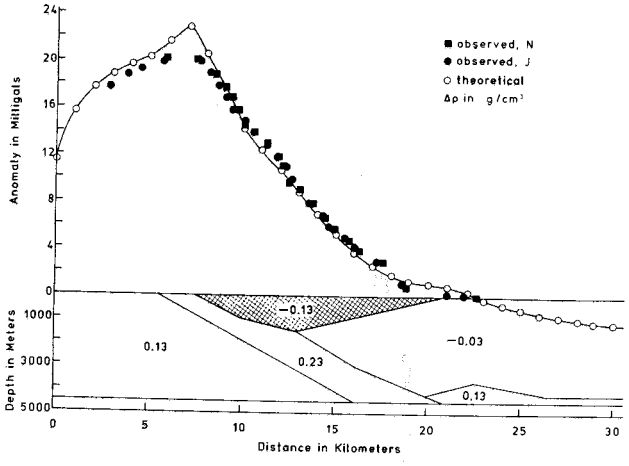

Figure 20. Interpretive model for the basin along profile R5. Maximum depth is about 1500 meters.

Figure 21 represents an interpretation of profile R6 which traverses about 13.5 km of the basin. The western edge of the basin is rather steep, but its eastern edge has a gentle dip, and its maximum depth is about 1500 meters. This profile intersects two dikes which were not modeled in the subsurface structure. Their effects on the profile are seen by a difference between the observed anomaly and the theoretical anomaly at a distance of 14 to 16 km on the cross section.

Figure 22 is an interpretation of profile R7. It is very similar to profile R6, except the thickness of denser material is slightly increased and the thrust fault at a distance of 20 to 24 km is more pronounced. The depth of the basin is about 1500 meters.

The surface geology surrounding the basin changes south of approximately 37°22.5'N latitude, where along both the eastern and western borders of the basin, a mica gneiss is exposed. The effects of these changes in geology are seen in the form of observed gravity anomalies. Profile R7 is mainly

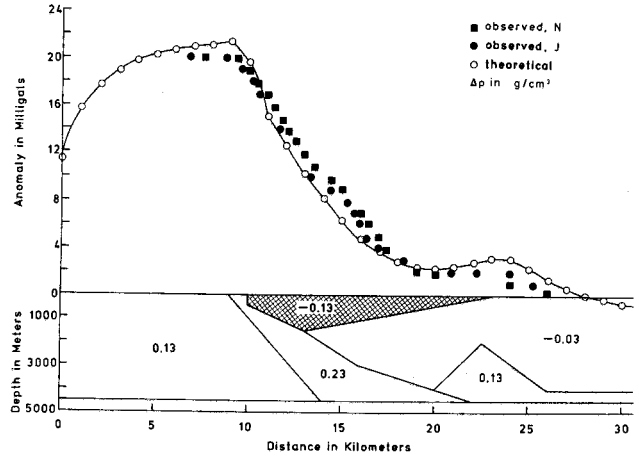

Figure 21. Interpretive model for the basin along profile R6. Maximum depth is about 1500 meters. The western edge is steeply faulted.

affected by the Hylas fault zone (Figure 22). There is a sharp contrast between the form of this profile and profiles R8 and R9, (Figures 23 and 24). In these profiles, a local minimum is observed which can be approximately correlated with the boundary of the basin in profiles R8, Figure 23, and well correlated with the boundary of the basin for profile R9, Figure 24. Profile R8 traverses about 11 km of the basin; a mica gneiss is present on the basin boundary and was given a density contrast of 0.23 g/cm³ (Figure 23). The maximum thickness of the basin fill in this area is about 2000 meters. Profiles R11 and R12 traverse 2.5 and 1.3 km of the basin respectively. These profiles do not indicate a major anomaly due to the basin and are not shown.

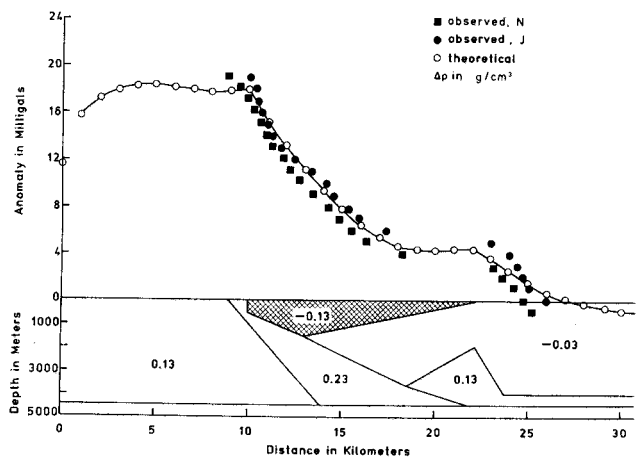

Figure 22. Interpretive model for the basin along profile R7. Maximum depth is about 1500 meters.

Profile R9 (Figure 24) is located in the vicinity of State Road 602, and it reflects the basin's shape and geometry. The effects of the Hylas fault zone are not particularly evident on this profile, probably because the fault lies west of the basin's margin. Two methods are used for interpretation

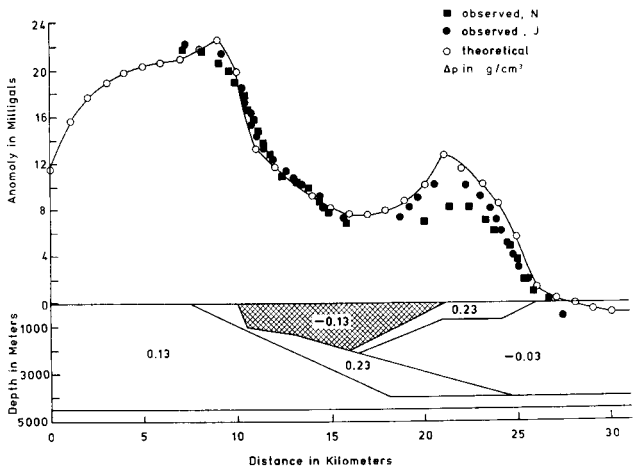

Figure 23. Interpretive model for the basin along profile R8. Note that the character of this profile and profile R9 is different from that of the preceding profiles because of a local depression which can be correlated with the basin boundary. The maximum depth is about 2000 meters and there are two down-slope faults along the western border.

of this profile. The first method, as discussed before, is based on local geology and the technique proposed by Talwani andothers (1959). Geological information indicates that the basin is bounded by a mica gneiss on both sides. The basin has a depth of about 2300 meters at this locality. Both profiles R8 and R9 indicate a step fault near the western margin.

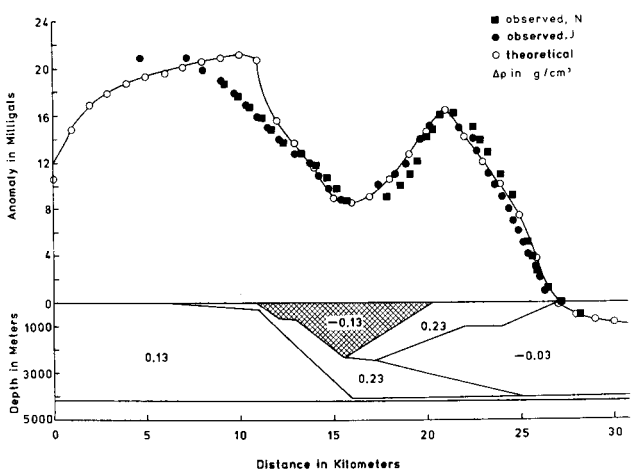

Figure 24. Interpretive model for the basin along profile R9. The maximum depth is about 2300 meters.

In the second method, the shape of the basin is obtained in a direct way. As was mentioned before, an observed gravity profile can be the result of an infinite number of different subsurface masses. However, the uncertainty in this method may be reduced or even eliminated, if certain valid geological assumptions can be made. In an ideal situation a unique solution may be obtained if the density contrast between the basin rock and the surrounding rock is known and the regional anomaly is completely corrected for, or if a regional anomaly does not exist. In practice, it is possible to determine the shape of the cross section of a two- dimensional basin from regionally corrected gravity anomalies using trial and error technique. Bott (1960) proposed this technique and applied it to the Dumfries New Red Sandstone basin in southern Scotland. The technique is based on equations derived by Heiland (1940) for the vertical attraction of a rectangular prism.

A gravity profile along State Highway 602, which is close to profile R9, is suitable for interpretation by the "Bott technique" because it appears that there is no regional field superimposed on the profile. Density contrasts of -0.10, -0.13, and -0.15 g/cm^3 were used for the interpretation (Figure 25). Assuming that Δp = -0.13 g/cm^3 is reasonable, the smoothed depth is about 2000 meters. This depth is in agreement with our previous interpretation of profile R9 using the modeling technique of Talwani and others (1959). The irregularities in depth near the western margin of the basin and at its middle part are interpreted as a possible step fault.

Profiles R10, R11, and R12 are not shown because profile R10 is probably affected by a fault on its eastern border, and the maximum widths of the basin along these profiles are about 6, 3, and 2 km respectively.

INTERPRETATION OF THE MAGNETIC DATA

The northwest boundary of the Richmond basin is well marked on the aeromagnetic map by a gradient which is associated with the Hylas fault zone (Figure 26). The other segments of the basin's boundary are not associated with this magnetic gradient. Much of the basin is magnetically featureless. Magnetic anomalies over the eastern part of the basin are probably related to crystalline rocks of the shallow floor of the basin. A discussion of a linear feature, which is related to a dike, is presented.

A long, narrow linear magnetic anomaly in the southwest area of the basin is interpreted as a major dike (Figures 26 and 27). Ten vertical-component magnetic profiles were measured across this feature by Lutz (1986).

The doubly plunging Sabot amphibolite unit west of the basin is well marked by a concentrated narrowing of the magnetic gradient which forms a closed contour pattern (Figure 26).

The State Farm gneiss is magnetically featureless. The mica phyllite and hornblende gabbro which occur outside the southern border of the Richmond basin are marked by a series of linear magnetic contour lines. Some downslope high-magnetic anomalies which are associated with the mica gneiss occur outside of the southwest border of the basin. A pattern of closed contour lines, associated with the Petersburg

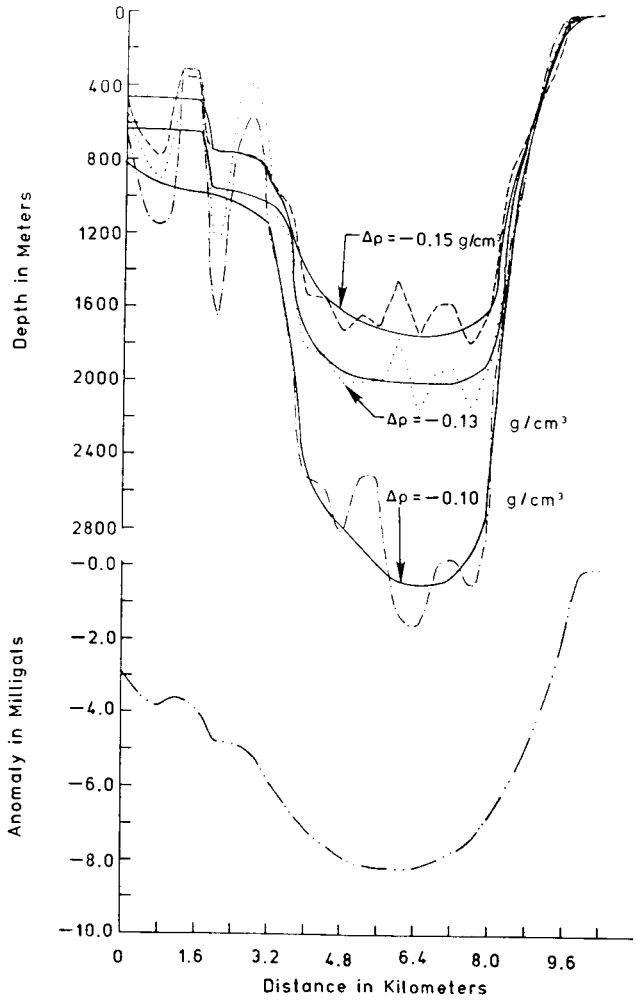

Figure 25. Three structural interpretations of the gravity profile along State Road 602 assuming Δp = -0.1, -0.13 and -0.15 g/cm^3, using Bott's technique. The position of this profile is near the position of profile R9. This technique gives an average maximum depth of 2000 meters for Δp = -0.13 g/cm^3, but it extends to a depth of 2150 meters. The variations in the observed anomaly near the western edge and middle of the basin are interpreted as possible faults. Solid lines are the smoothed depth profiles obtained from the three density contrasts.

granite, is the dominating feature east of the basin margin (Figure 26).

Figures 28 through 37 present ten vertical-component magnetic profiles measured at ground level across a diabase dike. The position of each profile is shown on Figure 27. These profiles were modeled using the technique proposed by Talwani (1965). Data pertaining to the magnetic susceptibility of the Triassic lithologies and diabase are not abundant. Sumner (1977) gives a range of 73 x 10 to 100 x 10 emu and 3000 x 10 emu for the Triassic lithologies and diabase in the Newark-Gettysburg basins. Various geometries were used to model the dike. Because the magnetic anomaly is very narrow and almost linear between the position of profiles 1 and 10 a vertical dike model, with sides marked by the arrows (Figures 28 to 37) was used. The agreement between the observed and calculated values is relatively good. The profiles indicate that the thickness of the dike ranges from 15 to 30 meters and the depth to the top of the dike ranges from 5 to 35 meters. These depths are plausible from surface geological observations (Lutz, 1986). The depth is greatest at both ends of the dike and is least in between.

DISCUSSION

Interpretation of the gravity anomaly due to the Richmond basin is complicated because the gravitational signature of the basin appears to be masked by the gravity gradient associated with the Hylas fault zone. Many of the gravity profiles do not show a depression in the anomaly as would be expected from the less-dense lithologies in the basin. The depression is visible only on profiles R8 and R9 and to some extent on profile R10. On this latter profile the depression in the anomaly may be masked by the gravity gradient associated with the basin's eastern boundary fault. Theoretical modeling of profiles R1 through R7 (Figures 16 through 22) indicates that the form of the theoretical curve is very sensitive to the shape of the basin. For example, in profiles R1 and R2, a slight variation in the shape of the two proposed basin models causes a relatively large deviation between the corresponding theoretical anomalies and the observed anomaly.

In interpreting the profiles attempts were made to use only a few "lumped-sum" mass layers. For example, the entire Hylas fault zone is represented by two layers of the Petersburg granite (a density of 2.64 g/cm^3 or a Δp = -0.03 g/cm^3, and a layer with a density of 2.8 g/cm^3 or a Δp = 0.13 g/cm^3).

Geologic data (Figure 2) indicate that in the northwestern area of the basin the State Farm gneiss, Sabot amphibolite, and Maidens gneiss are exposed. The interpretation of the seismic profile along I-64 (Harris and others, 1982) extends these formations under the basin through a series of thrust faults which are connected to a nearly horizontal, master decollement. The data in Table 1 indicate that the range of densities for the Sabot amphibolite, State Farm gneiss, and Maidens gneiss is 2.71 to 2.81, 2.72 to 3.12, and 2.61 to 2.76 g/cm^3 respectively. In modeling, the effect of the fault is represented by a layer of material with a density of 2.8 g/cm^3 and the effect of the splay-faulted Sabot amphibolite, under the basin is represented by a layer with a density of 2.9 g/cm^3. The density of the mica gneiss which is exposed on both sides of the southern segment of the basin is shown by layers with a density of 2.9 g/cm^3 or Δp = 0.23 g/cm^3. This is within the range of 2.59 to 3.00 g/cm^3 given for the density of gneiss in Table 1 (see also Telford and others, 1976). Because of non-uniqueness associated with interpretation of gravitational data, these layers could be

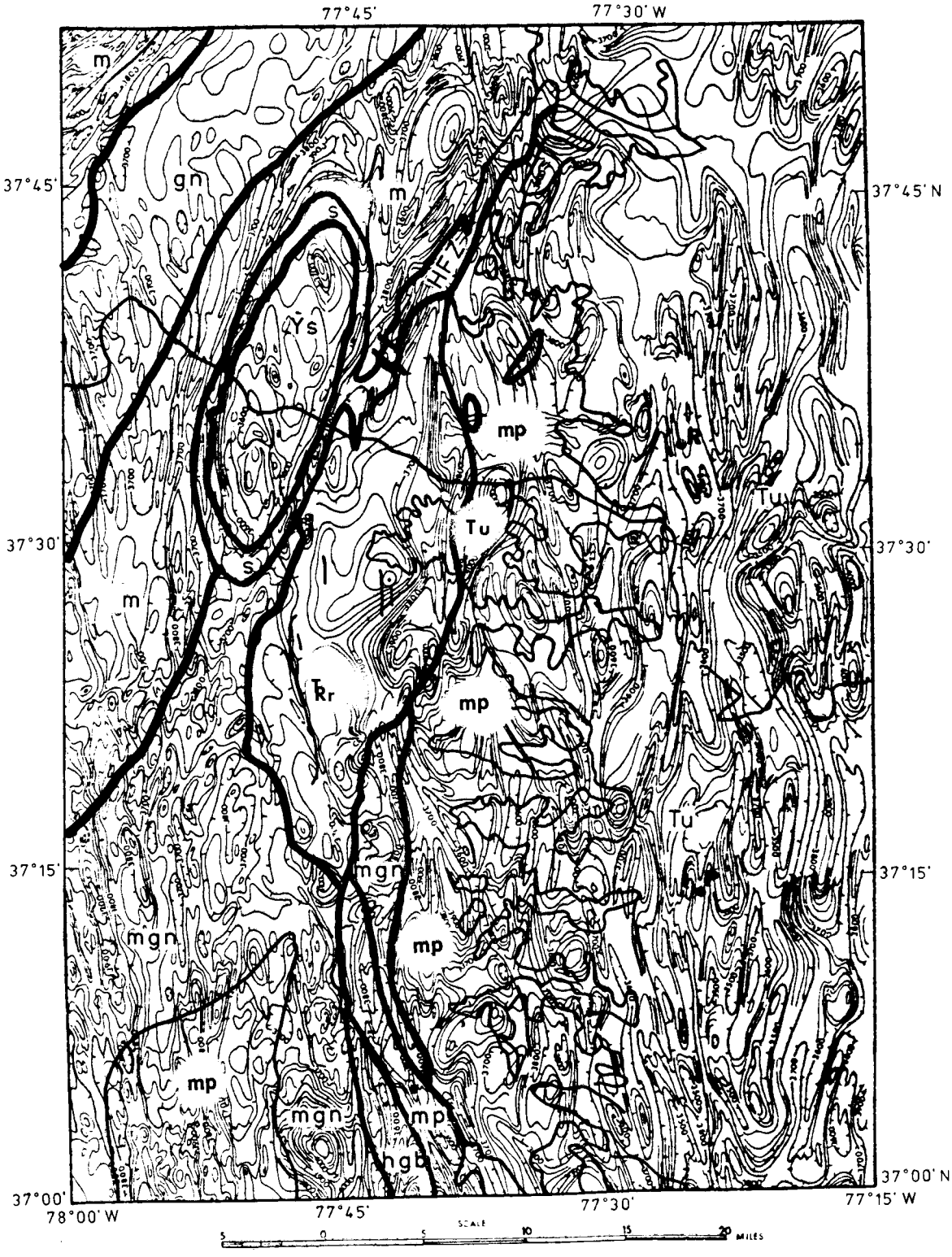

Figure 26. General interpretation of the total magnetic field of the Richmond basin and vicinity. Magnetic data are taken from various aeromagnetic maps prepared for the U. S. Geological Survey and the Commonwealth of Virginia. The designated nomenclatures are the same as in Figure 2. The contour intervals are 20 gammas.

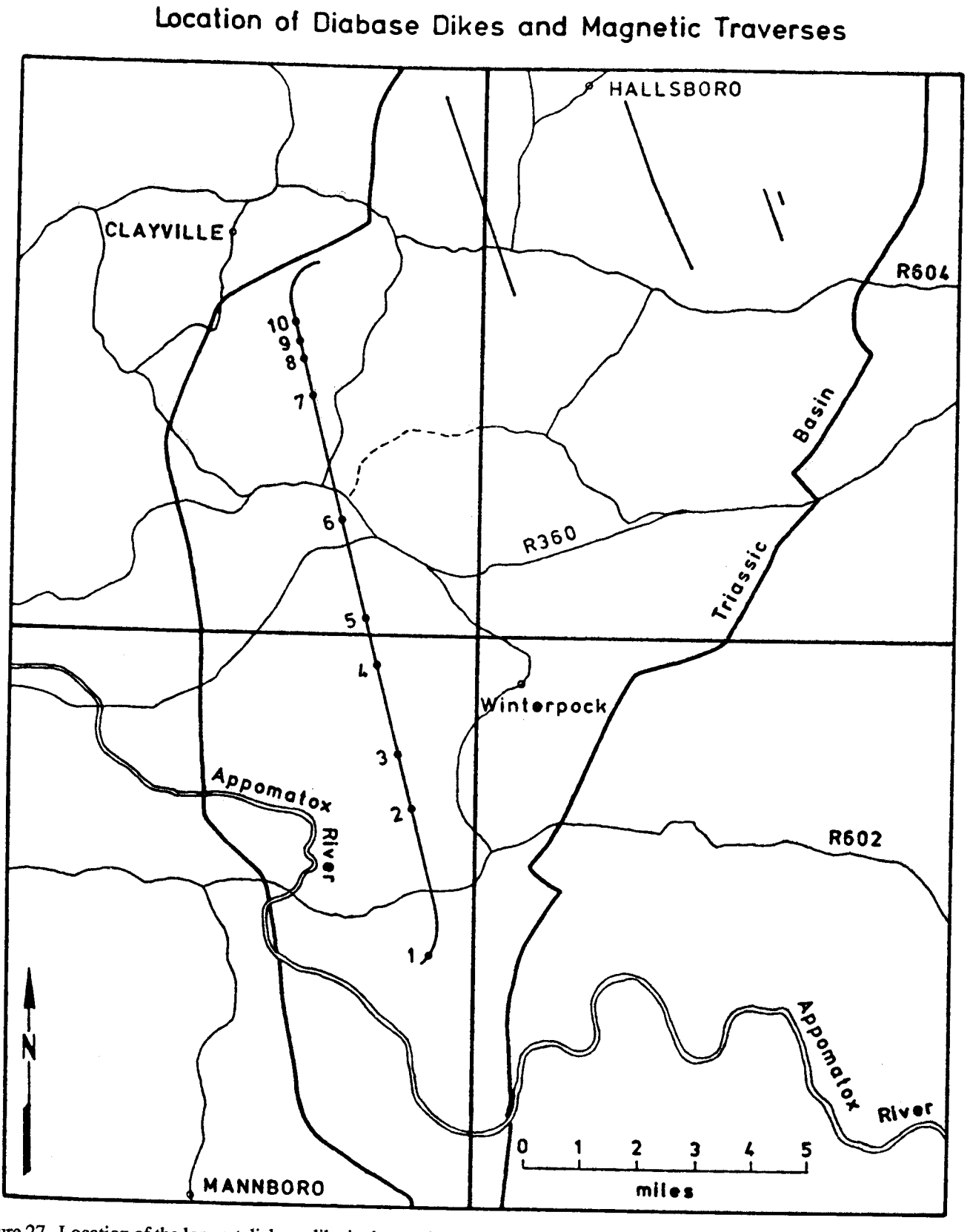

Figure 27. Location of the longest diabase dike in the southern part of the Richmond basin and position of the 10 profiles across the dike.

thinner with a higher density contrast or thicker with lower density contrast. In order to resolve the exact shape and the thickness of these layers a detailed seismic survey would be necessary.

The Hylas fault zone is not the western border of the basin in all of the profiles. In profile R1 (Figure 16), it is nearer to the eastern border at a depth of about 300 to 400 meters. In this profile, the denser layer was not included as it is not seen on the surface, but this layer was included in profiles R2 through R8. In general, the thickness of this layer increases from north to south. Two fault planes are indicated in profiles R2 through R8 as the contact between the Petersburg granite and the denser layer, $\Delta p = 0.23$ g/cm^3, and the contact between the denser layer and another layer with a density contrast of $\Delta p = 0.13$ g/cm^3. The first fault plane is terminated at the deepest part of the basin, and the other plane is seen slightly west of the basin margin. Profiles R6, R7, R8, and R9 (Figures 21 through 23) indicate step faults at the western margin of the basin. It may be concluded that the western boundary of the basin is not a simple onlap. Available geologic, magnetic, and gravity data support step faulting. Sumner (1977) came to a similar conclusion, using gravity, magnetic, and geologic data, for the southern margin of the Newark-Gettysburg Triassic basins in Pennsylvania. In many of the models, the Hylas fault zone and the border faults are basinward of the margin and the margin indicates an onlap. The shape of the models indicates a half graben basin, where the western border fault is near the western margin, and Triassic sediments are in depositional contact with the Petersburg granite on the eastern margin. In the southern part of the basin, the mica gneiss is exposed at both sides of it. This is interpreted in profiles R8 and R9 (Figures 23 and 24) as the mica gneiss thrusted upward by the granite; the bottom of the basin is formed by mica gneiss. This may be the reason for the development of a depression in the observed anomalies on profiles R8 and R9. Because of this particular situation, the effect of the Hylas fault is not discernible on these profiles. These profiles may be interpreted by the Bott method (1960). The effective density is the only parameter needed for this method. Because of uncertainties a range of -0.10 to -0.15 g/cm^3 is used. Figure 25 indicates a thickness of 1650 meters for $\Delta p = -0.15$ g/cm^3; a thickness of 2950 meters for $\Delta p = -0.10$ g/cm^3; for $\Delta p = -0.13$ g/cm^3 this value is 2000 meters which is a reasonable thickness for the southern part of the basin. The maximum depth is, however, about 2200 meters. This depth is close to the reported depth of 7300 feet of the Triassic rocks in the middle of the Richmond basin by Johnson and others (1985). The profile also indicates two step faults near the western border and a possible small central fault at the deepest part of the basin. This would be in the form of a small horst. The horst may be indicated by a slight relative high in the depression seen on profile 602, (Figure 25).

A diabase dike crosses the basin from its southern tip to its western border (Figure 27) in a north-northwest direction and coincides with a linear magnetic anomaly. Magnetic modeling indicates that the dike has a width of about 15 to 30 meters, has a range of depth of 5 to 35 meters, and is nearly vertical.

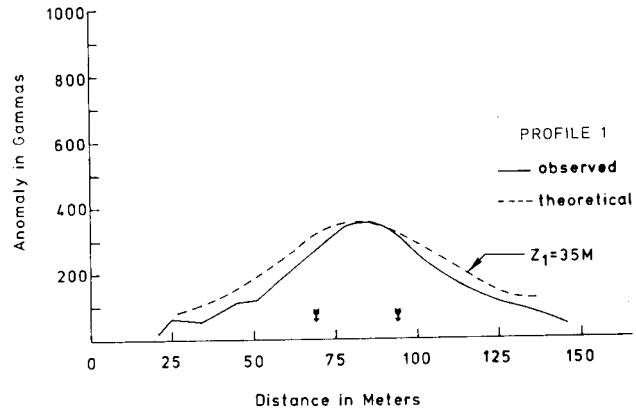

Figures 28 through 37. Observed and calculated values of the vertical component of the magnetic field. The Y-axis is the anomaly in gammas, the X-axis is the horizontal distance in meters. Position of the dikes are marked by the two downward arrows. The parameter Z indicates the depth to the top of the dike. A susceptibility contrast of 5000 x 10 emu was used in modeling. A total field intensity of 65,000 gammas and an inclination angle of 70° were used for the model. The trend of the dike is about north 15° west.

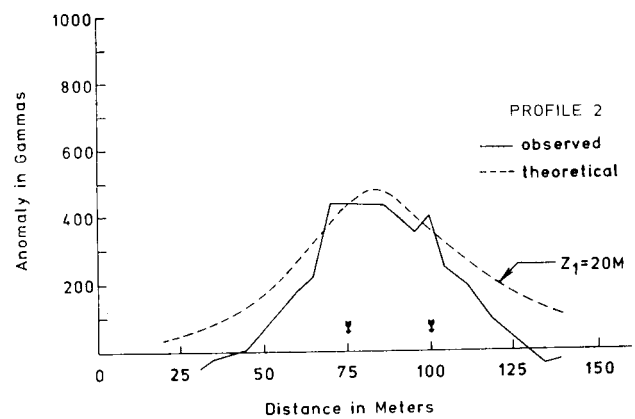

Figure 29.

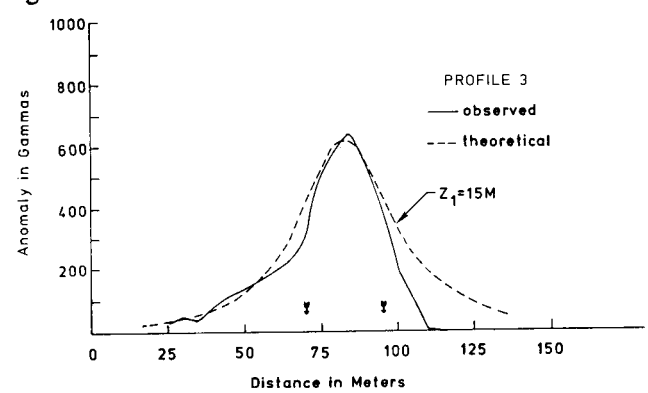

Figure 30.

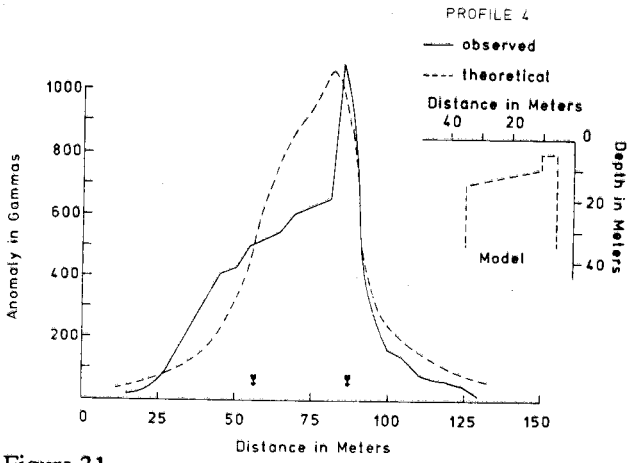

Figure 31.

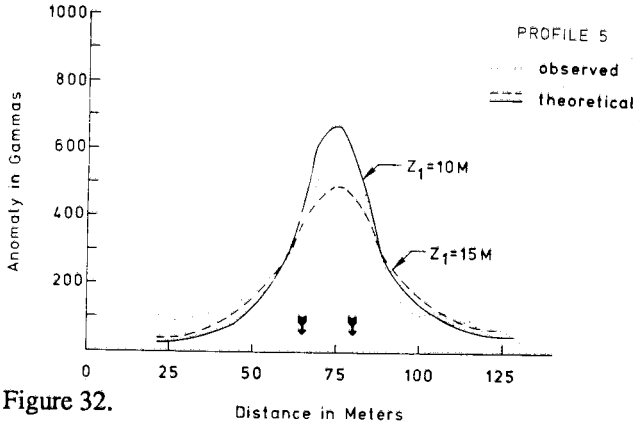

Figure 32.

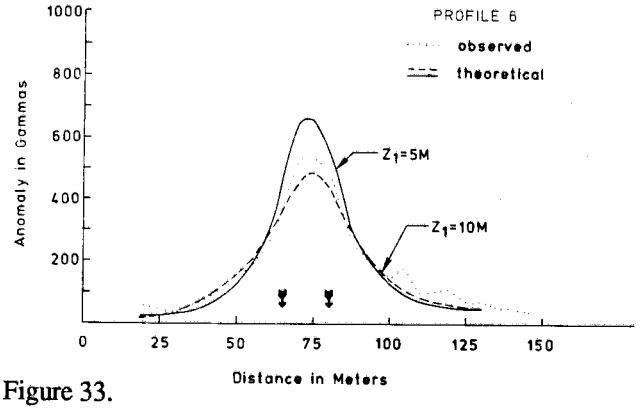

Figure 33.

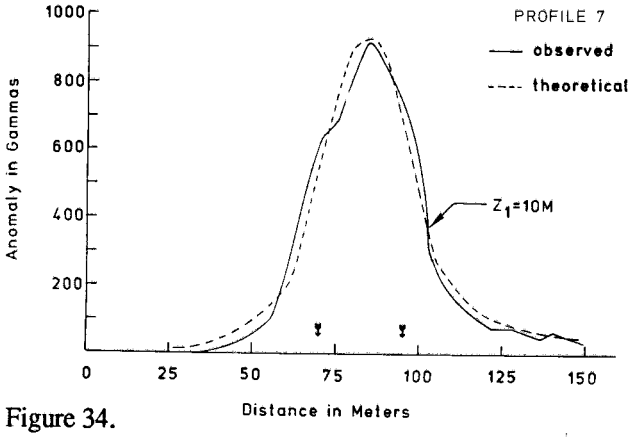

Figure 34.

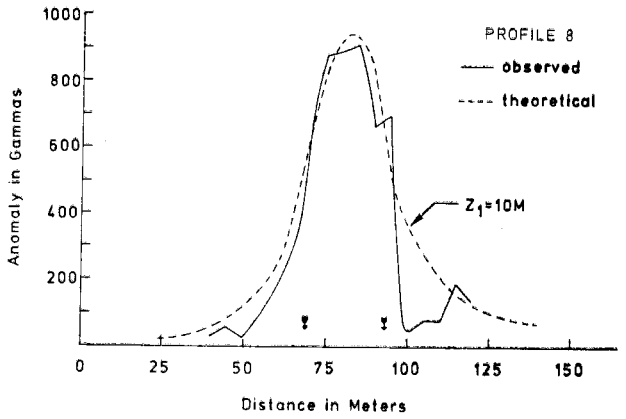

Figure 35.

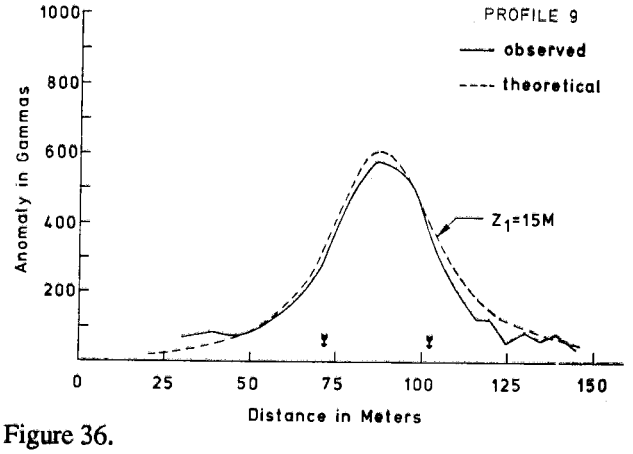

Figure 36.

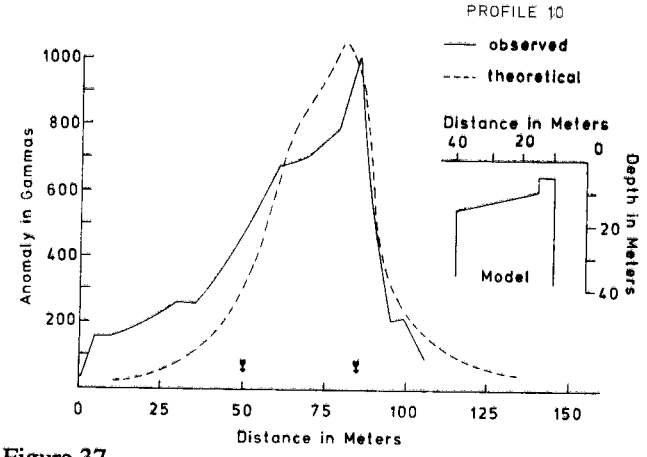

Figure 37.

Table 1. Densities and susceptibilities of certain rock units and specified lithologies.

Geologic Unit or Lithology	Legend	Density (g/cm³) Range	Density (g/cm³) Average	Density Contrast[1] Range	Density Contrast[1] Average	Susceptibility[2] (x 10 emu) Range	Susceptibility[2] (x 10 emu) Average
State Farm Gneiss	Ys	2.71 - 2.81	2.75	+0.04 - +0.14	+0.08	0-400	-
Sabot Amphibolite	s	2.72 - 3.12	2.90	+0.05 - +0.45	+0.23		1000
Maidens Gneiss	m	2.61 - 2.76	2.71	-0.06 - +0.09	+0.04		0
Triassic sediments	Tr	2.42 - 2.52	2.48	-0.25 - - 0.15	-0.19		0
Triassic sediments (Richmond basin)	Tr	-	2.58	-	-0.09		NA
Petersburg granite	Mp	-	2.64	-	-0.03		40
Catoctin Formation (metabasalt, greenschists)	Yc	2.89 - 3.19	3.00	+0.22 - +0.52	+0.33	100-17.200	-
Garrisonville mafic complex (metagabbros, amphibolites)		2.88 - 3.20	3.01	+0.21 - +0.53	+0.34		NA
Chopawamsic Formation (metavolcanic rocks)	ch	2.62 - 3.04	2.84	-0.05 - +0.37	+0.17		NA
Metavolcanics, W-3317			NA				<1
Culpeper Basin							
Triassic sediments	Tr	2.49 - 2.62	2.58	-0.18 - -0.05	-0.09		NA
Diabase		-	2.92	-	+0.25	500-5500	1000
Basalt		2.91 - 2.98	2.94	+0.24 - +0.31	+0.27		NA
General Lithologies							
Amphibolite		2.90 - 3.04	2.96	+0.23 - +0.37	+0.29		60
Anorthosite		2.64 - 2.94	2.78	-0.03 - +0.27	+0.11		NA
Basalt		2.70 - 3.30	2.99	+0.03 - +0.63	+0.32	20-14.500	6000
Gabbro		2.70 - 3.50	3.02	+0.03 - +0.83	+0.35	80-7200	6000
Gneiss		2.59 - 3.00	2.80	-0.08 - +0.33	+0.13	10-2000	-
Granite		2.50 - 2.81	2.64	-0.17 - +0.14	-0.03	0-4000	200
Schist		2.39 - 2.90	2.64	-0.28 - +0.23	-0.03	25-240	120
Serpentine		2.40 - 3.10	2.78	-0.27 - +0.43	+0.11	250-1400	-
Granodiorite		-	2.73	-	-	-	-
Slate		-	2.79	-	-	-	-

NOTES: 1. Density contrast = density - 2.67 (g/cm³)
2. Reilly's (1980) data are based on determinations from three-dimensional magnetic modeling; the susceptibility of 400 x 10 e.m.u. for the State Farm Gneiss represents a biotite-rich section of gneiss, from Davison (1985) with some modification.

ACKNOWLEDGMENTS

We are grateful to Stanley S. Johnson, Division of Mineral Resources, Albert Froelich and David Daniels, U.S. Geological Survey, for their interests in our work and their comments and editorial suggestions. This study was supported by the U.S. Geological Survey and the Old Dominion University Research Foundation

REFERENCES CITED

Bally, A. W., 1981, Atlantic-type margin, *in* Geology of passive continental margins: American Association of Petroleum Geologists Eastern Section Meeting and Atlantic Margin Energy Conference, Education Course Note Series No. 19, p. 1.11-1.48.

Bobyarchick, A. R., and Glover, Lynn, III, 1979, Deformation metamorphism in the Hylas zone and adjacent parts of the eastern Piedmont in Virginia: Geological Society of America Bulletin Part I, v. 90, p. 739-752.

Bott, M. H., 1960, The use of rapid digital computing methods for direct gravity interpretation of sedimentary basins: Geophysical Journal Royal Astronomical Society, p. 63-67.

Cochran, W. C., 1984, Newark rift activity reported: American Association of Petroleum Geologists, American Association of Petroleum Geologist Explorer, p. 34.

Conley, J. F., 1978, Geology of the Piedmont of Virginia - interpretations and problems, *in* Contributions to Virginia geology III: Virginia Division of Mineral Resources Publication 7, p. 115-149.

Davison, Gordon, 1985, A geophysical model of the central gravity-magnetic high, Virginia Coastal Plain [M. S. thesis]: Norfolk, Virginia, Old Dominion University, p. 147.

De Boer, J., and Snyder, F. G., 1979, Magnetic and chemical variations of Mesozoic diabase dikes from eastern North America: evidence for a hot spot in the Carolinas: Geological Society of America Bulletin, v. 90, p. 185-198.

Farrar, S. S., 1984, The Goochland granulite terrane: Geological Society of America Special Paper 194, 215 p.

Gentz, B., 1982, Newark basins draw new attention: East Coast sitting on Texas size basin?: American Association of Petroleum Geologists, American Association of Petroleum Geologist Explorer, p. 8-9.

Glover, Lynn, III, Mose, D. G., Costain, J. K., Poland, F. B., and Reilly, J. M., 1978, Grenville basement in the eastern Piedmont of Virginia [abs.]: Geological Society of America Abstracts with Programs, v. 10, n. 4, 169 p.

Goodwin, B. K., 1970, Geology of the Hylas and Midlothian quadrangles, Virginia: Virginia Division of Mineral Resources Report of Investigations 23, 51 p.

Grow, J. A., 1981, The Atlantic margin of the United States, in Geology of passive continental margins: American Association of Petroleum Geologists Eastern Section Meeting and Atlantic Margin Energy Conference; Education Course Notes Series No. 19, p. 3.1-3.41.

Harris, L. D., DeWitt, W., Jr., and Bayer, K. C., 1982, Interpretive seismic profile along I-64 from the Valley and Ridge to the Coastal Plain in central Virginia: U. S. Geological Survey Oil and Gas Investigation 123, 1 sheet.

Heiland, C. A., 1940, Geophysical exploration: Englewood Cliffs, New Jersey, Prentice-Hall, 1013 p.

Johnson, S. S., and Ziegler, R. E., 1972, Virginia gravity base net: Virginia Division of Mineral Resources Information Circular 17, 22 p.

Johnson, S.S., 1975, Bouger gravity in southeastern Virginia, Virginia Division of Mineral Resources Report of Investigations 39, 42 p.

Johnson, S. S., Wilkes, G. P., and Gwin, M. R., 1985, Simple Bouguer gravity anomaly map of the Richmond and Taylorsville basins and vicinity, Virginia: Virginia Division of Mineral Resources Publication 53, 1 sheet.

Le Van, D. C. and Pharr, R. F., 1963, A magnetic survey of the Coastal Plain in Virginia: Virginia Division of Mineral Resources Report of Investigations 4, 17 p.

Lutz, R. D., 1986, Lineament analysis in the Richmond Triassic basin area, Virginia, a kinematic model [M. S. thesis]: Norfolk, Virginia, Old Dominion University, p. 202.

Lyell, Charles, 1847, On the structure and probable age of the coal field of the James River, near Richmond, Virginia: Geological Society of London Quaternary Journal, v. 3, p. 261-280.

Mixon, R. B., and Newell, W. L., 1977, Stafford fault system: structures documenting Cretaceous and Tertiary deformation along the fall line in northeastern Virginia: Geology, v. 5, p. 436-441.

Ragland, P. C., Hatcher, R. D., and Whittington, D., 1983, Juxtaposed Mesozoic diabase dike sets from the Carolinas: A preliminary assessment: Geology, v. 11, p. 394-399.

Reilly, J. M., 1980, A geologic and potential field investigation of the central Virginia Piedmont [M. S. thesis]: Blacksburg, Virginia Polytechnic Institute and State University, p. 158.

Sumner, J. R., 1977, Geophysical investigation of the structural framework of the Newark-Gettysburg Triassic basin, Pennsylvania: Geological Society of America Bulletin 88, p. 935-942.

Talwani, M., Worzel, J. Lamar, and Landisman, M., 1959, Rapid gravity computations for two dimensional bodies with application to the Mendocino submarine fracture zone: Journal of Geophysical Research, v. 64, p. 49-59.

Talwani, M., 1965, Comparison with the help of a digital computer of magnetic anomalies caused by bodies of arbitrary shape: Geophysics v. 25, p. 203-225.

Telford, W. M., Geldard, L. P., Sheriff, R. E., and Keys, D. A., 1976, Applied geophysics: Cambridge, England, Cambridge University Press, p. 860.

U. S. Geological Survey, 1972, Total intensity aeromagnetic map, Dinwiddie and Petersburg quadrangles: U. S. Geological Survey, scale 1:62,500. Van

Houten, F. B., 1969, Late Triassic, Newark Group; north central New Jersey and adjacent Pennsylvania and New York, *in* S. Subinsky. ed., Geology of selected areas in New Jersey and eastern Pennsylvania: New Brunswick, New Jersey, Rutgers University Press, p. 314-317.

Virginia Division of Mineral Resources, 1963, Geologic map of Virginia: Virginia Division of Mineral Resources, scale 1:500,000.

Virginia Division of Mineral Resources, 1971, Total intensity aeromagnetic map Wellville quadrangle: Virginia Division of Mineral Resources, scale 1:62,500.

Watts, A. B., 1981, The U. S. Atlantic continental margin: subsidence history, crustal structure and thermal evolution, *in* Geology of passive continental margins: American Association of Petroleum Geologists Eastern Section Meeting and Atlantic Margin Energy Conference, Education

Course Note Series No. 19, p. 2.1-2.75.

Weems, R. E., 1974, Geology of the Hanover Academy and Ashland quadrangles, Virginia [M. S. thesis]: Blacksburg, Virginia Polytechnic Institute and State University, p. 100.

Weems, R. E., 1980, Geology of the Taylorsville basin, Hanover County, Virginia, *in* Contributions to Virginia geology IV: Virginia Division of Mineral Resources Publication 27, p. 23-28.

Wright, J. E., Sinha, A. K., and Glover, Lynn, III, 1975, Age of zircons of the Petersburg granite, Virginia, with comments on belts of plutons in the Piedmont: American Journal of Science, v. 275, n. 7, p. 846-856.

Zietz, I., Calver, J. L., Johnson, S. S., and Kirby, J. R., 1977, Aeromagnetic map of Virginia: Virginia Division of Mineral Resources, scale 1:1,000,000.

GRAVITY ANOMALIES AND GEOLOGY IN THE BLUE RIDGE PROVINCE NEAR FLOYD, VIRGINIA

Robert L. Stovall[1], Edwin S. Robinson[2], and Mervin J. Bartholomew[3]

CONTENTS

	Page
Abstract	62
Introduction	62
Geology	63
Gravity	65
Regional and local anomalies	67
Interpretation of local gravity anomalies	69
Interpretation of the regional gravity field	70
Conclusions	71
Acknowledgments	71
References cited	71
Appendix I: A vertical line source algorithm for computing gravity terrain corrections	71
Appendix II: Gravity data	74

ILLUSTRATIONS

Figure

1. Generalized geologic map and cross sections 63
2. Bouguer anomaly map 64
3. Local gravity anomaly map derived by subtracting the calculated regional gravity values from the Bouguer anomaly values 66
4. Quadratic polynomial representation of the regional gravity field 66
5. Local gravity anomaly map derived by subtracting the calculated regional gravity values from the Bouguer anomaly values 67
6. Observed gravity anomaly variation along profile A-A' 67
7. Observed gravity anomaly variation along profile B-B' 68
8. Observed gravity anomaly variation along profile C-C' 68
9. Difference between the plane and quadratic polynomial representations of the regional gravity field 69
10. Regional gravity variation along profile D-D' compared with computed gravity variation 70
11. Rectangular prism representation of topography 72
12. Zones used for calculation of terrain correction 72

TABLES

1. Density estimates for the principal lithologic units 64
2. Bouguer anomalies used to compute a plane regional gravity field 66
3. Average free-air anomaly values in the 7.5-minute quadrangles 70

1. Conoco, Inc., Ponca City, OK 74601
2. Department of Geological Sciences, Virginia Polytechnic Institute and State University, Blacksburg, VA 24061
3. Montana Bureau of Mines and Geology, Butte, MT 59701

ABSTRACT

Bouguer gravity anomalies in the Blue Ridge near Floyd, Virginia can be explained in terms of upper crustal geology and some combination of crustal thickening and anomaly sources at intermediate depths in the crust. Local gravity anomalies were separated from a regional gradient by polynomial filtering of the Bouguer anomaly field. Two-dimensional model analysis indicates that these local anomalies could result from density differences between steeply dipping rock units truncated by low-angle thrust faults at depths of less than 8 km. Density contrasts in Grenville rocks could be related to large scale folding.

The regional gravity gradient can be attributed to features of two contrasting crustal models. The study area is situated on the border of an earlier seismic refraction survey that indicates westward crustal thickening from approximately 47 km to 50 km. If this model is correct, then a significant density contrast must exist across a steep boundary at intermediate depth in the crust. An alternate model of northwestward crustal thickening from 30 km to 45 km can also account for the regional gravity gradient without requiring any intermediate crustal anomaly sources.

INTRODUCTION

The Blue Ridge Province in southwest Virginia is characterized by northeast trending low-angle imbricate faults that juxtapose terranes of different lithologies. Principal faults and lithologic units in the area of the Blue Ridge (Figure 1) have been identified by geologic mapping. However, in this complexly deformed region the subsurface distribution of lithologic units, and the existence in the subsurface of rock units not exposed at the surface, are difficult to infer without indirect evidence provided by geophysical surveys. In this study a gravity survey was undertaken to broaden our understanding of the geology in this area.

This report is concerned with analysis of Bouguer anomalies obtained from gravity measurements at 470 locations (Figure 2). This analysis involves separating by means of polynomial filtering the local gravity field, which is related to upper crustal geology, from broader regional patterns. Local anomaly variation along selected profiles is then interpreted by comparison with theoretical gravity variations computed for two-dimensional models which are consistent with mapped structural and lithologic features. The broader regional Bouguer anomaly field may be attributable to changes in crustal thickness or to deep crustal anomaly sources, as well as to large upper crustal geologic features. Limited information about crustal thickness in this area and evidence of deep crustal anomaly sources elsewhere close to the Blue Ridge are used in the interpretation of the regional Bouguer anomaly variation.

The interpretation of Bouguer anomaly patterns is constrained by available data on the characteristics of the lithologic units and structural features in the area. Locations of faults and the structural attitudes and densities of the exposed rocks are of particular value in the interpretation of gravity anomalies.

GEOLOGY

The study area crosses the tectonic boundary between the Valley and Ridge and Blue Ridge geologic provinces in a region dominated by thrust faults with large-scale displacements. Principal rock units and structures are displayed on a geologic map and on three representative cross sections (Figure 1). The Blue Ridge fault marks the leading edge of thrust sheets containing crystalline "basement" nonconformably overlain by metasedimentary and metavolcanic rocks. Northwest of, and structurally below, the Blue Ridge thrust are complexly deformed sedimentary rocks of Paleozoic age which make up the Pulaski thrust sheet. Windows through the Pulaski sheet reveal Paleozoic strata of the structurally lower Saltville sheet.

Southeast of the Blue Ridge thrust, the Fries ductile deformation zone juxtaposes contrasting packages of basement lithologies and cover rocks (Bartholomew and Lewis, 1984). The stratigraphic succession northwest of the Fries fault consists of Grenville-age gneisses nonconformably overlain by metasedimentary rocks of the Chilhowee Group. Chilhowee Group rocks are conformably overlain by the Cambrian-age sequence of Shady Dolomite, Rome Shale, Elbrook Dolomite, and Copper Ridge Dolomite, and by the Ordovician-age Beekmantown Group as well as younger Paleozoic rocks. The Grenville-age rocks include layered granulite gneisses intruded by the Bottom Creek charnockite suite. The Chilhowee Group consists of the Weverton (metasandstone), Harpers (metashale), and Antietam (metaquartzite) Formations.

Southeast of the Fries fault the stratigraphic succession consists of Grenville-age gneisses nonconformably overlain by metasedimentary and metavolcanic rocks of the late Precambrian (?) Ashe Formation, which are overlain by the Alligator Back Formation. In the southeastern portion of the area, the metavolcanic rocks of the Moneta Gneiss are roughly equivalent to the basal portion of the Ashe Formation. The layered gneisses are intruded by the Little River gneiss. In the vicinity of the study area displacements on the Pulaski, Blue Ridge, and Fries faults are estimated to be about 50 km (Bartholomew, 1979), 80 km (Hatcher, 1981; Boyer and Elliott, 1982), and 30 km (Bartholomew, 1983) respectively. Southeastward from the Fries fault the grade of Paleozoic metamorphism increases from the greenschist facies (biotite grade) to upper amphibolite facies (kyanite grade) (Espenshade and others, 1975).

Density values of rock specimens typical of formations in both the Valley and Ridge and Blue Ridge provinces

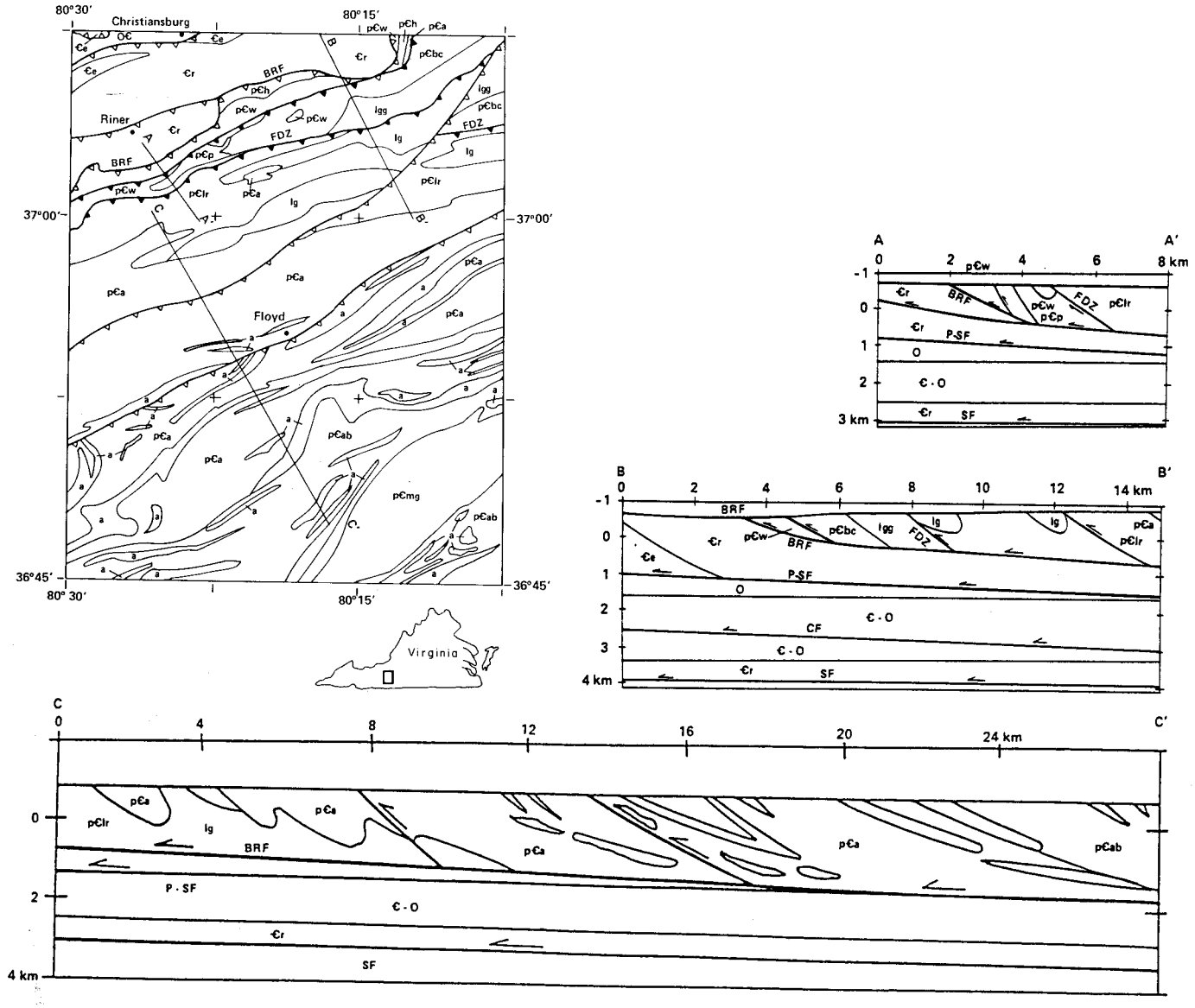

Figure 1. Generalized geologic map and cross sections of the area around Floyd, Virginia modified after: unpublished map of Riner quadrangle (Lewis and others); unpublished maps of Pilot and Check quadrangles (Bartholomew and others); Bartholomew and Lewis (1984); Conley (1978); Dietrich (1959); Epenshade and others (1975); P-SF - Pulaski-Salem fault; SF- Saltville fault; O - Ordovician shales; Є-O - Ordovician- Cambrian carbonates; Єe - Elbrook Formation; Єr - Rome Formation; pЄa - Antietam Formation; pCh - Harpers Formation; pCw - Weverton Formation; pCp - Pilot gneiss*; pCbc - Bottom Creek charnockite suite*; lgg - layered granulite gneiss; pCa - Ashe Formation (with amphibolite - a); pЄlr - Little River gneiss*; lg - layered gneiss; pЄab - Alligator Back Formation; pCmg - Moneta Gneiss; BRF - Blue Ridge fault; FDZ - Fries ductile deformation zone; solid teeth - faults of Fries fault system; open teeth - faults of Pulaski-Blue Ridge fault system; * - informal units.

of southwestern Virginia were determined by Kolich (1974) and Wells (1975). Estimates of density presented in Table 1 are based on measured values and on general relationships between density and lithology described by Clark (1966). Density approximations used in compiling the models are based on the geologic map and cross sections (Figure 1) and estimations of the proportions of different lithologies where two or more are interlayered.

GRAVITY

A total of 470 gravity stations were established (Figure 2) from June to September, 1982. Measurements were made using LaCoste-Romberg gravimeter No. G-612 along roads at bench marks, at landmarks where elevations are known within 1 foot, or at locations where elevation could be determined from the topographic contours within 5 feet. In the Check and Pilot 7.5-minute quadrangles, 286 of the sta-

Table 1. Density estimates for the principal lithologic units.

UNIT NUMBER	LITHOLOGY	DENSITY (g/cm^3)	THICKNESS (meters)
5	Beekmantown Group	2.77(k)	600
6	Copper Ridge Formation	2.80(k)	300
6	Elbrook Formation	2.80(k)	1300
1a	Rome Formation	2.75(w)	*
1b	Rome Formation (lower density)	2.68(c)	*
2	Chilhowee Group	2.75(c)	*
9	Alligator Back Formation	2.82(c)	*
7a	Ashe Formation (gneiss)	2.80-2.85(c)	*
7b	Ashe Formation (mica schist)	2.74(c)	*
7c	Ashe Formation (amphilobite)	2.88-3.00(c)	*
8a	Bottom Creek suite	2.85(c)	*
8b	layered granulite gneiss	2.90(c)	*
3a	Little River gneiss (granitoid)	2.75-2.83(c)	*
3b	Little River gneiss (mylonitic rock)	2.68(c)	*
4	Pilot gneiss	2.75	*

k - Kolich (1974), w - Wells (1975), c - Clark (1966), * indeterminate or not applicable.

tions were established with an average coverage of about nine stations per square mile, except close to Pilot Mountain and near the headwaters of Lick Fork in the Check quadrangle, where there were no access roads. The remaining 184 stations were situated in a 2-mile-wide corridor crossing the Blue Ridge province from Christiansburg to Woolwine paralleling State Highway 8 with a coverage of approximately nine stations per square mile. This corridor includes portions of the Riner, Alum Ridge, Floyd, and Woolwine 7.5-minute quadrangles.

Gravimeter readings were converted into relative gravity values using the instrument calibration table. Corrections for instrument drift were determined from daily reoccupation of a base station in Christiansburg and weekly readings at the Virginia Tech Gravity Base Station at Derring Hall in Blacksburg. The total instrument drift of 2.5 milligals during the survey period was corrected by linear adjustments using straight lines fitted to different portions of the drift data. The standard deviation of 0.13 milligal of the points from the straight line segments provides information for estimating the accuracy of the observed gravity values. Lunisolar tidal gravity variations were corrected using equations of Longman (1959) and a solid earth tidal gravity factor of 1.16.

Values of observed gravity (g_{ob}) were calculated by adjusting relative values obtained from gravimeter readings to the Derring Hall base value of 979718.89 milligals. This base value of absolute gravity is referenced to the new International Gravity Standardization Net 1971 (IGSN1971) that was reviewed by Woollard (1979).

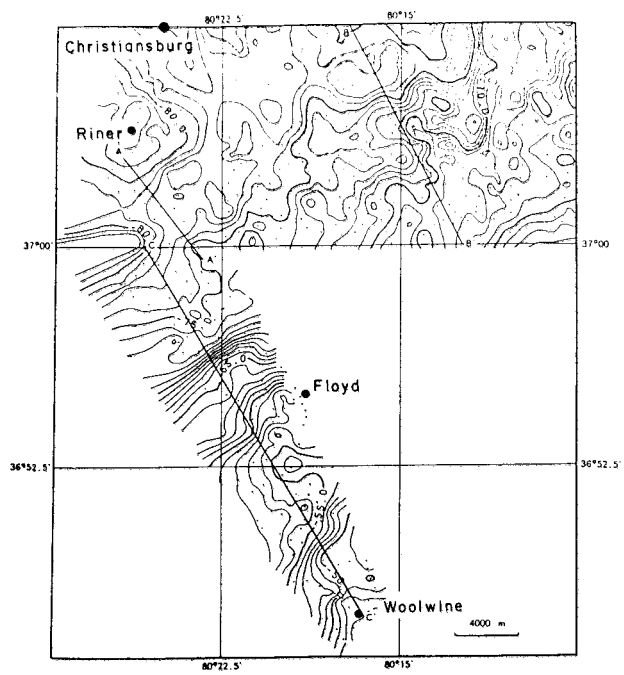

Figure 2. Bouguer anomaly map; observation sites indicated by dots; contour interval 1 milligal.

The well-known formulas for gravity data reduction (Nettleton, 1976) were used to obtain free air anomalies

$$g_f = g_{ob} - (g - 0.09406h),$$

and the complete Bouguer anomalies

$$g = g_{ob} - (g_t - 0.09406h + 0.01278ph - TC),$$

where normal gravity (g_t) was computed from the GRS-67 formula (Woollard, 1979), elevation h in feet was read from topographic maps, and a standard density of $p = 2.67$ g/cm^3 was used in the Bouguer plate corrections and the terrain corrections (TC). Results are tabulated in Appendix II. Bouguer anomalies are contoured at a 1-milligal interval in Figure 2.

Local topographic relief was sufficiently large to require terrain corrections. These were calculated by a new method that involves computer summation by means of a FORTRAN program called TERRCORR of the gravitational attraction of vertical line sources representing increments of topography. This method of terrain correction is described more fully in Appendix I. The increments of topography were determined from elevations read on a square grid at 1093.6 feet intervals from topographic maps. Elevation data used for this study were taken from a larger set of elevations compiled for the entire State as part of a research program supervised by Professor Robert H. Giles (School of Forestry and Wildlife Resources, Virginia Tech). The effect of topography within a distance of 15,000 feet from a gravity station was included in a terrain correction. This is approximately equivalent to the effect of topography extending as far as the J ring in a computation based on the terrain correction method of Hammer (1939).

The principal source of error in terrain corrections obtained with the program TERRCORR is related to the sampling interval of 1093.6 feet which is inadequate to represent smaller topographic features. Significant errors can be produced by inadequately sampled features within approximately 3000 feet of a gravity station. In areas of rugged relief these errors can exceed 1 milligal. Some insight into such errors is provided from comparative terrain corrections determined by the graphical method of Hammer (1939). Ordinarily the effect of terrain within a distance of approximately 3000 feet can be determined to an accuracy of better than 0.05 milligal by this method. At greater distances the errors in values obtained with TERRCORR caused by inadequate sampling diminish, and it becomes questionable if greater accuracy can be obtained by the Hammer method because of errors in estimates of average elevation within compartments of the template used to compute the terrain correction.

At two locations in Floyd County, terrain correction values were determined independently using the Hammer method by fifteen students as part of a class exercise. Values for one location range between 0.46 milligal and 0.61 milligal with an average of 0.54 milligal compared with the value of 0.50 milligal obtained with TERRCORR. At the other location, values are between 0.06 milligal and 0.14 milligal with an average of 0.10 milligal compared to a TERRCORR value of 0.10 milligal. These comparisons suggest that terrain corrections computed for most gravity stations using TERRCORR should be adequate for the purposes of this study. Nonetheless, at all locations where values larger than 1 milligal were obtained in this way terrain corrections were also determined by the Hammer method. Unacceptable discrepancies were found at 44 stations, which could be attributed to nearby topography that was not properly represented by elevations at 1093.6 feet intervals. The terrain corrections determined by the Hammer method were used for these stations.

Estimates of the precision of Bouguer anomalies (Appendix II) are based on the accuracy of observed gravity values (approximately 0.1 milligal) and uncertainties in the elevation and the terrain corrections. In areas of moderate to subdued relief where terrain corrections are smaller than 1 milligal and elevation is known within 1 foot, the Bouguer anomaly precision is close to 0.2 milligal. Where more extreme relief produces larger terrain corrections, and elevations are estimated within 5 feet, the Bouguer anomaly precision is probably closer to 0.5 milligal.

REGIONAL AND LOCAL ANOMALIES

A regional gravity gradient overprinted by local anomalies is evident on the Bouguer anomaly map (Figure 2). The local anomalies can be attributed entirely to upper crustal geology, but the sources of the regional gradient can include variation in crustal thickness and deep crustal density contrasts as well as broad upper crustal features. There are two basic methods of addressing the problem of separating regional and local gravity variations. The first requires explicit independent information about regional anomaly sources. For example, if crustal thickness is known independently from seismic data, the effect on the gravity field can be calculated and then subtracted from a Bouguer anomaly map of that area. The second basic method involves mathematical filtering to reveal the form of the regional field. This can be done by using a low order polynomial function determined by least squares analysis of the Bouguer anomalies (Mack, 1963) to represent the regional field. Both methods were applied in this study.

Seismic refraction measurements of crustal thickness were given by James and others (1968) for a large region that includes this study area along its western periphery. They used a time-term analysis of 860 P-wave travel time observations from numerous randomly oriented source-receiver pairs covering the middle Atlantic states to determine crustal thickness at locations common to several source to receiver mid-points. They also computed the gravity field that would be produced by this variation in crustal thickness.

Later seismic measurements by Bollinger and others (1980) at two locations confirm the results of James and others (1968).

Insofar as the results of James and others (1968) are correct, the variation in gravity related to crustal thickness in this area can be represented by a plane function

$$g_r(x, y) = a_1 + a_2 x + a_3 y \qquad (1)$$

where x and y are the east and north state grid coordinates (in feet) of a regional gravity value g_r. The coefficients $a_1 = 0.00037932$, $a_2 = 0.00019925$, $a_3 = 524.501595$ were found by solving the set of three linear equations obtained using the Bouguer anomalies and locations given in Table 2. The criteria for choosing these values are: a) they yield a linear gravity gradient with a direction and magnitude consistent with the results of James and others (1968), and b) they are situated (Figure 2) where the effects of local anomaly sources appear to be minimal.

Local gravity variations displayed in Figure 3 were found by subtracting from the Bouguer anomalies the corresponding regional field values obtained from Equation 1 and Table 2. In addition to local anomalies it is evident that a significant regional gradient remains in the residual field. This implies either that there are other regional anomaly sources, or that crustal thickness was not accurately determined in this peripheral part of the region described by James and others (1968). These possible implications are discussed in the following sections.

Table 2. Bouguer anomalies used to compute a plane regional gravity field.

STATION NUMBER	LAT (deg)	LONG (deg)	BOUGUER ANOMALY (mgal)
123	37.1	80.1	-75.0
232	37.1	80.3	-80.0
378	37.0	80.4	-80.0

An alternate approach is to represent the regional gravity field with the quadratic polynomial function

$$g_r(x,y) = a_1 + a_2 x + a_3 y + a_4 x^2 + a_5 xy + a_6 y^2 \qquad (2)$$

where x and y are the east and north state grid coordinates of a regional gravity value g_r. Coefficients a_1 through a_6 were determined directly from the Bouguer anomalies (Appendix II) using the least squares method. The regional gravity field that is contoured in Figure 4 was determined in this way. By subtracting it from the Bouguer anomaly field (Figure 2) the local gravity anomaly field was obtained (Figure 5).

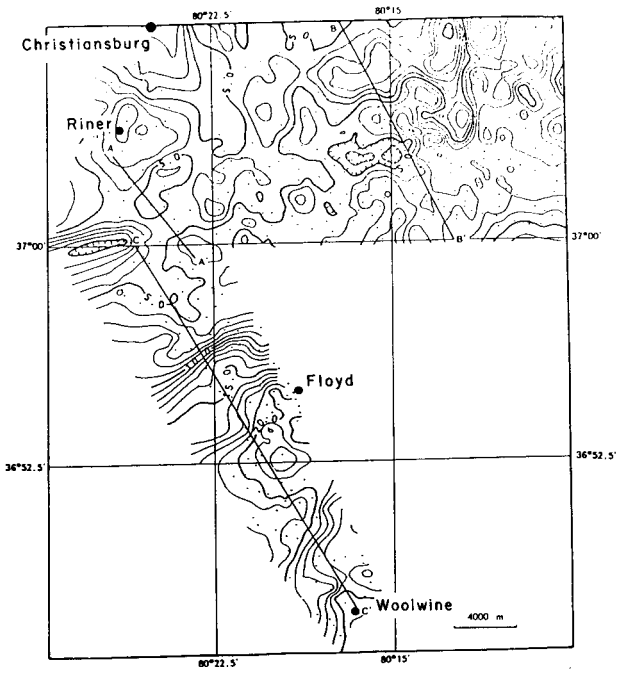

Figure 3. Local gravity anomaly map derived by subtracting the calculated regional gravity values (Equation 1) from the Bouguer anomaly values; contour interval 1 milligal.

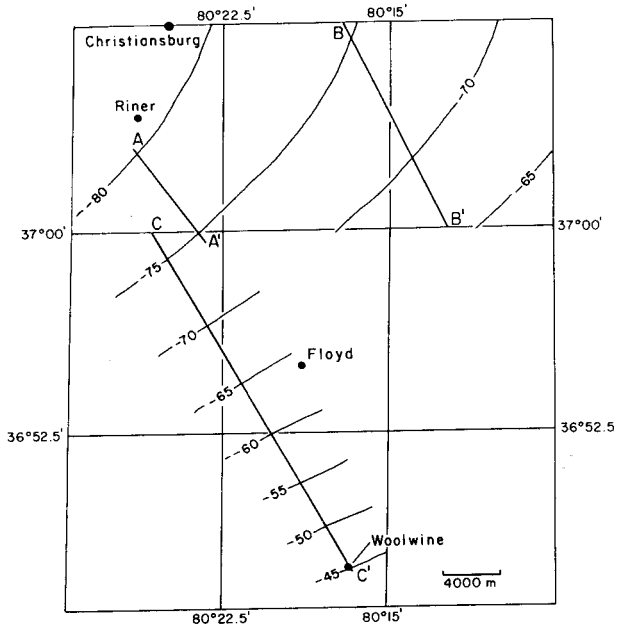

Figure 4. Quadratic polynomial representation of the regional gravity field calculated from Equation 2; contour interval 5 milligals.

In view of the thickness of the crust and the size of the study area, a function no more complicated than a quadratic polynomial should be sufficient to represent the regional gravity anomaly related to variations in crustal thickness. But the least squares method for determining the polynomial

coefficients does not distinguish between the effects of crustal thickness and equally broad anomalies produced by large upper crustal geologic features. This implies that while the local anomaly field (Figure 5) can be attributed entirely to upper crustal geology, it does not necessarily represent all of the gravity variation caused by upper crustal geology. Effects of larger features may remain in the regional field (Figure 4). For lack of evidence to the contrary, one possible interpretation is to attribute the regional gravity field entirely to variation in crustal thickness, which can then be computed for comparison with the James and others (1968) crustal model. This is discussed in a following section.

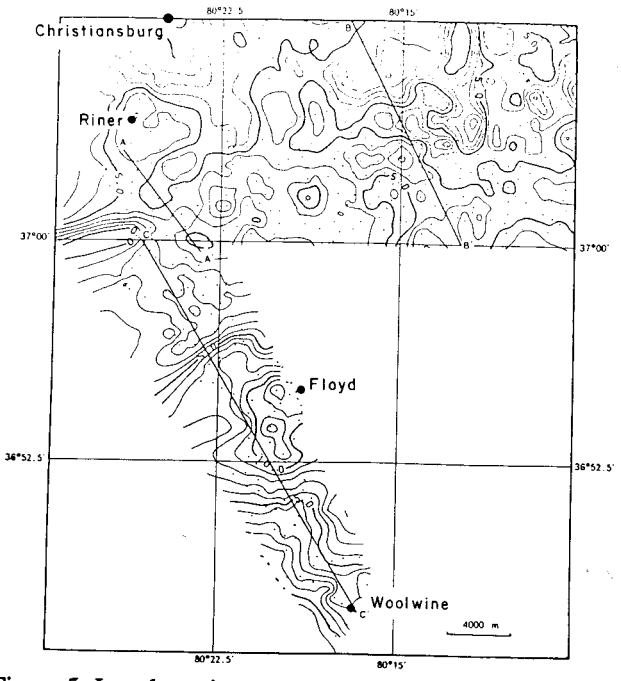

Figure 5. Local gravity anomaly map derived by subtracting the calculated regional gravity values (Equation 2) from the Bouguer anomaly values; contour interval 1 milligal.

INTERPRETATION OF LOCAL GRAVITY ANOMALIES

Local gravity anomalies provide information for estimating the subsurface extent of rock units and structures exposed along the three profiles shown in Figure 5. Values at contour intersections and projected from nearby observation sites are plotted in Figures 6, 7, and 8 to illustrate gravity variation along the profiles. These are the local gravity anomaly values found by subtracting the quadratic polynomial representation of the regional field (Figure 4) from the Bouguer anomaly field (Figure 2). They are analyzed by comparison with theoretical gravity variations computed over two-dimensional models by the method of Talwani, and others (1959). The shapes and densities of units in the models were adjusted in successive trials until the theoretical variations reproduced the observed anomaly patterns within the limits of Bouguer anomaly precision. Model units were constrained to be consistent with structural attitudes and lithologies of rock units determined from geologic mapping. Insofar as possible, densities close to values in Table 1 were used.

The practice of using a common reduction density of 2.67 g/cm^3 for computing Bouguer anomalies is likely to produce subtle elevation-dependent spatial variations. The existence of these variations, and the locally irregular contour patterns in Figure 5 near profiles A-A', B-B', and C-C' suggest that the two-dimensional models may be less than satisfactory for explaining local gravity variations along these profiles. Unfortunately, the geologic constraints are inadequate to substantiate more reliable three-dimensional models. Therefore, the two-dimensional models in Figures 6, 7, and 8 are more realistically viewed as confirmation of geologic style rather than explicit indications of density distribution.

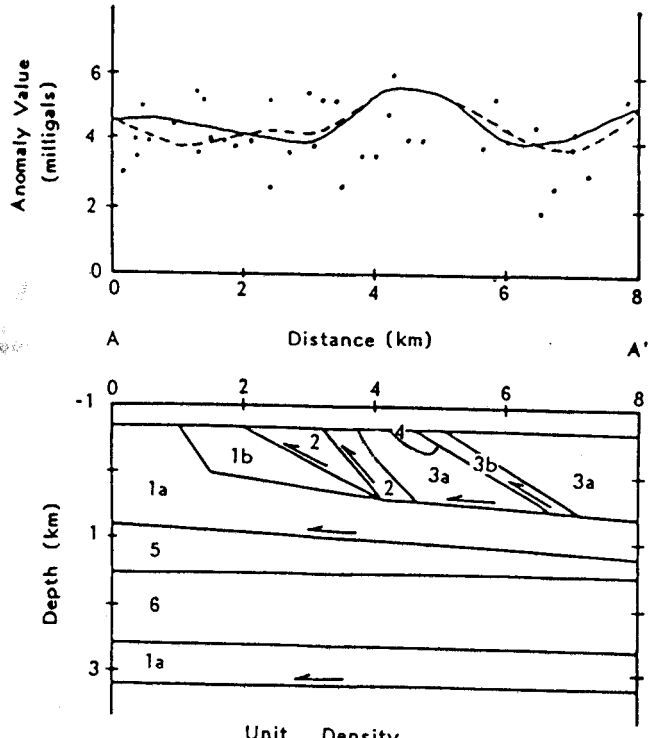

Unit	Density (gm/cc)
1a	2.73
1b	2.68
2	2.75
3a	2.76-2.79
3b	2.68
4	2.75
5	2.77
6	2.8

Figure 6. Observed gravity anomaly variation along profile A-A' (Figure 5) compared with gravity variation (dashed curve) computed for the two-dimensional model of density distribution.

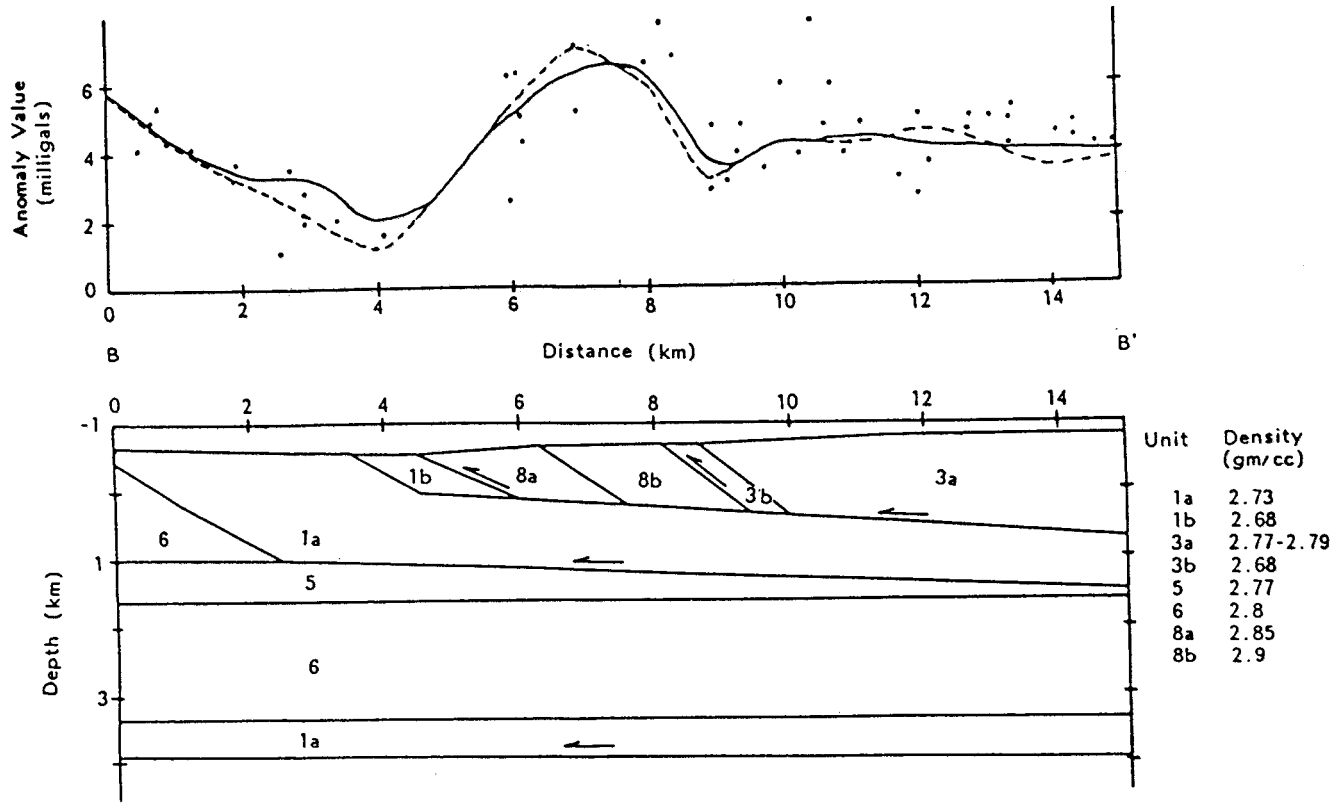

Figure 7. Observed gravity anomaly variation along profile B-B' (Figure 5) compared with gravity variation (dashed curve) computed for the two-dimensional model of density distribution.

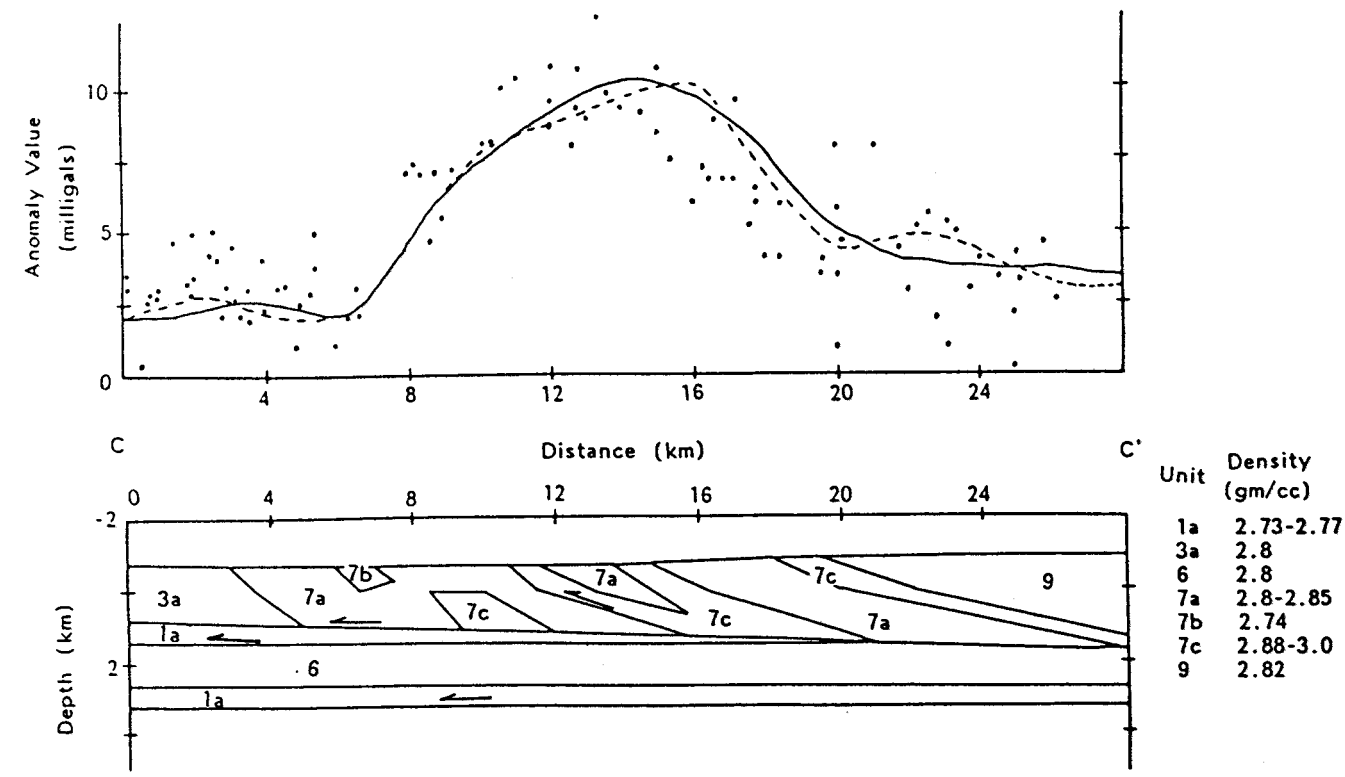

Figure 8. Observed gravity anomaly variation along profile C-C' (Figure 5) compared with gravity variation (dashed curve) computed for the two-dimensional model of density distribution.

Local gravity anomalies along profile A-A' can be attributed to the density distribution illustrated in Figure 6. This two-dimensional model is based upon the geology in Figure 1. The following geologic interpretation of the model units is proposed: (1a) the Rome Formation, (1b) a supposed low density zone within the Rome Formation suggested by a relative gravity low, (2) Chilhowee metasediments, (4) the Pilot gneiss, (3a) Little River gneiss, (3b) a supposed low density zone within the Little River gneiss suggested by a relative gravity low, (5) the Beekmantown Group, and (6) a combined section of Copper Ridge and Elbrook Formations. The Pulaski fault was located at an approximate depth of 1.6 km beneath the trace of the Blue Ridge fault near Riner by projecting the dip of about 10 degrees at a depth of 1 km determined from seismic measurements by Wells (1975) about 4 km southeast of profile A-A'. Although there is no local evidence of the deeper (Saltville) fault shown at about 3.9 km depth, such a fault is known to exist from geologic mapping northwest of the study area. The Rome Formation (unit la) with a density of 2.73 g/cm^3 differs slightly from the value listed in Table 1. Relatively low density (2.68 g/cm^3) zones extend along the trace of the Blue Ridge fault, which appears to be a zone of cataclasis, and along the Fries ductile deformation zone.

Local gravity anomalies along profile B-B' can be attributed to the density distribution illustrated in Figure 7. This two-dimensional model is based upon the geology in Figure 1. The following geologic interpretation is proposed for the density units of the model: (1a) the Rome Formation, (1b) a low density zone along the trace of the Blue Ridge fault, (8a, 8b) crystalline rocks of the Grenville basement complex (3b) a low density zone within the Little River gneiss, (3a) Little River gneiss, (5) the Beekmantown Group, and (6) the combined Copper Ridge and Elbrook Formations. This model includes the Salem and Saltville faults at the same depths as shown for profile A-A'. Low density zones are again introduced at the trace of the Blue Ridge fault and the Fries ductile deformation zone with densities consistent with those in profile A-A'. Again, a slightly lower density for the Rome Formation is indicated.

The two-dimensional model C-C' (Figure 8) is based upon mapping by Espenshade and others (1975) in the southern half of the area in Figure 1. The proposed geologic interpretation is that model unit number 3a corresponds to the Little River dioritoid, model units numbered 7a correspond to the individual metasedimentary and metavolcanic gneisses of the Ashe Formation, model unit 7b corresponds to the mica schist of the Ashe Formation, units 7c represent the amphibolites of the Ashe Formation, unit 9 represents the Alligator Back Formation, unit 6 represents the combined Copper Ridge and Elbrook Formations, and unit la the Rome Formation. The geometry seen in the model above the Max Meadows fault could be the result of large scale folding of units of the Grenville basement complex. Note that different densities are assumed for model units 3a and 7c, both of which lie beneath unit 7a. This may be explained by lithologic variations in the older Grenville basement. This model includes the Pulaski-Salem and Saltville faults at the approximate depths that are shown for profiles A-A' and B-B'.

INTERPRETATION OF THE REGIONAL GRAVITY FIELD

The regional variation of gravity determined from the crustal thickness model of James and others (1968) differs significantly from that represented by a quadratic polynomial (Figure 4). The difference illustrated in Figure 9 is a south-southwest to southwest trending gradient that extends across the entire study area. To the extent that the James and others model correctly depicts crustal thickness, this difference must be attributed to density contrasts within the crust. Because the study area is situated along the western margin of their survey where the seismic measurements are least reliable, it is probably more realistic to view this model as one limiting case. The other limiting case is to explain the regional gravity field entirely in terms of crustal thickening which requires significant modification of the James and others model.

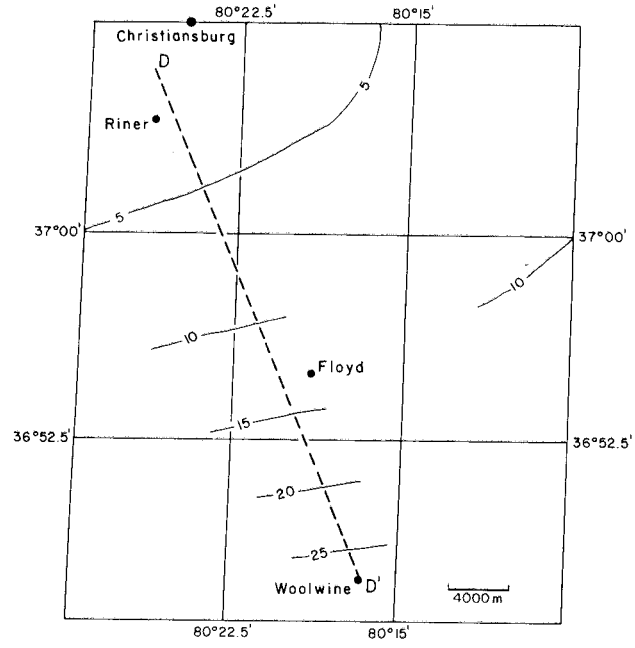

Figure 9. Difference between the plane (Equation 1 and Table 2) and quadratic polynomial (Equation 2 and Figure 4) representations of the regional gravity field; contour interval 5 milligals.

It is unlikely that more than a small part of the gradient in Figure 9 can be ascribed to upper crustal density contrasts. Acceptable changes of models shown in Figures 6, 7, and 8, in the inclination of faults and the depths to which different density units extend, would produce regional gradi-

ents of only a few milligals across the study area. Elsewhere, such gradients have been reported by Keller and others (1985). Deeper in the crust it would be difficult to justify a density contrast of more than 0.2 g/cm³. The gravity change of more than 25 milligals along profile D-D' in Figure 9 can be explained by the two-dimensional model of density distribution in Figure 10. This model is not meant to represent any particular geologic feature. Its purpose is to indicate that some kind of density contrast at intermediate depth in the crust could produce the gravity gradient seen in Figure 9. There is no independent geological evidence to justify such a feature and no seismic travel time anomalies are evident in this area (Bollinger and others, 1980; Carts, 1981). The values in Table 3 of free air gravity anomalies averaged over 7.5-minute quadrangles indicate possible local isostatic imbalance which might be associated with such a feature. Furthermore, the study area is situated where significant intracrustal density contrasts could be expected according to an analysis of gravity and tectonics in the Appalachian, Alpine, and Himalayan mountain systems by Karner and Watts (1983).

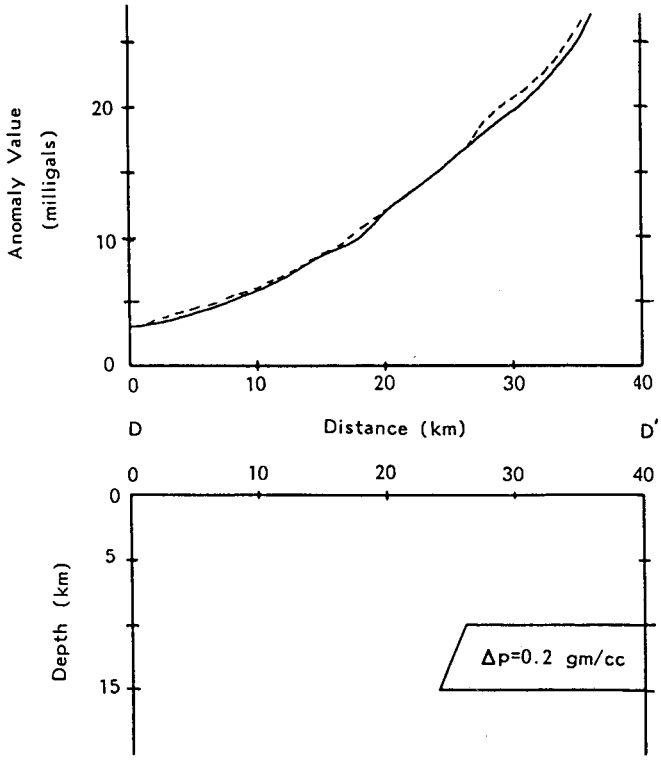

Figure 10. Regional gravity variation (solid curve) along profile D-D' in Figure 9 compared with gravity variation (dashed curve) computed for the two-dimensional horizontal plate with a steeply sloping edge and a density of 0.2 g/cm³.

An alternative interpretation is to attribute the regional field represented by the quadratic polynomial entirely to change in crustal thickness. Following this assumption, the method of Plouff (1976) was used to compute the variation of crustal thickness which would produce a regional gravity field closely resembling the pattern in Figure 4. This would require a northwestward thickening of the crust from approximately 32 km to 45 km across the area, which differs significantly from the 3 km change in crustal thickness in the James and others model. The direction also differs from the westward thickening described by James and others (1968). There is no independent evidence to confirm such a dramatic change in crustal thickness.

Table 3. Average free-air anomaly values in the 7.5-minute quadrangles.

QUADRANGLE	FREE-AIR ANOMALY (mgals)
Alum Ridge	4.8
Check	15.4
Floyd	18.4
Pilot	1.9
Riner	-7.7
Woolwine	16.9

CONCLUSIONS

Bouguer anomalies over this transect of the Blue Ridge can be explained in terms of upper crustal geology, and some combination of density contrast at intermediate depth in the crust and spatial variation of crustal thickness. Local gravity anomalies appear to result from density contrasts related to steeply inclined rock units bounded by low-angle thrust faults that extend beneath the area at depths of less than 8 km. Low density zones may extend along the Blue Ridge fault and the Fries ductile deformation zone. The gravimetric evidence is consistent with the idea of large scale folding of high density amphibolite units in the Grenville basement complex.

Two contrasting models of crustal structure are presented to explain regional Bouguer anomaly variation. One is the crustal model of James and others (1968) that was determined independently from seismic measurements. Because the westward thickening of the crust from 47 km to 50 km across the area is insufficient to explain the regional gravity gradient, this crustal model must be modified to include a significant northeast trending density contrast at intermediate depth. An alternative is to explain the regional gravity gradient in terms of a different, homogeneous crustal model that thickens from approximately 30 km to 45 km in a northwest direction across the area. There is no compelling evidence favoring one or the other of these crustal structures, or another model containing some features from both.

ACKNOWLEDGMENTS

This study received support from the Mining and Mineral Resources Research Institute, the Virginia Division of Mineral Resources, and the Computing Center of Virginia Polytechnic Institute and State University. Dr. Robert Giles kindly made available the array of elevation data, and Dr. Blair Jones provided much assistance in the computer processing of these data.

REFERENCES CITED

Bartholomew, M. J., 1979, Thrusting component of shortening and a model for thrust fault development at the central/southern Appalachian junction[abs.]: Geological Society of America Abstracts with Programs, v. 11, n. 7, p. 384-385.

Bartholomew, M.J., 1983, Palinspastic reconstruction of the Grenville terrane in the Blue Ridge geologic province, southern and central Appalachians, U.S.A.: Geological Journal, v. 18, p. 241-253.

Bartholomew, M. J., Dove, P. M., and Walsh, C. A., in preparation, The geology of the Check and Pilot quadrangles, Virginia: Virginia Division of Mineral Resources.

Bartholomew, M. J., and Lewis, S. E., 1984, Evolution of Grenville massifs in the Blue Ridge geologic province, southern and central Appalachians, *in* Bartholomew, M. J., and others, eds., The Grenville event in the Appalachians and related topics: Geological Society of America Special Paper 194, p. 229-254.

Bollinger, G. A., Chapman, M. C., and Moore, T. P., 1980, Central Virginia regional seismic network: Crustal structure in central and southwestern Virginia: NUREG/C-1217 (R6, RA) U.S. Nuclear Regulatory Commission, Division of Reactor Safety Research, Contract No. NRC-04-77-134, 187 p.

Boyer, S. E., and Elliot, David, 1982, Thrust systems: American Association of Petroleum Geologists Bulletin, v. 66, n. 9, p. 1196-1230.

Carts, D. A., 1981, A regional crustal velocity model for the southeastern U. S. [M. S. thesis]: Blacksburg, Virginia Polytechnic Institute and State University, 124 p.

Clark, S. P., Jr., ed., 1966, Handbook of physical constants: Geological Society of America Memoir 97, 587 p.

Conley, J. F., 1978, Geology of the Piedmont of Virginia - interpretations and problems, *in* Contributions to Virginia geology III: Virginia Division of Mineral Resources Publication 7, p. 115-149.

Dietrich, R. V., 1959, Geology and mineral resources of Floyd County of the Blue Ridge upland, southwestern Virginia: Virginia Polytechnic Institute, Engineering Experiment Station Series Bulletin, n. 134, 160 p.

Espenshade, G. H., Rankin, D. W., Shaw, K. W., and Neuman, R. B., 1975, Geologic map of the east half of the Winston-Salem quadrangle, North Carolina-Virginia: U. S. Geological Survey Miscellaneous Investigations Map I-709B, text and 1:250,000-scale map.

Hammer, S., 1939, Terrain corrections for gravimeter stations: Geophysics, v. 4, p. 184-194.

Hatcher, R. D., Jr., 1981, Thrusts and nappes in the North American Appalachian orogen: Journal of the Geological Society of London, v. 138, p. 491-499.

James, D. E., Smith, T. J., and Steinhart, J. S., 1968, Crustal structure of the middle Atlantic states: Journal of Geophysical Research, v. 73, n. 6, p. 1983-2008.

Karner, G. D., and Watts, A. B., 1983, Gravity anomalies and flexure of the lithosphere at mountain ranges: Journal of Geophysical Research, v. 88, n. B12, p. 10449-10477.

Keller, M. R., Robinson, E. S., and Glover, Lynn, III, 1985, Geologic framework of gravity anomalies in the central piedmont of Virginia: Geological Society of America Bulletin, v. 96, p. 1580-1584.

Kolich, T. M., 1974, Seismic reflection and refraction studies in the folded Valley and Ridge province at Price Mountain, Montgomery County, Virginia [M. S. thesis]: Blacksburg, Virginia Polytechnic Institute and State University, 130 p.

Lewis, S. E., Bartholomew, M. J., and Kaygi, P. B., in preparation, Geology of the Riner quadrangle, Virginia: Virginia Division of Mineral Resources.

Longman, I. M., 1959, Formulas for computing the tidal accelerations due to the moon and the sun: Journal of Geophysical Research, v. 64, n. 12, p. 2351-2355.

Mack, J. W., Jr., 1963, A least-squares method of gravity analysis and its applications in the study of sub-surface geology [Ph.D. dissert.]: Madison, University of Wisconsin, 122 p.

Nettleton, L. L., 1976, Gravity and magnetics in oil prospecting: New York, McGraw Hill Book Co., 464 p.

Plouff, D., 1976, Gravity and magnetic fields of polygonal prisms and applications to magnetic terrain corrections: Geophysics, v. 41, n. 4, p. 727-739.

Talwani, M. J., Worzel, J. L., and Landisman, M., 1959, Rapid gravity computations for two-dimensional bodies with application to the Mendocino submarine fracture zone: Journal of Geophysical Research, v. 64, p. 49-59.

Telford, W. M., Geldart, L. P., Sheriff, R. E., and Keys, D. A., 1976, Applied Geophysics: Cambridge University Press, p. 860.

Wells, P. K., 1975, A seismic reflection and refraction study near the Blue Ridge thrust in Virginia [M. S. thesis]: Blacksburg, Virginia Polytechnic Institute and State University, 91 p.

Woollard, G. P., 1979, The new gravity system-changes in international gravity base values and anomaly values: Geophysics, v. 44, n. 8, p. 1352-1366.

APPENDIX I

A VERTICAL LINE SOURCE ALGORITHM FOR COMPUTING GRAVITY TERRAIN CORRECTIONS

Edwin S. Robinson

A gravity terrain correction accounts for the reduction of the earth's downward gravitational attraction caused by the mass of terrain reaching higher than the observation site, and the lack of mass where the land surface is lower than

the observation site (Hammer, 1939). For purposes of calculating this correction let the land surface be represented by elevations on a rectangular grid. Differences (Δh) between these elevations and the elevation of the observation site indicate heights of rectangular prisms that approximate increments of higher terrain or increments of space between the observation site and the land surface at lower elevation. This is illustrated in two dimensions by the profile in Figure 11. The gravity terrain correction is the sum of the vertical components of gravitational attraction of these prisms at the observation site.

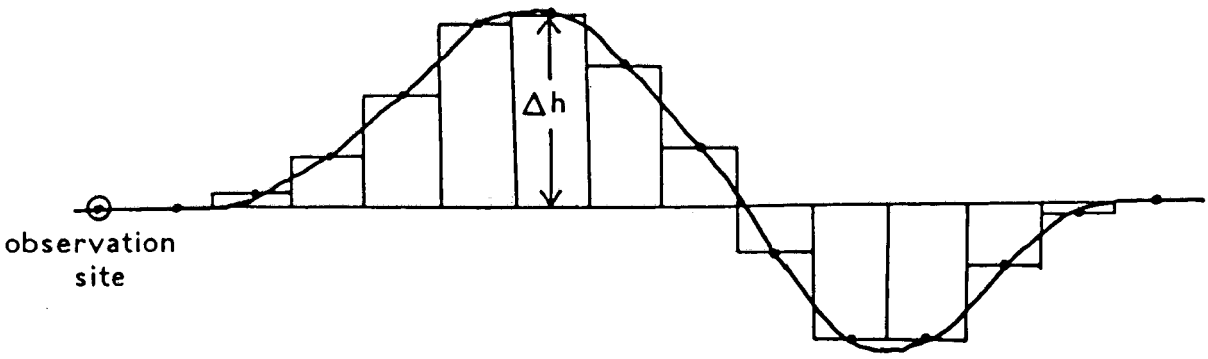

Figure 11. Rectangular prism representation of topography.

The vertical gravitational attraction of a rectangular prism is difficult to compute. The computation can be simplified by assuming that the mass of each prism is concentrated along a vertical line that is its central axis. The formula of Telford and others (1976) expresses the vertical component of gravitational attraction (g) of a vertical line mass:

$$g = .03 \times 10^{-3}\ m\ (1/r - (h^2 + r^2)^{-1/2}) \qquad \text{I-1}$$

where r is the horizontal distance to the observation site (feet), and h is the length of the vertical line. The mass per unit length (m) of the line is found from the product of the volume of the prism centered on the line and the density assumed for the terrain.

The vertical line approximation is satisfactory only where the dimensions of the prism are much smaller than its distance from the observation site. To insure this condition when using elevations given on a rectangular grid the following interpolation procedure can be used. The elevation grid surrounding an observation site is divided into the three zones shown in Figure 12. The inner zone is the grid cell ABCD that contains the observation site P. It is divided into four rectangular subcells. Values of h at subcell corners E, F, G, and H are calculated by linear interpolation along the lines AB, BC, CD, and DA respectively. Then h values at 100 evenly spaced points within each subcell are found by linear interpolation. First, 10 values are obtained along the top line and another 10 values are obtained along the bottom line of the subcell, for example, the lines AE and HP. These values of h are then used to interpolate 10 interior values along each of 10 equally spaced lines extending from the top to the bottom of the subcell.

The middle zone includes elevations within four grid intervals of the cell containing the observation site. Within each grid cell of this zone h is interpolated at 10 equally spaced points first along the top and then along the bottom, for example, along lines IJ and KL. These values are used to interpolate h at 10 intermediate points along each of 10 equally spaced lines from the top to the bottom of the cell.

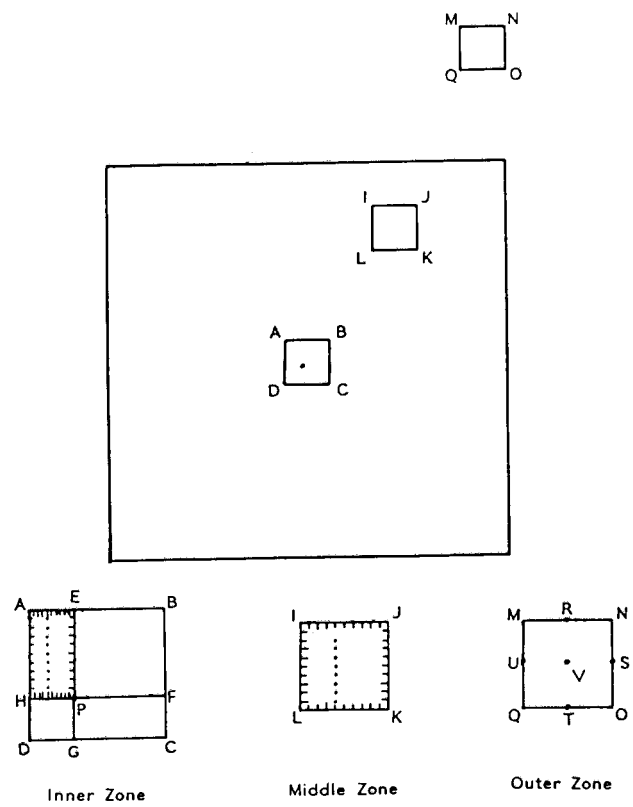

Figure 12. Zones used for calculation of terrain correction.

The outer zones include elevations to a distance beyond which terrain effects can be neglected. Within each grid cell additional values of h are interpolated for points at positions indicated by R, S, T, U, and V in the example.

The FORTRAN program called TERRCORR is used to compute the terrain corrections. Input includes an array of elevation data and its grid spacing, positions and elevations of observation sites, and the density assumed for the terrain. These data are used first to obtain values of h on the elevation grid. Then, intermediate values are interpolated, their distances (r) are found, and values of vertical gravitational attraction are computed using equation I-1. Finally, these latter values are summed to obtain a terrain correction.

The interpolation intervals and the sizes of the middle and outer zones can be changed from the sites and intervals described above, depending on the nature of the terrain. In the event that an observation site is so close to the side of the inner grid cell that spuriously steep terrain would be produced by the interpolation process, that site can be arbitrarily moved to a prescribed minimum distance for purposes of computation. Then, to the extent that topographic features are properly represented by the elevation grid, reliable terrain corrections can be calculated.

APPENDIX II

GRAVITY DATA

STATION	ELEVATION (FT)	LATITUTE (DEG)	LONGITUDE (DEG)	OBSERVED GRAVITY (MGAL)	FREE AIR ANOMALY (MGAL)	BOUGUER ANOMALY (MGAL)
1	2610	37.0367	80.2063	979682.0	19.9	-69.0
2	2533	37.0265	80.2040	979685.9	17.5	-68.8
3	2496	37.0205	80.1967	979687.4	16.5	-68.6
4	2489	37.0175	80.1972	979687.9	16.3	-68.5
5	2725	37.0128	80.2028	979674.0	25.5	-67.3
6	2707	37.0145	80.2077	979674.4	23.3	-68.9
7	2705	37.0177	80.2117	979674.5	23.2	-68.9
8	2765	37.0218	80.2157	979670.7	25.1	-69.1
9	2668	37.0212	80.2243	979676.5	21.7	-69.2
10	2760	37.0113	80.2130	979670.2	25.1	-69.0
11	2655	37.0133	80.2202	979677.5	21.5	-68.9
12	2580	37.0108	80.2267	979680.5	18.4	-69.5
13	2489	37.0052	80.2338	979684.3	13.6	-71.1
14	2426	37.0117	80.2447	979689.4	12.8	-68.8
15	2490	37.0202	80.2465	979686.3	14.8	-70.0
16	2615	37.0258	80.2347	979679.2	18.5	-70.6
17	2704	37.0333	80.2310	979673.7	21.4	-70.8
18	2737	37.0340	80.2183	979673.1	23.8	-69.4
19	2642	37.0423	80.2060	979680.2	21.2	-68.9
20	2360	37.0515	80.2087	979695.3	8.8	-71.6
21	2230	37.0582	80.2085	979702.6	2.9	-73.1
22	1922	37.0695	80.2160	979719.6	-10.1	-75.5
23	1785	37.0775	80.2093	979728.3	-14.2	-75.0
24	1688	37.0833	80.2068	979733.2	-19.4	-76.9
25	1637	37.0927	80.2075	979735.8	-22.4	-78.2
26	2175	37.1380	80.3422	979706.9	-4.4	-78.6
27	1990	37.0658	80.2142	979715.9	-6.4	-74.1
28	2290	37.0653	80.2200	979700.4	6.4	-71.6
29	2430	37.0597	80.2225	979691.7	10.9	-71.9
30	2630	37.0555	80.2155	979682.1	20.9	-68.7
31	2670	37.0503	80.2182	979677.2	19.9	-71.1
32	2610	37.0478	80.2158	979681.8	18.8	-71.1
33	2470	37.0432	80.2223	979689.3	14.0	-70.1
34	2450	37.0445	80.2305	979690.4	13.3	-70.2
35	2570	37.0402	80.2287	979679.6	13.7	-73.9
36	2686	37.0380	80.2428	979674.4	19.5	-72.0
37	2705	37.0453	80.2095	979676.0	21.9	-70.3
38	2005	37.0678	80.2230	979714.6	-7.2	-75.5
39	2069	37.0647	80.2292	979711.6	-3.2	-73.7
40	2125	37.0653	80.2335	979708.6	-1.0	-73.4
41	2195	37.0612	80.2332	979710.0	7.0	-67.8
42	2140	37.0555	80.2347	979705.3	-1.9	-74.8
43	2195	37.0503	80.2397	979702.2	0.2	-74.6
44	2360	37.0503	80.2397	979702.2	4.4	-76.0
45	2175	37.1380	80.3422	979706.2	-5.1	-79.2
46	2175	37.1380	80.3422	979706.4	-4.9	-79.1
47	1507	37.0983	80.2327	979745.1	-25.3	-76.7
48	2280	37.0767	80.2168	979704.9	9.0	-68.7
49	2375	37.0797	80.2167	979694.9	23.6	-73.9

STATION	ELEVATION (FT)	LATITUTE (DEG)	LONGITUDE (DEG)	OBSERVED GRAVITY (MGAL)	FREE AIR ANOMALY (MGAL)	BOUGUER ANOMALY (MGAL)
50	2673	37.0435	80.1632	979679.7	23.6	-67.5
51	2721	37.0515	80.1567	979678.8	26.2	-66.5
52	2664	37.0603	80.1520	979682.8	23.9	-66.9
53	2732	37.0685	80.1530	979679.1	25.6	-67.4
54	2730	37.0685	80.1578	979679.5	25.9	-67.1
55	2794	37.0665	80.1632	979674.3	27.6	-67.6
56	2720	37.0615	80.1668	979678.0	24.4	-68.3
57	2670	37.0563	80.1702	979680.5	22.2	-68.8
58	2727	37.0483	80.1817	979676.5	24.5	-68.4
59	2717	37.0552	80.1780	979677.5	24.1	-68.0
60	2702	37.0442	80.1825	979677.6	24.1	-67.9
61	2725	37.0503	80.1935	979676.1	23.8	-69.0
62	2632	37.0425	80.1895	979680.9	20.9	-68.8
63	1587	37.0983	80.2153	979737.9	-25.0	-79.1
64	1570	37.1062	80.2207	979743.8	-21.7	-75.1
65	1640	37.1105	80.2250	979740.1	-19.7	-75.6
66	1585	37.1110	80.2105	979739.2	-25.8	-79.8
67	1552	37.1045	80.2142	979740.9	-26.2	-79.1
68	1534	37.1008	80.2198	979743.0	-25.9	-78.1
69	2175	37.1380	80.3422	979706.7	-4.7	-78.8
70	2175	37.1380	80.3422	979706.9	-4.5	-78.6
71	2710	37.0402	80.1988	979676.9	24.2	-68.1
72	2578	37.0435	80.1717	979685.6	20.5	-67.3
73	2610	37.0365	80.1648	979683.3	21.2	-67.7
74	2522	37.0318	80.1720	979688.5	19.1	-66.9
75	2490	37.0270	80.1667	979690.6	18.2	-66.7
76	2535	37.0233	80.1592	979687.5	20.2	-66.1
77	2510	37.0140	80.1400	979690.3	20.7	-64.8
78	2480	37.0167	80.1467	979691.1	18.6	-65.9
79	2550	37.0112	80.1350	979688.5	23.6	-63.3
80	2510	37.0065	80.1430	979690.7	22.0	-63.5
81	2410	37.0063	80.1512	979696.6	18.5	-63.6
82	2448	37.0083	80.1613	979693.7	19.2	-64.2
83	2458	37.0060	80.1730	979692.4	18.8	-64.9
84	2539	37.0117	80.1742	979686.4	20.5	-66.0
85	2612	37.0167	80.1722	979681.8	21.8	-67.2
86	2658	37.0237	80.1720	979679.5	23.8	-66.8
87	2680	37.0342	80.1797	979677.5	22.9	-68.4
88	2720	37.0393	80.1835	979675.9	24.2	-68.5
89	2570	37.0308	80.1867	979685.1	20.2	-67.4
90	2545	37.0262	80.1948	979684.9	17.6	-69.1
91	2175	37.1380	80.3422	979706.9	-4.5	-78.6
92	2175	37.1380	80.3422	979706.7	-4.6	-78.7
93	2465	37.0150	80.1923	979688.9	15.0	-69.0
94	2450	37.0133	80.1843	979690.6	15.4	-68.1
95	2550	37.0135	80.1257	979688.6	22.7	-64.2
96	2475	37.0190	80.1305	979691.8	18.9	-65.4
97	2495	37.0247	80.1327	979690.6	18.6	-66.4
98	2589	37.0307	80.1308	979685.1	21.9	-66.3
99	2664	37.0367	80.1458	979681.0	24.0	-66.8
100	2635	37.0400	80.1563	979682.6	22.8	-67.0
101	2538	37.0388	80.1305	979689.6	20.7	-65.8
102	2550	37.0452	80.1337	979689.9	22.1	-64.8

STATION	ELEVATION (FT)	LATITUTE (DEG)	LONGITUDE (DEG)	OBSERVED GRAVITY (MGAL)	FREE AIR ANOMALY (MGAL)	BOUGUER ANOMALY (MGAL)
103	2590	37.0492	80.1452	979687.2	22.3	-65.9
104	2585	37.0598	80.1403	979687.7	21.4	-66.6
105	2738	37.0598	80.1252	979677.4	25.4	-67.8
106	2696	37.0603	80.1317	979678.9	23.1	-68.8
107	2640	37.0683	80.1347	979685.3	23.2	-66.7
108	2742	37.0767	80.1378	979679.5	27.0	-66.4
109	2675	37.0733	80.1463	979684.1	25.3	-65.9
110	1620	37.1233	80.2373	979740.1	-22.6	-77.8
111	1580	37.1184	80.2395	979742.2	-23.3	-77.1
112	1511	37.1157	80.2480	979745.6	-26.4	-77.9
113	1467	37.1000	80.2500	979747.4	-27.7	-77.7
114	1610	37.1100	80.2417	979739.7	-22.9	-77.8
115	1474	37.0983	80.2440	979745.9	-27.6	-77.8
116	2175	37.1380	80.3422	979707.4	-4.0	-78.1
117	2175	37.1380	80.3422	979707.7	-3.6	-77.7
118	2614	37.0553	80.2012	979678.3	15.6	-73.4
119	2856	37.0817	80.1343	979673.3	30.6	-66.7
120	2805	37.0850	80.1258	979680.2	32.7	-62.9
121	2656	37.1182	80.1333	979685.7	21.4	-69.1
122	2701	37.1220	80.1303	979683.1	22.1	-69.9
123	2616	37.1123	80.1325	979688.2	20.2	-68.9
124	2665	37.1068	80.1317	979685.9	23.4	-67.4
125	2638	37.1003	80.1312	979688.1	23.0	-66.8
126	2697	37.0935	80.1287	979685.1	26.5	-65.4
127	2462	37.0857	80.1467	979696.6	16.8	-67.1
128	2520	37.0820	80.1537	979693.9	19.6	-66.2
129	2340	37.0800	80.1620	979700.7	9.4	-70.3
130	2483	37.0957	80.1608	979693.5	14.8	-69.8
131	2429	37.0910	80.1588	979696.8	13.1	-69.7
132	2685	37.1032	80.1613	979681.6	21.0	-70.5
133	2835	37.1087	80.1558	979672.6	26.1	-70.5
134	2590	37.1040	80.1708	979686.6	17.0	-71.2
135	2590	37.0992	80.1780	979686.7	17.1	-71.1
136	2565	37.0927	80.1870	979688.9	17.9	-69.5
137	2450	37.0860	80.1887	979693.7	12.9	-70.6
138	2360	37.0987	80.1875	979698.6	8.4	-72.0
139	2470	37.1070	80.1815	979694.8	14.0	-70.2
140	2520	37.1122	80.1728	979693.6	16.6	-69.3
141	2507	37.1183	80.1733	979695.1	16.8	-68.6
142	2504	37.1233	80.1750	979694.2	14.7	-70.6
143	2540	37.1150	80.1625	979691.2	16.0	-70.5
144	2660	37.1233	80.1417	979685.4	20.6	-70.0
145	2766	37.1150	80.1483	979677.6	23.7	-70.5
146	2720	37.1183	80.1425	979679.8	21.6	-71.1
147	2590	37.1075	80.1365	979689.4	19.8	-68.4
148	2560	37.1020	80.1423	979690.6	18.2	-69.0
149	2515	37.0945	80.1438	979691.7	16.0	-69.7
150	2175	37,1380	80.3422	979706.9	-4.4	-78.6
151	2175	37.1380	80.3422	979707.4	-3.9	-78.1
152	2390	37.0525	80.3018	979691.0	7.3	-74.1
153	2594	37.0473	80.2858	979677.7	13.2	-75.2
154	2525	37.0458	80.2775	979682.0	11.0	-75.1
155	2660	37.0460	80.2648	979674.5	16.2	-74.5

STATION	ELEVATION (FT)	LATITUTE (DEG)	LONGITUDE (DEG)	OBSERVED GRAVITY (MGAL)	FREE AIR ANOMALY (MGAL)	BOUGUER ANOMALY (MGAL)
156	2689	37.0392	80.2598	979674.3	19.6	-72.0
157	2670	37.0330	80.2540	979676.5	21.0	-70.0
158	2680	37.0343	80.2637	979675.1	20.5	-70.8
159	2646	37.0318	80.2680	979676.3	18.5	-71.6
160	2579	37.0255	80.2642	979680.7	16.6	-71.3
161	2550	37.0237	80.2553	979683.0	17.1	-69.8
162	2535	37.0192	80.2582	979681.4	14.1	-72.3
163	2735	37.0217	80.2703	979672.1	23.6	-69.6
164	2690	37.0173	80.2733	979672.2	19.6	-72.1
165	2670	37.0140	80.2638	979674.6	20.0	-70.9
166	2680	37.0700	80.2605	979674.2	21.5	-69.8
167	2550	37.0007	80.2568	979682.1	18.1	-68.8
168	2683	37.0118	80.2770	979672.4	19.9	-71.5
169	2565	37.0075	80.2822	979679.0	15.5	-71.9
170	2485	37.0060	80.2920	979683.0	12.0	-72.7
171	2504	37.0118	80.2958	979681.7	12.5	-72.8
172	2650	37.0163	80.2898	979673.1	16.7	-73.6
173	2595	37.0213	80.2863	979676.9	15.3	-73.1
174	2729	37.0267	80.2815	979669.8	19.8	-73.1
175	2710	37.0290	80.2757	979672.2	20.4	-71.9
176	2540	37.0378	80.2733	979681.7	13.0	-73.5
177	2496	37.0512	80.2937	979684.1	10.4	-74.7
178	2175	37.1380	80.3422	979708.2	-3.2	-77.3
179	2175	37.1380	80.3422	979707.9	-3.4	-77.6
180	2242	37.0533	80.3588	979697.0	-0.6	-77.0
181	2448	37.0405	80.3505	979683.7	6.4	-77.0
182	2430	37.0360	80.3430	979684.8	5.8	-77.0
183	2532	37.0268	80.3453	979678.2	9.8	-76.5
184	2255	37.0175	80.3413	979693.2	-0.4	-77.2
185	2226	37.0120	80.3513	979694.5	-0.9	-76.7
186	2150	37.0087	80.3650	979698.2	-4.4	-77.6
187	2105	37.0062	80.3747	979700.6	-6.2	-77.9
188	2210	37.0047	80.3552	979695.4	-1.5	-76.8
189	2262	37.0175	80.3347	979693.4	0.4	-76.6
190	2380	37.0103	80.3350	979687.3	6.4	-74.7
191	2578	37.0043	80.3383	979674.9	12.6	-75.2
192	2327	37.0208	80.3245	979690.9	4.0	-75.3
193	2525	37.0102	80.3167	979679.3	12.0	-74.0
194	2687	37.0077	80.3062	979670.1	18.1	-73.5
195	2595	37.0008	80.2963	979680.0	16.4	-72.1
196	2510	37.0153	80.3203	979680.0	10.4	-75.1
197	2330	37.0233	80.3168	979691.5	4.9	-74.4
198	2412	37.0313	80.3125	979686.8	7.0	-75.1
199	2570	37.0370	80.3005	979678.0	12.1	-75.4
200	2674	37.0430	80.2900	979672.7	16.7	-74.4
201	2530	37.0470	80.2963	979681.7	11.1	-75.1
202	2175	37.1380	80.3422	979707.9	-3.5	-77.6
203	2175	37.1380	80.3422	979707.8	-3.6	-77.7
204	2430	37.0627	80.3717	979683.2	2.4	-80.4
205	2466	37.0565	80.3725	979681.7	4.2	-79.8
206	2338	37.0532	80.3682	979690.5	1.9	-77.8
207	2301	37.0575	80.3478	979693.7	1.7	-77.7
208	2338	37.0578	80.3342	979691.6	2.1	-77.6

STATION	ELEVATION (FT)	LATITUTE (DEG)	LONGITUDE (DEG)	OBSERVED GRAVITY (MGAL)	FREE AIR ANOMALY (MGAL)	BOUGUER ANOMALY (MGAL)
209	2457	37.0547	80.3262	979685.9	8.5	-75.2
210	2371	37.0525	80.3215	979691.2	5.7	-75.0
211	2358	37.0550	80.3125	979692.5	5.8	-74.6
212	2545	37.0392	80.2830	979681.1	12.9	-73.9
213	2668	37.0275	80.2930	979672.7	17.0	-73.9
214	2345	37.0478	80.3195	979692.2	4.2	-75.7
215	2488	37.0418	80.3150	979683.1	9.6	-75.2
216	2560	37.0355	80.3153	979678.0	11.2	-76.0
217	2610	37.0217	80.3492	979671.0	10.8	-78.1
218	2595	37.0208	80.3583	979671.8	10.2	-78.2
219	2515	37.0203	80.3725	979673.4	4.3	-81.4
220	2388	37.0263	80.3730	079685.1	3.1	-78.3
221	2238	37.0297	80.3662	979694.7	-1.5	-77.7
222	2183	37.0367	80.3725	979698.4	-3.9	-78.3
223	2207	37.0437	80.3688	979696.9	-3.1	-78.3
224	2220	37.0475	80.3632	979695.9	-3.8	-79.4
225	2310	37.0495	80.3558	979692.6	1.4	-77.3
226	2335	37.0342	80.3515	979690.8	3.8	-75.8
227	2334	37.0437	80.3358	979691.7	3.7	-75.8
228	2349	37.0465	80.3293	979691.5	3.9	-76.1
229	2175	37.1380	80.3422	979707.8	-3.6	-77.7
230	2175	37.1380	80.3422	979707.7	-3.7	-77.8
231	1406	37.1238	80.2690	979754.4	-28.7	-76.3
232	1422	37.1195	80.2767	979751.4	-28.9	-77.3
233	1460	37.1118	80.2950	979748.1	-28.7	-78.4
234	1720	37.1035	80.3030	979730.6	-18.7	-77.3
235	1600	37.1203	80.3017	979740.0	-23.6	-78.1
236	1410	37.1175	80.2677	979752.5	-29.0	-77.0
237	1425	37.1137	80.2620	979751.8	-28.2	-76.8
238	1450	37.1112	80.2568	979748.6	-29.1	-78.5
239	1455	37.1052	80.2625	979747.1	-29.2	.78.7
240	1510	37.1035	80.2693	979745.4	-25.7	-77.2
241	1590	37.0992	80.2770	979739.3	-24.3	-78.4
242	1821	37.0965	80.2887	979723.5	-17.4	-79.5
243	2080	37.0938	80.2943	979707.2	-9.3	-80.2
244	2350	37.0910	80.2840	979690.2	-1.0	-81.1
245	2575	37.0887	80.2903	979677.2	7.2	-80.6
246	2588	37.0848	80.3000	979679.0	11.2	-77.1
247	2544	37.0810	80.2937	979682.1	10.1	-76.6
248	2516	37.0747	80.2868	979684.2	10.5	-75.2
249	2540	37.0738	80.3020	979683.3	11.8	-74.7
250	2527	37.0717	80.3103	979683.4	10.7	-75.4
251	2500	37.0703	80.3213	979683.4	8.1	-77.1
252	2450	37.0670	80.3268	979686.0	6.0	-77.4
253	2175	37.1380	80.3422	979707.7	-3.6	-77.7
254	2175	37.1380	80.3422	979707.7	-3.7	-77.8
255	2035	37.1053	80.3705	979712.6	-9.2	-78.5
256	2194	37.1123	80.3637	979702.5	-5.2	-80.0
257	2175	37.1380	80.3422	979707.7	-3.7	-77.8
258	2175	37.1380	80.3422	979707.3	-4.1	-78.2
259	2250	37.1150	80.3542	979699.7	-2.8	-79.4
260	2061	37.1158	80.3463	979712.3	-7.9	-78.1
261	1682	37.1123	80.3308	979733.7	-22.2	-79.5

STATION	ELEVATION (FT)	LATITUTE (DEG)	LONGITUDE (DEG)	OBSERVED GRAVITY (MGAL)	FREE AIR ANOMALY (MGAL)	BOUGUER ANOMALY (MGAL)
262	1591	37.1080	80.3275	979738.6	-24.9	-79.1
263	1600	37.1097	80.3207	979739.6	-23.1	-77.6
264	1510	37,1125	80.3133	979744.4	-27.6	-79.1
265	1650	37.1032	80.3413	979734.6	-23.3	-79.5
266	1675	37.1003	80.3525	979732.6	-23.0	-80.1
267	1750	37.0947	80.3677	979726.8	-20.8	-80.4
268	1625	37,1017	80,3295	979735.7	-24.6	-80.0
269	1695	37.0957	80.3353	979731.3	-21.5	-79.2
270	1775	37.0917	80.3437	979725.7	-19.6	-80.0
271	2175	37.1380	80.3422	979707.8	-3.6	-77.7
272	2175	37.1380	80.3422	979708.1	-3.3	-77.4
273	2710	37.0512	80.2567	979671.8	18.2	-74.1
274	2732	37.0562	80.2498	979670.9	18.4	-74.6
275	2210	37.0637	80.2417	979705.0	3.4	-71.9
276	2626	37.06333	80.2558	979678.7	16.3	-73.2
277	2652	37.0680	80.2537	979677.0	16.0	-74.3
278	2603	37.0713	80.2568	979680.1	14.6	-74.1
279	2575	37.0758	80.2580	979681.4	13.2	-74.6
280	2500	37.0813	80.2502	979684.7	8.6	-76.6
281	2510	37.0832	80.2387	979686.1	10.8	-74.7
282	2350	37.0860	80.2342	979696.3	6.0	-74.1
283	2612	37.0543	80.2695	979678.7	15,8	-73.1
284	2550	37.0587	80.2740	979682.3	12.7	-74.2
285	2480	37.0620	80.2842	979687.8	11.6	-72.9
286	2510	37.0675	80.2882	979684.7	10.4	-75.1
287	2175	37,1380	80.3422	979707.9	-3.4	-77.6
288	2175	37.1380	80.3422	979708.1	-3.3	-77.4
289	2085	37.1112	80.4235	979710.0	-8.0	-79.0
290	2032	37.1040	80.4313	979711.4	-10.6	-79.8
291	2156	37.0985	80.4438	979702.6	-6.8	-80.3
292	2135	37.0938	80.4480	979703.2	-8.2	-80.9
293	2104	37.0887	80.4513	979704.3	-10.0	-81.7
294	2083	37.0792	80.4532	979705.7	-9.7	-80.7
295	2037	37.0667	80.4413	979704.6	-13.2	-82.6
296	2025	37.0553	80.4408	979705.2	-12.9	-81.9
297	2135	37.0398	80.4365	979699.1	-7.7	-80.4
298	2267	37.0332	80.4397	979690.6	-2.8	-80.0
299	2345	37.0270	80.4400	979686.4	0.3	-79.6
300	2290	37.0258	80.4325	979689.0	-2.3	-80.3
301	2162	37.0237	80.4210	979697.4	-5.0	-78.6
302	2109	37.0167	80.4253	979699.6	-7.7	-79.6
303	2097	37.0073	80.4260	979698.9	-8.6	-80.0
304	2116	37.0228	80.4117	979700.0	-6.7	-78.8
305	2083	37.0153	80.4047	979701.8	-8.0	-78.9
306	2354	37.0203	80.3932	979686.2	1.9	-79.3
307	2346	37.0300	80.4083	979686.7	0.8	-79.2
308	2311	37.0347	80.4113	979689.6	-0.7	-79.4
309	2399	37.0423	80.4170	979683.6	1.6	-80.1
310	2150	37.0442	80.4263	979698.5	-6.9	-80.1
311	2074	37.0515	80.4203	979703.1	-10.4	-81.0
312	2175	37.1380	80.3422	979708.3	-3.1	-77.2
313	2175	37.1380	80.3422	979708.6	-2.8	-76.9
314	2145	37.1132	80.4375	979707.7	-4.6	-77.7

STATION	ELEVATION (FT)	LATITUTE (DEG)	LONGITUDE (DEG)	OBSERVED GRAVITY (MGAL)	FREE AIR ANOMALY (MGAL)	BOUGUER ANOMALY (MGAL)
315	2035	37.0912	80.4420	979709.5	-11.3	-80.6
316	2085	37.0487	80.4470	979702.1	-10.3	-81.3
317	2101	37.0452	80.4550	979700.7	-9.3	-80.9
318	2225	37,0325	80.4508	979693.6	-3.8	-79.6
319	2295	37.0085	80.4020	979689.0	0.1	-78.1
320	2390	37.0012	80.3983	979683.9	4.8	-76.6
321	2341	36.9908	80.4008	979685.7	3.0	-76.8
322	2327	36.9815	80.4025	979685.8	1.8	-77.5
323	2468	36.9740	80.3993	979677.1	7.2	-76.9
324	2475	36.9697	80.3885	979676.2	8.0	-76.3
325	2170	36.9653	80.3758	979694.4	-2.5	-76.4
326	2315	36.9870	80.4103	979687.3	2.2	-76.7
327	2201	36.9908	80.4225	979693.0	-2.9	-77.9
328	2152	36.9948	80.4262	979695.9	-5.6	-78.9
329	2271	36.9918	80.4332	979688.8	-1.4	-78.8
330	2243	37.0030	80.4358	979687.4	-6.4	-82.8
331	2112	37.0030	80.4253	979699.0	-7.1	-79.1
332	2071	37.0032	80.4150	979701.8	-8.2	-78.7
333	2110	37.0615	80.4272	979701.2	-9.8	-81.6
334	2078	37.0650	80.4282	979704.7	-9.3	-80.1
335	1975	37.0685	80.4165	979710.2	-14.4	-81.7
336	1911	37.0712	80.4100	979714.3	-16.3	-81.4
337	1875	37.0787	80.4070	979717.3	-17.7	-81.5
338	1890	37.0887	80.4125	979719.3	-15.1	-79.5
339	1897	37.0880	80.4215	979718.8	-14.1	-78.7
340	1931	37.0945	80.4263	979716.3	-14.3	-80.1
341	2175	37.1380	80.3422	979708.6	-2.8	-76.9
342	2175	37.1380	80.3422	979708.6	-2.8	-76.9
343	2060	37.0720	80.4372	979703.9	-12.7	-82.9
344	1985	37.0797	80.4358	979709.4	-15.3	-82.9
345	2421	36.9803	80.4463	979677.5	3.3	-79.2
346	2606	36.9728	80.4403	979667.2	10.3	-78.4
347	2568	36.9683	80.4292	979669.6	10.1	-77.4
348	2486	36.9720	80.4147	979675.1	6.9	-77.8
349	2445	36.9725	80.4042	979678.1	6.1	-77.2
350	2170	36.9592	80.3825	979694.4	-2.5	-76.5
351	2485	36.9537	80.3967	979675.5	9.1	-75.5
352	2508	36.9412	80.4048	979674.0	10.7	-74.8
353	2440	36.9418	80.3938	979679.2	9.5	-73.6
354	2329	36.9492	80.3800	979686.4	5.4	-73.9
355	2300	36.9518	80.3700	979689.6	5.8	-72.6
356	2228	36.9558	80.3672	979693.2	2.7	-73.3
357	2362	36.9510	80.3605	979686.5	8.6	-71.9
358	2455	36.9438	80.3592	979684.5	16.2	-67.4
359	2564	36.9418	80.3648	979676.4	18.4	-69.0
360	2496	36.9113	80.3200	979689.4	27.8	-57.2
361	2447	36.9153	80.3213	979692.3	26.1	-57.3
362	2195	36.9292	80.3313	979703.2	11.4	-63.4
363	2189	36.9320	80.3347	979702.4	10.0	-64.6
364	2180	36.9398	80.34.53	979697.7	3.5	-70.8
365	2175	37.1380	80.3422	979708.7	-2.6	-76.7
366	2175	37.1380	80.3422	979708.6	-2.8	-76.9
367	1940	37.0982	80.4275	979715.8	-13.9	-80.0

STATION	ELEVATION (FT)	LATITUTE (DEG)	LONGITUDE (DEG)	OBSERVED GRAVITY (MGAL)	FREE AIR ANOMALY (MGAL)	BOUGUEER ANOMALY (MGAL)
368	2040	37.0722	80.4603	979707.4	-11.1	-80.6
369	2047	37.0637	80.4613	979706.2	-10.7	-80.4
370	2135	37.0175	80.4432	979698.3	-6.6	-79.3
371	2279	36.9848	80.4387	979687.4	-1.2	-78.8
372	2555	36.9763	80.4420	979671.1	9.5	-77.6
373	2325	36.9572	80.4113	979684.7	3.4	-75.9
374	2480	36.9503	80.4018	979676.4	9.6	-74.9
375	2205	36.9468	80.4080	979692.2	0.4	-74.7
376	2505	36.9593	80.3947	979673.5	8.1	-77.3
377	2122	36.9720	80.3713	979698.6	-3.8	-76.1
378	2115	36.9770	80.3717	979699.8	-3.2	-75.3
379	2110	36.9758	80.3785	979699.4	-4.1	-76.0
380	2105	36.9800	80.3870	979699.2	-4.7	-76.4
381	2100	36.9867	80.3918	979699.5	-5.9	-77.4
382	2423	36.9207	80.3887	979685.2	15.8	-66.8
383	2340	36.9198	80.3802	979691.2	13.9	-65.8
384	2385	36.9170	80.3737	979689.5	16.5	-64.8
385	2255	36.9137	80.3652	979697.6	13.3	-63.6
386	2415	36.9103	80.3523	979691.9	22.7	-59.6
387	2250	36.9087	80.3402	979702.5	17.7	-58.9
388	2313	38.9087	80.3320	979700.9	22.1	-56.7
389	2480	36.9137	80.3258	979689.5	26.4	-58.1
390	2415	36.9160	80.3352	979701.7	23.5	-58.8
391	2220	36.9195	80.3453	979701.7	13.2	-62.4
392	2376	36.9250	80.3483	979691.5	17.6	-63.3
393	2175	37.1380	80.3422	979708.8	-2.6	-76.7
394	2175	37.1380	80.3422	979708.7	-2.6	-76.7
395	2010	37.0657	80.4498	979706.4	-14.0	-82.4
396	2086	37.0403	80.4580	979703.1	-8.3	-79.3
397	2211	37.0312	80.4555	979694.7	-3.9	-79.3
398	2501	36.8958	80.3558	979684.7	24.5	-60.8
399	2550	36.9030	80.3547	979682.4	26.8	-60.1
400	2550	36.8887	80.3543	979683.1	28.4	-58.5
401	2625	36.8783	80.3542	979679.2	32.5	-56.9
402	2533	36.8742	80.3487	979685.0	29.7	-56.6
403	2482	36.8683	80.3647	979685.6	26.4	-58.2
404	2534	36.8613	80.3550	979682.2	28.8	-57.5
405	2750	36.8592	80.3467	979669.2	36.1	-57.6
406	2630	36.8578	80.3402	979677.4	33.1	-56.5
407	2520	36.8640	80.3303	979685.7	30.1	-55.8
408	2400	36.8708	80.3337	979693.8	26.9	-54.9
409	2560	36.9075	80.3175	979686.4	30.8	-56.5
410	2575	36.9037	80.3168	979684.0	30.7	-57.0
411	2484	36.8990	80.3187	979689.4	27.6	-57.0
412	2336	36.8800	80.3297	979697.9	24.1	-55.5
413	2483	36.8595	80.3238	979687.0	28.8	-55.8
414	2510	36.8535	80.3280	979684.5	28.9	-56.6
415	2644	36.8482	80.3342	979674.2	32.2	-57.9
416	2454	36.8595	80.3153	979688.6	27.7	-55.9
417	2440	36.8652	80.3142	979690.4	27.3	-55.8
418	2515	36.8548	80.3092	979685.3	30.1	-55.5
419	2678	36.8445	80.3180	979673.0	34.1	-57.1
420	2610	36.8438	80.3065	979679.6	34.3	-54.6

STATION	ELEVATION (FT)	LATITUTE (DEG)	LONGITUDE (DEG)	OBSERVED GRAVITY (MGAL)	FREE AIR ANOMALY (MGAL)	BOUGUER ANOMALY (MGAL)
421	2590	36.8480	80.2977	979683.1	36.0	-52.3
422	2744	36.8397	80.3205	979668.7	36.9	-56.6
423	2556	36.8320	80.3200	979678.2	29.7	-57.7
424	2350	36.8252	80.3263	979688.8	20.9	-59.1
425	1750	36.8098	80.3257	979725.3	2.0	-57.7
426	1590	36.8103	80.3163	979737.6	-0.8	-54.9
427	1634	36.8070	80.3075	979735.3	1.9	-53.8
428	2175	37.1380	80.3422	979708.7	-2.7	-76.8
429	2175	37.1380	80.3422	979708.7	-2.6	-76.7
430	1590	36.8025	80.2967	979737.3	-0.2	-54.4
431	1480	36.7982	80.2920	979747.8	-0.1	-50.5
432	1435	36.7947	80.2868	979750.6	-0.5	-49.4
433	1410	36.7900	80.2775	979753.6	0.1	-47.9
434	1545	36.7983	80.2732	979745.7	4.0	-48.6
435	1410	36.8058	80.2688	979752.6	-1.8	-49.9
436	1598	36.8168	80.2737	979742.6	4.9	-49.5
437	1653	36.8212	80.2745	979740.3	6.9	-49.4
438	1655	36.8208	80.2862	979739.0	5.8	-50.6
439	1620	36.8190	80.2940	979739.3	3.7	-51.5
440	1575	36.8123	80.2725	979742.6	2.8	-50.9
441	2175	37.1380	80.3422	979708.8	-2.6	-76.7
442	2175	37.1380	80.3422	979708.8	-2.6	-76.7
443	2330	36.9203	80.3247	979698.4	20.3	-59.1
444	2280	36.9042	80.3363	979699.6	18.6	-59.1
445	2255	36.9013	80.3405	979702.3	18.9	-57.9
446	2270	36.8953	80.3392	979702.6	20.7	-56.7
447	2335	36.8865	80.3392	979697.5	22.6	-56.9
448	2415	36.8798	80.3450	979691.7	25.3	-57.0
449	2565	36.8692	80.3563	979681.7	30.3	-57.1
450	2575	36.8653	80.3470	979681.1	30.6	-57.1
451	2700	36,8497	80.3413	979671.4	34.6	-57.4
452	2871	36.8403	80.3480	979658.7	38.9	-58.9
453	2756	36.8447	80.3512	979666.9	35.3	-58.6
454	2662	36.8370	80.3353	979672.4	32.9	-57.8
455	1479	36.7763	80.2907	979747.6	1.5	-48.9
456	1435	36.7822	80.2953	979747.9	-2.3	-51.2
457	1495	36.7887	80.3070	979741.2	-4.3	-55.2
458	1430	36.7858	80.2982	979747.5	-3.2	-51.9
459	1415	36.7828	80.2835	979752.4	0.3	-47.9
460	1575	36.8163	80.3070	979740.4	0.6	-53.1
461	1669	36.8215	80.3048	979738.6	6.7	-50.1
462	2868	36.8335	80.3277	979659.6	39.5	-58.2
463	2515	36.8522	80.3180	979683.3	28.1	-57.5
464	2297	36.8883	80.3222	979699.7	21.3	-57.0
465	2480	36.9342	80.3755	979683.7	18.7	-65.8
466	2565	36.9303	80.3830	979677.7	20.7	-66.7
467	2175	37.1380	80.3422	979708.8	-2.6	-76.7

PILLOW LAVAS IN THE CATOCTIN FORMATION OF CENTRAL VIRGINIA

Edgar W. Spencer[1], Christopher Bowring[1], and J. D. Bell[2]

CONTENTS

	Page
Abstract	83
Introduction	83
Geologic setting	84
Geology of the metabasalts	85
Petrology	86
Geochemistry	87
Environment of formation	87
Conclusions	88
Acknowledgments	88
References cited	90

ILLUSTRATIONS

Figure

1. Regional sketch map showing the areal distribution of the Catoctin Formation 84
2. Geologic map of the study area 85
3. Strongly developed penetrative cleavage dipping to the southeast 86
4. Large pillow-shaped masses of greenstone 86
5. Pillow rinds 86
6. Pillow and pillow breccia 87
7. Geochemical oxide percents measured across Catoctin pillow lava samples 89
8. Ti-Zr-Y discrimination diagram 90

TABLE

1. Composition of Catoctin metabasalts from the northwest flank of the Blue Ridge, central Virginia 88

ABSTRACT

Metabasalts of tholeiitic basalt and basaltic andesite composition near Oronoco, Virginia contain pillow structures. The study area is close to the southern end of the Catoctin Formation outcrop belt on the northwestern flank of the Blue Ridge anticlinorium. The flows in this area are interbedded with thick, shallow-water arkosic and conglomeratic metasedimentary rocks. The metabasalts were extruded into a basin now bounded by faults, which is interpreted as an early Cambrian rift valley. Ti-Zr-Y plots indicate that the rocks are "within-plate" basalts. The plots of the metabasalts from Oronoco, Virginia resemble the plots of the basalts from the Rio Grande Rift.

INTRODUCTION

The name Catoctin schist was first given to exposures of metamorphosed basaltic and rhyolitic lavas and metasedimentary rocks at Catoctin Mountain in northern Virginia by Geiger and Keith (1891). At Catoctin Mountain the basalts are so extensively altered in places that Keith (1894) called them the Catoctin schist. Bloomer and Werner

1. Geology Department, Washington and Lee University, Lexington, VA 24450
2. Department of Earth Sciences, University of Oxford, Oxford, OX1 3PR, England

(1947) named the metamorphosed lavas and the interlayered sedimentary and metasedimentary rocks the Catoctin Formation. Along the northwestern limb of the Blue Ridge anticlinorium, the Catoctin Formation has been mapped from Pennsylvania to the James River in central Virginia (Figure 1).

In Maryland, the Catoctin Formation has been traced around the northern end of the Blue Ridge anticlinorium. In central Virginia, on the eastern limb of the Blue Ridge anticlinorium, metabasalts associated with the Catoctin Formation are situated between the Precambrian Lynchburg Group (Furcron, 1969) and the Candler Formation (Brown, 1958). The metabasalts of the eastern limb have not been traced into the Catoctin Formation to the northeast (Conley, 1985). The precise stratigraphic position of the Catoctin on the western limb of the Blue Ridge has been debated. Bloomer and Werner (1955) concluded that the Catoctin lies above the Swift Run Formation and is conformably overlain by the Lower Cambrian Unicoi Formation. Reed (1969) included the Swift Run Formation as part of the Catoctin Formation. Bartholomew (1971) proposed a Catoctin group that includes the Catoctin, Swift Run, and the former Loudoun Formations.

Thickness measurements reported for the Catoctin Formation show considerable variation from 150 and 550 meters in the Luray area (Reed, 1969) to approximately 300 meters in the Elkton area (Conley, personal communication, 1988). When these thicknesses are considered, one should remember that the Catoctin has been subjected to considerable tectonic shortening, including thrusting, and that exposures in the Blue Ridge rarely afford optimum conditions for section measurement.

The evidence of columnar jointing, large amygdules, scoriaceous flow tops, lava blisters, and tuff-filled paleostream beds (Nunan, 1980) at other places on the western limb of the Blue Ridge anticlinorium has been taken to indicate subareal extrusion. In contrast the greenstones on the eastern limb of the anticlinorium (presently about 32 km to the east of the west limb) are reported to contain pillow lavas, indicating subaquatic extrusion (Brown, 1958, 1970; Conley, 1978; Evans, 1983; Kline and others, 1987).

GEOLOGIC SETTING

The metabasalts examined in this study occur north of the James River, northeastern Buena Vista 7.5-minute quadrangle. This southernmost large outcrop belt of the Catoctin is on the western limb of the Blue Ridge anticlinorium (Figure 2). The Catoctin Formation was first reported in this area by Bloomer and Bloomer (1947), and was mapped by Bloomer and Werner (1955).

In the study area, the Catoctin comprises a northeast trending belt of greenstones and interbedded sedimentary rocks, which is fault-bounded on the northwest and southeast margins. Blue Ridge basement rocks are thrust onto the

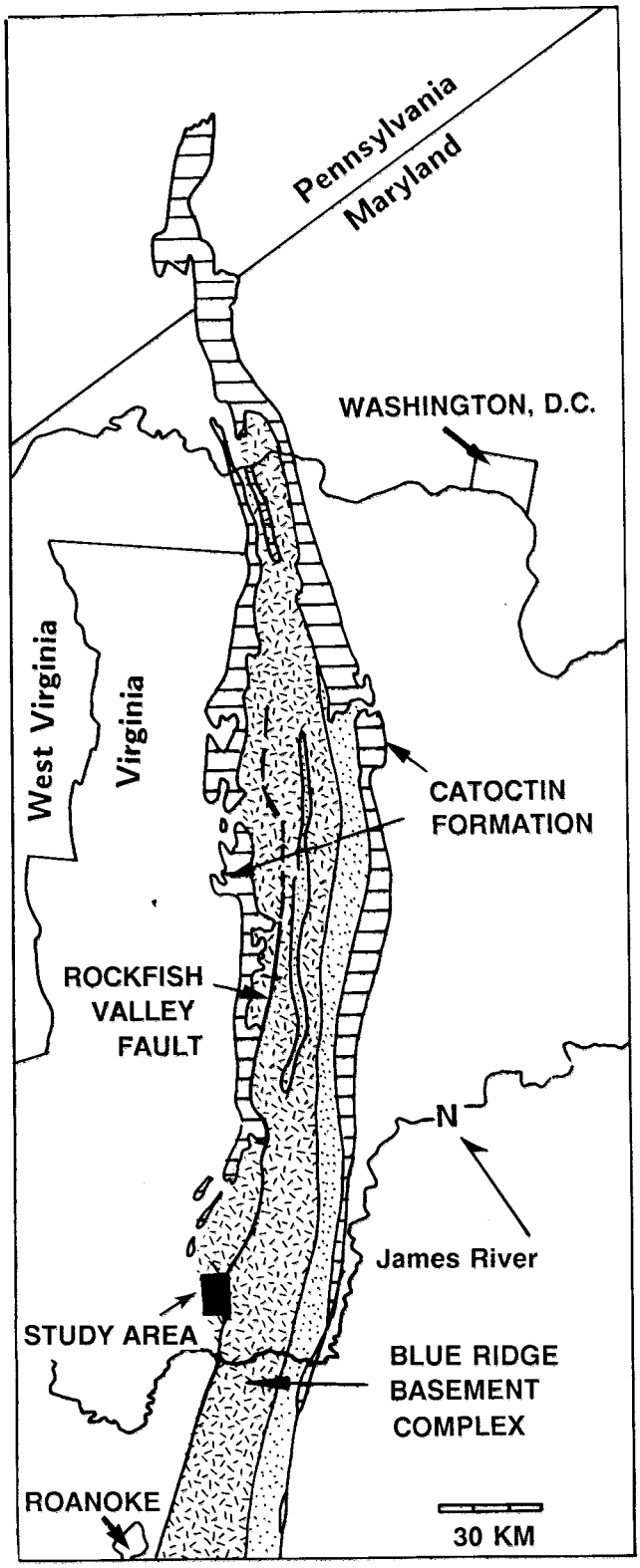

Figure 1. Regional sketch map showing the areal distribution of the Catoctin Formation. Metabasalts occur in the Catoctin Formation on both flanks of the Blue Ridge anticlinorium; study area, at the southern end of the Catoctin exposures, shown by black rectangle.

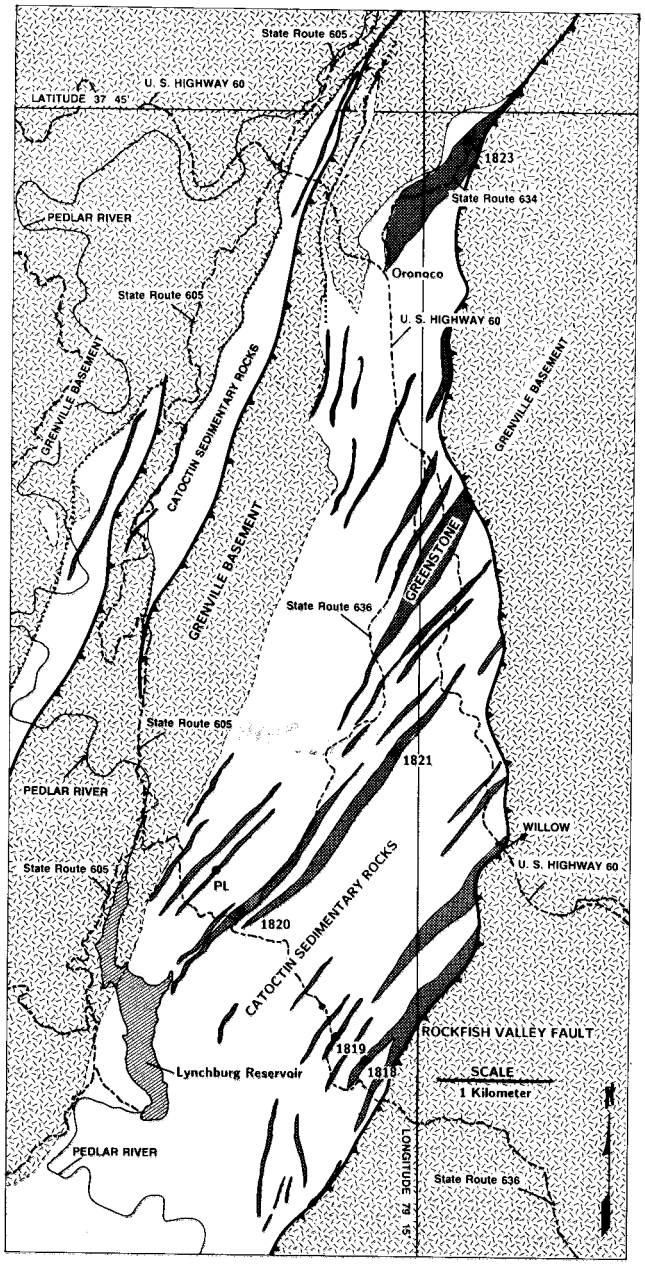

Figure 2. Geologic map of the study area. No pillow lavas have been found south of this area; however, a thin flow and several greenstone dikes occur in the James River Gap about 10 kilometers southwest of the area shown on this map. Blue Ridge basement complex is shown by hash marks; metabasalt is indicated by dark shading; sedimentary rocks interlayered with the greenstones are shown in white. Numbers indicate specimen localities. Heavy barbed lines indicate thrust faults. Heavy dotted lines indicate the approximate position of faults of uncertain character.

Catoctin along its southeastern margin. This thrust may be part of the Rockfish Valley shear zone (Bartholomew, 1984). Rocks of the Blue Ridge basement complex are in fault contact with the Catoctin on the northwest by a series of early Cambrian normal faults which are partially concealed by later thrusts (Spencer and Waterbury, 1987).

The metabasalts and interlayered slightly metamorphosed tuffaceous rock, slate, arkose, feldspathic pebble conglomerate, siltstone, and sandstone lie nonconformably on the Precambrian Blue Ridge basement complex. In a few places, the metabasalt is separated from basement rock by only a few centimeters of metasedimentary rock. The rocks in the study area are physically separated from Chilhowee Group rocks in outcrop belts to the west by faults. Therefore, the relationship of the Catoctin Formation to the Chilhowee Group in the study area is unclear. The metabasalt outcrops become thinner and less numerous toward the southwest. Sections in the northern part of the study area containing greenstone, arkose, and tuffaceous rock grade into shale, siltstone, and sandstone toward the southwest (Bowring, 1987).

GEOLOGY OF THE METABASALTS

In this area, greenstones occur as lava flows on the basement, interlayered with metasedimentary rocks, and as dikes that cut the Virginia Blue Ridge complex. Lava flows are well exposed along Davis Mill Creek, U.S. Highway 60, State Road 636, and on the Appalachian Trail north of the Lynchburg reservoir. Individual flows can be traced for distances of several kilometers and range from a few meters to a few tens of meters thick. Generally, outcrops of the greenstones stand out topographically.

The thickest sections of greenstone are north of Oronoco along Davis Mill Creek and on the crest of Long Mountain where thicknesses of individual flows are on the order of 30 to 40 meters. The true thickness of the greestones and associated sedimentary rocks has not been determined. A calculation based on average dips and outcrop width yields a maximum possible thickness of 1400 meters for the section. this estimate assumes no duplication by folding or faulting. It is probable that tectonic shortening is likely to have caused some duplication of the section. Because evidence of movement parallel to layers is commonly present, and hinges of isoclinal folds were not seen, duplication by thrusting is considered most likely.

Most of the lava flows have southeast dips of 20° to 50°. Generally, they exhibit well developed northeast-trending southeast-dipping continuous (penetrative) cleavage (Figure 3). Tectonic movement is indicated by southeastward-dipping slickensides and by zones of shearing along the base of flows and in the underlying metasedimentary rocks.

Pillow structures have been found in about half of the 36 individual flow units. The pillows range in size from a few centimeters to nearly a meter in diameter (Figure 4). Some are nearly circular or oval in form; others have been

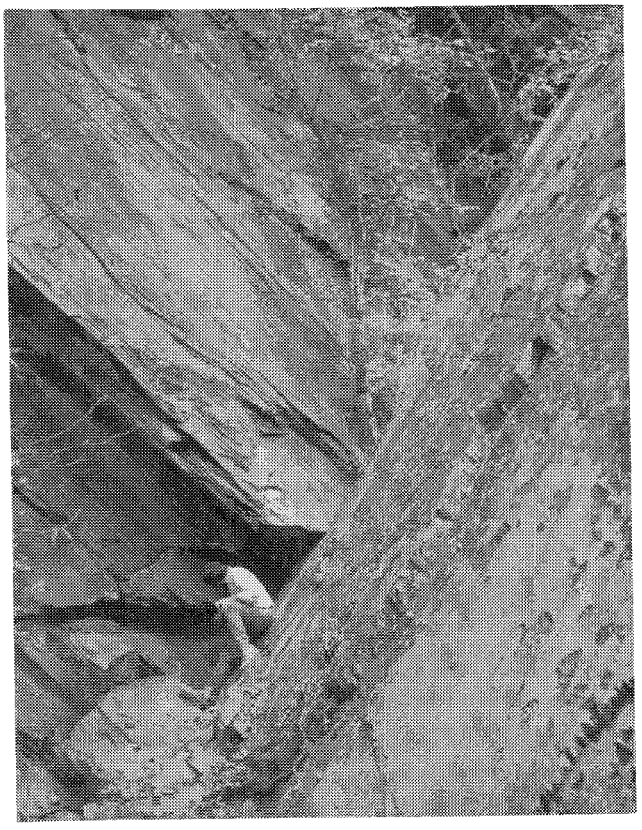

Figure 3. Strongly developed penetrative cleavage dipping to the southeast (right in this photograph) is present in most outcrops of greenstone. This outcrop is located east of the State Road 636 label in Figure 2.

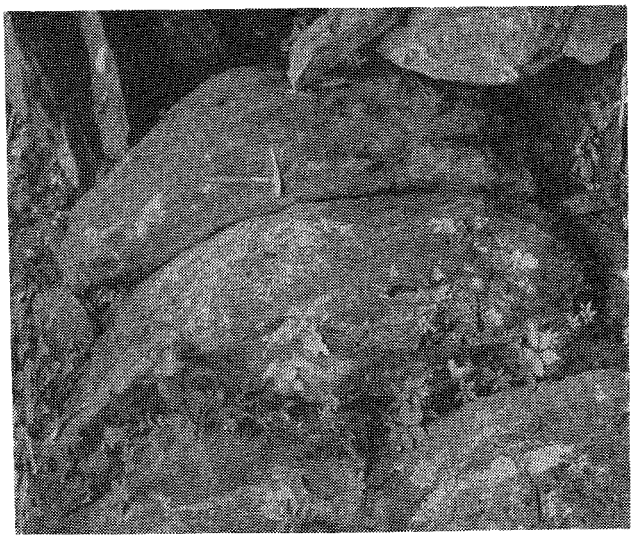

Figure 4. Large pillow-shaped masses of greenstone occur in a few places. These are near the locality labeled PL in Figure 2. Generally the external form of pillows is not preserved.

flattened so that their long axis is three to four times greater than the short axis (see cover photograph). These pillows are generally oriented so that the plane containing the long and short axes lies in the plane of the cleavage. Ratios of length to thickness vary greatly both within single outcrops and from one locality to another. Highly altered greenstone thought to be rinds of pillows (Figure 5) commonly occurs as breccias associated with pillows. Greenstone dikes cut through pillow-bearing greenstones in several localities.

In a few localities, such as 1823, in Figure 2, pillows and fragments of pillows are enclosed in coarse metasedimentary rock, clasts of which are embedded in the outer edge of the greenstone (Figure 6). These metasedimentary rocks are similar to those interlayered with the flows.

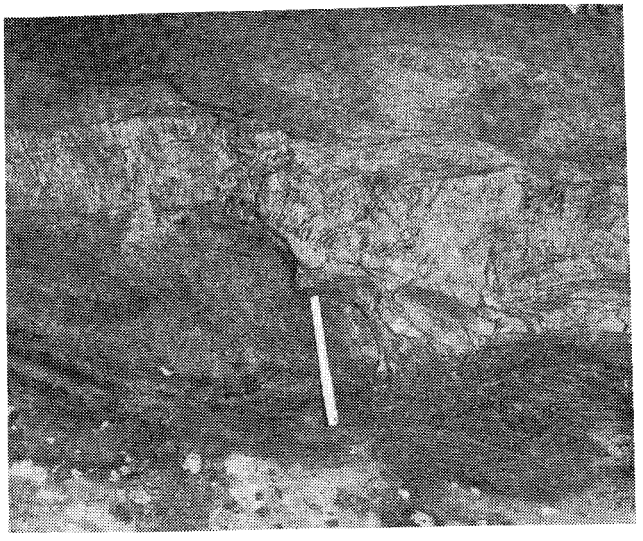

Figure 5. Pillow rinds (?) are commonly fractured and broken up; along Appalachian Trail northeast of Lynchburg Reservoir; PL on Figure 2.

PETROLOGY

The lavas examined are mostly greenstones that preserve identifiable igneous textures, although greenschist fabrics develop in the more-deformed rocks. Porphyritic and amygdaloidal textures are common with plagioclase the most abundant phenocryst phase. Directional fabrics result in some cases from a combination of original flow alignment and subsequent deformation. The mineralogy is typical of low-grade metabasites in which plagioclase has been altered to more sodic compositions, original ferromagnesian minerals have been replaced by chlorite and fibrous amphibole, and by clusters of epidote crystals representing original amygdaloidal and/or ferromagnesian phenocryst phases. An opaque oxide mineral occurs abundantly in the groundmass as small equant grains or in the more-deformed rocks as streaky aggregates. Thin veins containing epidote, quartz, and feldspar occur in most of the samples.

Two dikes are represented among the analyses in Table 1. Specimen 1811 is relatively undeformed and similar in mineralogy to the lavas, although it has much less epidote and contains a carbonate phase in irregular-shaped

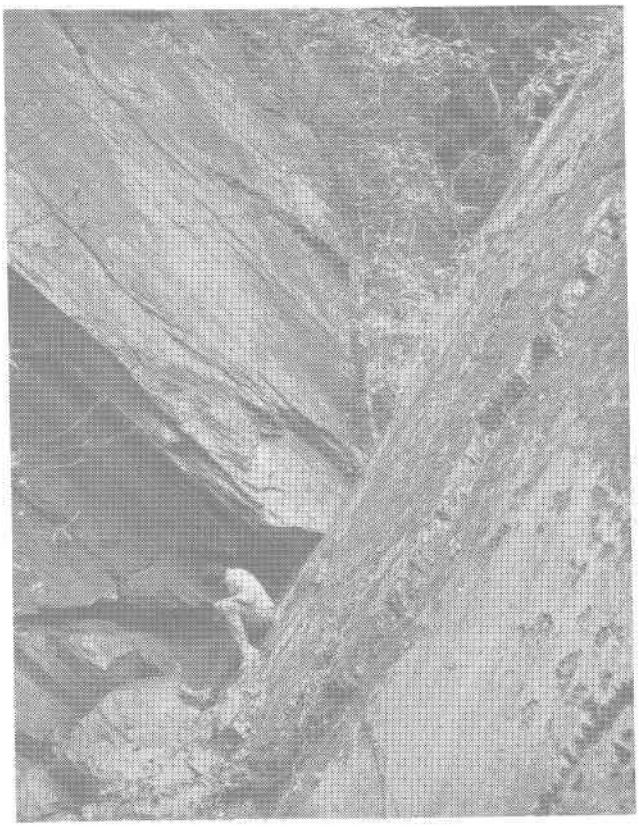

Figure 3. Strongly developed penetrative cleavage dipping to the southeast (right in this photograph) is present in most outcrops of greenstone. This outcrop is located east of the State Road 636 label in Figure 2.

Figure 4. Large pillow-shaped masses of greenstone occur in a few places. These are near the locality labeled PL in Figure 2. Generally the external form of pillows is not preserved.

flattened so that their long axis is three to four times greater than the short axis (see cover photograph). These pillows are generally oriented so that the plane containing the long and short axes lies in the plane of the cleavage. Ratios of length to thickness vary greatly both within single outcrops and from one locality to another. Highly altered greenstone thought to be rinds of pillows (Figure 5) commonly occurs as breccias associated with pillows. Greenstone dikes cut through pillow-bearing greenstones in several localities.

In a few localities, such as 1823, in Figure 2, pillows and fragments of pillows are enclosed in coarse metasedimentary rock, clasts of which are embedded in the outer edge of the greenstone (Figure 6). These metasedimentary rocks are similar to those interlayered with the flows.

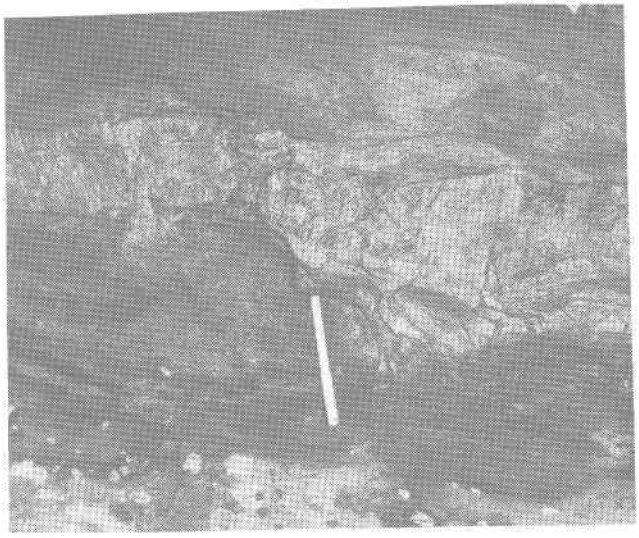

Figure 5. Pillow rinds (?) are commonly fractured and broken up; along Appalachian Trail northeast of Lynchburg Reservoir; PL on Figure 2.

PETROLOGY

The lavas examined are mostly greenstones that preserve identifiable igneous textures, although greenschist fabrics develop in the more-deformed rocks. Porphyritic and amygdaloidal textures are common with plagioclase the most abundant phenocryst phase. Directional fabrics result in some cases from a combination of original flow alignment and subsequent deformation. The mineralogy is typical of low-grade metabasites in which plagioclase has been altered to more sodic compositions, original ferromagnesian minerals have been replaced by chlorite and fibrous amphibole, and by clusters of epidote crystals representing original amygdaloidal and/or ferromagnesian phenocryst phases. An opaque oxide mineral occurs abundantly in the groundmass as small equant grains or in the more-deformed rocks as streaky aggregates. Thin veins containing epidote, quartz, and feldspar occur in most of the samples.

Two dikes are represented among the analyses in Table 1. Specimen 1811 is relatively undeformed and similar in mineralogy to the lavas, although it has much less epidote and contains a carbonate phase in irregular-shaped

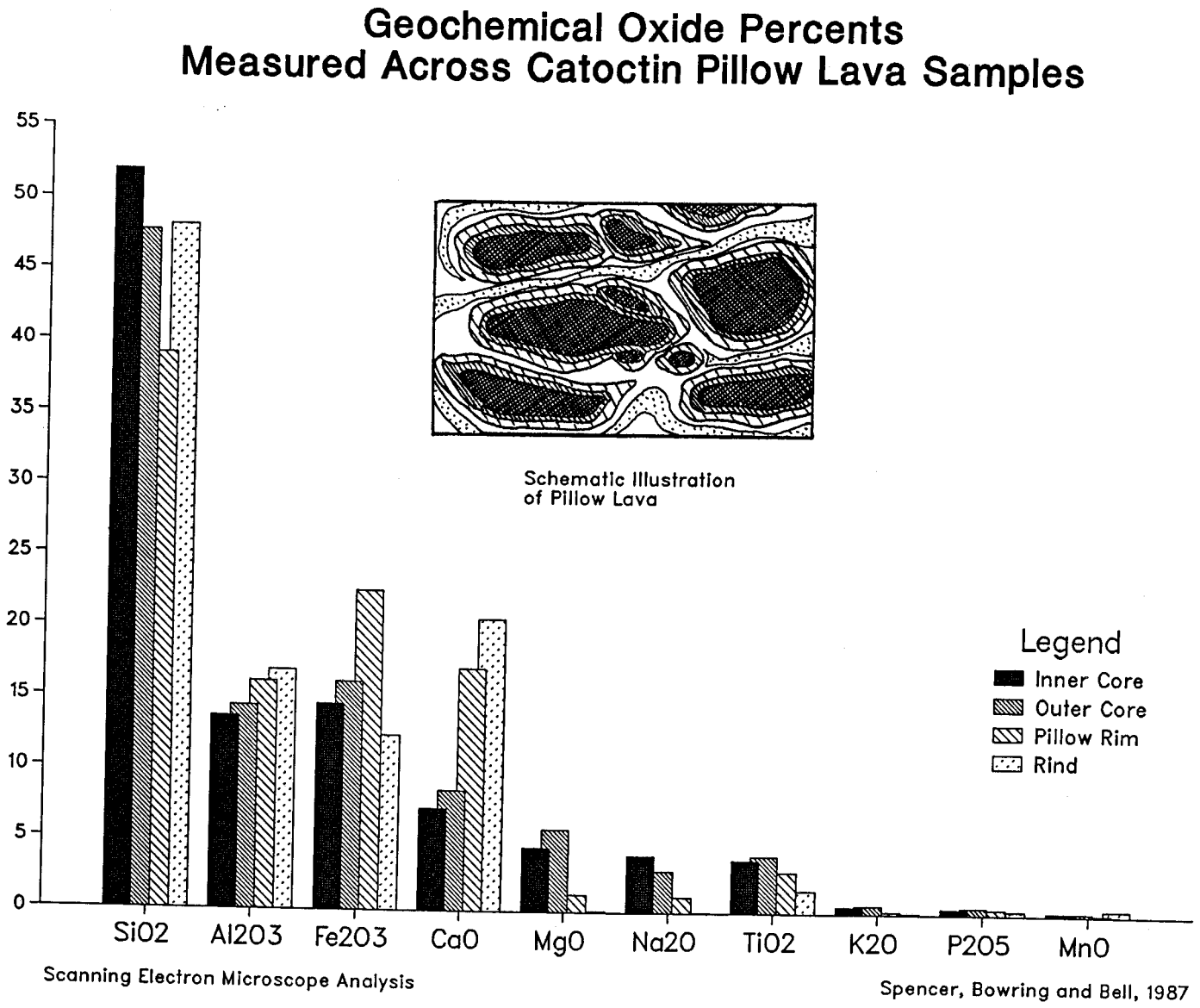

Figure 7. Catoctin pillow lava structures are recognized in the field by zonational differences of color and texture. The core is usually darker and slightly raised when compared to the rim. Oxide analyses using a scanning electron microscope revealed a gradational variation between the inner core and the rim. As silica and sodium oxides decrease, the oxides of aluminum, iron, and calcium increase. Each pillow was analyzed from the center to the outer edge. The data were grouped into three divisions: inner core, outer core, and pillow rim. The rind, an epidote-rich vein surrounding the pillow structure, is comprised almost entirely of silica, aluminum, iron, and calcium oxides.

Conley, D. C. Le Van, Douglas Rankin, and T. M. Gathright, II, who gave us the benefit of their critical reading of the manuscript.

Major- and trace-element analyses were performed in the Department of Earth Sciences, University of Oxford, on a Phillips PW 1400 X-ray fluorescence spectrometer, with data processing using the X14 package on a PDP 11 microcomputer. Fused glass beads were used for major-element analyses. FeO was determined independently by titration. Chemical analyses performed at Washington and Lee University were done on an ISI-40 scanning electron microscope with Edax 9100 analytical equipment. Major dikes are presented in Table 1.

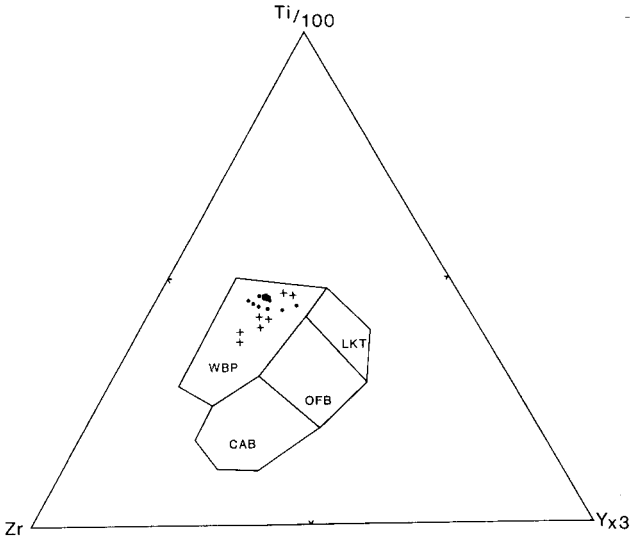

Figure 8. Ti-Zr-Y discrimination diagram (after Pearce and Cann, 1973) showing plots of the Blue Ridge metavolcanic rocks (filled circles) with plots of lavas from the Taos Plateau Volcanic Suite, Rio Grande Rift (Basaltic Volcanism Study Project, 1981) for comparison. WPB: within-plate basalts; CAB: calc-alkali basalts; OFB: ocean-floor basalts; LKT: low-potassium tholeiites.

REFERENCES CITED

Bartholomew, M. J., 1971, Geology of the Humpback Mountain area of the Blue Ridge in Nelson and Augusta counties, Virginia: [Ph.D. dissert.]: Blacksburg, Virginia Polytechnic Institute and State University, 211 p.

Bartholomew, M. J., 1984, Structural evolution of a portion of the eastern (Appalachian) overthrust belt; a new model [abs.]: Geological Society of America Abstracts with Programs, v. 16, p. 438.

Bartholomew, M. J., Gathright, T. M., II, and Henika, W. S., 1981, A tectonic model for the Blue Ridge in central Virginia: American Journal of Science, v. 281, p. 1164-1183.

Basaltic Volcanism Study Project, 1981, Basaltic volcanism on the terrestrial planets: New York, Pergamon Press, 1286 p.

Blackburn, W. H., and Brown, W. R., 1976, Petrochemical evidence relating the Catoctin volcanic series to late Precambrian continental separation [abs.]: Geological Society of America Abstracts with Programs, v. 8, p. 136-137.

Bloomer, R. O., 1950, Late Pre-Cambrian or lower Cambrian formations in central Virginia: American Journal of Science, v. 248, p. 753-783.

Bloomer, R. O., and Bloomer, R. R., 1947, The Catoctin formation in central Virginia: Journal of Geology, v. 55, p. 94-106.

Bloomer, R. O., and Werner, H. J., 1955, Geology of the Blue Ridge region in central Virginia: Geological Society of America Bulletin, v. 66, p. 579-606.

Bowring, C. B., 1987, The stratigraphic relationship of the Catoctin, Unicoi, and Harpers formations within a fault bounded rift basin in central Virginia [Honor thesis]: Lexington, Virginia, Washington and Lee University, 29 p.

Bowring, C. B., and Spencer, E. W., 1987, Catoctin pillow lavas [abs.]: The Geological Society of America Abstracts with Programs, v. 19, p. 77.

Brown, W. R., 1958, Geology and mineral resources of the Lynchburg quadrangle, Virginia: Virginia Division of Mineral Resources Bulletin 74, 99 p.

Brown, W. R., 1970, The Piedmont, investigations of the sedimentary record in the Piedmont and Blue Ridge of Virginia, in Fischer, G. W., Pettijohn, F. J., Reed, J. C., Jr., and Weaver, K. N., eds., Studies of Appalachian geology, central and southern: New York, Wiley-Interscience, p. 335-349.

Conley, J. F., 1978, Geology of the Piedmont of Virginia — interpretations and problems, *in* Contributions to Virginia geology III: Virginia Division of Mineral Resources Publication 7, p. 115-149.

Evans, N. H., 1984, Late Precambrian to Ordovician metamorphism and orogenesis in the Blue Ridge and western Piedmont, Virginia Appalachians [Ph.D. dissert.]: Blacksburg, Virginia Polytechnic Institute and State University, 322 p.

Gathright, T. M., II, 1976, Geology of the Shenandoah National Park, Virginia: Virginia Division of Mineral Resources Bulletin 86, 93 p.

Geiger, H. R., and Keith, Arthur, 1891, The structure of the Blue Ridge near Harpers Ferry: Geological Society of America Bulletin, v. 2, p. 155-164.

Keith, Arthur, 1894, geology of the Catoctin Belt: U. S. Geological Survey Annual Report 14, pt. 2, p. 285-395.

Kline, S. W., Conley, J. F., and Evans, N. H., 1987, The Catoctin formation in the eastern Blue Ridge of Virginia: Evidence for submarine volcanism[abs.]: Geological Society of America, Southeastern Section Meeting,March 25-27, p. 93.

Nunan, W. E., 1980, Stratigraphy of the Weverton formation, northern Blue Ridge anticlinorium [Ph.D. dissert.]: Chapel Hill, University of North Carolina, 225 p.

Pearce, J. A., and Cann, J. R., 1973, Tectonic setting of basic volcanic rocks determined using trace elements analyses: Earth and Planetary Science Letters, v. 19, p. 290-300.

Rankin, D. W., 1976, Appalachian salients and recesses: Late Precambrian continental breakup and the opening of the Iapetus Ocean: Journal of Geophysical Research, v. 81, p. 5605-5619.

Reed, J. C., Jr., 1955, Catoctin Formation near Luray, Virginia: Geological Society of America Bulletin, v. 66, p. 871-896.

Reed, J. C. Jr., 1964, Chemistry of greenstone of the Catoctin Formation in the Blue Ridge of central Virginia: U. S. Geological Survey Professional Paper 501-C, p. C69-C73.

Reed, J. C., Jr., 1969, Ancient lavas in Shenandoah National Park near Luray, Virginia: U. S. Geological Survey Bulletin 1265, p. 1-42.

Schwab, F. L., 1986, Latest Precambrian-earliest Paleozoic sedimentation, Appalachian Blue Ridge and adjacent areas: review and speculation, *in* McDowell, R. C., and Glover, Lynn, III, eds., The Lowry volume: studies in Appalachian geology: Virginia Polytechnic Institute and State University Memoir 3, p. 115-137.

Spencer, E. W., and Waterbury, M. J., 1987, Basement-cover interaction on the northwestern flank of the Blue Ridge in the James River Gap area [abs.]: Geological Society of America Abstracts with Programs, v. 19, p. 130-131.

Wehr, Frederick, and Glover, Lynn III, 1985, Stratigraphy and tectonics of the Virginia-North Carolina Blue Ridge: evolution of a late Proterozoic-

early Paleozoic hinge zone: Geological Society of America Bulletin, v. 96, p. 285-295.

Werner, H. J., 1966, Geology of the Vesuvius quadrangle, Virginia: Virginia Division of Mineral Resources Report of Investigations 7, 53 p.

Whitaker, J. C., 1955, Geology of Catoctin Mountain, Maryland and Virginia: Geological Society of America Bulletin, v. 66, p. 436-462.